DELINEATING THE ROLE OF OXYGEN IN BIOFILM FORMATION IN *ESCHERICHA COLI* URINARY TRACT ISOLATES

By

Allison Rae Eberly

Dissertation

Submitted to the Faculty of the

Graduate School of Vanderbilt University

in partial fulfillment of the requirements

for the degree of

DOCTOR of PHILOSOPHY

in

Microbiology and Immunology

May 10, 2019

Nashville, Tennessee

Approved:

James E. Cassat, M.D. Ph.D., Chair

David M. Aronoff, M.D.

Douglass B. Clayton, M.D.

Timothy L. Cover, M.D.

Andries Zijlstra, Ph.D.

Maria Hadjifrangiskou, Ph. D.

DEDICATION

I dedicate this work to my siblings-

we can do anything we set our minds to.

ACKNOWLEDGEMENTS

I first thank my advisor, Dr. Maria Hadjifrangiskou, for mentoring me over the last five years. Her strength, intelligence, perseverance, passion for outreach, and ability to excite others about her work are just a few qualities I admire most. I am also appreciative to have a female mentor with a family, showing me that work-life balance is possible in science. I'd be remorse if I did not thank her for pushing me beyond my limits in order to realize my full potential. I am grateful for her continuous support of my ever-evolving project tailored towards my long-term career goals.

I thank my thesis committee, chair Dr. Jim Cassat, Dr. Dave Aronoff, Dr. Douglass Clayton, Dr. Timothy Cover, and Dr. Andries Zijlstra. Their expertise, tough questions, and thoughtful insights undoubtedly strengthened me and my thesis work, and I am appreciative of their support.

My sincere appreciation goes to Drs. Jonathan Schmitz, Charles Stratton, and Gerald van Horn for their conversations about clinical microbiology and scientific collaborations. Their graciousness to discuss their career path and show me what it truly means to be a clinical microbiology director is valued. Without their expertise and willingness to collect clinical isolates, much of this work would not have been possible.

I thank my fellow lab mates, past and present, for all of their conversations- both personal and intellectual. To the first generation of mighty Hadjis: thank you for welcoming me with open arms and nurturing me into the scientist I am today. I especially thank Dr. Erin Breland for all the conversations at every hour of the day and constantly reminding me that there are bigger things. Had Dr. Kyle Floyd never

painstakingly taught me how to do that first FimA blot, I would not have the love and appreciation for peculiar technical details, and more importantly, biofilms. He is the original father of the #BiofilmFamilyDynamics. I was so fortunate to work with Madison Fitzgerald during her undergraduate career at Vanderbilt; she challenged me to be both a better mentor and scientist. To the F1c: thank you for tolerating me, especially since among you extreme introverts, the extrovert in me was brought out. Dr. John Brannon's bad dad jokes never went without an eye roll, but more importantly, his ability to constantly challenge me scientifically has made me a stronger scientist. Melanie Hurst is always willing to take a walk for food or coffee when a break was needed. She is an incredible listener and technical rockstar. Connor Beebout pushed me to an entirely new level with his impeccable literature skills, resistance to what has been done, and desire to know more. Let it be known that he now color codes his samples, and he is keeping the #BiofilmFamilyDynamics alive! My time and success in lab would have been very dull and truly impossible without all of you.

I would like to acknowledge the Department of Pathology, Immunology, and Microbiology and the Vanderbilt Institute for Infection, Immunology, and Inflammation (VI4). To all the staff who was always willing to help book meeting rooms with a smile including Helen Chomicki, Megan Schladt, Carolyn Berry, Jamie Phillips, James Rudolph, Kaleigh Johnson, Liz Roelofsz, and Pradeep Srivastava- thank you. Without the funding and support from the Monroe Carell Jr. Children's Hospital Division of Pediatric Urologic Surgery at Vanderbilt, microVU supported by Vanderbilt Trans-Institutional Programs and VI4, and NIH funding to Dr. Hadjifrangiskou, this work would

not have been possible. To all of my peers and friends in the department, thank you for supporting me both emotionally and scientifically.

Last and certainly not least, I would like to thank my family and friends. To my mom and my dad, thank you for your unending love and support, especially answering the phone no matter what time of day and calling me when it had been too long since I called. My siblings Andrew, Austin, Claire, Tegan, and Rylan are my biggest motivators. To my grandparents, for asking more questions to try to understand what I was talking about, believing in me, and always reminding me what my last name is. Aunt Mickey and Uncle Dave, thank you for showing me all things Nashville, inviting me for all of the meals, and especially making your house feel like home. Mike, thank you for the sacrifices you have made, being my rock— pushing me to be my best yet keeping me composed— and finding a way to always make me smile. To my friends both local and distant, thank you for supporting me, understanding when I could not always be there, and never turning down dinner or drinks. All of these small things have not gone unnoticed.

TABLE OF CONTENTS

LIST OF TABLES

LIST OF FIGURES

LIST OF ABBREVIATIONS

%	percent
ß	beta
µ	micro
$\Delta\Delta C_T$	log fold-change
Δ	deletion
>	greater than
<	less than
~P	phosphorylated
^oC	degrees Celsius
A-motility	adventurous motility
ABC	ATP-binding cassette
ADP	adenosine diphosphate
Ag43	Antigen 43
AI	autoinducer
APEC	avian pathogenic *Escherichia coli*
ASB	asymptomatic bacteriuria
ATEA	alternative terminal electron acceptor
ATP	adenosine triphosphate
$C_4H_2O_4^{-2}$	fumarate
c-di-GMP	bis-(3'-5')-cyclic dimeric guanosine monophosphate
cAMP	cyclic adenosine monophosphate
CAUTI	catheter-associated urinary tract infection
CFU	colony forming unit
CIT	Center for Innovative Technology
CLSM	confocal laser-scanning microscopy
CR	Congo red dye
CRE	carbapenem-resistant *Enterobacteriaceae*
CUP	chaperone-usher pathway
DMSO	dimethyl sulfoxide
DNA	deoxyribonucleic acid
E. coli	*Escherichia coli*
E. faecalis	*Enterococcus faecalis*
Ebp	endocarditis- and biofilm-associated pili
ECM	extracellular matrix
eDNA	extracellular DNA
EPEC	enteropathgenic *Escherichia coli*
EPS	exopolysaccaride
ESBL	extended-spectrum beta (ß) –lactamase

et al	and others
ExPEC	extra-intestinal pathogenic *Escherichia coli*
IBC	intracellular bacterial community
IMS	imaging mass spectrometry
IRB	Institutional Review Board
H^+	hydrogen ion
hpi	hours post infection
HSL	homoserine lactone
K. pneumoniae	*Klebsiella pneumoniae*
kan	kanamycin
kDa	kiloDaltons
L	liter
LB	lysogeny broth
LC	liquid chromatography
LPS	lipopolysaccharide
M	molar
MAEC	meningitis-associated *Escherichia coli*
MALDI-TOF	matrix-assisted laser desorption/ionization time of flight
MDR	multi-drug resistant
mg	milligram
mL	milliliter
mm	millimeter
mM	millimolar
MSCRAMM	microbial surface components recognizing adhesive matrix molecules
MS/MS	tandem mass spectrometry
N. meningitidis	*Neisseria meningitidis*
NADH	nicotinamide adenine dinucleotide
nm	nanometer
NMEC	neonatal meningitis-causing *Escherichia coli*
NO^{2-}	nitrite
NO^{3-}	nitrate
NS	not significant
O_2	oxygen
OD_{600}	optical density at 600 nanometers
OMP	outer membrane protein
P. aeruginosa	*Pseudomonas aeruginosa*
P_i	phosphate
PAGE	polyacrylamide gel electrophoresis
PBS	phosphate-buffered saline
PCA	principle component analysis
pH	potential hydrogen
PVC	polyvinyl chloride
Q	ubiquinone
QH	ubiquinone (reduced form)
QIR	quiescent intracellular reservoir

qPCR	quantitative polymerase chain reaction
RNA	ribonucleic acid
rUTI	recurrent urinary tract infection
S. aureus	*Staphylococcus aureus*
S. pneumoniae	*Streptococcus pneumoniae*
S-motlity	social motility
SDS	sodium dodecyl sulfate
SEM	standard error of the mean
SNP	single nucleotide polymorphism
spp.	species
TBST	Tris-buffered saline with Tween 20
TCA	tricarboxylic acid
TMAO	trimethylamine *N*-oxide
Tn	transposon
TSB	tryptic soy broth
UPEC	uropathogenic *Escherichia coli*
UTI	urinary tract infection
V. cholerae	*Vibrio cholerae*
VUMC	Vanderbilt University Medical Center
VUTI	Vanderbilt Urinary Tract Isolate
x	times
YESCA	Yeast extract/Casamino acids

CHAPTER I

INTRODUCTION

Portions of this introduction have been adapted from:

(A) Breland, **Eberly**, Hadjifrangiskou. "An overview of two- component signal transduction systems implicated in extra-intestinal pathogenic *E. coli* infections". Review in *Frontiers in Cellular and Infection Microbiology.* 2017. (PMID: 28536675)

(B) Floyd, **Eberly**, & Hadjifrangiskou. Biofilms and Implantable Medical Devices: Infection and Control – Chapter 4: "Adhesion of Bacteria to Surfaces and Biofilm Formation on Medical Devices". 2016.

(C) Floyd*, Mitchell*, **Eberly**, Colling, Zhang, dePas, Chapman, Conover, Rogers, Hultgren, Hadjifrangiskou. "The UbiI (VisC) ubiquinone synthase is a biofilm requisite in uropathogenic *Escherichia coli* that impacts type 1 pili formation and pathogenesis." *J Bact.* 2016. (PMID: 27161114)

(D) Floyd, Moore, **Eberly**, Good, Shaffer, Zaver, Almqvist, Skaar, Caprioli, Hadjifrangiskou. "Adhesive Fiber Stratification in Uropathogenic *Escherichia coli* Biofilms Unveils Oxygen-Mediated Control of Type 1 Pili". *PLoS Pathogens*. 2015. (PMID: 25738819)

1.1 The burden of urinary tract infections

Urinary tract infections (UTIs) are among the most common bacterial infections, accounting for approximately 20 million ambulatory visits annually in the United States and Europe (1-4). Though UTIs are very common, the infection severity can encompass a broad range of clinical diagnoses, including asymptomatic bacteriuria (ASB), acute cystitis, and pyelonephritis (**Figure 1**). In most cases, patient symptoms point towards the infection state. ASB is diagnosed by the presence of bacteria in urine without other symptoms. Patients with ASB are typically not prescribed antibiotics, with pregnant women being the exception to this (5). The most common form of symptomatic UTI is bladder infection termed cystitis. Patients with cystitis have bacteriuria, pyuria, and

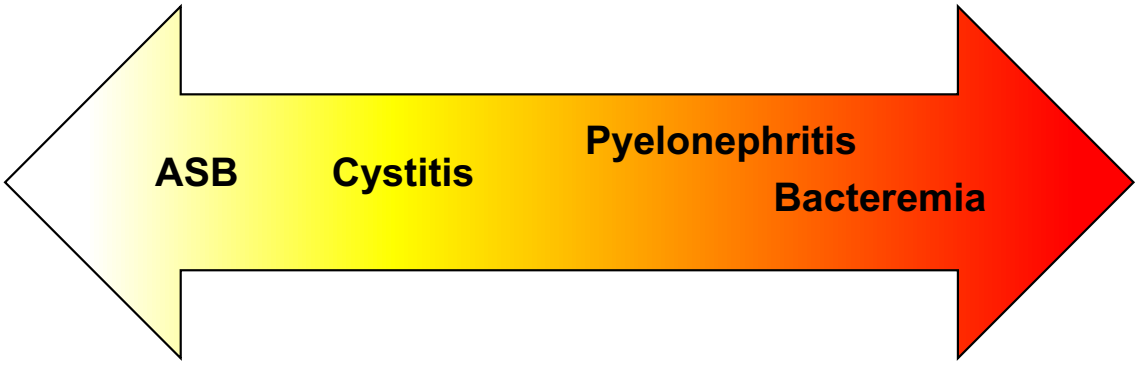

Infection State	ASB	Cystitis	Pyelonephritis	Bacteremia
Symptoms	bacteriuria	bacteriuria, dysuria, pyuria, frequency or urgency of urination, incontinence, foul-smelling urine, and blood in urine	bacteria in kidneys, high fever, chills, flank pain, nausea, and vomiting in addition to any cystitis symptoms	bacteria in the bloodstream with a combination of the following: fever, low blood pressure, increased heart, rapid breathing, gastrointestinal symptoms, and often disorientation or confusion; can lead to death
Prevalence	~3% of young women; increases with age in both men and women, especially when catheter present	estimated 1 million per year in US	4x increased risk after cystitis; ~250,000 cases in US annually	up to 15% of patients presenting with UTI can have bacteremia

Figure 1. UTIs are dynamic infections. Urinary tract infections can occur in the bladder (cystitis) and kidneys (pyelonephritis), with infection outcomes ranging from minor to life-threatening. Arrow depicts less severe (left, yellow) to most severe (right, red) sequelae. The table describes the symptoms associated with and the prevalence of each infection outcome (2, 6-9).

exhibit a combination of frequency, urgency, and dysuria (painful urination). Foul-smelling urine, blood in urine, and incontinence are less common symptoms that can occur with cystitis (1, 2). In bladder infection, bacteria can also ascend to the kidney, where they can asymptomatically colonize or induce inflammation and renal damage, leading to pyelonephritis (2, 9). Patients with pyelonephritis may or may not have symptoms associated with cystitis, but present with one or more of the following: high fever, chills, back pain, nausea, and vomiting (10). If bacteria traverse the kidneys and enter the bloodstream, the resulting bacteremia can lead to urosepsis that is accompanied by symptoms including fever, low blood pressure, increased heart rate, rapid breathing, gastrointestinal symptoms, and often disorientation or confusion (11). Urosepsis can lead to death, especially in hospitalized individuals and more vulnerable populations like the elderly and immunosuppressed (12).

In the community, females are disproportionally affected by UTIs, with fifty percent of all females experiencing at least one UTI during their lifetime (2, 13, 14). This is largely attributed to anatomical differences between males and females— specifically the distance from the urethra to anus being shorter in females— thus facilitating bacterial movement to the urethra. Though men are less susceptible to UTIs than women, their risk of infection increases with age. Furthermore, upon infection, men are more likely to experience more severe sequelae such as pyelonephritis and urosepsis (15, 16). In the hospital setting, UTIs are a common complication, particularly among the elderly and patients with diabetes, bladder cancer, or indwelling catheters (17, 18).

Given the broad range of symptoms associated with UTIs, there are two classifications used to define severity: location of infection and complication state.

Location clarifies if the infection is in the lower (bladder) or upper (kidney) portion of the urinary tract. The complication state is referred to as complicated or uncomplicated. The classification of “uncomplicated” refers to an individual with no other structural or functional abnormalities, is not catheterized, has no immunosuppression, and is not pregnant. The term “complicated UTI” refers to those individuals who have one or more comorbidities, such as bladder obstruction or the presence or a catheter (1, 2). Though there are several comorbidities that are attributed to increased risk for UTI, urinary catheters arguably provide the most risk. Catheter-associated urinary tract infections (CAUTIs) account for nearly thirty percent of all hospital acquired infections (19). This high infection rate is caused by a combination of contamination introduced during catheter insertion and host microflora (20). Furthermore, in catheterized patients, the infection risk— regardless of bacteriuria— increases *by three percent for each day that a catheter is in place*, even if the catheter has an antibiotic coating (21). CAUTIs are diagnosed by the presence of bacterial burdens greater than 1,000 colony forming units (CFU) per milliliter (mL) and one or more of the following symptoms: new or worsening fever, chills, altered mental state, flank and/or pelvic pain, presence of blood in urine, lethargy from no other identifiable cause (19).

In addition to the vast range of disease severity, UTIs also have a very high rate of recurrence, especially in the female population. Greater than thirty percent of women with cystitis will experience a second infection within ninety days, even after treatment with antibiotics (2). Aside from gender, other risk factors for recurrent UTI (rUTI) include structural abnormalities and chronic catheterization. rUTIs can be the result of infection by the same bacterial strain or by distinct strains (22, 23). In cases involving rUTI by

the same bacterial strain, there are multiple locations that may serve as reservoirs including the gastrointestinal tract (24) and vaginal cavity (25), as well as bacteria evading the host immune response and remaining in underlying layers of the bladder epithelium (26, 27).

1.2 Clinical standards for diagnostics and treatment

Since the 1950s, the gold standard for UTI diagnosis has been a positive urine culture that contains greater than (>) 100,000 bacterial CFU/mL of urine (28). Physciians also note increased pyuria as a hallmark of UTI. This standard, however, is continually questioned by both clinicians and researchers. For example, Patient A has multiple urinary symptoms— likely cystitis— but the positive culture contains less than (<) 100 CFU/mL. Patient B has >100,000 CFU/mL without any urinary tract symptoms, quite possibly ASB. Patient B matches the gold standard and may unnecessarily be treated with antibiotics, while Patient A does not meet the standard and could remain untreated with a continual infection that could lead to more severe sequelae. In nearly all cases, physicians would treat Patient A with antibiotics against the standard because of the patient symptoms, but many may also unnecessarily treat Patient B. There are no clear-cut guidelines in place to differentiate between symptomatic and asymptomatic infections, leading to significant over prescription of antibiotics because ASB is often treated with antibiotics.

With the ongoing rise in antibiotic resistance, it is clear that clinical diagnostic improvements are needed. There is constant research in this area, but studies these often meet challenges. In one study, Price *et al.* developed improved culture

techniques, requiring increased volume of urine collected from a catheter (29). One major shortcoming, however, is that not all patients are catheterized, and it is unjustifiable to catheterize every patient for a urine sample due to the risks of urinary tract injury. Thus, a critical need remains to improve diagnostic measures, especially towards deciphering asymptomatic from symptom-causing bacteria.

In addition to the need for improved diagnostics, current therapies for UTIs also need augmentation. This is due to the increased incidence of UTIs caused by bacteria resistant to common antimicrobials (30, 31), along with inherent bacterial strategies that thwart antibiotic effectiveness (discussed in 1.3). The most common treatment for UTI is a regimen of antibiotics. The fluoroquinolones, such as ciprofloxcin, levofloxacin, and ofloxacin, were the first line of treatment against UTI (32). However, as of 2010, the International Clinical Practice Guidelines suggest the following oral antibiotic treatments as a first line of defense: 100 milligrams (mg) nitrofurantoin once a day for 5 days; 160/800 mg trimethoprim/sulfamethoxazole once a day for three days; or 3 grams (g) fosfomycin in a single dose (33, 34).

Unfortunately, the rise in antibiotic resistance is prevalent in the uropathogens and has dictated the antibiotics used to treat UTIs. This is in part due to the ability of bacteria to acquire resistance markers through horizontal gene transfer (35). Documented as early as 1983 in Germany, extended-spectrum beta (ß)- lactamase (ESBL)-producing strains began causing outbreaks worldwide (36). These ESBL enzymes are plasmid-encoded, most often found in *Escherichia coli*, and confer resistance to many penicillins and cephalosporins (37, 38). ESBL-producing strains are most often treated with carbapenems; however, carbapenem resistant isolates are

becoming more prevalent (37). This leads to multi-drug resistant (MDR) strains with very limited susceptibility to antibiotic treatment. For example, the MDR ST131 lineage in *E. coli* is resistant to extended-spectrum cephalosporins and fluoroquinolones. In 2017, the World Health Organization listed carbapenem-resistant and ESBL-producing *Enterobacteriaceae*, the family classification of *E. coli*, as the third class of pathogens on the critical priority list for which new antibiotics are needed (39). More alarmingly, in addition to heritable antibiotic resistance markers, pathogenic strategies employed by uropathogens enable persistence through multiple rounds of antibiotic therapy. One such pathogenic strategy that augments persistence in the host is biofilm formation.

1.3 Biofilm formation

Biofilms are three-dimensional, multicellular communities, in which microbes are held together by a self-produced extracellular matrix (ECM) (40-43). Biofilms are ubiquitously found in nature and are formed by both bacteria and fungi. A biofilm can be composed of one or more microbial species and can form on both biotic and abiotic surfaces. The transition from the planktonic lifestyle to the biofilm state involves the microorganisms sensing the environment and responding by changing gene expression of factors necessary to ensure survival in the encountered environmental condition (24, 40-45).

Bacterial motility and sensing that lead to surface contact

This motile to sessile transition begins with sensing and interacting with a surface (**Figure 2A-B**). Motility plays a key role in this initial step and is influenced by Brownian

motion and the production of appendages that directly facilitate movement through fluids. Brownian motion is the random, uncontrolled movement of particles in a fluid as they constantly collide with other molecules (46). Brownian motion is in part responsible for facilitating movement in bacteria that do not encode motility appendages, such as *Streptococcus* and *Klebsiella* species. Brownian motion can also affect "deliberate" movement exhibited by inherently motile bacteria that harbor pili or flagella. For example, an *E. coli* cell that is swimming towards an area of higher oxygen concentration may "fall off-track" if it physically encounters a particle moving by Brownian motion or if such a particle obstructs the bacterial cell's path of motion. This form of "interference" adds to the stochasticity with which bacterial direction can change.

Arguably the most common appendage associated with motility is the flagellum. Flagella are flexible, motor-based, filamentous appendages that utilize the flux of ions to rotate and propel bacteria through fluids (known as swimming motility) or enable gliding across a surface (known as swarming motility). A typical bacterial flagellum consists of three parts: the basal body, the hook, and the flexible filament (47). Most bacteria studied to date use protons that are generated from the electron transport chain to power flagella rotation (48). Unlike the majority of bacteria that require proton motive force, *Vibrio* species pump sodium ions across the membrane to power flagellar rotation (49, 50). The ability to elaborate and power the flagellum allows for bacterial movement, and the way in which the flagellar rotation is controlled determines the type of movement that occurs. Some bacteria, such as *Vibrio cholerae* harbor a single flagellum at one pole of the cell while others harbor multiple flagella that can be arranged in

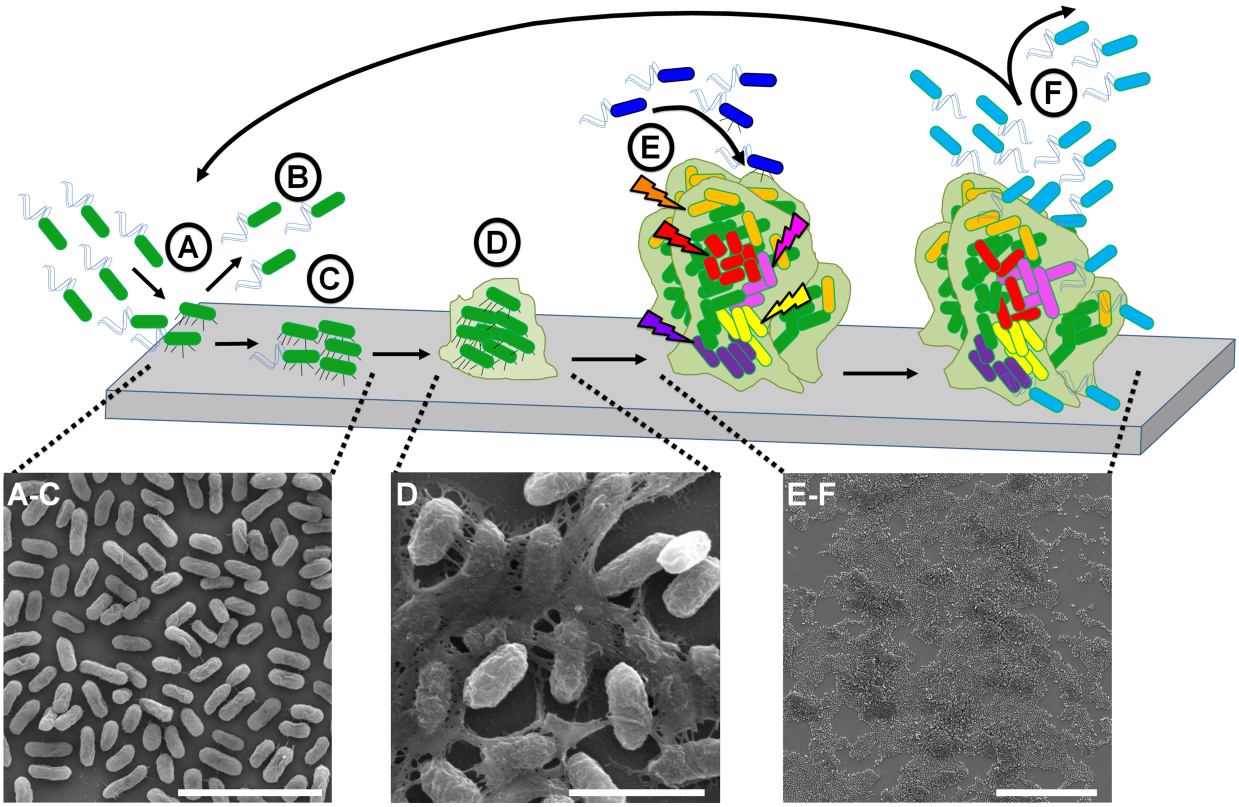

Figure 2. Stages of biofilm formation. A-B. The first, and perhaps most critical, step of biofilm formation is attachment to the surface. This process is often mediated by adhesive fibers, such as pili. Some bacteria may come into contact with the surface and return to the planktonic environment, while others can attach to the surface and proceed to form a micro-colony. **C-D.** Second, micro-colony formation begins as the bacteria begin to secrete extra cellular matrix (ECM), which acts as the glue that encases the bacteria and protects them from the outside environment. The ECM can be composed of a milieu of adhesive fibers, polysaccharides, and/or extracellular DNA. Composition of the ECM varies in a strain- and growth condition- dependent manner. **E-F.** As the biofilm matures, bacteria within the ECM are protected from outside assaults, such as antibiotics, represented as lightning bolts; other bacteria from outside may also add to the growing biofilm. Bacteria can disperse from the mature biofilm, returning to the planktonic state and able to reinitiate the biofilm formation cascade. *Figure from Floyd, Eberly, & Hadjifrangiskou. Biofilms and Implantable Medical Devices: Infection and Control – Chapter 4: Adhesion of Bacteria to Surfaces and Biofilm Formation on Medical Devices. 2016.*

multiple ways along the bacterial cell surface (51, 52). Some bacteria like *E. coli* and *Salmonella* spp. elaborate 5 – 10 flagella that are either bundled together (lophotrichous) or are placed at various locations along the cell surface (peritrichous), depending on the mode of motility engaged by the bacteria (53). There are three distinct types of flagellar-based motility: swimming, swarming, and tumbling.

In addition to flagellar-based motility, bacteria may also exhibit twitching, gliding, or sliding motility. Bacteria may harbor specific types of flexible pili fibers that can facilitate these types of motility across a surface via a combination of adhesive properties and dynamic pilus movement. Twitching motility involves the active extension and retraction of type IV pili (54, 55). A wide variety of bacteria like *Myxococcus, Neisseria,* and *Pseudomonas* species encode type IV pili that are typically found at one or both poles of the bacterial cell (55). There is evidence that individual cells are capable of moving short distances, generally the length of their type IV pili. However, twitching is usually associated with social group movement requiring cell-cell contact that allows and/or accompanies group movement of bacteria from the center of the colony outward (54, 56). Twitching motility is useful both for bacteria to group together to form micro-colonies and to flux out of biofilms (57). Gliding defines the smooth group movement over a surface that resembles swarming and twitching motility, and though it can utilize flagella or pili for movement, it does not require them. Gliding is common in myxobacteria and cyanobacteria (57, 58). In *Myxococcus xanthus*, there are two distinct mechanisms that control gliding. These two movements are termed social motility (S-motility) and adventurous motility (A-motility) (59). S-motility refers to the group movement that depends on cell-to-cell contact and the protrusion and retraction of type

IV pili; A-motility is the movement of single cells independent of pili or cell-to-cell contact and takes advantage of a self-produced “slime” to achieve movement across a surface (60, 61). Finally, sliding is a passive mode of movement that is thought to play an important role in surface colonization in many bacteria (62). Sliding occurs as a bacterial colony grows and produces surfactants such as lipopolysaccharides (LPS), which combined with reduced surface tension, allows the colony to spread along the surface (57, 58). Together, these different types of motility enable bacteria to move through space and sample the surfaces that may surround them.

Several environmental stimuli influence how these types of motility are engaged, and bacteria constantly cue changes in their direction of motion in response to their surrounding environments. Thus, the composition and hydrodynamics of the environment surrounding a surface are critical factors influencing bacterial movement and adherence. There are three main signaling pathways that control movement, though they have diverse outcomes in different bacteria: chemotaxis, quorum sensing and the secondary signaling molecule bis-(3’-5’)-cyclic dimeric guanosine monophosphate (c-di-GMP).

Chemotaxis, or the movement of a cell along a chemical gradient towards or away from nutrients, is crucial for bacterial survival. A typical chemosensory system comprises trans-membrane chemoreceptors that are generally found at the cell poles (63). These chemoreceptors bind different ligands, and in response, undergo differential methylation (via the action of cytoplasmic accessory proteins) and a conformational change that allows for the formation of complexes with a cytoplasmic histidine kinase, CheA. In *E. coli*, reduction of a chemo-attractant in the medium leads to CheA auto-

phosphorylation and subsequent phosphotransfer to another cytoplasmic functional regulator, CheY. Phosphorylated CheY (CheY~P) binds to the FliM component of the flagellar motor and forces a change in the rotation of the flagella from counterclockwise to clockwise (64-66). The counter-clockwise to clockwise rotation leads to bacterial tumbling, and thereby, a switch in the direction of movement until they swim towards high concentrations of the chemo-attractant they are lacking. In other bacterial species, the binding of CheY~P to FliM can lead to “molecular braking”, causing the flagella to slow down or stop entirely (64). Reduction of flagellar rotation due to nutritional cues can provide enough stasis to engage a surface and initiate the formation of a biofilm.

Quorum sensing is one method by which bacteria communicate within and between species. Through the production and release of chemical signals termed autoinducers (AIs), bacteria are able to sense changes in population density. As the population of bacteria releasing AIs increases, the extracellular AI concentration rises until it reaches a threshold level, at which the AI re-enters the bacterial cells. Interaction of the AI with a specific transcriptional regulator or two-component system (depending on the quorum sensing system) leads to changes in gene expression and population-dependent bacterial behavioral changes (67-70). In very simplified terms, prototypical quorum sensing systems in Gram-negative bacteria are those of *Vibrio* and *Pseudomonas* species, comprising of what is known as a LuxI/R like system (68). The LuxI protein synthesizes the AI, which in this case is an acylated homoserine lactone (HSL). LuxR is a regulatory protein that the HSL binds when it seeps back in the bacterial cells once the threshold population density has been reached. The LuxR-HSL complex activates transcriptional changes that alter the behavior of the highly dense

population (71, 72). Gram-positive bacterial species such as *Staphylococcus aureus* and *Streptococcus pneumoniae* secrete peptides as AIs. These peptides are sensed through two-component systems or are actively transported via adenosine triphosphate- (ATP-) binding cassette (ABC) transporters to engage a cytoplasmic regulator (67, 73). A significant body of work continues to shed light on additional regulatory elements present in different quorum sensing networks, and their role in the compact populations within biofilms are now beginning to be elucidated.

The secondary messenger c-di-GMP is a key determinant in the change from a motile to sessile lifestyle, where it down-regulates flagella and actively promotes biofilm formation in Gram-negative bacteria (74). In most cases, the transition from a motile state to initiating biofilm formation requires high levels of c-di-GMP. In *E. coli*, one of the critical proteins identified is a phosphodiesterase (PDE) that degrades c-di-GMP, called YhjH (75). YhjH is active during exponential phase of growth, but its expression decreases as the cell enters stationary phase (75). Reduction in *yhjH* expression allows c-di-GMP levels to rise, facilitating interaction of c-di-GMP with the flagellar "molecular brake" protein YcgR. The complex of c-di-GMP and YcgR binds to the flagellar motor to slow flagellar rotation and promote adherence to the surface (76). Likewise, a decrease in c-di-GMP levels can inhibit biofilm formation. In *V. cholerae,* the two-component system response regulator VieA regulates cholera toxin production, but also maintains PDE activity that can decrease c-di-GMP levels. VieA expression decreases the cellular levels of c-di-GMP and has also been shown to repress expression of genes involved in *V. cholerae* exopolysaccharide (EPS) synthesis to ultimately prevent biofilm formation (77, 78). Downstream targets, proteins, and ribonucleic acid (RNA) riboswitches sense

the relative abundance of c-di-GMP, and in turn, influence quorum sensing, production of ECM, and other virulence factors. For example, in *E. coli* the levels of c-di-GMP regulate the expression of curli amyloid fibers that are a component of the ECM in biofilms (79, 80). Combined, the hydrodynamic and nutritional stimuli surrounding the bacteria, along with appendages that mediate motility, and coupled with stochasticity, guide the first interactions of a bacterial cell with a surface. For steadfast adherence to take place, a combination of contact-dependent signaling and the presence of appropriate adherence factors must be present.

Adherence

After bacteria come into contact with a surface, the cells must be able to adhere (**Figure 2C**). Adherence mechanisms vary among bacterial species and strains, and each strain generally harbors multiple adhesion mechanisms that allow them to maintain hold on a surface once contact is made. Protein adhesins, adhesive pili, amyloid fibers, and non-proteinaceous factors will be described.

Microbial surface components recognizing adhesive matrix molecules (MSCRAMMs) are a family of bacterial cell surface adhesins that mediate the initial attachment to the surface of host cells. Described mostly in Gram-positive bacteria, MSCRAMMs recognize and bind specific host ECM components, such as fibronectin, lectin, and collagen (81, 82). Bacteria can harbor multiple MSCRAMMs that are specific for certain ligands. For example, *S. aureus* encodes the following MSCRAMMs: FnBA and FnBB (fibronectin), *cna* (collagen), *clfA* (laminin, vitronectin, fibrinogen), as well as others (83, 84). *S. aureus* infection can lead to various disease outcomes, and the panel

of adhesins expressed on the bacterial surface plays a critical part in determining these outcomes. One example is the collagen adhesion gene *cna* that is crucial for adherence during septic arthritis, but is not crucial for osteomyelitis infections (85).

In Gram-negative bacteria, the outer membrane can harbor adhesive proteins that belong to the outer membrane protein (OMP) group. Some OMPs are crucial for the elaboration of adhesive pili (86, 87) and have been reportedly found in the ECM of *Pseudomonas aeruginosa, E. coli,* and *V. cholerae* (88-90). In addition to OMPs, Gram-negative bacteria can code for adhesins that reach the bacterial surface via a type V secretion pathway. These types of proteins known as auto-transporters are large proteins with three distinct domains: a cleavable N-terminal signal sequence, an internal passenger domain that carries out the functions specific to each auto-transporter, and a C-terminal transmembrane domain that allows for their insertion in the outer membrane (91, 92). Notably, not all auto-transporters are adhesins; many contribute significantly to bacterial pathogenesis by acting as proteases or carrying out different functions (92). Examples of adhesin auto-transporters are the *Neisseria meningitidis*, AutA that stimulates auto-aggregation on surfaces (93) and the uropathogenic *E. coli* (UPEC) Ag43 that is critical for long-term persistence of bacteria in the urinary tract (94).

Both Gram-negative and Gram-positive bacteria utilize surface-anchored macromolecular complexes known as pili to adhere to host cells and abiotic surfaces. Gram-negative pilus assembly has been very well characterized for some systems, but the discovery of Gram-positive pili is much more recent (95). Representative Gram-positive and Gram-negative systems are depicted in **Figure 3**.

Gram-negative bacteria, more specifically Enterobacteriaceae such as *E. coli, Pseudomonas, Klebsiella, and Burkholderia* species, utilize the chaperone-usher pathway (CUP) to elaborate multi-subunit pili with adhesive properties, primarily mediated by the tip adhesins (96-99). CUP pilus biogenesis takes its name from the requirement for a periplasmic "chaperone" protein that interacts with pilin subunits after their translocation to the periplasm to stabilize folding and escort them to the outer membrane "usher" (**Figure 3B**). The pilus subunits are taken up by their cognate periplasmic chaperones as soon as they exit the Sec machinery. Pilus subunits are characterized by an incomplete immunoglobulin-like fold, which lacks the C-terminal beta-strand (100). This incomplete fold is stabilized by the interaction of one of the chaperone strands, called the G1 strand that is "donated" by the chaperone during chaperone-subunit interaction (100). This process is termed "donor strand complementation". The usher is a pilus-specific component located in the outer membrane that facilitates the assembly of the pilus on the surface of the bacterial cell (100, 101).

In UPEC, type 1 pili mediate adherence to mannosylated uroplakin receptors on the bladder epithelial surface (102-108), while P pili are crucial for binding to digalactoside receptors (109, 110). Both of these pili are also capable of mediating attachment to extracellular surfaces, such as silicone urinary catheters. Increased sequence information that has recently emerged has revealed the presence of many yet not thoroughly characterized CUPs in each of the UPEC isolates evaluated (111, 112). Each of these CUP systems' adhesins is predicted to have specificity for a different receptor or moiety, suggesting an expanded repertoire of surfaces that UPEC can

adhere to in the environment and within the host. *K. pneumoniae* also harbor type 1 pili and use them to adhere to surfaces like epithelial cells and catheters (113). *K. pneumoniae* express another CUP pilus system called type 3 pili that have also been shown to play a role in adherence to cells and silicone catheters (114, 115).

Besides CUP pili, type IV pili are also well characterized and fairly ubiquitous among the culturable bacteria studied to date. Notably, type IV pili are encoded by both Gram-negative and Gram-positive bacterial species. The formation of Gram-negative type IV pili is modeled in **Figure 3C**. Unlike CUP and sortase-dependent pili that have not yet been shown to possess the ability to disassemble, type IV pili are able to both assemble and disassemble (54). In Gram-negative bacteria, type IV pilus biogenesis occurs through a machinery that spans both membranes and requires ATP for energy production (**Figure 3C** and (96)). The double-membrane spanning machinery supporting the extrusion of the type IV pili can vary depending on the bacterial species (116). Type IV pili are also known as bundle forming pili because bacteria like *V. cholerae* and enteropathogenic *E. coli* (EPEC) can express these pili in bundles to promote twitching motility, aggregation, and biofilm formation (117-119). *Clostridium* species are reported to utilize type IV pili for gliding across surfaces, therefore mediating primary engagement with a surface (120). *Mycobacterium* species use type IV pili to adhere to host cell- and abiotic surfaces (121).

Many bacteria can also produce amyloid fibers, a class of beta sheet fibers that are homologous in structure to the amyloids that are associated with human diseases like Parkinson's and Alzheimer's (122, 123). Bacterial amyloid fibers are distinct from their eukaryotic counterparts in that they are functional and play a critical role in surface

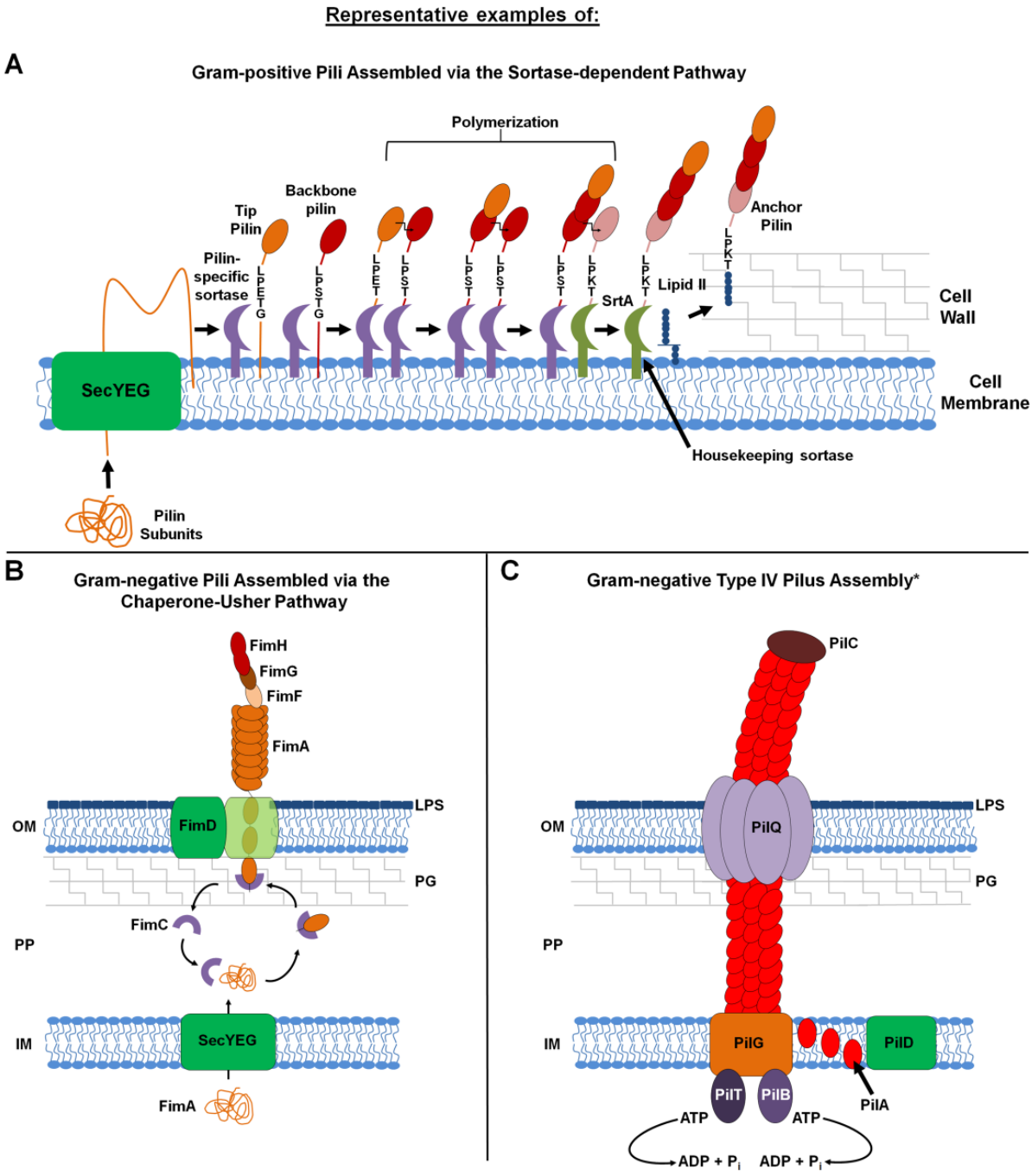

Figure 3. Examples of adhesive fiber formation by three different mechanisms. A. Schematic depicts the model describing sortase-dependent pilus biogenesis as it has been defined for *Enterococcus faecalis* Ebp pili (124). Pilin subunits are escorted across the membrane by the SecYEG translocon. Upon translocation, a pilin-specific sortase recognizes a specific sorting signal at the C-terminus of each protein and facilitates folding of the pilin subunit, as well as cleavage of the G within the sorting signal. In the case of *E. faecalis,* the tip adhesin EbpA harbors the signal LPETG recognized by the pilin-specific sortase. The EbpC backbone pilin contains the sorting signal LPSTG. All

tip and backbone pilin subunits will undergo this interaction with the pilin-specific sortase. Polymerization of the pilin subunits occurs through sortase transpeptidation of the most recently integrated pilin subunit and the next pilin subunit being incorporated. When the anchor pilin is incorporated, its sorting signal undergoes cleavage of its sorting signal by the housekeeping sortase A, SrtA. SrtA is the sortase responsible for facilitating the anchoring of proteins to the cell wall. SrtA will facilitate a series of chemical reactions, including transpeptidations and transglycosylations, with the anchor pilin and lipid II to anchor the pilus to the cell wall. **B.** Modeled here is the assembly of the CUP type 1 pili in *E. coli*. All pilin subunits are transported into the periplasm via the Sec translocon. FimC serves as the chaperone protein to bind, fold, and transport pilus subunits through the periplasm to the FimD usher in the outer membrane. FimD facilitates the transport of pilus subunits to the exterior surface of the cell and pilus elaboration in a helical fashion. The tip adhesin FimH serves at the starting point for pilus elaboration followed by FimF and FimG. Pilus assembly continues with >1,000 copies of the major type 1 pili subunit FimA incorporated in the growing pilus. For a comprehensive review of this process, please refer to the review by (100). **C.** Schematic depicts a model representative of type IV pili biogenesis in Gram-negative bacteria, though both Gram-positive and Gram-negative bacteria can both produce type IV pili. Here, the model depicts biogenesis of type IV pili in *V. cholerae* (125). PilC serves as the tip adhesin, and PilA is the major pilin subunit with hundreds to thousands of copies making up each pilus. The pilin subunits are translocated across the inner membrane via the Sec translocon and folded by the peptidase, PilD. Once folded, the PilG inner membrane protein allows for the assembly of the pilus in a helical manner that is driven by the ATPase PilB (also named PilF). The pilus begins amassing in the periplasm until it reaches the outer membrane, where it is shuttled through the secretin PilQ that forms a channel and allows the protrusion of the pilus onto the cell surface. The PilT ATPase drives disassembly and retraction of the pilus (126). For a comprehensive review on the biogenesis of type IV pili please refer to these cited reviews ((116, 117, 127). Abbreviations in figure: IM, inner membrane; LPS, lipopolysaccharide; OM, outer membrane; PG, peptidoglycan; PP, periplasm. *Figure from Floyd, Eberly, & Hadjifrangiskou. Biofilms and Implantable Medical Devices: Infection and Control – Chapter 4: Adhesion of Bacteria to Surfaces and Biofilm Formation on Medical Devices. 2016.*

attachment (128). Functional bacterial amyloids have been characterized in *Corynebacterium*, *Gordonia*, and *Mycobacterium* species (121, 129), but their role in pathogenesis is not yet thoroughly characterized. In *E. coli* and *Salmonella* spp., curli amyloid fiber subunits are transported through the Sec translocon to the periplasm, where they are shuttled through the outer membrane protein CsgG. Curli fibers are then assembled via nucleation precipitation of the major subunit, CsgA, onto the minor subunit CsgB on the cell surface (96, 130-132). Curli amyloid fibers in *Salmonella* spp. and *E. coli* have been shown to contribute to adhesion on abiotic surfaces, are a component of the ECM of biofilms, promote host cell invasion in murine models, and have recently been shown to induce an innate immune response (128, 133-142).

Along with protein adhesins and proteinaceous macromolecular adhesive structures, bacteria can also utilize non-proteinaceous components for adherence to a surface. One key component for many bacteria is the production of the virulence factor capsule. The capsule is a well-organized layer typically made up of polysaccharides (143), though some bacteria such as *Bacillus anthracis* produce a non-polysaccharide capsule (144, 145). The primary role of a capsule is protection from desiccation and predation, such as the host immune response. However, in some cases, the capsule has been demonstrated to mediate adherence of pathogenic bacteria to surfaces. Select strains of Group A *Streptococcus* species have been shown to bind to human keratinocytes through interactions of their hyaluronic acid capsule with the CD44 protein on the cell surface (146). Likewise, interactions of the bacterial capsule with a surface have been implicated in device-associated infections of different *Staphylococci* species (147).

Another adherence/aggregation factor that has been shown to play a role in the initial adherence of bacteria to a surface is secreted/extracellular deoxyribonucleic acid DNA (eDNA). In many bacteria, eDNA is a critical component of the ECM surrounding the biofilm residents. eDNA can alter the hydrophobicity of the bacterial cell surface modulating bacterial interactions with surfaces of varying hydrophobicity (148). For example, eDNA on the surface of the mouth-colonizing *Streptococcus mutans* has been shown to increase bacterial adhesion to hydrophobic surfaces (149). Some strains of the Gram-negative pathogen *N. meningitidis* have been shown to rely on eDNA for the initiation of pathogenic biofilm formation (150). Similarly, the initiation of biofilm formation by *P. aeruginosa* has been shown to be dependent upon eDNA that secures surface attachment (151).

These examples highlight the diversity of adhesive moieties elaborated by bacteria. Most bacteria use different combinations of these adhesive moieties, which depend on the chemistry and type of surface encountered and may alter the combination in response to differing environments or conditions (149, 152-155). However, stochastic heterogeneity within a given bacterial population also contributes to the phenotype and adhesive properties of each cell. For example, UPEC type 1 pili are critical for binding to bladder epithelial cells as discussed above (102, 156-159). Only a subset of bacteria within a UPEC population expresses type 1 pili on their surface at any given time (160). Therefore, out of a large number of UPEC cells, only a fraction succeeds in engaging the bladder surface; their non-piliated brethren forgo binding to the bladder and are subsequently voided by urination or transverse the ureters via swimming motility to adhere to and colonize the kidneys if they express P pili (156, 161).

The same is true for all bacteria; not all members of a population harbor the same adhesive appendages on their cell surface, even though they are genetically identical. This phenotypic heterogeneity adds to the dynamics of bacteria-surface interactions.

Micro-colony formation, biofilm maturation, and dispersal

Following initial attachment, a series of signal transduction events occur as a function of microbe-surface interactions. Mechano-sensing, or the ability to sense and respond to the physical forces by the local environment, results in changes in transcription in response to surface attachment (162, 163). One example of contact-dependent changes mediating irreversible attachment comes from the opportunistic pathogen *P. aeruginosa.* The EPS Psl is a major component of the ECM of *P. aeruginosa* and has been shown to induce the production of c-di-GMP by nearby sessile and planktonic cells to promote aggregation into micro-colonies (164-166). The Psl-producing bacteria move around the surface, leaving a trail of Psl, which attracts other Psl-producing bacteria, ultimately resulting in micro-colony formation (164-166). Though other bacterial species utilize molecules other than Psl, c-di-GMP is a universal signal. As c-di-GMP levels in the microenvironment rise, the bacteria sense this and prepare for a biofilm lifestyle (79, 80, 167).

Micro-colony formation begins with adherent bacteria that begin replicating and producing ECM (**Figure 2D**). The ECM is the hallmark feature of biofilms that serves to protect the resident bacteria from outside immune assaults or environmental stressors such as temperature and nutrient resources. Typical ECM components are proteinaceous fibers like curli and pili, lipids, eDNA, and EPS (42, 43, 168-180). In many

biofilm-forming pathogens, the EPS component is one of the most prevalent ECM constituent. Depending on the strain and growth conditions, the composition of the ECM varies. The EPS produced by *E. coli* is cellulose (179-181). In UPEC strain UTI89, cellulose and curli amyloid fibers produce rugose and wrinkled colony biofilms (**Figure 4A** and (182, 183)). Cellulose makes up one sixth of the ECM, while curli amyloid fibers make up the other five-sixths of the total ECM mass, with additional variable components contributing to spatial organization depending on growth conditions (180). Recent work from the Cegelski group reported the identification of a phosphoethanolamine modification of cellulose in UPEC that facilitates adherence to bladder cells (184, 185). The combination of ECM components make up a strong protective cover that excludes diffusion of agents (**Figure 4A**) and can thus protect against antibiotic treatment (**Figure 4B-C**).

As the biofilm matures by expanding in terms of ECM production and number of cells, bacteria at different depths of the community begin to respond to signals from the immediate micro-environment, becoming phenotypically distinct over time (**Figure 2E**). Mature biofilms range in size from a few cells thick to several millimeters (mm) thick and can persist for extended periods of time due to the protective ECM and subpopulations that arise within the biofilm. However, at some point, some bacterial cells disperse from the biofilm into the surrounding environment (**Figure 2F**). The mechanistic details behind dispersal is not well understood, but it is likely that the bacteria within the biomass reach a threshold cell density and/or run out of nutrients, which become limiting factors for biofilm growth (186). Quorum sensing and c-di-GMP levels play a major role in mediating population density-dependent changes and has thus been

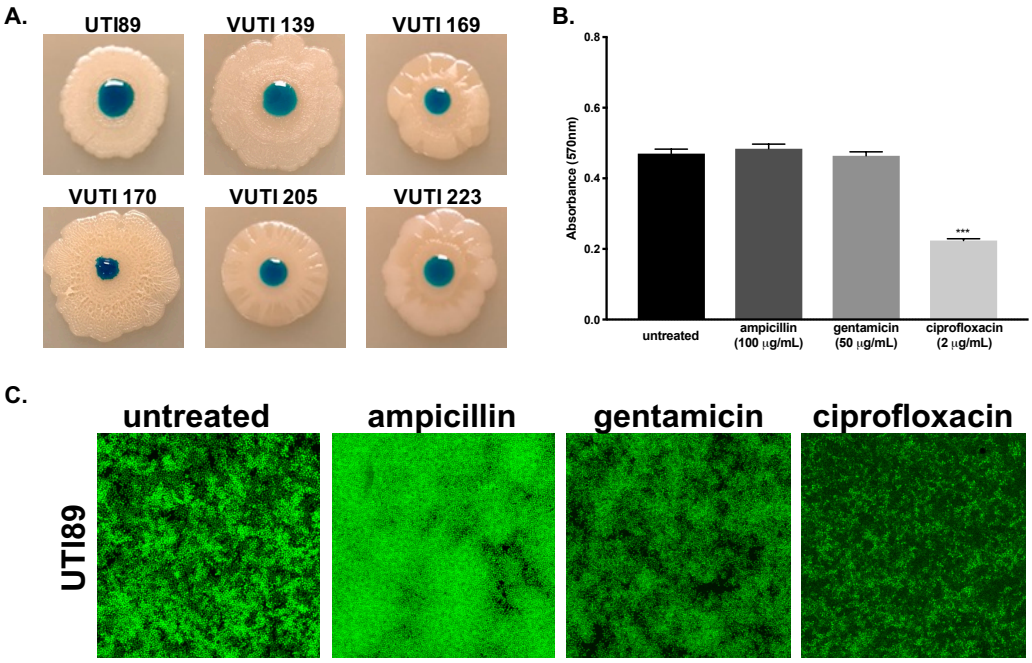

Figure 4. Biofilm formation complicates treatment of urinary tract isolates. **A.** Water droplet assay performed by adding 5 microliters (μL) colored water on mature, day 11 colony biofilms. After 1 minute, each colony biofilm is imaged. Isolates tested were obtained from patients with diverse clinical outcomes: UTI89 (cystitis isolate), VUTI 139 (ASB), VUTI 169 (pyelonephritis), VUTI 170(ASB), VUTI 205 (bacteremia), VUTI 223 (cystitis). **B.** Biofilm formation by crystal violet assay shows that preformed biofilms withstand antibiotic treatment. 96-well plates were seeded with pan-sensitive cystitis isolate UTI89 and allowed to grow for 48 hours. At 48 hours, biofilms were treated with antibiotic for an additional 72 hours prior to plate washing and crystal violet staining following the O'Toole method (187). *** p-value <0.0001 by Kruskal-Wallis test. **C.** Biofilms were grown on plastic coverslips and treated with antibiotics as described above. After 72 hours of antibiotic treatment, coverslips were washed and stained with SYTO9, a DNA stain, and imaged using confocal laser-scanning microscopy to visualize overall biofilm architecture.

implicated in biofilm dispersal (186). Dispersed bacteria can seed secondary-site infection in biofilm- or planktonic states. In the case of UTIs, bacteria can form biofilms on and within bladder epithelial cells, on the surface of kidneys, and on urinary catheters (21, 188, 189). When bacteria disperse from one of these sites, they can move on to re-seed infection in either the bladder or kidney. In catheter-associated infections, the bacteria are coating the catheter and are likely in the bladder lumen as well. Even though the contaminated catheter is removed and replaced by a sterile one, there is a high risk for contaminating the new catheter due to the bacteria in the bladder lumen. Because the biofilm to planktonic lifestyle is cyclical, biofilms greatly contribute to chronic infection and recurrent infections.

In the context of infection treatment, biofilms pose complications in two ways: 1) the self-secreted ECM in which they reside serves as a physical barrier to antibiotic treatment (**Figure 4**), and 2) the biofilm community exhibits “division of labor” in response to chemical gradients within the biofilm resulting in phenotypically distinct subpopulations that serve different roles in the biofilms. One of those subpopulations— termed “persisters”— are metabolically quiescent, resist treatment and serve as reservoirs for recurrent infection (190). Other subpopulations include ECM secretors that eventually lyse to increase amounts of ECM, as well as “explorers” that are flagellated and disperse from the biofilm (191-193). Ongoing work in our lab— part of which is described in this thesis— includes identifying and understanding the role of each subpopulation within the biofilm.

Because biofilms are difficult to eradicate, they contribute to significant healthcare burdens in terms of patient care and costs. Since standard antibiotic

treatment is not always sufficient to treat biofilms, several years and billions of dollars have been dedicated to the development of antibiofilm strategies. Research on different device materials, including urinary catheters coated or embedded with antimicrobial properties, have been tested with very marginal success (194-196). Several studies have been devoted to utilizing or designing anti-biofilm compounds to inhibit particular steps in biofilm formation such as ECM production, the enhancement of dispersal, interference with c-di-GMP signaling, or blocking of adhesive fiber biosynthesis (197). Another approach to biofilm treatment is to detect early stages of biofilm formation through improved diagnostic techniques; however, to date, this has only been successful through genetic manipulation of the bacteria to express fluorophores (198). In order to either prevent or remove infection-causing biofilms, it is pertinent that we better understand the intricacies of the biofilm residents and the dynamics of changing behaviors within biofilms. My thesis work has focused on better understanding the nature of UPEC biofilms.

Though several bacterial species such as *K. pneumoniae*, *P. aeruginosa*, and *Staphylococcus saprophyticus* cause UTIs, greater than eighty percent of all UTIs are caused by UPEC, a Gram-negative facultative anaerobe (**Figure 5** and (1, 2)).

1.4 Uropathogenic *Escherichia coli*

The UPEC pathogenic cascade (**Figure 6**) initiates with ascension of the bacteria to the bladder. Ascension requires flagella, but it is still uncertain as to whether bacteria swim against the urine flow or if they use their flagella to swarm across the urothelial surface (199, 200). Upon ascension to the bladder, attachment to the urothelium is

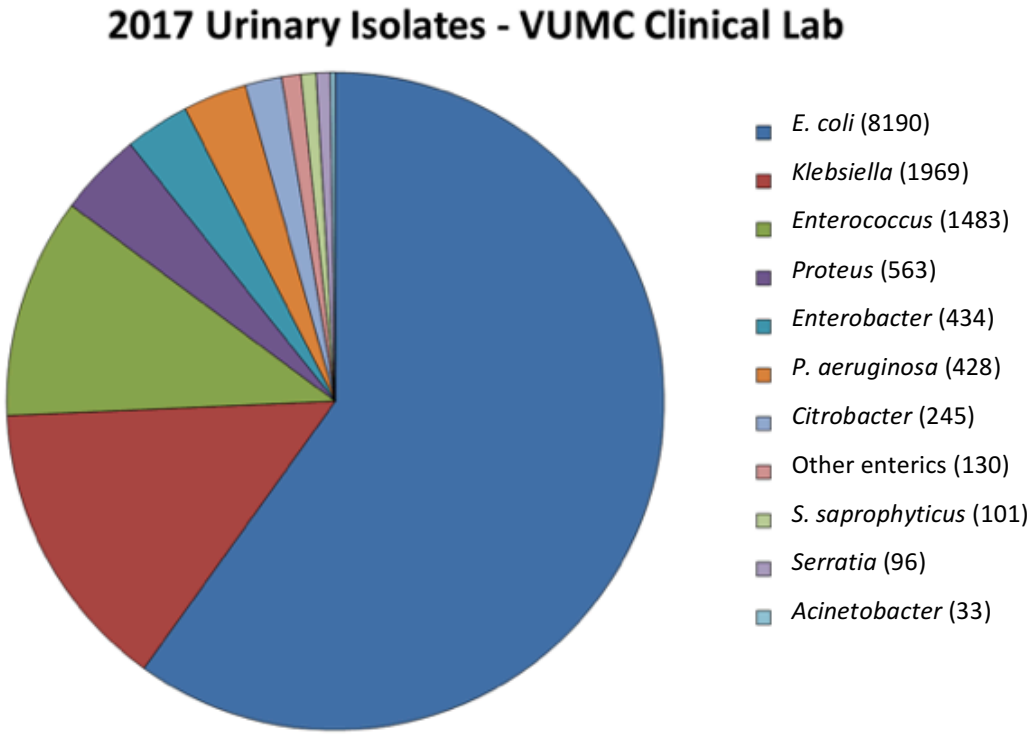

Figure 5. Urinary isolate classification during 2017 from the Vanderbilt University Medical Center. Pie chart shows bacterial species isolated from urine samples collected in 2017 at the Vanderbilt University Medical Center Clinical Laboratory. *Figure provided by Dr. Jonathan Schmitz.*

mediated by adhesive pili, with type 1 pili (Fim) reported to be the most critical in this process. Type 1 pili assemble via the CUP, and their tip adhesin FimH recognizes mannosylated receptors on the bladder epithelial cells (100, 102, 156, 201). FimH-mediated adherence leads to bacterial internalization followed by vacuolar escape and bacterial expansion into a biofilm-like intracellular bacterial community (IBC) (102, 156). If bladder epithelial cells do not exfoliate, the bacterial cells eventually filament and flux out of the bladder epithelial cells. At this stage, the filaments can infect neighboring host cells and repeat the IBC cascade.

The innate immune system is responding at several points throughout this IBC cascade, at any which point UPEC reaches an infection bottleneck and may be cleared. When UPEC enters into the vacuole reported to be a fusiform vesicle, there is an increase in TLR4 from the LPS reminants. The elevated levels of TLR4 signal an increase in cyclic adenosine monophosphate (cAMP), which causes exocytosis of the fusiform vesicle out of the bladder cell (27, 202-204). If the bacteria escape the vacuole into the bladder cell cytosol, they are targeted for expulsion by autophagy and taken to the lysosome. Meanwhile, due to TLR4 activation, antimicrobial peptides such as cathelicidin and ß-defensin and chemokines and chemokine receptors are produced, including CXCL1 and CCR5 (203-205). These soluble factors signal to resident immune cells like macrophages and mast cells to recruit neutrophils to clear the targeted bacterial cells. Caspase 3- and 8-dependent apoptosis is triggered by
bacteria inside the bladder cells, which ultimately causes exfoliation of the infected bladder epithelial cell (204, 206).

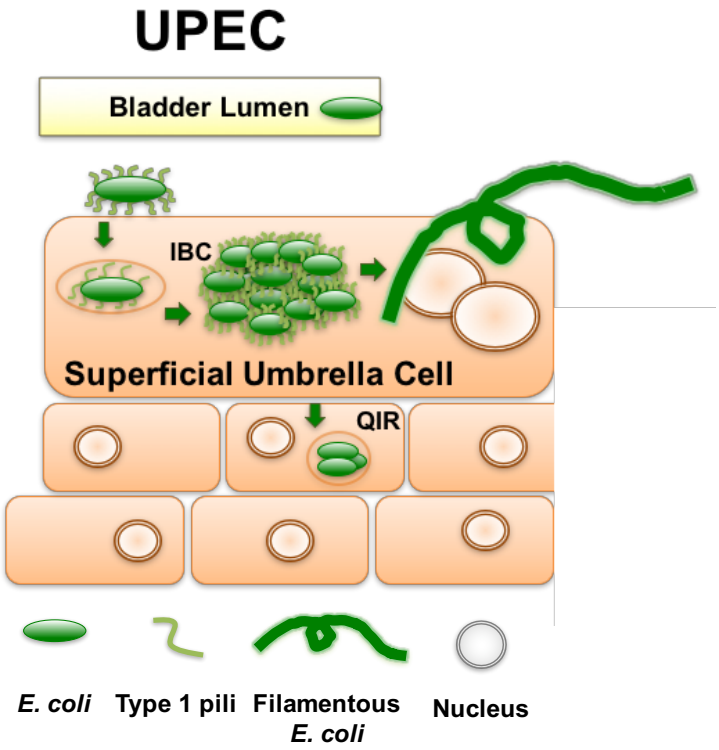

Figure 6. UPEC intracellular life-cycle. The intracellular bacterial community (IBC) cycle that leads to acute UTI is similar to biofilm formation. First, the bacterial cell binds to mannosylated receptors on the surface of the bladder epithelium primarily via type 1 pili adhesive fibers, although recent studies have also demonstrated a key role for phosphoethanolamine-modified cellulose mediating this process. The bacterial cell then invades the host cell via a zipper mechanism. The mechanism by which UPEC escapes the endocytic vacuole and exits into the host cell cytoplasm remains unknown. Once in the host cell cytoplasm, the bacteria clonally expand into a biofilm-like IBC encased in ECM. Over time, cells can filament and flux out of the infected host cell and attach to neighboring host cells, ultimately repeating this cycle. Quiescent intracellular reservoirs (QIRs) can form in the underlying urothelial layers and cause infection at a later time. This intracellular acute cystitis can lead to a chronic infection if the host is unable to clear the infection. *Adapted from Breland, Eberly, & Hadjifrangiskou. Front. Cell. Infect. Microbiol. 2017.*

This acute, intracellular lifestyle of UPEC can lead to chronic cystitis infection if the host immune system is unable to clear the infection. In areas where exfoliation has occurred, bacteria gain access to undifferentiated bladder cells (188). The bacteria can become internalized in underlying layers of the urothelium, forming quiescent intracellular reservoirs (QIRs) (**Figure 6**). The QIRs can remain dormant inside the bladder cell, do not respond to antibiotic treatment, and can seed infection at a later time (188, 207, 208). For these reasons, QIRs are considered one for the contributors for rUTI.

1.5 Unknowns and gaps in the field

Given the prevalence of biofilms both on catheters and in the acute and chronic phases of infection, we need to understand basic chemical and physical cues that drive adherence and biofilm expansion. Previous studies have teased apart the metabolic requirements of UPEC in human urine and in an *in vivo* mouse model (209-211). These results show that mutations in the glycolysis pathway do not impact UPEC pathogenesis, but the import and utilization of amino acids and tricarboxylic acid (TCA) cycle products are requisite for pathogenesis (210, 211). These same requirements impact biofilm formation *in vitro* and *in vivo* (210, 212). Furthermore, aerobic respiration is required for infection in the bladder. To show this, a gene deletion of *ubiI*, which encodes for an aerobic ubiquinone synthase enzyme, was created and used as a proxy to gauge the mode of respiration in the bladder. Though the *ubiI* mutant is capable of colonization, IBC formation was entirely ablated in the murine bladder in the *ubiI* mutant compared to the wild-type strain (**Figure 7A-B** and(209)). Furthermore, *in vitro* biofilm

formation in the *ubiI* mutant had decreased abundance and loss of architecture compared to the wild-type strain (**Figure 7C** and (209)). These data indicated that aerobic respiration enhances UPEC biofilm formation.

Further studies by Floyd *et al*. unveiled that an oxygen gradient exists within the biofilm and that it dictates protein stratification within the biofilm by developing a matrix-assisted laser desorption/ionization time-of-flight (MALDI-TOF) imaging mass spectrometry (IMS) technique for biofilms (213). This study then went on to validate and verify localization known constituents of UPEC biofilm, namely type 1 pili and curli fibers. Type 1 pili are found primarily at the air-exposed region, while curli fibers are found at the air-liquid interface of the biofilm, where oxygen concentrations are below atmospheric levels (**Figure 8** and (213)).

The implication of oxygen gradients in organizing biofilm structure raises the following questions that that will be addressed in this thesis:

1) Is the requirement for oxygen a broad phenomenon across urinary isolates? (**Chapter II**)
2) Is the oxygen-induced spatial organization driven by terminal oxidase expression? (**Chapter III**)
3) Can biofilm formation be used as a distinguishing feature for isolates coming from asymptomatic versus symptomatic patients? (**Chapter IV**)

I show that oxygen enhances substantial biofilm formation in a diverse range of non-domesticated urinary tract isolates cultured under infection-relevant conditions (**Chapter II**). I reveal that the high-affinity terminal oxidase cytochrome *bd* is critical for

UPEC biofilm architecture and infection establishment (**Chapter III**), while several additional oxygen-regulated factors were uncovered via a transposon screen (**Appendix A**). Finally, I demonstrate that biofilm abundance does not correlate with asymptomatic strains as previously reported, but preliminary evidence point towards distinct metabolic signatures that may distinguish ASB from cystitis isolates (**Chapter IV**).

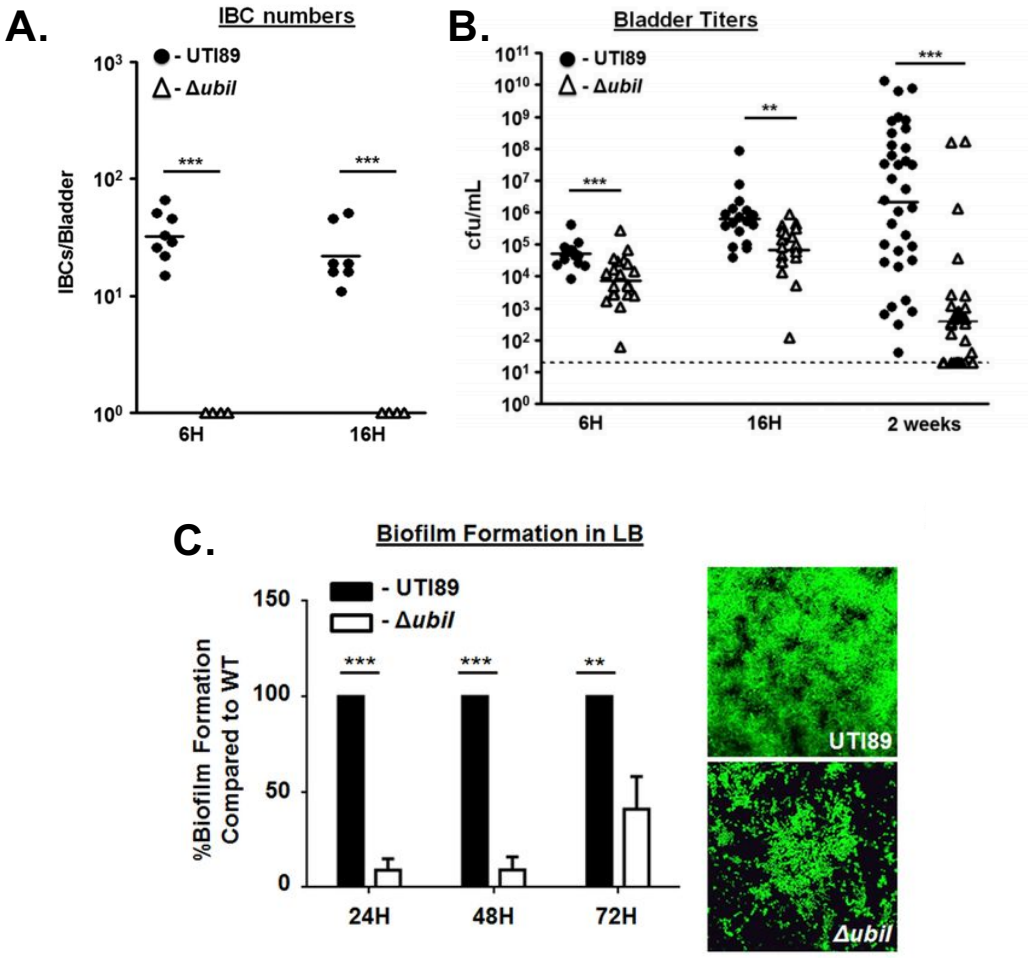

Figure 7. Deletion of *ubil* attenuates IBC formation, chronic colonization, and biofilm formation. A. Intracellular bacterial community (IBC) numbers at 6 and 16 h post infection with WT UTI89 or UTI89Δ*ubil* mutant. A representative from two experiments is shown and a two-tailed Mann-Whitney test was performed to determine significance (*, $P < 0.05$; **, $P < 0.001$; ***, $P < 0.0001$). **B.** Numbers of CFU recovered from the bladders of mice infected with either WT UTI89 or UTI89Δ*ubil* mutant at stages of acute or chronic UTI. The graph depicts numbers from two independent experiments. **C.** Graph shows percent biofilm formation of UTI89Δ*ubil* compared to WT UTI89 performed in 96-well PVC plates in lysogeny broth (LB) medium under ambient oxygen. On the right, representative images of 72-h confocal laser scanning microscopy (CLSM) images of WT UTI89 and the *ubil* deletion mutant are shown. Statistical significance was determined by one-way ANOVA with a P of <0.05 (95% confidence interval). *Figure adapted from Floyd, Mitchell, Eberly et. al. J. Bacteriol. 2016.*

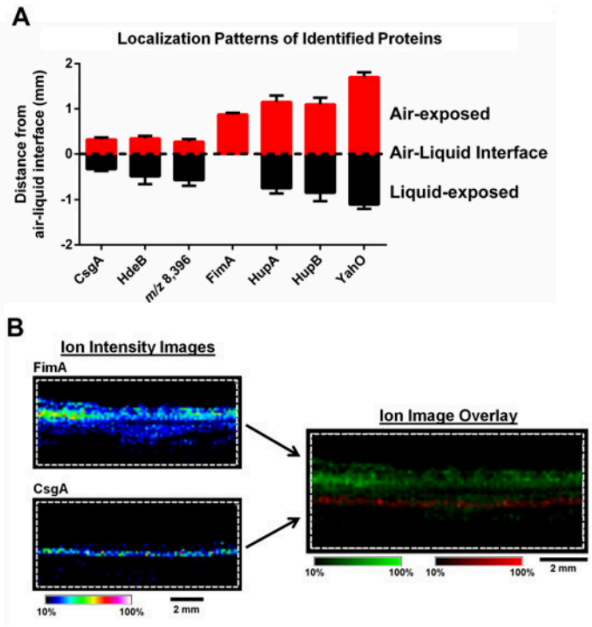

Figure 8. IMS analysis reveals stratification of identified UPEC proteins and distinct localization of FimA and CsgA within the biofilm. A. The localization of each protein identified, along with the unidentified ion *m/z* 8,396 is shown in graphical form. The localization of the major curli subunit, CsgA, was used to demarcate the air-liquid interface. Localization of ions were measured as the distance (mm) from the middle of CsgA localization to the middle of the localization of each individual ion using Fiji Image J software. **B.** IMS ion images of FimA and CsgA localization are depicted ± 5 Da for each ion, and data are presented as a heat map intensity of relative abundance from 10 (blue)– 100% (Red/White). FimA (green) and CsgA (red) ion overlay image presented using the same criteria, with single color distribution instead of a heat map from 10–100% intensity. Scale bar = 2 mm. *Adapted from Floyd, Moore, Eberly, et. al. PLoS Pathogens. 2015.*

CHAPTER II

BIOFILM FORMATION BY UROPATHOGENIC *ESCHERICHIA COLI* IS FAVORED UNDER OXYGEN CONDITIONS THAT MIMIC THE BLADDER ENVIRONMENT

Portions of this chapter have been published in: **Eberly** *et al.* "Biofilm Formation by Uropathogenic *Escherichia coli* Is Favored under Oxygen Conditions That Mimic the Bladder Environment". *Intl. J. Mol. Sci.* 2017. (PMID: 28973965)

2.1. Introduction

E. coli strains are facultative anaerobes, meaning that oxygen is the preferred source to fuel aerobic respiration if it is available, but that in the absence of oxygen, *E. coli* strains can generate energy via anaerobic respiration or fermentation (**Figure 9** and (214, 215)). While utilization of oxygen as the terminal electron acceptor leads to maximal ATP generation (36-38 ATP molecules), *E. coli* can produce variable ATP numbers by utilizing five alternative electron acceptors in the following order: nitrate (NO^{3-}), nitrite (NO^{2-}), dimethyl sulfoxide (DMSO), trimethylamine *N*-oxide (TMAO), and fumarate (214, 215). The energy produced by the different electron acceptors varies from 2 to 36 ATP molecules. In the absence of terminal electron acceptors, *E. coli* can generate up to two ATP through fermentation by converting pyruvate to lactate, formate, or acetate and ethanol (215, 216).

Uropathogenic *E. coli* are exposed to varying oxygen concentrations throughout the route to the urinary tract. In the gastrointestinal tract, where UPEC asymptomatically reside, oxygen concentrations range from 8% to 0% (217). The bladder lumen ranges from 4 to 5.5% oxygen (217, 218), while the kidneys have oxygen concentrations that range from 12 to 14% (219). Thus, UPEC transition from a hypoxic (gastrointestinal tract) to a normoxic (exterior) and back to a hypoxic environment (bladder) when they

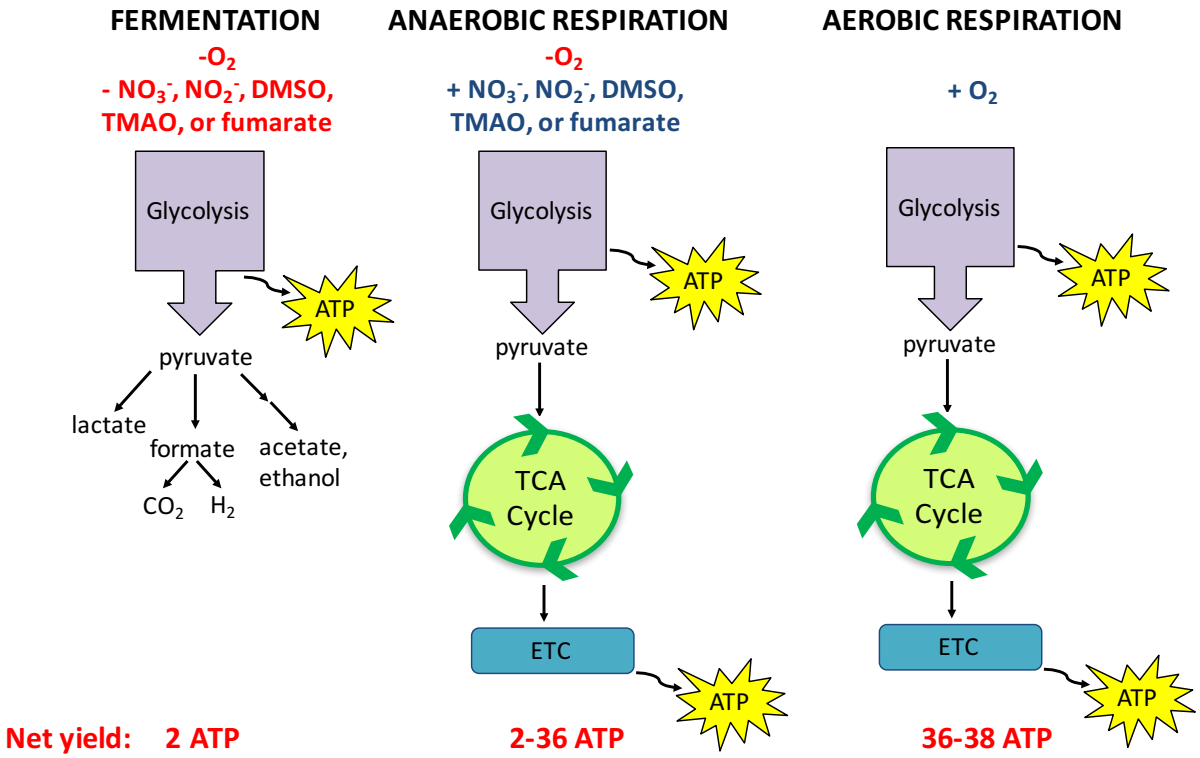

Figure 9. Overview of energy production by *E. coli*. As a facultative anaerobe, *E. coli* can undergo fermentation, as well as respiration using oxygen or one of 5 different alternative electron acceptors. In the absence of oxygen and in order of preference, *E. coli* can utilize the following alternative terminal electron acceptors to fuel anaerobic respiration: nitrate (NO^{3-}), nitrite (NO^{2-}), dimethyl sulfoxide (DMSO), trimethylamine *N*-oxide (TMAO), and fumarate. In the absence of these electron acceptors, fermentation produces the least amount of ATP, yielding only 2 molecules. Anaerobic respiration is more favorable than fermentation, producing between 2 and 36 molecules of ATP depending on the alternative electron acceptor used. Oxygen is the most favorable electron acceptor, producing between 36 and 38 ATP molecules.

traverse host anatomical niches on their way to the bladder (**Figure 10**). The mechanisms driving UPEC biofilm formation have not been studied in the context of the actual oxygen conditions encountered by the bacteria during a UTI. All studies performed to date have only investigated UPEC biofilm formation under atmospheric oxygen conditions. In addition, the vast majority of studies in UTI pathogenesis use specific isolates that have been in the laboratory setting for many years. As discussed above, *E. coli* can utilize alternative terminal electron acceptors (ATEAs) in the absence of oxygen (**Figure 11**). The goal of this study was to expand upon previous observations that demonstrated increased biofilm levels in the presence of oxygen (209, 213). In this study, we asked the questions:

1) how broad is this phenomenon of biofilm regulation by oxygen?

2) what is the impact of ATEAs on biofilm formation?

2.2 Methods

Bacterial strains

Cystitis isolate UTI89 (220) and previously constructed mutant *UTI89ΔfimA-H* (213) were used as reference strains. Urine-associated *E. coli* strains VUTI1 – VUTI112 (VUTI for Vanderbilt Urinary Tract Isolate) were isolated from positive-culture urines (mono-species culture) by the Vanderbilt University Medical Center (VUMC) clinical microbiology laboratory under Institutional Review Board (IRB) #151465. Of the collected isolates, 50 strains were randomly selected for the biofilm studies presented in this chapter.

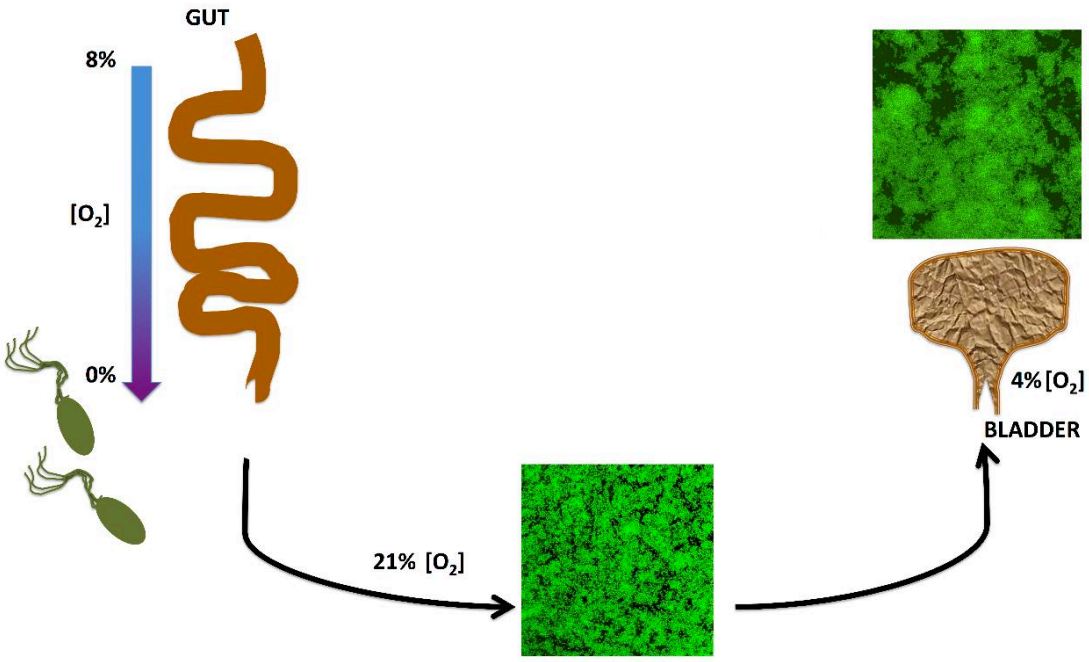

Figure 10. UPEC can occupy a variety of environmental niches. UPEC resides asymptomatically in the gastrointestinal tract (gut), where oxygen decreases from about 8% to 0%. Upon exiting the gastrointestinal tract, the bacteria are exposed to atmospheric (21%) oxygen before entering the urethra. The oxygen concentration in the bladder is hypoxic, ranging from 4-5.5% oxygen. UPEC must adapt to the different environments encountered during the route to infection. *Figure adapted from Eberly et. al. Int. J. Mol. Sci. 2017.*

A.

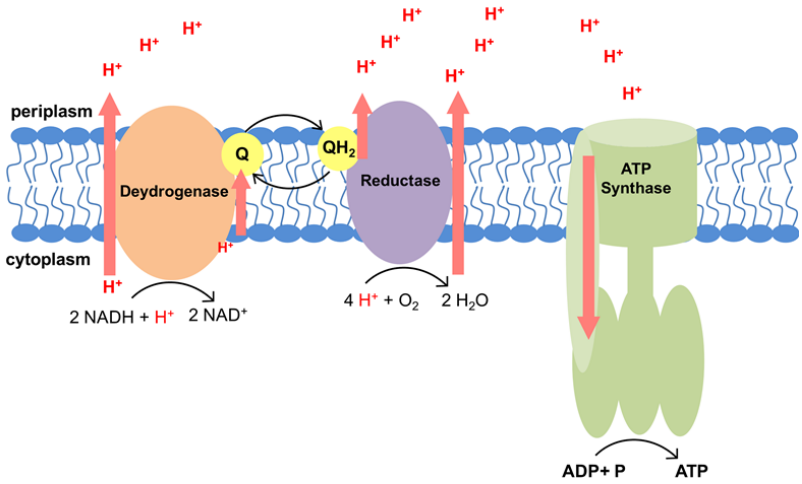

B.

Terminal Electron Acceptor	Dehydrogenase	Reductase
O_2	NADH dehydrogenase	Cytochrome oxidase
NO_3^-	Formate dehydrogenase	Nitrate reductase
NO_2^-	Formate dehydrogenase	Nitrite reductase
TMAO	Formate dehydrogenase	TMAO reductase
DMSO	Formate dehydrogenase	DMSO reductase
$C_4H_2O_4^{-2}$	Formate dehydrogenase	Fumurate reductase

Figure 11. Schematic depicting critical enzymes in the Electron Transport Chain. A. The schematic represents the enzymes utilized to generate energy when oxygen is the terminal electron acceptor. Aerobic respiration yields the most ATP, undergoing glycolysis and the tricarboxylic acid (TCA) cycle to feed nicotinamide adenine dinucleotide (NADH) molecules to the electron transport chain (ETC), where the bulk of ATP is produced. In the case of aerobic respiration when oxygen is abundant, the electron transport chain, which is located in the inner membrane, consists of an NADH dehydrogenase that donates electrons to the cytochrome *bo* oxidase. The transfer of electrons between the enzymes is mediated by ubiquinones (Q, QH_2). The reduction of oxygen to water by the cytochrome oxidase creates a proton motive force across the membrane, and these protons are used to drive ATP synthase to produce ATP. In the absence of oxygen and in the presence of an alternative terminal electron acceptor, *E. coli* undergo anaerobic respiration. *E. coli* encodes two NADH- and at least two formate dehydrogenases that are utilized under different respiration conditions. **B.** The table shows the dehydrogenase and reductase enzymes used for each terminal electron acceptor. *E. coli* can utilize five additional terminal electron acceptors in the absence of oxygen (O_2) in the following preferential order: nitrate (NO_3), nitrite (NO_2^-), dimethyl sulfoxide (DMSO), trimethylamine-*N*-oxide (TMAO), and fumarate ($C_4H_2O_4^{-2}$). *Figure from Eberly et. al. Int. J. Mol. Sci. 2017.*

Biofilm assays

All strains were grown statically overnight at 37 degrees Celsius (^{o}C) in lysogeny broth (LB). Cultures were then diluted to an optical density at 600 nanometers (OD_{600}) of 0.06 in fresh LB and seeded into 96-well polyvinyl chloride (PVC) plates as previously described (209). Plates were incubated statically at room temperature as previously described (209), but with varying oxygen concentrations: a) aerobic (ambient/21%); b) hypoxic gradient (shown in results); or c) anoxic (0% oxygen) conditions. Biofilm plates grown under anoxic conditions were incubated in a vinyl anaerobic chamber (Coy Lab Products) maintained at 0% oxygen and 2-3% hydrogen. Hypoxic oxygen concentrations were achieved in a Herthem incubator (ThermoFisher) equipped with a ProOx 110 compact oxygen controller (BioSpherix) that displaces oxygen with nitrogen gas. All biofilm plates were incubated for 48 hours at room temperature prior to quantitation. Biofilm abundance was quantified using crystal violet staining method of O'Toole *et al* (187). For the ATEA biofilm experiments, the following procedure was performed in addition to what is described above: A 3.2 molar (M) stock concentration of nitrate, DMSO, or TMAO was diluted with sterile water to the desired final concentration in each well (ranging from 160 mM to 20 mM) so that the final volume in each well was equal. Fumarate was diluted in LB to a stock concentration of 160 mM and further diluted in fresh LB to achieve the desired final concentrations. Each experiment was performed at least 3 independent times, with at least 24 technical replicates per biological replicate.

Congo red (CR) uptake was qualitatively assessed by spotting 5 µL of overnight culture on 1.2x Yeast extract/Casamino acid (YESCA) CR agar plates. The 1.2x YESCA

CR agar plates are comprised of 12 g casamino acids, 1.2 g Yeast extract, and 22 g of agar in one liter of water. The media is then autoclaved and after it cools, 1.5 mL of CR dye (40mg/mL stock) and 10µL of Bromophenol blue (10mg/mL stock) added. The colonies are monitored for CR uptake and rugose morphology as previously described (221, 222). Plates were incubated at room temperature and imaged on day 7. At least two independent experiments were performed.

Growth curves and CFU enumeration

Bacterial cultures were grown in LB overnight shaking at 37^{o}C. Overnight cultures were diluted to an OD_{600} of 0.06 in fresh LB. 100 µL of diluted culture was added to each well in a flat bottom 96-well plate. Absorbance measurements at an optical density at 600nm were recorded at 15-minute intervals for 24 hours. Growth curves under ambient oxygen conditions were performed using a SpectraMax i3 (Molecular Devices) plate reader, while measurements under anoxic conditions were performed using a Synergy H1 hybrid reader (BioTek). In addition to absorbance readings, samples were collected at 60-minute intervals for CFU enumeration. Obtained samples were serially diluted and plated on LB plates (8-10 technical replicates per sample) for enumeration. Experiments were performed independently at least two times.

Immunoblot analyses

FimA immunoblots were performed as detailed in Floyd, *et al* (213). Briefly, all strains were grown statically overnight at 37^{o}C. Culture was normalized to an OD_{600} of

1, pelleted by centrifugation, and resuspended in Laemmli buffer with 5% 2-mercaptoethanol. Samples were then acidified with 1M hydrochloric acid and boiled for 10 minutes at 100^{o}C. After cooling, samples were neutralized with 1M sodium hydroxide and then resolved on 16% sodium dodecyl sulfate (SDS) polyacrylamide gel electrophoresis (PAGE) gel. Proteins were transferred to nitrocellulose by Trans-Blot Turbo Transfer System (BioRad) for 7 minutes at 1.3 amps and 25 volts. After transfer, membranes were blocked overnight at 4^{o}C with 5% non-fat milk in 1x tris-buffered saline with Tween 20 (TBST), washed three times with 1x TBST and incubated with a 1:5,000 dilution of primary anti-FimA antibody (212) in 2% non-fat milk in TBST for one hour at room temperature. Membranes were again washed three times with 1x TBST and then incubated for 30 minutes at room temperature with HRP-conjugated goat-anti-rabbit secondary antibody (Promega) (1:10,000) in 2% non-fat milk in TBST. Membranes were washed three times with 1x TBST before treatment with SuperSignal West Pico Chemiluminescent Substrate (ThermoScientific) and subsequent visualization of bands on x-ray film.

2.3 Results

UPEC biofilm formation is diminished under anoxic conditions

One of the most critical adherence factors identified in UPEC is a class of fibers termed type 1 pili (157). Type 1 pili mediate UPEC adhesion to bladder epithelial cells, and their deletion greatly diminishes biofilm formation under laboratory and *in vivo* conditions (156). We have previously shown that in the complete absence of oxygen, expression of type 1 pili is reduced in cystitis strain UTI89 (213), and mutants unable to

aerobically respire also display a defect in type 1 pili production and biofilm formation (209). These observations have led to the hypothesis that anoxic conditions reduce biofilm formation due to the reduction of type 1 pili. We therefore compared *in vitro* biofilm formation at atmospheric (21% oxygen) and anoxic conditions (0% oxygen) for a panel of urine-associated *E. coli* isolates obtained from the VUMC clinical microbiology laboratory (IRB #151465). As expected, cystitis isolate UTI89 exhibited decreased biofilm formation under anoxic conditions (**Figure 12A**), presumably due to reduced expression of type 1 pili (213). Reduction in biofilm formation did not appear to be a function of reduced bacterial cell viability (**Figure 12B-C**).

To ascertain how broad the effect of oxygen is on diverse *E. coli* isolates, a collection of urine-associated *E. coli* was obtained under IRB #151465. A total of 50 strains were then assessed for biofilm formation *in vitro* in the presence of 21% or 0% oxygen (**Figure 13**). Biofilm levels varied overall among the urine-associated *E. coli* isolates, with Vanderbilt Urinary Tract Isolate 41 (VUTI41) forming the highest levels of biofilm (**Figure 13**, **Table 1**). This variability in biofilm abundance does not appear to be solely attributed to growth differences (**Figure 14**). Interestingly, VUTIs also expressed variable levels of type 1 pili. Variable abundance of the main type 1 pilin subunit FimA was observed (**Fig. 15**) that did not correlate with biofilm abundance (**Figure 13**). Striking variability was also observed in the ability of VUTIs to bind Congo Red (**Figure 16**), a dye that stains cellulose and curli within the biofilm matrix (223), indicating high variability in the matrix composition and possibly architecture among different isolates. Irrespective of the variability in type 1 pili expression and CR uptake, 96% (48/50) of

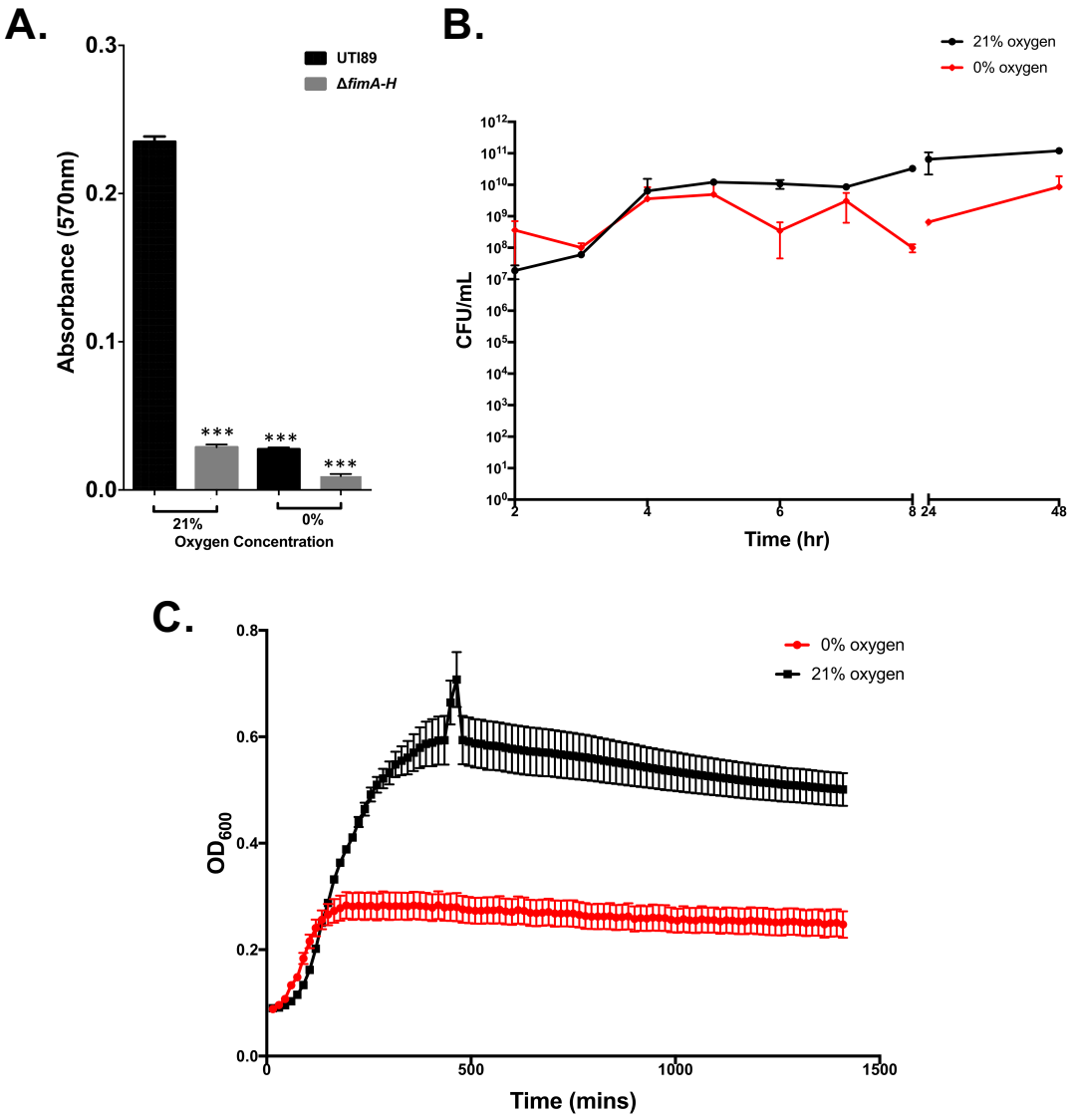

Figure 12. UPEC biofilm levels are decreased under anoxic conditions. A. UTI89 biofilm levels at 0% and at 21% oxygen. Biofilm abundance is measured as OD_{570} after crystal violet staining. UTI89Δ*fimA-H*, a strain that lacks the ability to form type 1 pili, is used as a negative control. *** p value <0.0001 by one-way ANOVA compared to UTI89 at 21% oxygen. Data shown are representative of at least 3 independent experiments with 24 technical replicates. **B.** Graph depicts fluctuations in CFU in liquid cultures grown in 21% and 0% conditions over the biofilm growth period. Error bars represent standard deviation between replicates at each time point. CFU enumeration was performed at least two independent times. **C.** Growth curves measuring the optical density at 600 nm over time during growth in 21% or 0% oxygen. Error bars show standard error of the mean among technical replicates. These data are representative of at least two independent experiments, with at least 5 technical replicates per experiment. *Figure from Eberly et. al. Int. J. Mol. Sci. 2017.*

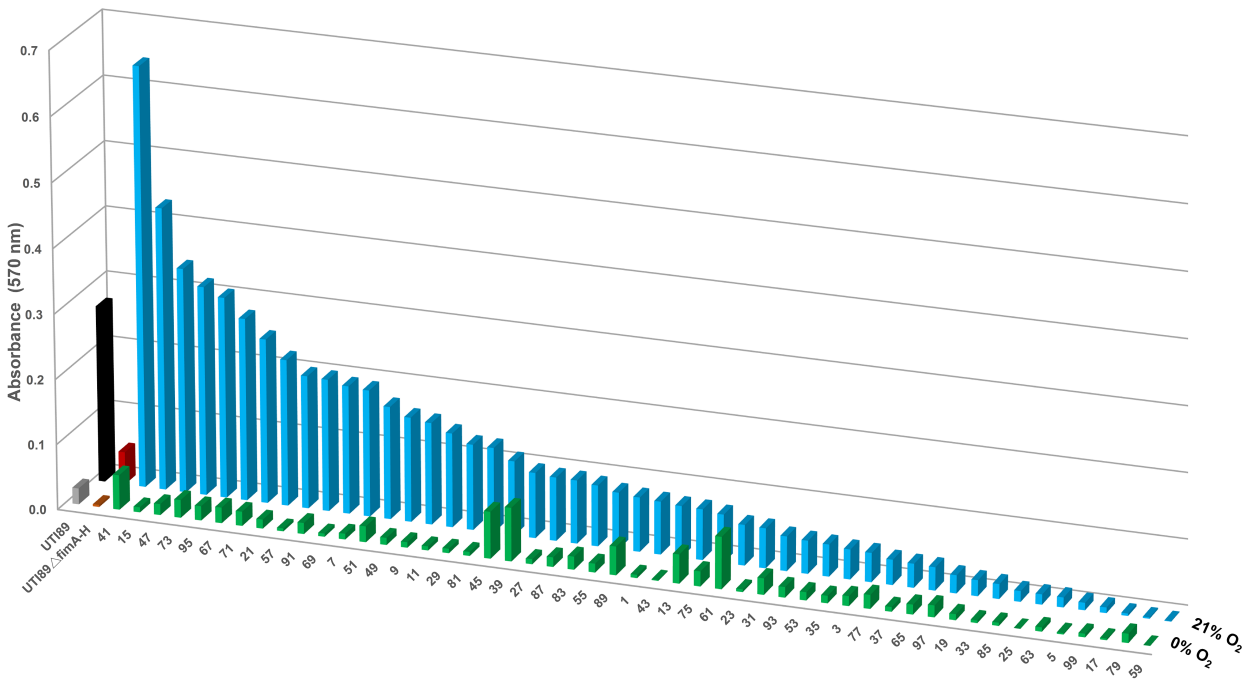

Figure 13. Most urine-associated *E. coli* clinical isolates tested exhibit decreased biofilm formation under anoxic conditions. Graph depicts the quantified biomass for 50 *E. coli* clinical strains isolated from the urine of patients at VUMC. Biofilms were grown at ambient oxygen (blue bars) or in the complete absence of oxygen (green bars). UTI89 (black bars) and the isogenic UTI89Δ*fimA-H* mutant (red bars) were used as controls. All isolates exhibited significantly-reduced biofilm compared to their own growth under ambient oxygen conditions, except isolates VUTI39 and VUTI61 (green bars). The average of a minimum of two independent experiments is shown, with a minimum of eight technical replicates per experiment. The standard error of the mean for each VUTI isolate is shown in **Table 1**. *Figure from Eberly et. al. Int. J. Mol. Sci. 2017.*

Isolate	Absorbance (570nm)	SEM	Absorbance (570nm)	SEM
UTI89	0.2701	0.00552	0.02453	0.001282
UTI89Δ*fimA-H*	0.0495	0.009396	0.00319	0.0002592
41	0.6450	0.0148	0.0531	0.001221
15	0.4328	0.012	0.0079	0.002335
47	0.3440	0.01738	0.0169	0.0002466
73	0.3201	0.04663	0.0273	0.001568
95	0.3076	0.01034	0.0219	0.0006946
67	0.2792	0.01418	0.0240	0.00157
71	0.2517	0.009984	0.0219	0.0008916
21	0.2241	0.02204	0.0138	0.002798
57	0.2033	0.01022	0.0045	0.0001542
91	0.2020	0.01758	0.0170	0.000289
69	0.1960	0.01282	0.0050	0.00081
7	0.1936	0.005538	0.0089	0.001046
51	0.1724	0.004367	0.0243	0.0007479
49	0.1601	0.01033	0.0109	0.0006613
9	0.1559	0.005457	0.0085	0.0006204
11	0.1439	0.01062	0.0063	0.001054
29	0.1309	0.01029	0.0069	0.0009281
81	0.1300	0.02071	0.0061	0.0003683
45	0.1136	0.002577	0.0718	0.0018
39	0.1000	0.006192	0.0819	0.006554
27	0.0971	0.002637	0.0078	0.00086
87	0.0968	0.01159	0.0147	0.0006153
83	0.0931	0.01722	0.0201	0.0002811
55	0.0864	0.007154	0.0136	0.0005828
89	0.0831	0.0167	0.0439	0.003411
1	0.0809	0.01481	0.0050	0.001282
43	0.0784	0.01003	0.0015	0.000119
13	0.0775	0.003347	0.0445	0.005697
75	0.0737	0.01636	0.0231	0.001676
61	0.0621	0.0106	0.0797	0.004079
23	0.0611	0.004755	0.0042	0.001644
31	0.0529	0.004267	0.0252	0.002312
93	0.0506	0.003049	0.0162	0.000741
53	0.0491	0.003226	0.0126	0.0007044
35	0.0457	0.003509	0.0114	0.00153
3	0.0447	0.007167	0.0152	0.0002592
77	0.0385	0.004075	0.0213	0.001182
37	0.0367	0.003119	0.0072	0.0005375
65	0.0356	0.006035	0.0152	0.0006716
97	0.0276	0.003931	0.0182	0.001619
19	0.0244	0.007798	0.0092	0.00109
33	0.0228	0.005141	0.0041	0.001327
85	0.0164	0.009211	0.0049	0.0004652
25	0.0157	0.004549	0.0000	0
63	0.0153	0.0009836	0.0065	0.0007633
5	0.0114	0.001413	0.0022	0.0003968
99	0.0086	0.001982	0.0055	0.0003715
17	0.0038	0.00164	0.0025	0.001025
79	0.0022	0.0004589	0.0141	0.0005627
59	0.0008	0.0003623	0.0003	0.0001268

Table 1. VUTI crystal violet biofilm formation average absorbance. Table lists the average of the absorbance at 570 nm for each of the 50 isolates screened for biofilm formation at 21% oxygen and 0% oxygen along with the standard error of the mean (SEM). *Table from Eberly et. al. Int. J. Mol. Sci. 2017.*

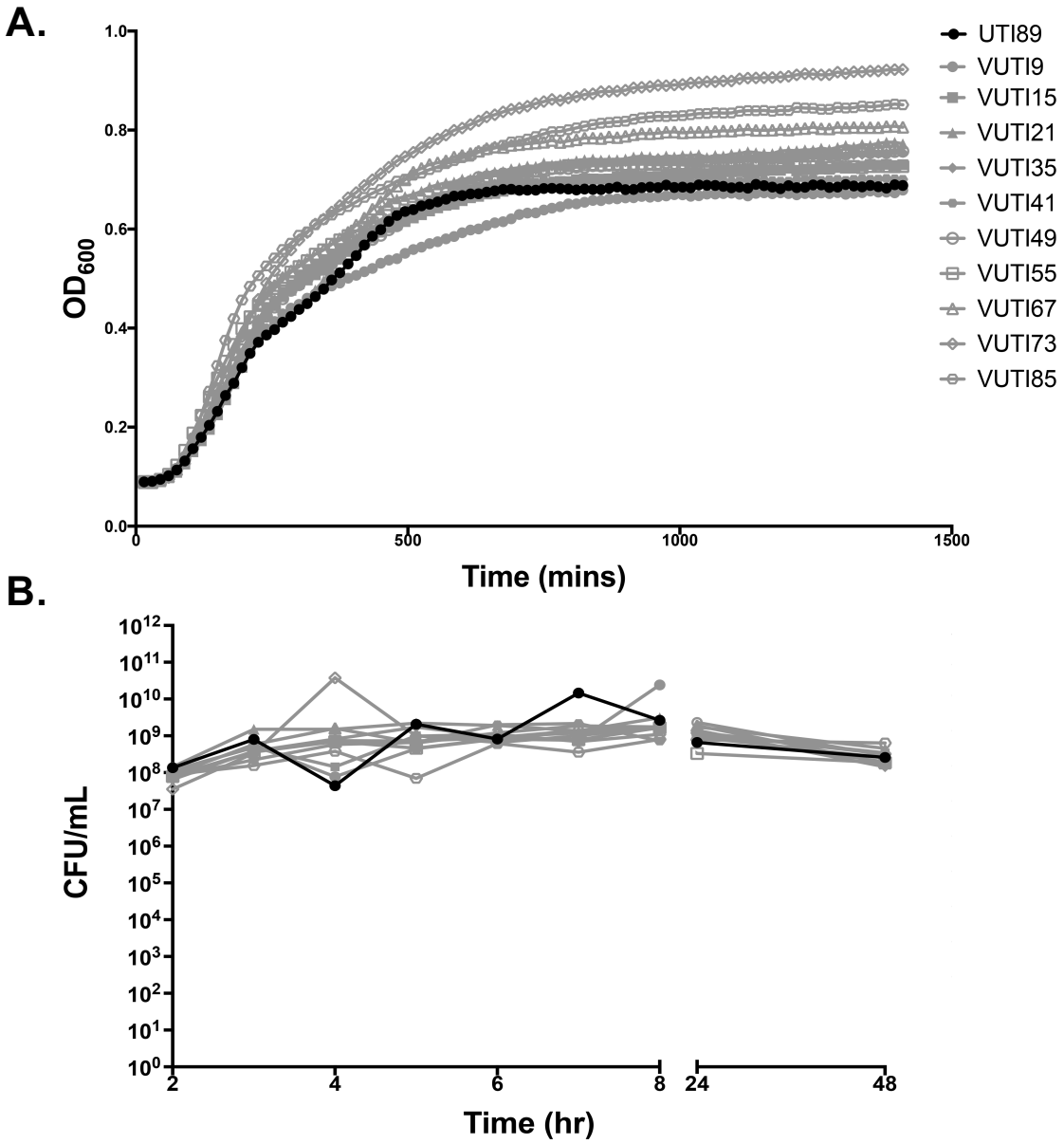

Figure 14. VUTI isolates do not exhibit gross growth differences. A. Growth curves measuring the optical density at 600 nm over time as described in **Figure 12C**. These data are representative of one independent experiment, with at least 8 technical replicates per isolate. **B.** Colony forming units (CFU) show that the bacteria are viable throughout the duration of biofilm assays performed. Assay was performed one time as described in **Figure 12B**. *Figure from Eberly et. al. Int. J. Mol. Sci. 2017.*

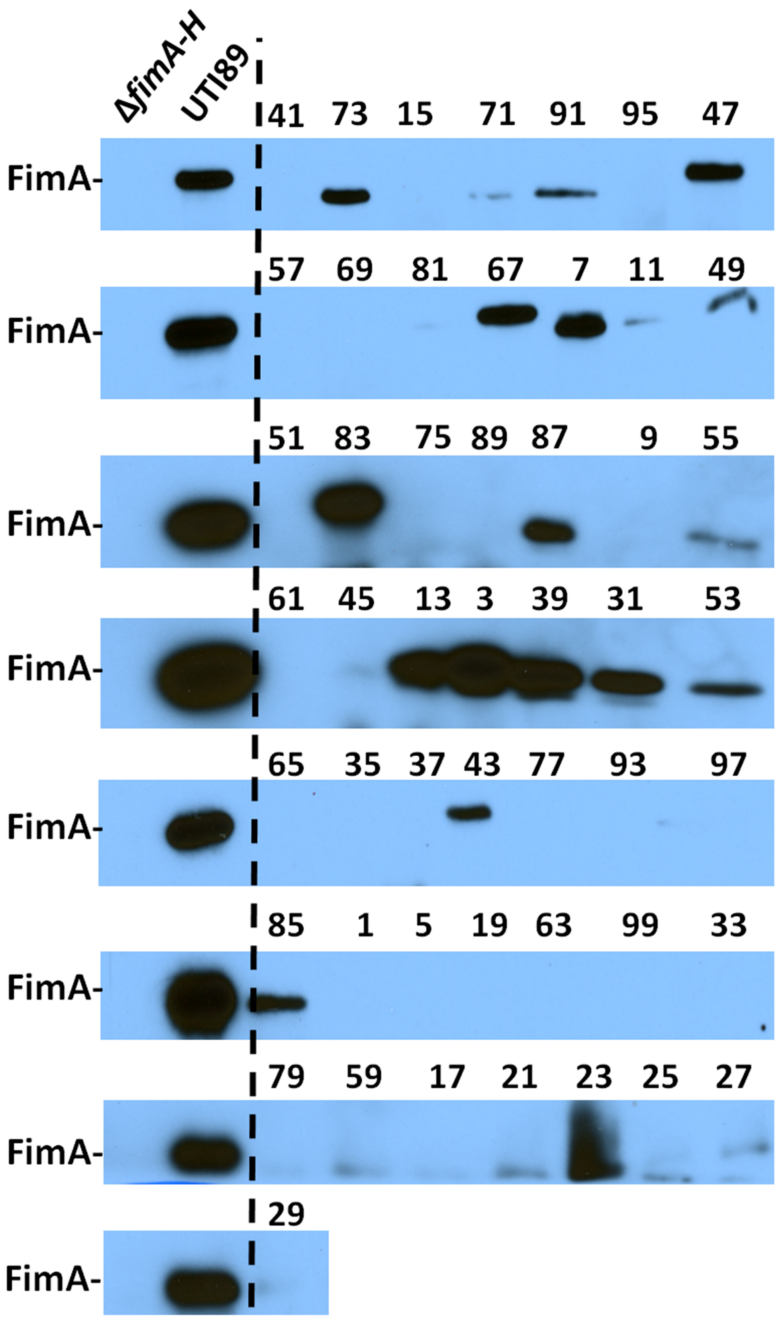

Figure 15. FimA expression is variable among VUTI isolates. Immunoblot depicts the abundance of FimA pilin subunit in the 50 VUTI strains. Cultures were grown statically overnight under atmospheric conditions. The antibody used to probe for FimA production was raised against the FimA antigen of cystitis strain UTI89 (224), which is used here as a positive control. The size of UTI89 FimA is roughly 18.5 kiloDaltons (kDa). An isogenic strain deleted for the entire *fim* operon (Δ*fimA-H*) is used as a negative control. This immunoblot indicates that 27/50 isolates express a FimA isoform or a pilin subunit recognized by the anti-FimA antibody used. The immunoblot shown is representative of a minimum of two biological replicates. *Figure from Eberly et. al. Int. J. Mol. Sci. 2017.*

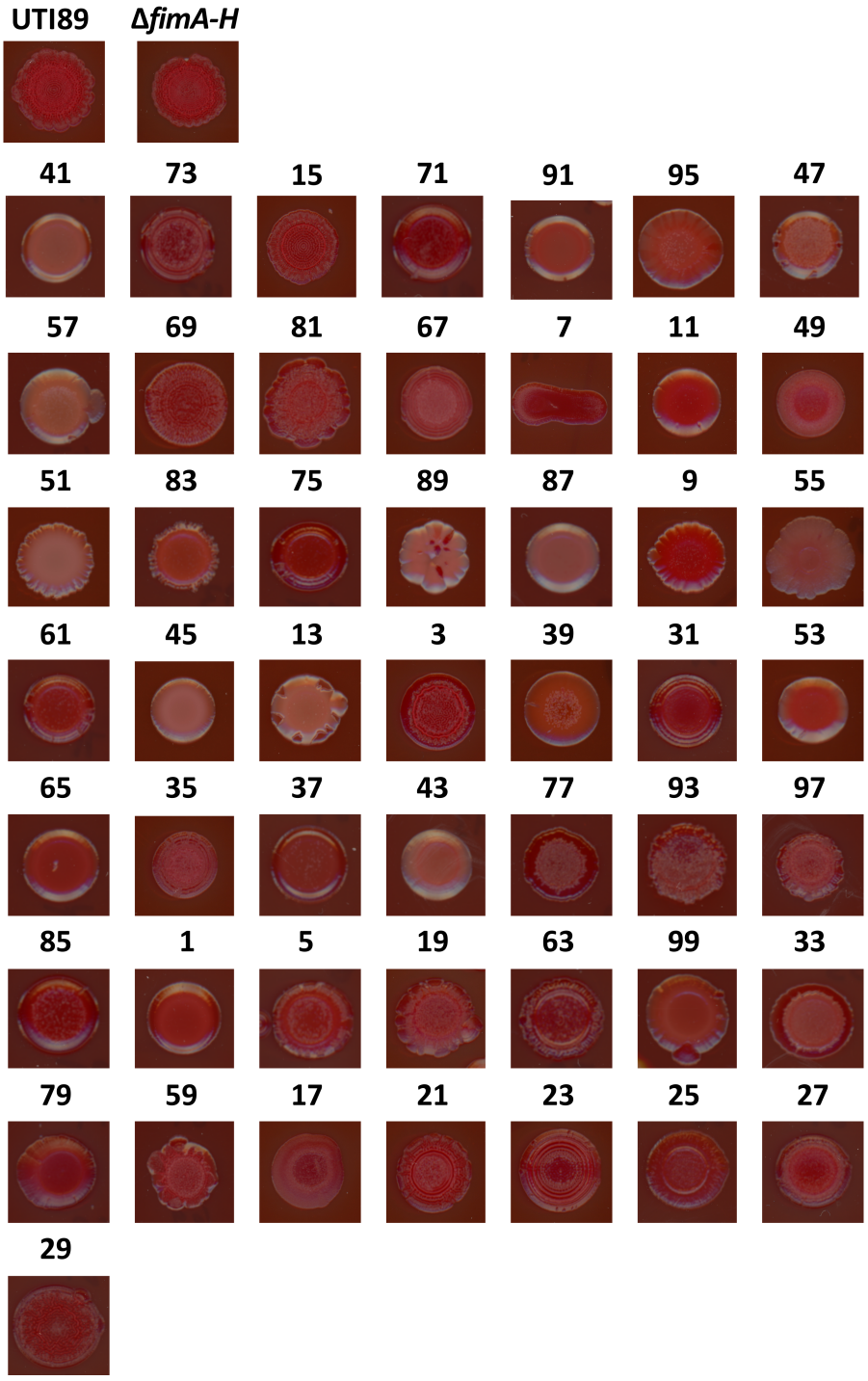

Figure 16. Inter-strain heterogeneity in matrix components among VUTI strains. VUTIs were spotted on YESCA–Congo Red agar and grown at room temperature for seven days. Congo Red uptake serves as a proxy to cellulose and curli presence in the ECM and also allows for better visualization of colony architecture. Representative images of two independent experiments are shown here. *Figure from Eberly et. al. Int. J. Mol. Sci. 2017.*

urine-associated E. coli *isolates exhibited reduced biofilm levels under anoxic conditions* (**Figure 13**).

Biofilm formation in UPEC is not restored in the presence of ATEAs

E. coli can use different (i.e. alternative) terminal electron acceptors when oxygen is unavailable (**Figure 11**). Depending on a person's diet, urine can be rich in TMAO (225) and nitrate (226). Moreover, high levels of nitrite are suggestive of a UTI, as members of the Enterobacteriaceae family will reduce nitrate to nitrite (226). DMSO has been used for the intravesical treatment of cystitis (227, 228). It is therefore possible that biofilm formation may be restored under anaerobic conditions provided an ATEA is present. Our previous work has demonstrated that the addition of nitrate partially restored type 1 pili expression under anaerobic conditions (213). We therefore tested biofilm formation under anaerobic conditions but in the presence of 40 mM of an ATEA (**Figure 17**). Under these conditions, cystitis strain UTI89 did not form appreciable biofilm (**Figure 17A**). The presence of an ATEA also failed to restore biofilm formation in ten randomly selected urine-associated *E. coli* isolates (**Figure 17B-C**), indicating that our observations were not strain-specific.

Oxygen concentrations that mimic the bladder support robust biofilm formation

Given that the urinary oxygen tension varies in the different genitourinary niches— from 4-5.5% in the bladder (218) to a range of 0%-8% in the gastrointestinal tract (217)— we asked how such variable oxygen concentrations influence biofilm formation. These experiments revealed that biofilm formation decreased in a step-wise

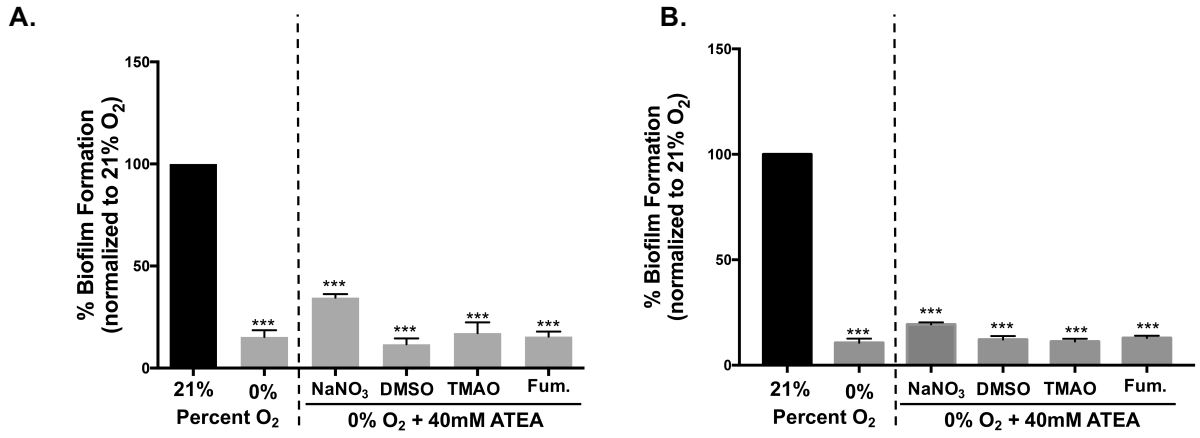

C.

Strains	21% oxygen	0% oxygen	Nitrate	DMSO	TMAO	Fumarate
UTI89	100	15.27	**34.41**	11.56	17.15	15.44
9	100	5.21	8.55	5.02	8.61	**9.61**
15	100	6.86	**11.81**	4.03	6.96	6.74
21	100	9.11	7.45	4.93	**14.31**	6.16
35	100	20.40	**33.98**	26.01	26.10	30.45
41	100	6.26	12.82	7.26	**15.06**	13.63
49	100	10.63	**19.32**	12.19	11.26	12.96
55	100	12.67	16.81	11.02	18.62	**32.00**
67	100	12.87	**20.01**	9.15	18.29	13.45
73	100	23.10	**31.08**	22.68	23.60	24.22
85	100	12.11	**31.17**	15.56	19.33	25.65

Figure 17. Alternative terminal electron acceptors do not restore biofilm formation. A. Graph showing percent biofilm formation by UTI89 in different ATEAs. UTI89 biofilm formation at 21% oxygen is artificially set to 100%, while the absorbance of the biofilm formed at 0% oxygen as well as at 0% oxygen with other terminal electron acceptors (40 mM) is averaged and then divided by the 21% oxygen average to calculate the percentage. Error bars represent the standard error of the mean (SEM) compared to UTI89 grown under 21% oxygen. *** p <0.001. **B.** Clinical isolate VUTI49 was tested under 21% oxygen and 0% oxygen with 40 mM of each alternative terminal electron acceptor. Percentages were calculated as in panel A and SEM is calculated compared to VUTI49 grown at 21% oxygen. *** p <0.001. **C.** Table including the percentages of biofilm formed by UTI89 and 10 randomly selected urine-associated *E. coli* from the panel tested in **Figure 11**. The highest percent biofilm formed by each strain is bolded to show the ATEA that had most effect on biofilm. The percentages were calculated as described above. Experiments were performed a minimum of three independent times. *Figure from Eberly et. al. Int. J. Mol. Sci. 2017.*

fashion from 21% to 10% oxygen (**Figure 18**). However, biofilm levels fluctuated as oxygen decreased from 8% to 2% oxygen, with biofilm levels at 4% oxygen reaching those obtained during growth under atmospheric oxygen conditions (**Figure 18**).

2.4 Discussion

In this investigation, we have demonstrated that oxygen is the terminal electron acceptor that supports the most robust biofilm production by UPEC. Though biofilm production under ambient oxygen conditions varied among isolates (**Figure 13**), the decrease in biofilm abundance in the absence of oxygen was consistent in 96% of all urine-associated *E. coli* tested, suggesting that the requirement for oxygen is a broad phenomenon. These results are aligned with previous studies that showed aerobic respiration is required for infection in the bladder (209). Specifically, deletion of *ubiI*— a gene that codes for an aerobic ubiquinone synthase that is dispensable for anaerobic respiration but needed in aerobic conditions— abolished IBC formation in the murine bladder (**Figure 7A** and (209)). The *ubiI* mutant was also more effectively cleared from the host by four weeks of infection compared to the wild-type (**Figure 7B** and (209)). It is thus evident that although *E. coli* is a facultative anaerobe that can and does utilize nitrate and other ATEAs during infection, it relies on aerobic respiration for infection establishment and robust biofilm expansion.

Notably, under ambient oxygen concentrations, a wide variability in biofilm production was exhibited by urine-associated *E. coli* strains (**Figure 13**). This exemplifies the extensive inter-strain variability that characterizes *E. coli*, especially in the extra-intestinal pathogenic strains (229). Colorimetric assays, such as the crystal

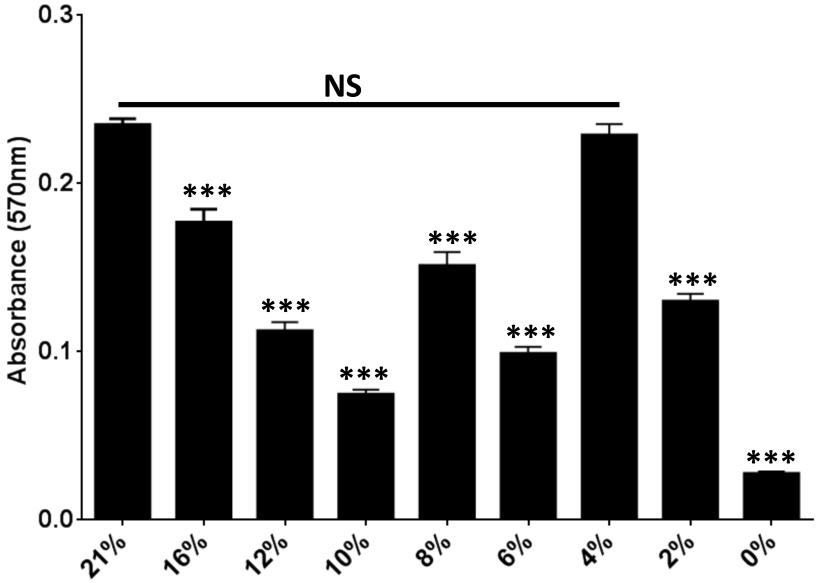

Figure 18. UTI89 biofilm formation is affected by oxygen concentration changes. Graph depicting the relative abundance of biofilm formed by UTI89 during growth in decreasing oxygen concentrations. This graph depicts the average of a minimum of three biological replicates per condition tested. Statistical analysis was performed using two-tailed Mann-Whitney method, comparing values for each condition to the values of biofilm formed under atmospheric (21%) oxygen. *** $p < 0.0001$, NS not significant. *Figure from Eberly et. al. Int. J. Mol. Sci. 2017.*

violet biofilm abundance and the CR uptake used in these studies, serve as indicators of biofilm production (187). Biofilm production can vary as a function of bacterial numbers within the biofilm colony, as well as the amount and type of ECM produced by a given strain. For example, the high biofilm levels of strain VUTI41 could be due to higher numbers of bacterial cells within the biofilm or due to higher levels of ECM produced by that particular strain. The diversity in CR uptake and in colony architecture suggests that ECM production, abundance, and/or kinetics vary across diverse strains.

Adherence is arguably the most critical step in for biofilm formation by *E. coli*. Similarly, adherence to a surface can vary as a function of the expression, abundance and the type of adhesive fibers expressed by each *E. coli* strain. We have previously reported that type 1 pili expression is decreased during UPEC growth in the absence of oxygen and that type 1 pili are localized to the air-exposed region of biofilms formed by strain UTI89 in ambient oxygen conditions (213). Though the majority of *E. coli* strains harbor the genes encoding type 1 pili, only 27 out of 50 isolates produced FimA under the growth conditions tested (**Figure 15**). Furthermore, there is variation in the FimA-reactive bands in the immunoblots, indicative of the presence of different FimA isoforms, as in the case of UPEC strain CFT073 FimA (**Figure 19** and (44, 230)). It is, however, also possible that the FimA antibody cross-reacts with a pilus subunit from another chaperone-usher pathway system. Most notably, there was no correlation between type 1 pili expression and biofilm abundance, as exemplified by VUTI41, which formed the most biofilm of the isolates screened but did not produce type 1 pili (**Figures 13** and **15**). This strongly suggests that type 1 pili are only partially responsible for the loss of biofilm production in the absence of oxygen. Previous studies have established

that the regulation of adhesive fibers is inter-connected (210, 231). It is possible that the urine-associated *E. coli* strains that do not express type 1 pili possess other functional adhesins on their cell surfaces that allow adherence. In addition to the variability in type 1 pili production, diverse heterogeneity was observed in colony morphology and CR uptake properties of the VUTIs (**Figure 16**). In summary, we have confirmed that oxygen supports robust biofilm formation by UPEC and that ATEAs do not restore biofilm under anaerobic conditions.

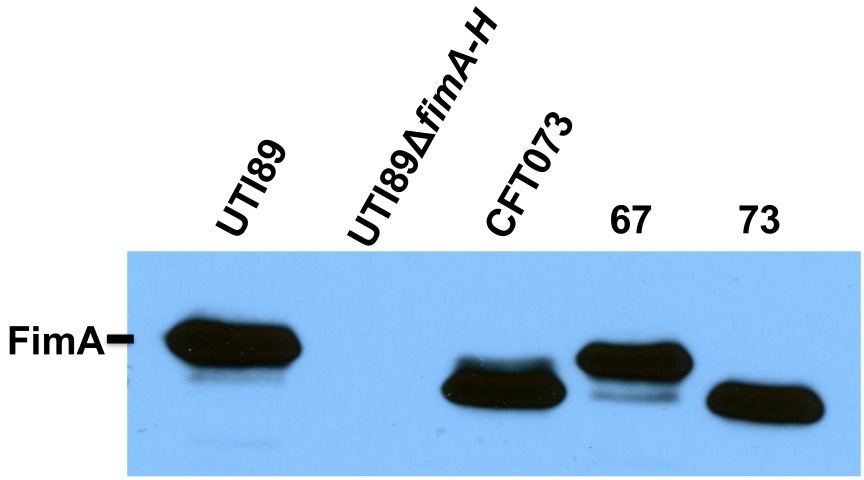

Figure 19. Isolates VUTI67 and VUTI73 express FimA as robustly as UTI89 and CFT073. FimA immunoblots were performed using normalized cultures that were grown statically overnight and used to seed biofilm assays. *Figure from Eberly et. al. Int. J. Mol. Sci. 2017.*

CHAPTER III

A ROLE FOR CYTOCHROME BD IN ACUTE URINARY TRACT INFECTION AND BIOFILM FORMATION

Portions of this chapter have been adapted from: Beebout, **Eberly** *et al.* "Respiratory heterogeneity shapes biofilm formation and host colonization in uropathogenic *Escherichia coli*." *mBio*. 2019; 10: e02400-18.

3.1 Introduction

The studies described in **Chapter II** uncovered that even though *E. coli* are facultative anaerobes, uropathogenic isolates exhibit enhanced biofilm formation under aerobic conditions (**Chapter II** and (232)). These observations are in agreement with our previous work that demonstrated the need for aerobic respiration during infection (209). To identify the factors and mechanisms regulating biofilm formation under different oxygen conditions, I followed two approaches. First, I developed a new tool that can be applied not only towards the identification of oxygen-regulated factors, but also has utility for diverse screening analyses. Specifically, I constructed a saturated transposon library (6x coverage) in the well characterized cystitis isolate UTI89. Partial screening of this library allowed the identification of 57 mutants that will be pursued outside the scope of this dissertation (outlined in **Appendix A**). Second, in parallel to the transposon library construction, I followed a directed mutagenesis approach to delineate the role of the three terminal oxidases of UPEC in biofilm formation and pathogenesis.

E. coli has three different cytochrome oxidases that are utilized under different oxygen conditions. In the presence of oxygen, aerobic respiration is always preferred, but different oxygen concentrations induce the expression of respiration oxidase

enzymes to mediate nicotinamide adenine dinucleotide (NADH) oxidation (214-216). Under high oxygen concentrations, NADH dehydrogenase transfers electrons to cytochrome *bo* oxidase (**Figure 20A**), creating a proton motive flux across the inner membrane. The proton gradient outside the membrane then flows through the ATP synthase pump that uses the kinetic energy of the hydrogen ions to create ATP from adenosine diphosphate (ADP) and phosphate (P_i) (215, 216, 233). When oxygen levels drop between 2-15%, cytochromes *bd* and *bd*$_2$ appear to take over as the principal cytochrome oxidases (**Figure 20B** and (234)). Intriguingly, the functions of the cytochrome *bd* oxidases have only been studied in non-pathogenic K12 strains of *E. coli* and are reported to be functionally redundant. Here, I examine the role of each of the terminal oxidases on biofilm formation and infection. Based on the fact that urinary oxygen concentration ranges from 4-6%, oxygen, I hypothesized that the high-affinity cytochrome oxidases are important for UPEC infection and biofilm formation.

3.2 Methods

Bacterial Strains

All studies were performed in *E. coli* cystitis isolate UTI89 (220). Isogenic deletion mutants UTI89Δ*cyoAB*, UTI89Δ*appBC*, and UTI89Δ*cydAB* were created using the λ-red recombinase mediated method of Murphy & Campellone (235). Complementation constructs were created in plasmid pTRC99a with *cydABX* under the control of its native promoter using primers shown in Table 2 and indicated restriction sites (XbaI and SacI, **Table 2**). as previously described (236). Primers used for gene deletions and complementation plasmid construction are listed in **Table 2**.

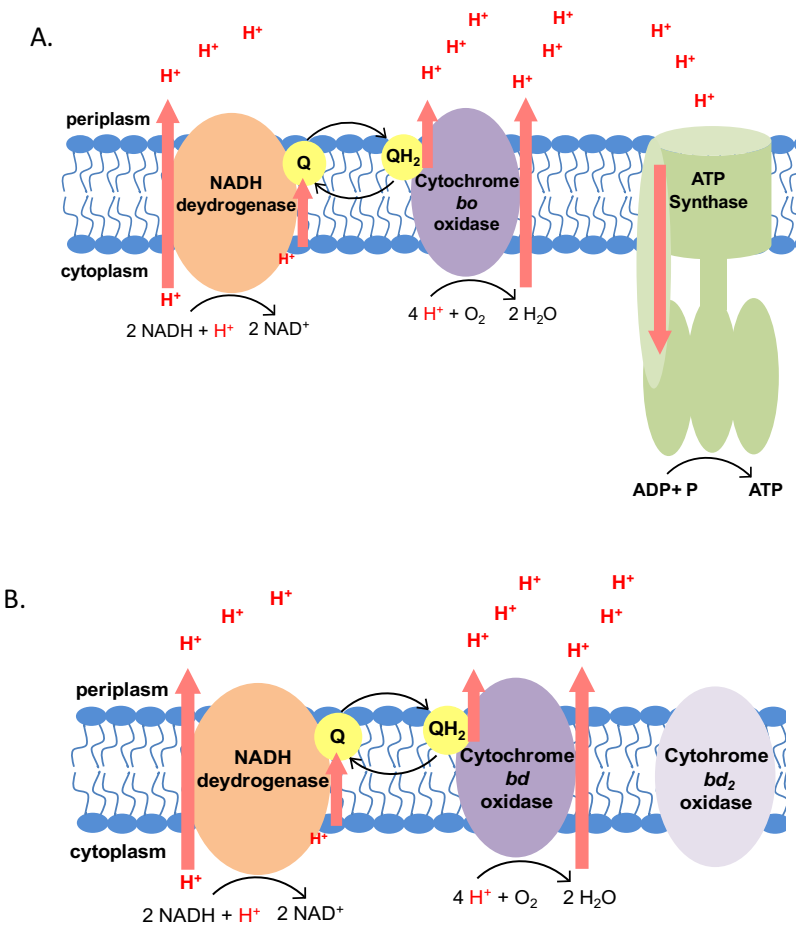

Figure 20. Three cytochrome oxidases are implicated in aerobic respiration in *E. coli*. A. In the case of aerobic respiration when oxygen is abundant, the electron transport chain, located in the inner membrane, consists of an NADH dehydrogenase that donates electrons to the cytochrome *bo* oxidase. The transfer of electrons between the enzymes is mediated by ubiquinones (Q, QH_2). The reduction of oxygen to water by the cytochrome *bo* oxidase creates a proton motive force across the membrane, and these protons are used to drive ATP synthase to produce ATP. **A.** In addition to cytochrome *bo* oxidase, E. *coli* encodes cytochrome *bd* and *bd*$_2$. Cytochrome *bd*$_2$ appears to be functionally redundant in K12 strains, but a role for cytochrome *bd*$_2$ in UPEC is unknown. When oxygen levels are low (2-15%), these cytochromes are expressed. Electrons are transferred from the dehydrogenase to the oxidase and generates a hydrogen ion (H^+) gradient across the membrane, similar to the cytochrome *bo*, but cannot pump protons through ATP synthase.

Primer/Probe	Sequence (5' → 3')	Purpose
cydA_KO_Fwd	ATGATGTTAGATATAGTCGAACTGTCGCGCTTACAGTTTGCCTTGACCGCGATGTACGTGTAGGCTGGAGCTGCTTC	cydAB knockout
cydB_KO_Rev	GTTACGTTCAATATCTTCTTTGGTGATACGACCGAACATTTTCCAGTCATATGAATATCCTCCTTAG	cydAB knockout
cydA_KO_Test_Fwd	GATCAAATTGGTGAGATCGTGAC	cydAB knockout
cydB_KO_Test_Rev	CTAACAGAAGTGCCATCACG	cydAB knockout
cydA1_Fwd_XbaI	CTGCAGTCTAGACTGGTCAAGTTATCCATCATTCACT	cydABX complementation
cydX_Rev_SacI	CGTATTGAGCTC/TTGCGATAATCTTACTCATCAGATGTC	cydABX complementation
appC_KO_Fwd	ATGTGGGATGTCATTGATTTATCGCGCTGGCAGTTTGCTCTGACCGCGGTGTAGGCTGGAGCTGCTTC	appBC knockout
appB_KO_Rev	TTAGTACAGCTCGTTTTCGTTACGGCGGAGAGTTTCTGTCGTCATGCCATATGAATATCCTCCTTAG	appBC knockout
appC_KO_Test_Fwd	ACGCAGACGTCACGGCG	appBC knockout
appB_KO_Test_Rev	TGCACAGTCAGGTGCCAGC	appBC knockout
cyoB_KO_Fwd	TCAGTTGCCATTTTTCAGCCCTGCCTTAGTAATCTCATCGGTGTAGGCTGGAGCTGCTTC	cyoAB knockout
cyoA_KO_Rev	GTCATTATTTGCAGGCACTGTATTGCTCAGTGGCTGTAATTCTGCGCTGCATATGAATATCCTCCTTAG	cyoAB knockout
cyoB_KO_Test_Fwd	CATCCAGATAAGACCGGAAGTG	cyoAB knockout
cyoA_KO_Test_Rev	GCAACATATGTGACCTGATAGC	cyoAB knockout

Table 2. Primers and probes used in Chapter III. *Table adapted from Beebout, Eberly, et al. mBio. 2019.*

Biofilm assays

All strains were grown overnight in LB (Fisher) pH 7.4 at 37°C with shaking unless otherwise specified. Colony biofilms were seeded using 10 µL of overnight culture that was spotted onto 1.2x YESCA agar (recipe in **Appendix A**) and allowed to grow at room temperature for a period of 72 hours to 11 days. The diameter of colony biofilms was measured and recorded over time.

Biofilm abundance (which comprises CFUs and the self-secreted matrix) was quantified using the crystal violet method of O'Toole (237). In brief, overnight cultures were diluted to OD_{600} = 0.05 and a volume of 100 µL was transferred to a 96 well PVC plate. After 48 hours, biofilms were rinsed in sterile water, stained with 0.5% crystal violet, and disaggregated with 35% acetic acid. When used, antibiotics were added to biofilm wells at 48 hours, followed by an additional 72-hour incubation before rinsing and staining. Absorbance of the disaggregated biofilm was measured at 570 nm using a SpectraMax i3 plate reader (Molecular Devices).

For air-liquid interface biofilms, overnight cultures were first diluted to OD_{600} = 0.05 in 12-well plates. Polyvinyl chloride (PVC) coverslips were placed in the diluted culture onto which bacteria adhered and expanded for grow 48 hours at room temperature. After 48 hours, the coverslips were washed with PBS, fixed in 4% paraformaldehyde (PFA), and stained using SYTO 9 (ThermoFisher) for subsequent confocal laser scanning microscopy (CLSM) analysis. When used, antibiotics were added to biofilm wells at 48 hours, followed by an additional 72-hour incubation before fixation and staining. Images were taken using a Zeiss 710 confocal laser scanning microscope. To obtain a representative sample of the biofilms, at least three Z stacks

were taken along the air-liquid interface from at least five biological replicates. Biofilms were analyzed using Comstat2 plugin for ImageJ (238-240). Surface reconstructions were created from Z stack data using the Interactive 3D Surface Plot plugin for ImageJ.

Murine infections

Murine infections were performed as described previously (241). In brief, UTI89 and each mutant strain were inoculated individually into 5 mL LB medium and grown shaking at 37˚C for 4 hours. This culture was diluted 1:1000 into 10 mL fresh media and grown statically at 37˚C for 24 hours. After 24 hours, this culture was diluted 1:1000 into 10 mL fresh media and grown for another 24 hours at 37˚C statically. Each 7-8 week-old C3H/HeN female mice was transurethrally inoculated with 50 µL phosphate-buffered saline (PBS) containing 10^7 CFU bacteria. Mice were sacrificed at 24 hours post infection, at which time bladders were removed and homogenized for CFU enumeration. All animal studies were approved by the Vanderbilt University Medical Center Institutional Animal Care and Use Committee (IACUC) (protocol number M/12/191) and carried out in accordance with all recommendations in the Guide for the Care and Use of Laboratory Animals of the National Institutes of Health and the IACUC.

Statistical analysis

All statistical analyses were performed in GraphPad Prism using the most appropriate test. Details of test used, error bars, and statistical significance cutoffs are presented in figure legends.

3.3 Results

Cytochrome bd deletion impairs bladder colonization by UPEC

We previously reported that aerobic respiration is critical for UPEC infection (209). Given that the bladder environment is hypoxic, we hypothesized that cytochrome *bd* and bd_2 play a role in bladder colonization and biofilm formation. To test this hypothesis, we created isogenic deletion mutants lacking one of the following terminal oxidases: cytochrome *bo* (*cyoAB*), cytochrome *bd* (*cydAB*), or cytochrome bd_2 (*appBC*). We first compared planktonic growth to record any growth defects (**Figure 21A**). These analyses indicated a 2-hour lag in growth for the *cydAB* mutant, which however, did not manifest in significant changes in CFUs. We then tested the fitness of the three quinol oxidase mutants in the bladder. To account for the early growth lag and following well-established protocols of infection, normalized inocula of 10^7 bacteria in 50 µL of PBS were used to inoculate female 7-8 week old C3H/HeN mice, bladder colonization was assessed at 24 hours post infection. While deletion of cytochrome *bo* (*cyoAB*) and cytochrome bd_2 (*appBC*) did not alter colonization, the *cydAB* deletion mutant had a 2-log reduction in CFUs recovered from the bladder (**Figure 21B**).

Deletion of cytochrome bd imparts architectural defects to biofilms

Given the significance of oxygen to biofilm formation and the observed defect of the *cydAB* mutant in murine colonization, I tested the hypothesis that cytochrome *bd* is critical for biofilm expansion. Three biofilm parameters were tested: 1) optical density at 570 nm that measures CFUs and ECM combined using the colorimetric method of O'Toole (**Figure 22A** and (187)); 2) infrastructure characteristics using microscopy and

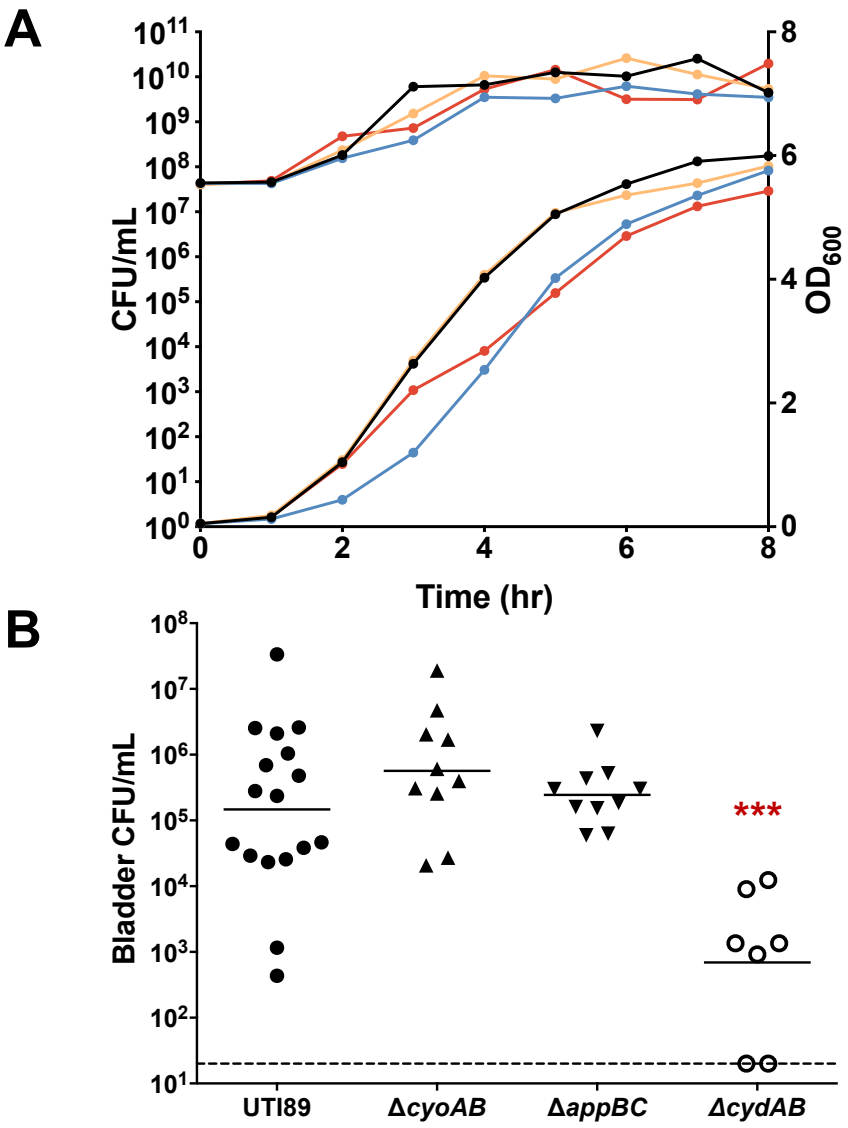

Figure 21. Cytochrome *bd* is important for UPEC fitness in the bladder. A. Graph shows growth by optical density and CFU over time. The optical density was measured at 600 nm at each hour over 8 hours. These data are representative of at least three independent experiments, with at least 5 technical replicates per experiment. Growth by CFU show that though there is little difference in the number of cells in mutant strains compared to the parent. CFU enumeration was performed at least three independent times. **B.** Bladder titers were obtained from mice infected with UTI89 or quinol oxidase mutant strains at 24 hours post infection. Each point represents a mouse. UTI89 and Δ*cydAB* are representative of two independent experiments. Δ*cyoAB* and Δ*appBC* are representative of one experiment. Statistical analysis was performed in GraphPad Prism using a two-tailed Mann-Whitney test. Line represents geometric mean. *** p <0.001. *Figure adapted from Beebout, Eberly, et al. mBio. 2019.*

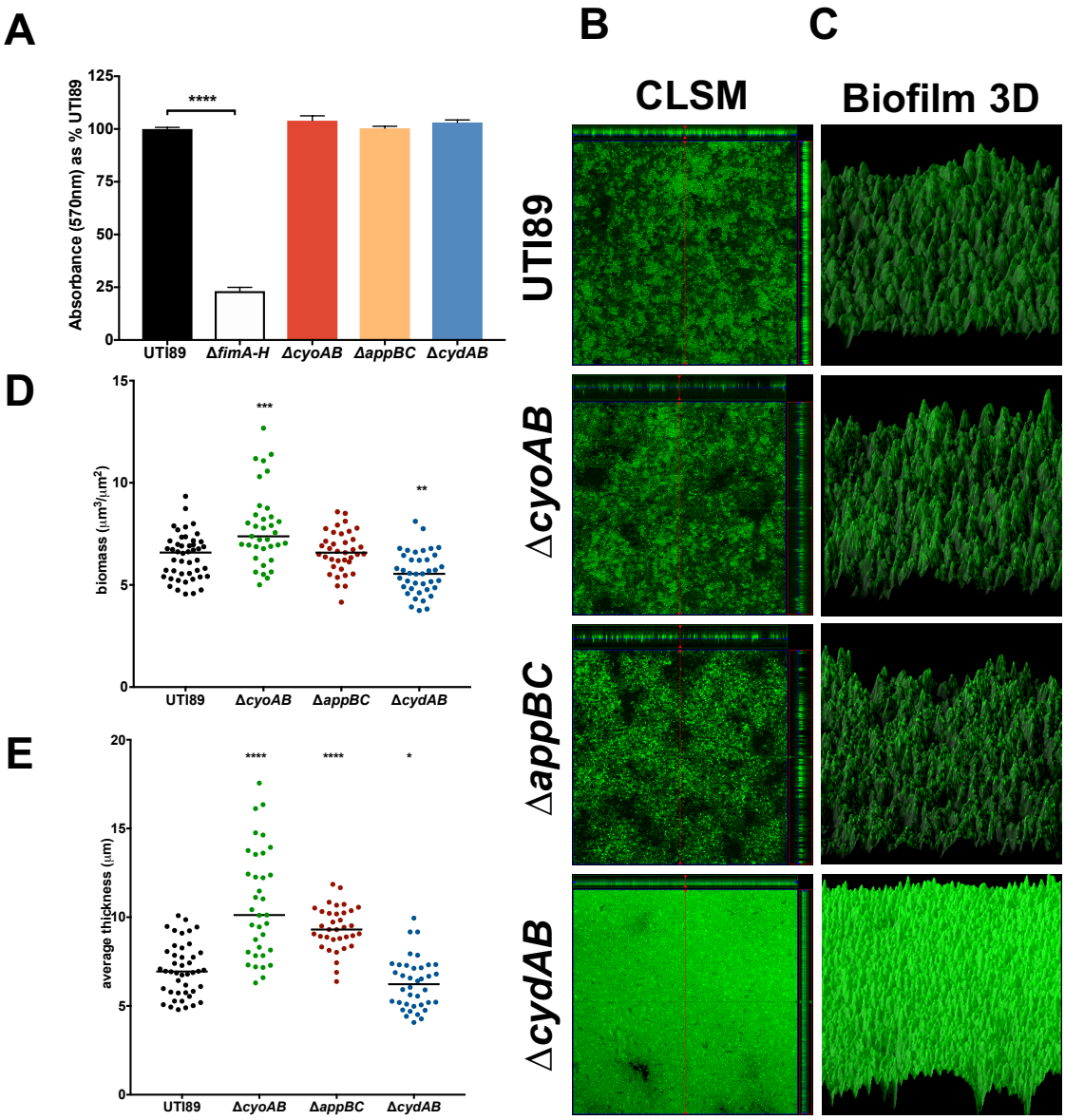

Figure 22. Cytochrome oxidases exhibit unique contributions to UPEC biofilm architecture. A. Air-liquid interface biofilms were grown for 48 hours on PVC material using the strains UTI89, Δ*fimA-H*, and each cytochrome deletion mutant. After 48 hours, biofilms were stained with crystal violet and absorbance at 570 nm was measured as a proxy of total biomass. Absorbance values are normalized as percentage of UTI89 absorbance on the same plate to account for variability between days. Data is representative of at least three biological replicates. Statistical analysis was performed in GraphPad Prism using Welch's t test. **** p< 0.0001. **B.** CLSM images of biofilms grown for 48 hours on PVC slides and stained with SYTO 9 nucleic acid stain. Images are representative of at least 5 biological replicates. **C.** Three-dimensional surface reconstruction of biofilms were created from Z-stack data shown in **B** using the Interactive 3D surface plot plugin on ImageJ. **D-E.** Biofilm volume per area (**D**) and average biofilm thickness (**E**) were quantified from Z-stack data using the Comstat2 plugin for ImageJ. Statistical analysis was performed in GraphPad Prism using the Mann-Whitney test. * p <0.05, ** p <0.01, *** p <0.001, **** p< 0.0001.

colony biofilms (**Figures 22B-E** and **23**); and 3) wet biomass and CFUs of colony biofilms (**Figure 24**). While the colorimetric method indicated no differences in biofilm formation (**Figure 22A**), visualization of biofilms using CLSM revealed changes in overall architecture (**Figure 22B**). Each mutant exhibited differences from the wild-type, which were quantified using ImageJ and COMSTAT2 software. The Δ*cyoAB* mutant displays taller, sharper peaks compared to the parent strain, while the Δ*appBC* displays spires that more closely resemble the parent strain. Both of these mutants have significantly increased thickness compared to wild-type UTI89 (**Figure 22C, E**). Most strikingly, the biofilm formed by Δ*cydAB* is the least complex, with the most pronounced decreases in thickness and biomass (**Figure 22 B-E**).

The architectural defects of the *cydAB* mutant were most apparent during colony biofilm formation (**Figure 23**). While wild-type UTI89 typically expands to an average diameter of 17 mm over an 11-day period and has rugose architecture with distinct central and peripheral regions (**Figure 23**), the Δ*cydAB* colonies have an average diameter of 10 mm and lack the rugosity of the parent strain (**Figure 23**). The Δ*cyoAB* colony biofilms (average diameter of 22 mm) display increased diameter with less rugosity, while quite oppositely, Δ*appBC* colony biofilms (average diameter 16 mm) are more compact with increased rugosity compared to the parent (**Figure 23**).

The development of the *cydAB* mutant colony biofilm appears to be stunted after 3 days of incubation compared to the wild-type and other cytochrome oxidase mutants (**Figure 23**). To assess if this was due to cell proliferation or ECM abundance, wet mass and CFUs of UTI89 and Δ*cydAB* were measured at days 3, 7, and 11 (**Figure 24**). By

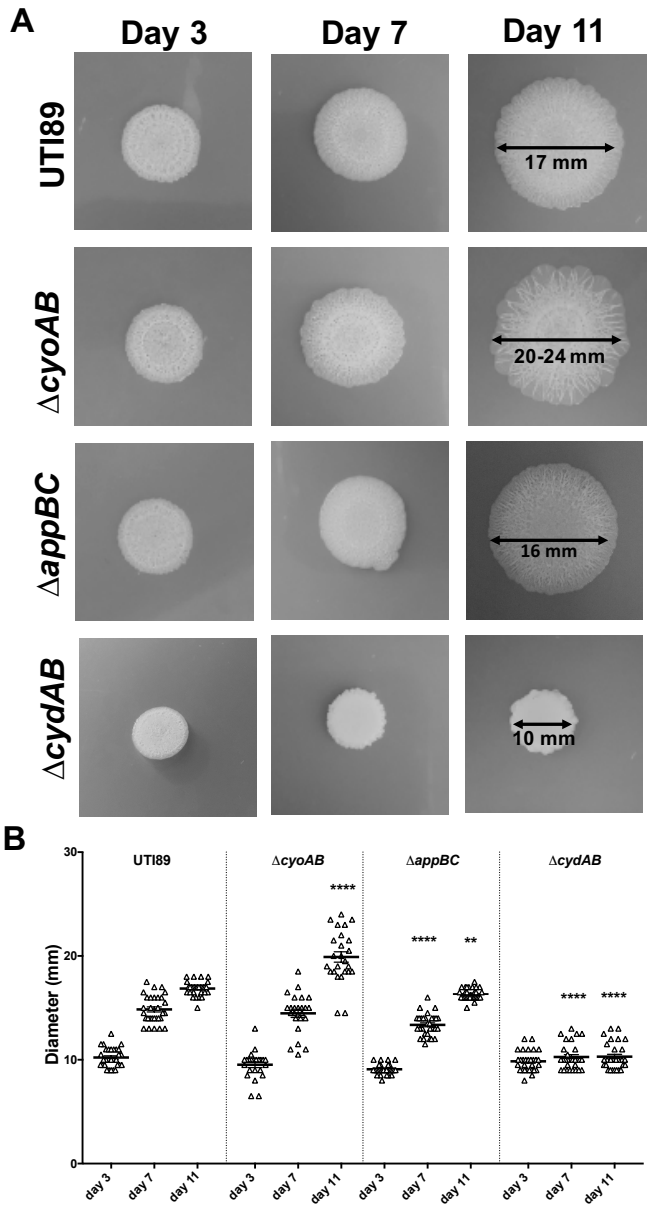

Figure 23. Colony biofilm development reveals macroscopic architectural differences between the parental strain and cytochrome mutants. A. Representative images of UTI89 and cytochrome oxidase mutant colony biofilms grown on YESCA agar taken on day 3, 7, and 11 of growth. **B.** Graph depicting colony biofilm diameter at days 3, 7, and 11 of growth. Each triangle represents an individual colony biofilm. Data is representative of at least 30 biological replicates and statistical analysis was performed in GraphPad Prism using Welch's t test. * $p < 0.05$, ** $p < 0.01$, *** $p < 0.001$, **** $p < 0.0001$. *Figure adapted from Beebout, Eberly, et al. mBio. 2019.*

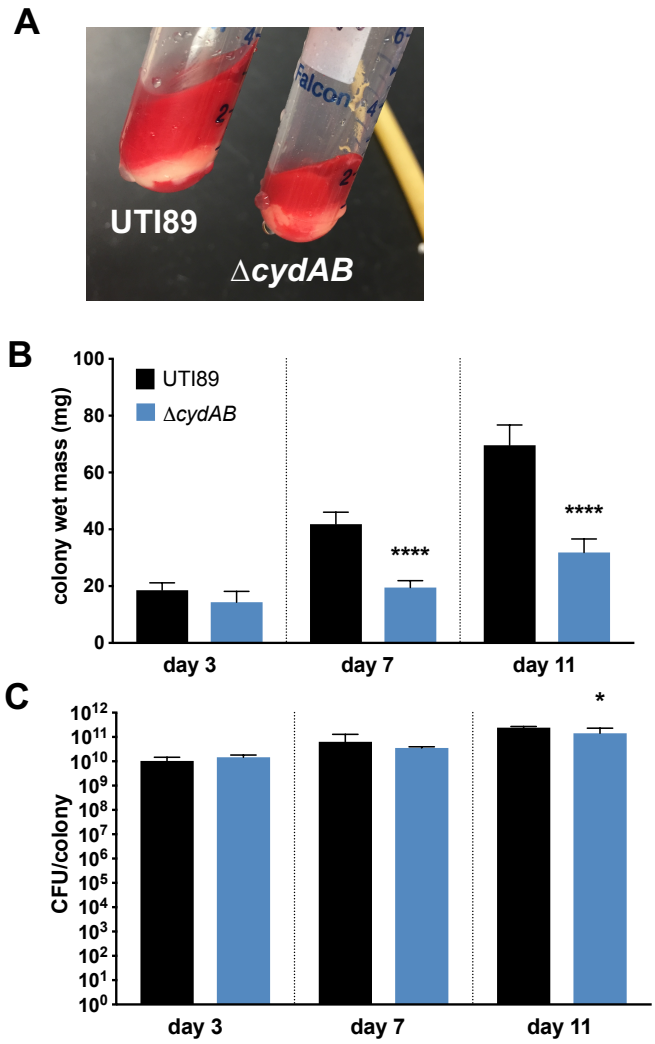

Figure 24. Cytochrome *bd* mutant colony biofilms exhibit a decrease in wet mass. **A.** Image depicting gross changes to extracellular matrix (ECM) abundance between UTI89 and Δ*cydAB* colony biofilms. ECM is stained red by the presence of CR in the growth medium. **B.** Graph depicting wet mass of individual colony biofilms at days 3, 7, and 11 of growth. Data is the average of five biological replicates per day. Data are presented as mean ± SD. **C.** CFU per colony biofilm was measured at days 3, 7, and 11 of growth. Data are presented as mean ± standard deviation. Data are representative of five biological replicates. All statistical analysis was performed in GraphPad Prism using a two-tailed unpaired t test. * p <0.05, ** p< 0.01, *** p <0.001, **** p <0.0001. *Figure adapted from Beebout, Eberly, et al. mBio. 2019.*

day 7, Δ*cydAB* presents a colony wet mass that is approximately 50% of the wild-type, even though the CFU per colony are comparable between the two strains. This indicates that there is a defect in ECM production or localization. A complementation construct of Δ*cydAB* with an extra-chromosomal copy of *cydABX* under its promoter rescues the mutant, restoring biofilm architecture to the wild-type phenotype (**Figure 25**). Combined, these data suggest that cytochrome *bd* is a key component required for proper biofilm development and architecture.

Altered biofilm architecture in the cytochrome bd mutant correlates with higher sensitivity to antibiotics treatment

The striking architectural changes in the Δ*cydAB* mutant are suggestive of altered ECM composition or localization. To test the Δ*cydAB* physical properties, a simple water droplet assay was used (242). The Δ*cydAB* colony biofilms were more permissive by aqueous solutions compared to the parent UTI89 and Δ*cyoAB* or Δ*appBC* mutants (**Figure 26A**). Higher penetrance by an aqueous solution indicates greater porosity or lower hydrophobicity in the ECM. To determine whether the Δ*cydAB* cells in the biofilm would be more accessible to antibiotics, biofilms were grown on PVC slides for 48 hours, treated with antibiotics commonly used to treat UTIs for a duration of 72 hours, washed and stained with SYTO9, and imaged by CLSM. Despite treating the biofilms with doses of antibiotics commonly used to treat urinary tract infections, antibiotic treatment had minimal effects on the structural characteristics of the UTI89 parent strain (**Figure 26B-C**). However, the Δ*cydAB* biofilms appeared significantly more vulnerable, with large regions devoid of bacteria readily visible (**Figure 26B**). In

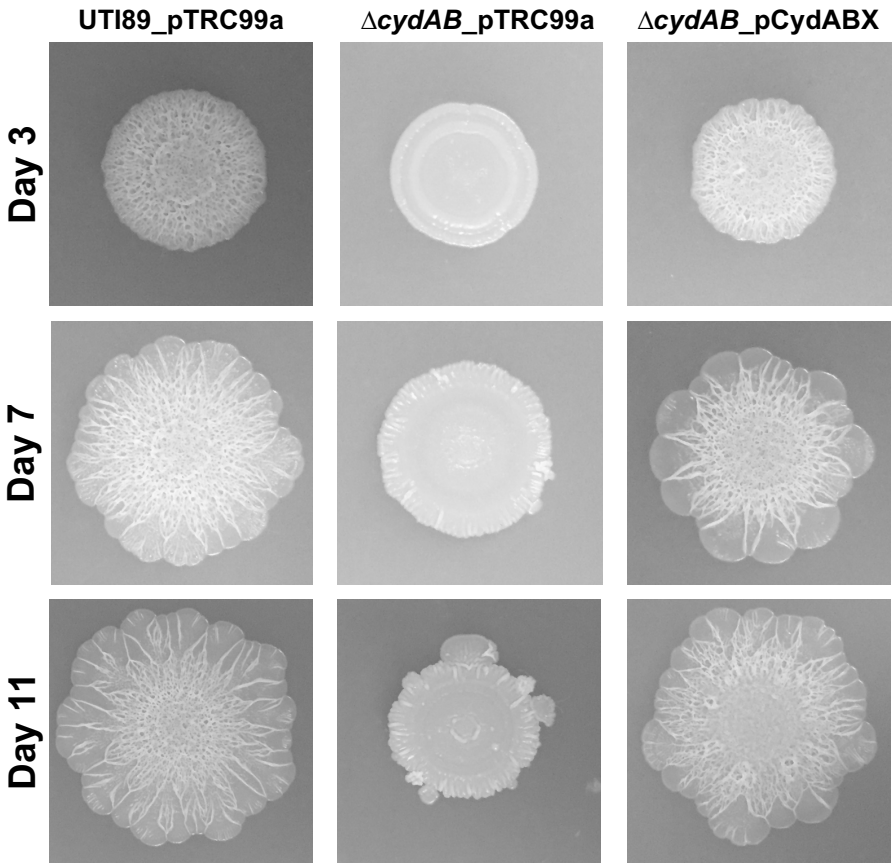

Figure 25. Complementation of Δ*cydAB* rescues biofilm defects. Representative images on UTI89_pTRC99a, Δ*cydAB*_pTRC99a, and complemented Δ*cydAB*_pCydABX under the control of a native promoter. Images were taken of colony biofilms grown on YESCA agar at days 3, 7, and 11 of growth. Images are representative of at least five biological replicates. *Figure from Beebout, Eberly, et al. mBio. 2019.*

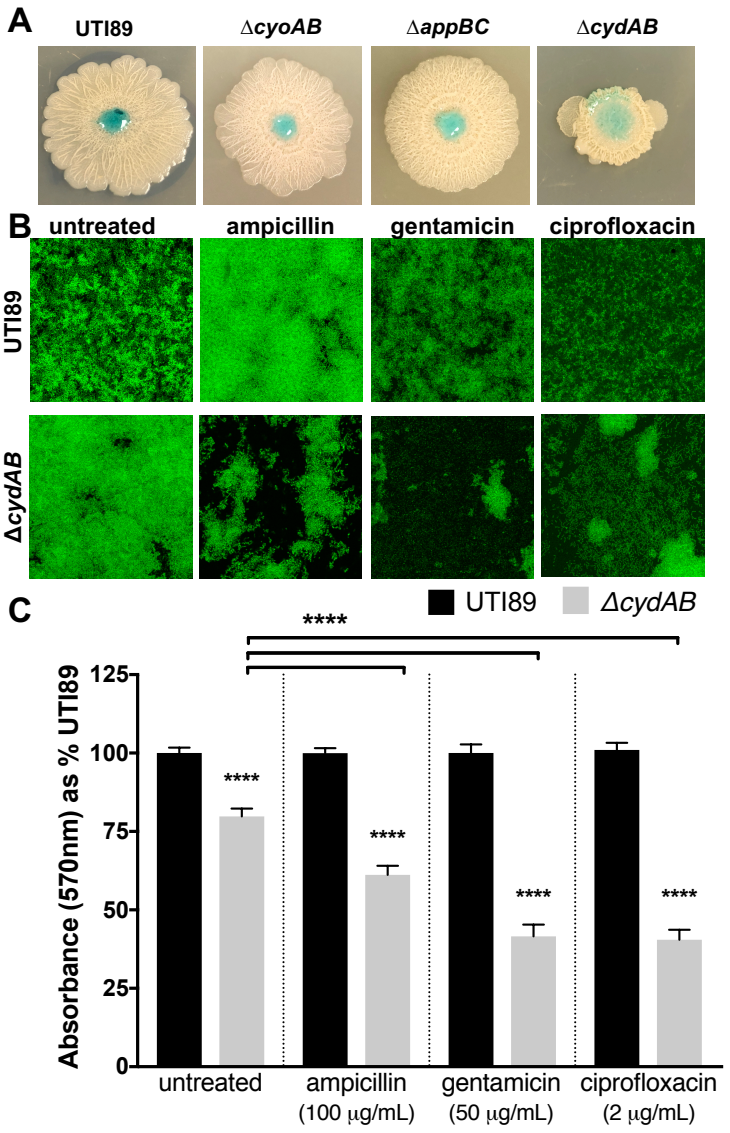

Figure 26. Deletion of cytochrome *bd* sensitizes biofilm matrix to aqueous penetration and antibiotic treatment. A. Colored water droplets were added to the top of day 11 colony biofilms to probe biofilm barrier function. **B.** UTI89 and Δ*cydAB* air-liquid interface biofilms were grown on PVC slides for 48 hours and then treated with either ampicillin (100 μg/mL), gentamicin (50 μg/mL), or ciprofloxacin (2 μg/mL) for 72 hours. After treatment biofilms were stained with SYTO 9 nucleic acid stain and imaged using CLSM. **C.** Biofilms were grown as in **B.** After 72 hour antibiotic treatment, biofilms were stained with crystal violet, and absorbance at 570 nm was measured as a proxy of total biomass. Absorbance values are normalized as percentage of UTI89 absorbance on the same plate to account for variability between days. Data is representative of at least three biological replicates. Statistical analysis was performed in GraphPad Prism using Welch's t test. * $p < 0.05$, ** $p < 0.01$, *** $p < 0.001$, **** $p < 0.0001$. *Figure adapted from Beebout, Eberly, et al. mBio. 2019.*

agreement with CLSM observations, a significant reduction in biofilm abundance was detected for the *cydAB* mutant treated with antibiotic compared to the parent strain (**Figure 26C**). Combined, these studies demonstrate that cytochrome *bd* is not only required during infection, but also imparts architectural integrity of the biofilm state.

3.4 Discussion

Cytochrome *bd* (*cydAB*) has previously been shown to have decreased colonization in the murine model (243), but there are no other studies to date that have assessed the role of each terminal oxidase. Surprisingly, the data presented in this chapter indicate that cytochrome *bd* is the only quinol oxidase that significantly impacts both biofilm architecture and bladder colonization. Furthermore, the deletion of *cydAB* leads to increased matrix penetration by aqueous substances and to sensitization of the biofilm to antibiotics. This suggests that there is a defect in the ability of the cytochrome *bd* mutant to either produce or correctly place the ECM components during biofilm formation. Current studies in the lab are investigating these possibilities, along with tracking the temporal roles for each quinol oxidase.

Future work will also establish the requirement of the other quinol oxidases by creating double deletion mutants and assessing how virulence and biofilm is impacted when bacteria operate using only one quinol oxidase. Gaining these insights will allow us to determine if targeting cytochrome *bd* through small molecule inhibition is feasible for developing novel anti-biofilm therapeutics to aid in the treatment of urinary tract infections and other biofilm-associated infections. However, in order to effectively design therapeutics or diagnostics based on an observation, the broad applicability of

that observation must be tested. Intriguingly, the nature of urine-associated *E. coli* isolates poses substantial barriers to accurate diagnosis and treatment, as will be discussed in **Chapter IV**. **Chapter IV** describes studies aimed towards the definition of a pathogenic signature— which may include cytochrome *bd* function in the future— that could distinguish asymptomatic or disease-causing urine-associated *E. coli*.

CHAPTER IV

TOWARDS DEFINING A PATHOGENIC SIGNATURE FOR UPEC: DISSECTING PHENOTYPIC DIVERSITY OF URINE-ASSOCIATED *ESCHERICHIA COLI* ISOLATES

Portions of this introduction have been adapted from: Breland, **Eberly**, Hadjifrangiskou. "An overview of two- component signal transduction systems implicated in extra-intestinal pathogenic *E. coli* infections". Review in *Frontiers in Cellular and Infection Microbiology.* 2017. (PMID: 28536675)

4.1 Introduction

Although UTIs are very common, the disease severity can encompass a broad range of clinical diagnoses, including acute cystitis, pyelonephritis, catheter-associated infection, and asymptomatic bacteriuria (ASB). Greater than eighty percent of UTIs are caused by *E. coli*, which has the ability to invade bladder epithelial cells and establish a transient intracellular lifestyle. The formation of these intracellular biofilms, as well as biofilms on catheter material and the kidney surface, greatly impedes treatment efforts by protecting resident bacteria from external stressors, such as the innate immune response and antibiotic treatment. In addition, genetic exchange within the biofilm greatly promotes the spread of antibiotic resistance markers**.** Intriguingly, there still remains a lack of a distinctive pathogenic signature for UPEC strains.

Unlike the intestinal *E. coli* pathotypes that can be readily identified by the presence of genes associated with attaching and effacing lesions (244, 245), UPEC strains lack a defined set of classical virulence factors that distinguish them from other extra-intestinal *E. coli* (**Figure 27**). For example, all UPEC isolates carry at least one iron acquisition system (with some encoding six or more), but only about fifty percent of the isolates harbor the hemolysin toxin (**Figure 27** and (246-249)). Though most UPEC isolates harbor type 1 and P pili, which have both been associated with UTI, the

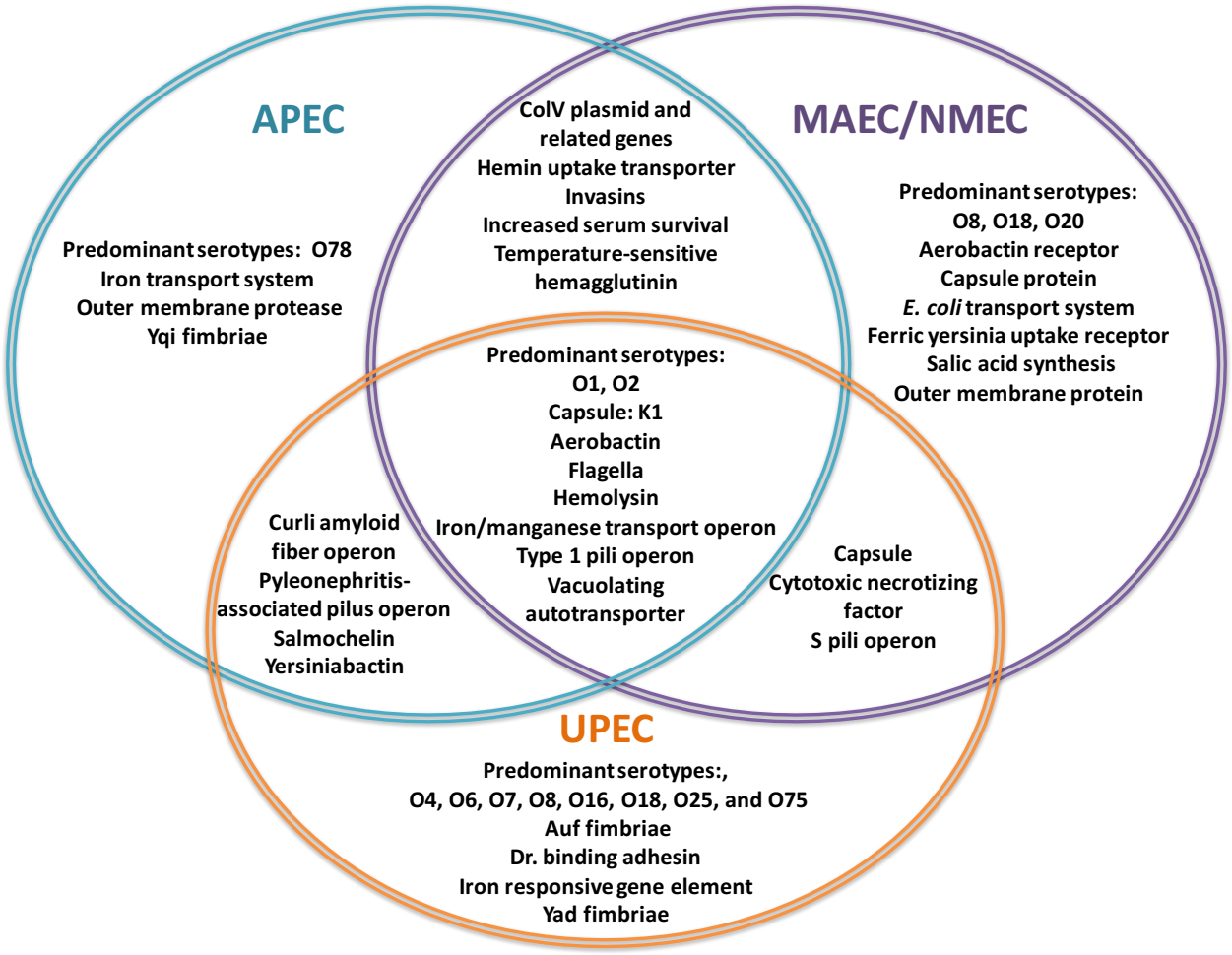

Figure 27. Virulence factors involved in ExPEC infections. The Venn Diagram represents the most commonly reported, shared and individual, virulence factors for APEC (blue), MAEC/NMEC (purple), and UPEC (orange). (250-261). *Figure from Breland, **Eberly**, & Hadjifrangiskou. Front. Cell. Infect. Microbiol. 2017.*

carriage of other CUP pili is variable (220, 262). Cystitis isolate UTI89 harbors ten intact chaperone-usher pathway pili systems, CFT073 isolated from the blood of a patient with pyelonephritis harbors eleven, and the multi-drug resistant ST131 EC958 isolated from urine harbors nine. These genes are often shared with avian pathogenic *E. coli* (APEC) and meningitis-associaed/neonatal meningitis-casuing *E. coli* (MAEC/NMEC) (100, 263-265). Furthermore, distinguishing signatures between symptomatic and asymptomatic strains are lacking. This prevents reliable identification of patients at risk for UTI if they present with bacteruria but not symptoms at the time of specimen collection.

Moreover, diagnostics of UTIs are based off of a threshold of bacteria present in a urine specimen and patient reported symptoms. Because of the inability to differentiate asymptomatic from symptomatic cases, physicians overprescribe antibiotics for UTIs, ultimately contributing to the rise in antibiotic resistance. To address this issue, this work utilizes a metabolomics approach to initiate efforts to identify a predictive signature to identify asymptomatic from symptomatic strains.

4.2 Methods

Urine-associated E. coli database

Urine-associated *E. coli* isolates and de-identified patient data were collected in accordance with IRB #151465. VUTI 113-VUTI 415 were isolated from mono-culture *E. coli* urine cultures by the Vanderbilt University Medical Center Clinical Microbiology Laboratory. Medical records were reviewed by a clinical microbiologist and de-identified patient information was collected following schematic in **Figure 29A**. To avoid bias, de-identified patient data was input by one individual, while freezer stocks of each VUTI

were grown overnight in LB from a single colony from MacConkey or blood agar plate by other individuals, blinded to the de-identified patient data to avoid bias.

Bacterial strains

Cystitis isolate UTI89 (220) and isogenic mutants UTI89Δ*fimA-H* (213) and UTI89Δ*flhDC* (200) were used in all phenotypic analyses as positive and negative controls.

Biofilm assays

All strains were grown overnight in LB (Fisher) pH 7.4 at 37°C with shaking unless otherwise specified. Colony biofilms were seeded using 10 µL of overnight culture that was spotted onto 1.2x YESCA CR agar (recipe in **Chapter II** and **Appendix A**) and allowed to grow at room temperature for a period of 11 days. Plates were incubated on the bench and imaged by digital camera on day 11. Images represent at least two biological replicates. Description of Congo red uptake and rugose morphology was qualitatively recorded as described previously (179, 222).

Biofilm abundance, comprising of CFUs and the self-secreted matrix, was quantified using the crystal violet method of O'Toole (237). Overnight cultures were diluted to OD_{600} = 0.05 and a volume of 100 µL was transferred to a 96 well PVC plate. Biofilms were rinsed in sterile water, stained with 0.5% crystal violet, and disaggregated with 35% acetic acid after 48 hours. Absorbance of the disaggregated biofilm was measured at 570 nm using a SpectraMax i3 plate reader (Molecular Devices).

Murine infections

Murine infections were performed as previously described (**Chapter III** and (241)). Mice were sacrificed at 24 hours post infection after which bladders were removed and homogenized for CFU enumeration. All animal studies were approved by the Vanderbilt University Medical Center Institutional Animal Care and Use Committee (IACUC) (protocol numbers M/12/191 and M1500017-01) in accordance with all recommendations in the Guide for the Care and Use of Laboratory Animals of the National Institutes of Health and the IACUC.

Immunoblot analyses

FimA immunoblots were performed as detailed in **Chapter II** and Floyd, *et al* (213). All strains were inoculated individually into 5 mL LB medium and grown shaking at 37˚C for 4 hours. This culture was diluted 1:1000 into 10 mL fresh media and grown statically at 37˚C for 24 hours. After 24 hours, this culture was diluted 1:1000 into 10 mL fresh media and grown for another 24 hours at 37˚C statically. Each culture was normalized to an OD_{600} of 1, pelleted by centrifugation, and prepped for SDS-PAGE. Proteins were transferred to nitrocellulose by Trans-Blot Turbo Transfer System (BioRad) for 7 minutes at 1.3 amps and 25 volts and blocked overnight with 5% milk. Nitrocellulose was washed and incubated with primary anti-FimA antibody (1:5,000 dilution) (212), and then washed and incubated with secondary HRP-conjugated goat-anti-rabbit secondary antibody (Promega) (1:10,000). Membranes were washed again before treatment with SuperSignal West Pico Chemiluminescent Substrate (ThermoScientific) and subsequent visualization of bands on x-ray film.

Motility Assay

Motility assays were performed as previously described (200). Approximately 5 µl portions of cells from each overnight were then stabbed into 0.25% LB agar supplemented with 0.001% 2,3,5-triphenyltetrazolium chloride. Plates were incubated at 37°C for 7 hours. Motility was evaluated by measuring the motility diameters. At least three technical replicates were tested per strain.

Pooled human urine

Urine was collected from healthy human volunteers in accordance with the IRB. A healthy volunteer was defined as one who is not menstruating and who has not taken antibiotics in the last 90 days. Equal volumes of male and female urine were pooled together from at least two volunteers of each sex for metabolomics experiments. Urine was filtered through a 0.22 µM filter prior to use.

Growth conditions for metabolomics analysis

A single colony from a LB agar dish was inoculated in 5 mL LB and grown overnight shaking at 37°C under ambient oxygen conditions for each individual isolate. The cultures were then individually diluted 1:1000 in pooled donated human urine and grown for 6 hours to mid-log growth phase at 37°C shaking at 4% oxygen to emulate the bladder environment. After 6 hours, OD_{600} of each isolate was measured and cultures were normalized by volume to contain the equal number of cells from each strain prior to pooling samples in groups of 8 isolates (**Table 3**). CFUs were plated for each sample to confirm cell number, which was approximately 10^9 cells per sample.

Each sample group was then centrifuged to separate the cellular portion (pellet) and supernatant fraction. Pellets and supernatants were flash frozen and stored at -80°C until submission for metabolomic analysis. Five biological replicates encompassing 60 pellets and 60 supernatant fractions were collected in total, along with a blank urine sample for each biological replicate.

Metabolomics Analysis

Samples were subjected to methanol extraction prior to ultra-high-performance LC/MS/MS of metabolite extracts. The samples were run on a Q Exactive HF Hybrid Quadrupole-Oribtrap mass spectrometer (ThermoFisher) for hydrophobic species analysis using Hypersil Gold reverse phase LC separation over a 30 minute gradient using 0.1% formic acid in water mobile phase A and 0.1% formic acid in acetonitrile. Retention time and mass spectra were aligned and statistical analysis performed using Progenesis QI 2.0 and MetaboAnalyst 4.0. Confidence levels of candidate metabolites were assigned as previously described (266). Chemometrics and hierarchical cluster analyses were performed on peak intensity values using the MetaboAnalyst 4.0 to generate principal component analysis (PCA) plots and heat maps, respectively. Log transformation and Pareto scaling were performed to normalize the data.

4.3 Results

Epidemiology from retrospective urine-associated E. coli isolate collection

To begin to investigate whether a phenotypic signature exists to distinguish ASB from symptom-causing strains, a retrospective study was performed in collaboration

with the Vanderbilt University Medical Center Clinical Microbiology Laboratory. Over 300 isolates were collected from monoculture, *E. coli*-positive urine specimens over the course of one month. These isolates were assigned the designation "VUTI" for Vanderbilt Urinary Tract Isolate, followed by a number, annotated based on the order the strains were collected. Along with the isolates, de-identified patient information was collected (**Figure 28A**). Cases that were unclear (n=18) were removed from downstream analyses. Of the 300 isolates, the majority were associated with putative cystitis (56%). Intriguingly, over 25% of the isolates collected were associated with asymptomatic bacteriuria (ASB) (**Figure 28B**). As reported in other studies, the majority (86%) of all isolates collected were from females (**Figure 28C**). **Appendix B** contains the database of patient information collected from each isolate.

Biofilm formation does not correlate with UTI symptomatology

To test the hypothesis that biofilm formation correlates with symptomatology, the 300 VUTI isolates were blindly tested for *in vitro* extracellular biofilm formation during growth in LB media. The results indicate that there is no specific correlation between biofilm formation and strains that cause symptomatic UTI (**Figure 29A**). Biofilm formation was tested both under atmospheric (21%) and under hypoxic (4%) bladder-like oxygen conditions for all 300 isolates (bar graphs in **Appendix C**). These assays demonstrated similar variability in the biofilm forming abilities of non-comorbid (**Figure 29B**) and comorbid (**Figure 29C**) cases of asymptomatic bacteriuria strains and strains collected from patients with putative cystitis. These data are contradictory to previous

A.

Strain/ Specimen V-UTI-_____

Sex: F M

Age: 18-35 36-50 51-60 61-70 71-80 81+

Collection setting: Outpatient Inpatient ED

Other (specify): _____

Recent indwelling urinary catheter: N Y

Pregnant: N Y

Diabetes: N Y

Asymptomatic bacteruria: N Y

Structural/ functional urinary tract abnormality:
N Y (specify): _____

Immunocompromised:
N Y (specify): _____

Associated infections:
None Pyelonephritis Prostatitis
Bacteremia Other (specify): _____

B.

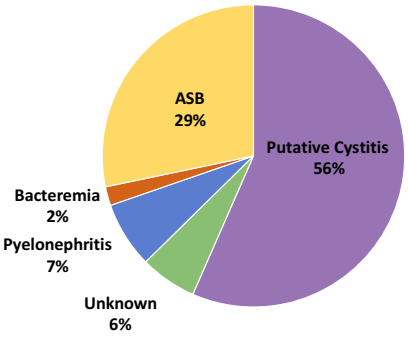

C.

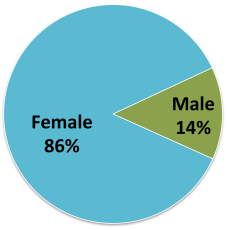

D.

	Female	Male
Total	259	41
18-35	68	3
36-50	46	3
51-60	40	8
61-70	46	16
71-80	40	8
81+	19	3

Figure 28. Collection parameters and distribution of Vanderbilt Urinary Tract Isolates. A. Panel represents patient parameters collected that pertain to urinary tract infections including collection setting, sex, age, collection setting, presence of a urinary catheter, pregnancy, diabetes, structural or functional abnormality, immunocompromised, and associated infection. **B.** Pie-chart with percentages of associated infection from all 300 isolates collected. **C.** Pie chart of sex of patients from which isolates were collected. **D.** Chart shows age breakdown by sex of patients from which isolates were collected.

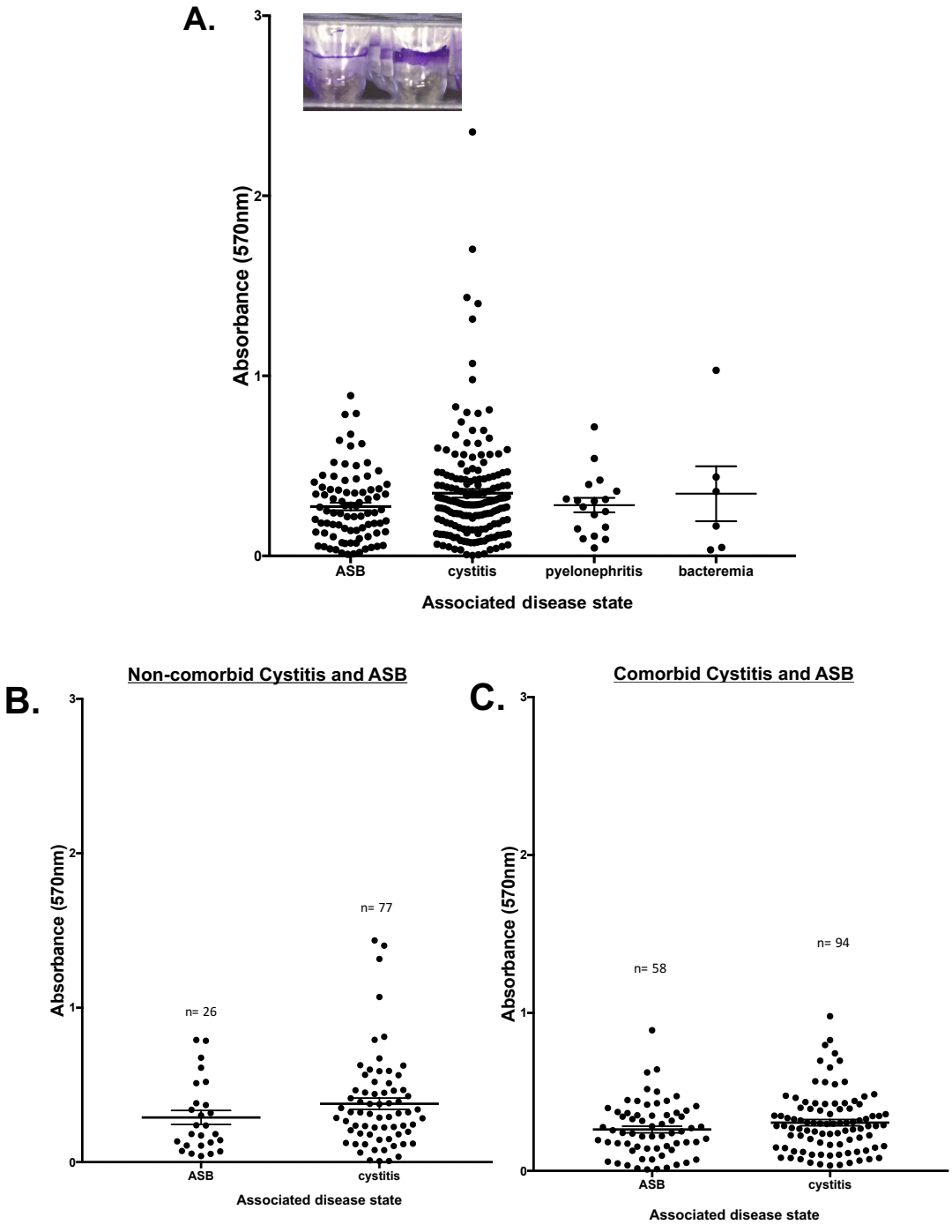

Figure 29. Vanderbilt Urinary Tract Isolates exhibit variable biofilm formation. A. *In vitro* crystal violet biofilm formation dot plot of the 282 isolates grouped by associated disease state. No statistical differences between groups by Kruskal-Wallis one-way ANOVA (p=0.475). Inset shows crystal voiolet stained biofilm formed on the PVC 96-well plate. **B.** Non-comorbid cases of cystitis and ASB from panel **A**. These isolates were used in metabolomics experiment. **C.** Comorbid cases of cystitis and ASB from panel **A**.

reports, as ASB isolates are suggested to be protective from symptomatic strains due to their high biofilm forming capabilities (267-269).

To further justify our results, we next tested five select ASB strains in an acute cystitis murine model to assess bacterial colonization in the bladder and kidneys. These results showed only VUTI 170 colonized the bladder at detectable levels 24 hours post infection (**Figure 30A**). Kidney colonization was detectable in at least one mouse by 4 of the 5 asymptomatic VUTI isolates (**Figure 30B**). Previous reports have noted that type 1 pili are essential for bladder colonization (156, 270, 271), so we subjected the ASB isolates to immunoblot analysis of FimA, the major subunit of type 1 pili. Though VUTI 142 produces a faint band, only VUTI 170 expresses FimA under the conditions tested (**Figure 31A**). Furthermore, since colonization in the kidneys was observed in 4 out of the 5 ASB isolates, I tested for hyper-motility of these isolates using a soft-agar motility assay. In parallel, representative cystitis and pyelonephritis isolates were also screened to test the hypothesis that pyelonephritic isolates are hyper-motile to colonize the kidneys. The results indicate that motility is variable among isolates of the same disease prognosis (**Figure 31B**). Type 1 pili production and Congo red (CR) dye uptake as a proxy for curli and cellulose production in 50 clinical isolates have previously been studied and show variation among the clinical isolates (**Figure 17** and (232)). Taken together, these results indicate that the virulence factors tested do not correlate with UTI symptomatology.

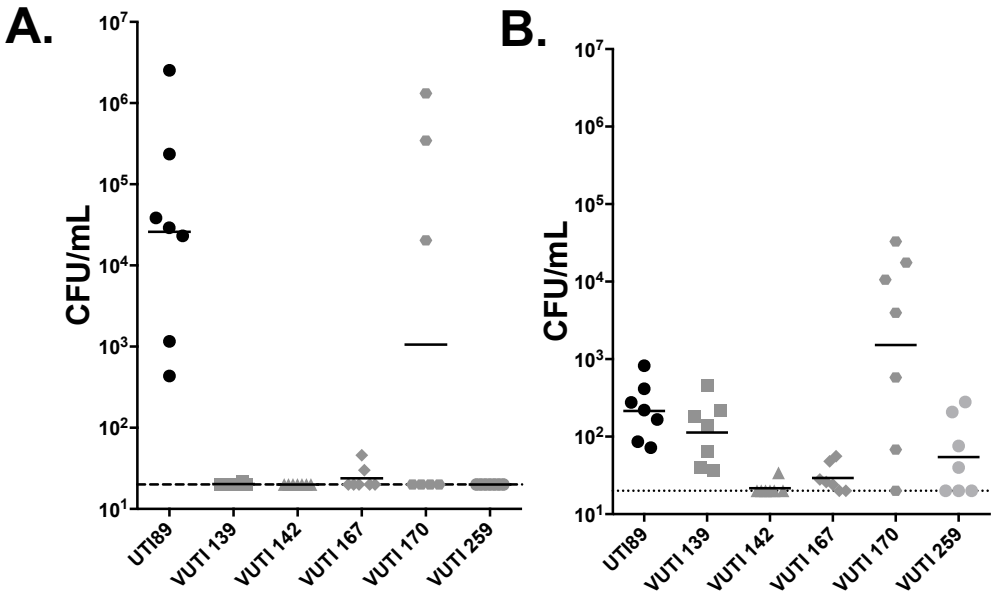

Figure 30. Select asymptomatic bacteriuria isolates do not exhibit robust colonization of the murine bladder or kidneys. A. Bladder titers were obtained from mice infected with UTI89 or ASB isolates at 24 hours post infection. Each point represents a mouse. **B.** Kidney titers were obtained from mice infected with UTI89 or ASB isolates at 24 hours post infection.

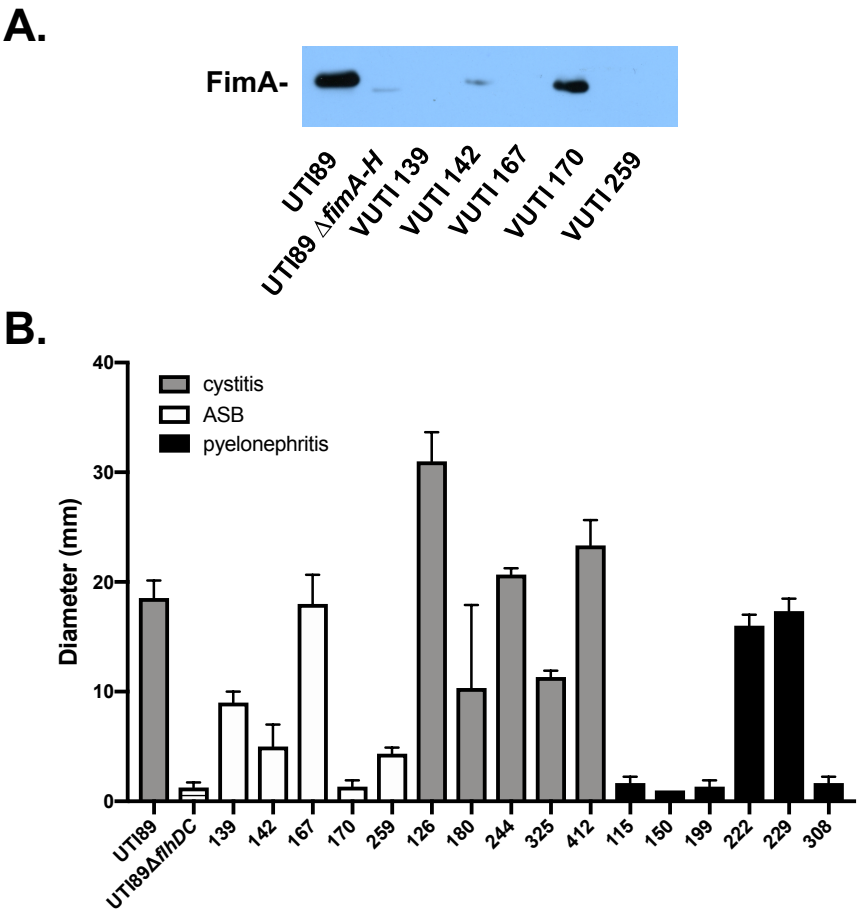

Figure 31. FimA expression and motility vary in VUTI isolates. A. Immunoblot of FimA, the major subunit of type 1 pili that are critical for host bladder colonization. This is representative of at least two biological replicates. **B.** Graph shows motility diameters of UTI89 and select VUTI isolates. Motility diameters were measured after bacteria were stabbed in soft agar supplemented with tetrazolium chloride and incubated at 37°C for approximately 7 hours. Data is representative of at least 3 technical replicates.

Profiling urine-associated E. coli isolates reveals a unique metabolic signature

Unlike other pathogenic *E. coli* like the enteropathogenic/enterohemorrhagic strains that have a defined set of virulence factors required for infection, there is no genetic signature that defines UPEC strains (23, 229). **Figure 32** demonstrates the inter- and intra-strain heterogeneity among select urinary tract isolates. Colony rugosity, diameter, and CR uptake vary among the clinical isolates. VUTI 150 is smooth (non-rugose) and uptakes CR primarily in the center. In contrast, VUTI 263 is rugose and uptakes CR throughout the colony biofilm. Some colonies, such as VUTI 167, display heterogeneous CR uptake throughout the biofilm. I hypothesize that there are subtle differences between the metabolic inventory of asymptomatic and symptomatic urinary tract isolates.

In collaboration with the Center for Innovative Technology (CIT) at Vanderbilt University, we designed an experiment to assess the metabolic differences between asymptomatic and symptom-causing strains (**Figure 33**). In order to simulate the *in vivo* environment that these isolates are exposed to in the bladder, non-comorbid isolates of ASB and cystitis isolates were grown individually in human urine for 6 hours (to reach mid-log growth phase). Eight isolates were then pooled in equal cell number by optical density measurement and pooled in groups of eight shown in **Table 3**, then pelleted and split into supernatant and pellet fractions, flash-frozen, and stored at -80^{o}C. Each sample was subjected to liquid chromatography tandem mass spectrometry (LC-MS/MS) to obtain elution times and mass spectra. **Figure 34A** shows separation analysis of the supernatant of the ASB groups and the cystitis groups in a principle

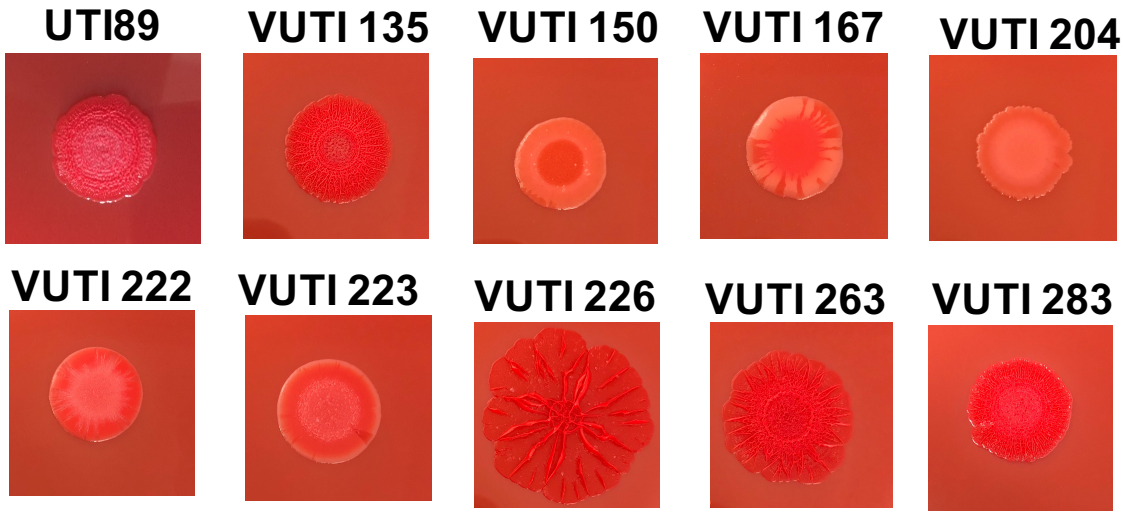

Figure 32. Inter- and intra-strain heterogeneity among urinary isolates. Mature colony biofilms show inter-and intra-strain heterogeneity. YESCA –CR agar plates were spotted with 10 µL of overnight culture and incubated on the bench for 11 days.

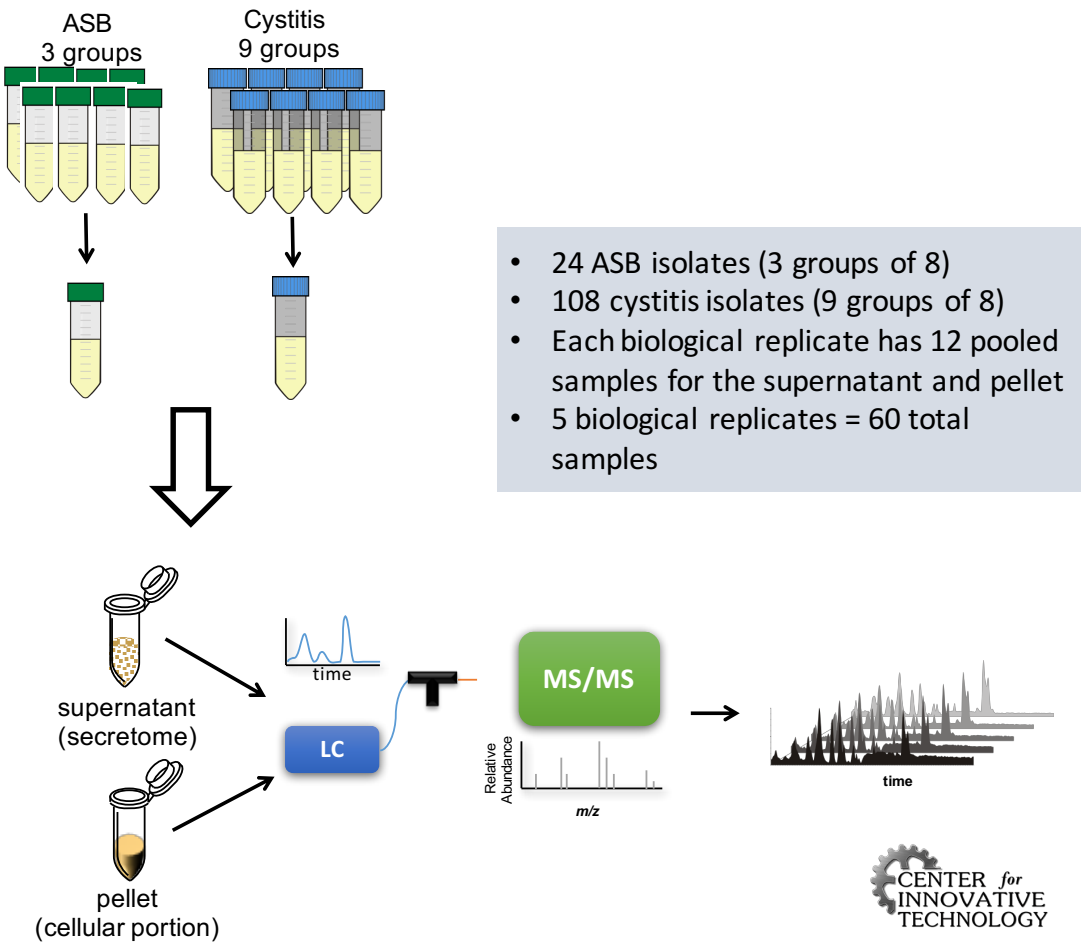

Figure 33. Schematic of metabolomics experimental design. Isolates were grown individually to mid-log, then pooled together in groups (**Table 3**), centrifuged and then seperated into two fractions: supernatant and pellet. Samples were flash-frozen and stored at -80°C. Samples were then subjected to LC-MS/MS, collecting both elution times and mass spectra for each metabolite.

Group A	Group B	Group C
139	151	142
167	170	161
219	231	183
280	269	190
318	285	259
359	302	298
388	372	313
398	406	324

Group D	Group E	Group F	Group G	Group H	Group I	Group J	Group K	Group L
163	135	129	412	152	175	198	125	117
215	204	168	145	180	217	236	188	172
256	272	207	182	194	371	249	265	213
270	317	263	239	223	244	312	290	237
335	365	300	286	230	266	342	333	264
404	403	362	337	288	275	382	361	325
193	164	390	374	316	307	407	389	353
224	232	409	405	380	314	126	113	366

Table 3. VUTI isolate grouping used in metabolomics experiment. Top: ASB isolates. Bottom: Cystitis isolates.

component analysis (PCA) of the first biological replicate. Within this first biological replicate, 6,711 features have been detected. The 6,711 were filtered by a p-value <0.05 and a q-value of <0.01 for a total of 1,211 and 580 significant compounds, respectively. The significant features by q-value of <0.01 are shown in a heat map where blue indicates low abundance and red indicates high abundance in **Figure 34B**. Significantfeatures were then blasted against databases by ProGenesis 2.0 software and were assigned a candidate identifications with a level of confidence, as described in Schrimpe-Rutledge *et al.* (266). Level 1 validated and level 2 putative top candidates were input into Metaboanalyst program to construct a heat map (**Figure 35**). These results indicate that there are differences in the metabolic profile of ASB isolates compared to the cystitis. **Appendix D** contains all top candidate identifications for all confidence levels of significant compounds.

4.4 Discussion

The need for improved diagnostic tools for distinguishing asymptomatic from symptomatic urinary tract isolates is prominent as antibiotic resistance rates continue to rise and current therapeutic measures are failing. This work is an example of how powerful isolate databases can be. We provide evidence that there are metabolic differences between asymptomatic and symptomatic urinary tract isolates. This urine-associated *E. coli* database is one of the largest composites of urine-associated *E. coli* isolates reported. We report 300 isolates in this study, though the database now encompasses over 400 urine-associated *E. coli* isolates collected to date and continues to grow. Furthermore, the de-identified patient data provide information that allows more

in-depth analysis and has potential for studying specific infection scenarios such as diabetes or pregnancy.

Our previous work showed that there is heterogeneity among clinical isolates and their production of biofilm factors including type 1 pili, cellulose, and curli, however, no patient data was associated with those isolates (232). Here, we are able to group the 300 isolates by disease state and observe that biofilm abundance is not a predictor of disease state. This contradicts previous work that indicates that ASB isolates form more biofilm than cystitis isolates to provide protection against recurrent infection (267-269). However, these studies tested less than 10 ASB isolates and less than 5 cystitis isolates for *in vitro* biofilm formation. The data presented here evaluated biofilm formation in over 80 ASB isolates and over 160 cystitis isolates, and variable levels of biofilm abundance is observed in both groups (**Figure 29**).

Because of the breadth of the VUTI database, we were able to design a large metabolomics experiment comparing 24 ASB isolates against 72 cystitis isolates from patients without comorbidities. Preliminary analyses indicate differences in the metabolic profile of supernatant fractions from ASB compared to cystitis (**Figures 34-35**). Intriguingly, hypoxanthine is found at lower levels in the supernatant of ASB isolates. Hypoxanthine is part of purine metabolism pathway, and our lab has previously reported purine biosynthesis is necessary for UPEC intracellular survival (236). **Figure 36** shows a portion of purine synthesis in *E. coli* where hypoxanthine is found, as well as the enzymes and metabolites directly up- or down-stream of hypoxanthine. Purines are essential to many processes, including DNA and RNA synthesis and energy production for both the bacterium and the host. Higher levels of the free purine base

hypoxanthine in the supernatant of cystitis isolates suggest that hypoxanthine is in excess to the bacteria, so they are utilizing other portions of the purine synthesis pathway up for purine catabolism to allow for intracellular survival in the bladder. Ongoing work is to mine the metabolite hits to identify additional metabolites in purine biosynthesis. We next will use genetic tools to delete the enzymes (individually or in combination) surrounding hypoxanthine (**Figure 36**) in both ASB and cystitis strain backgrounds. *In vitro* and *in vivo* analyses including metabolic flux analysis to measure the rate of consumption of specific metabolites and murine infections will be performed to interrogate the role of each metabolite in UPEC infection. Purine synthesis is one known pathway that is implicated in UPEC infection, but this data set allows for us to identify additional pathways and repeat these same biological validations to understand the biological importance of each pathway to eventually lead to distinct metabolic signatures for ASB and cystitis isolates.

In addition to interrogating the biological role of each pathway in asymptomatic or symptomatic isolate colonization, candidate metabolites will be validated by mass spectrometry. First, we will scramble the groups in **Table 3** and repeat this same experiment to determine if hypoxanthine is again identified as decreased in ASB supernatant, as well as other metabolites of interest. If these are validated, we will then use a targeted mass spectrometry approach where urine samples from the clinic will be pelleted and the supernatant subjected to mass spectrometry to measure levels of certain metabolites and predict whether the isolate is asymptomatic or symptomatic. Intriguingly, elevated hypoxanthine is reported to be a biomarker of inflammation in other injury and infection scenarios (272, 273) If a panel of metabolites are validated, a

new mass spectrometry assay can be implemented into clinical laboratories for rapid diagnostics of symptomatic and asymptomatic UTIs. This work has the potential to eliminate the issue of differentiating asymptomatic from symptomatic UTIs that has been plaguing microbiologists and clinicians alike for decades.

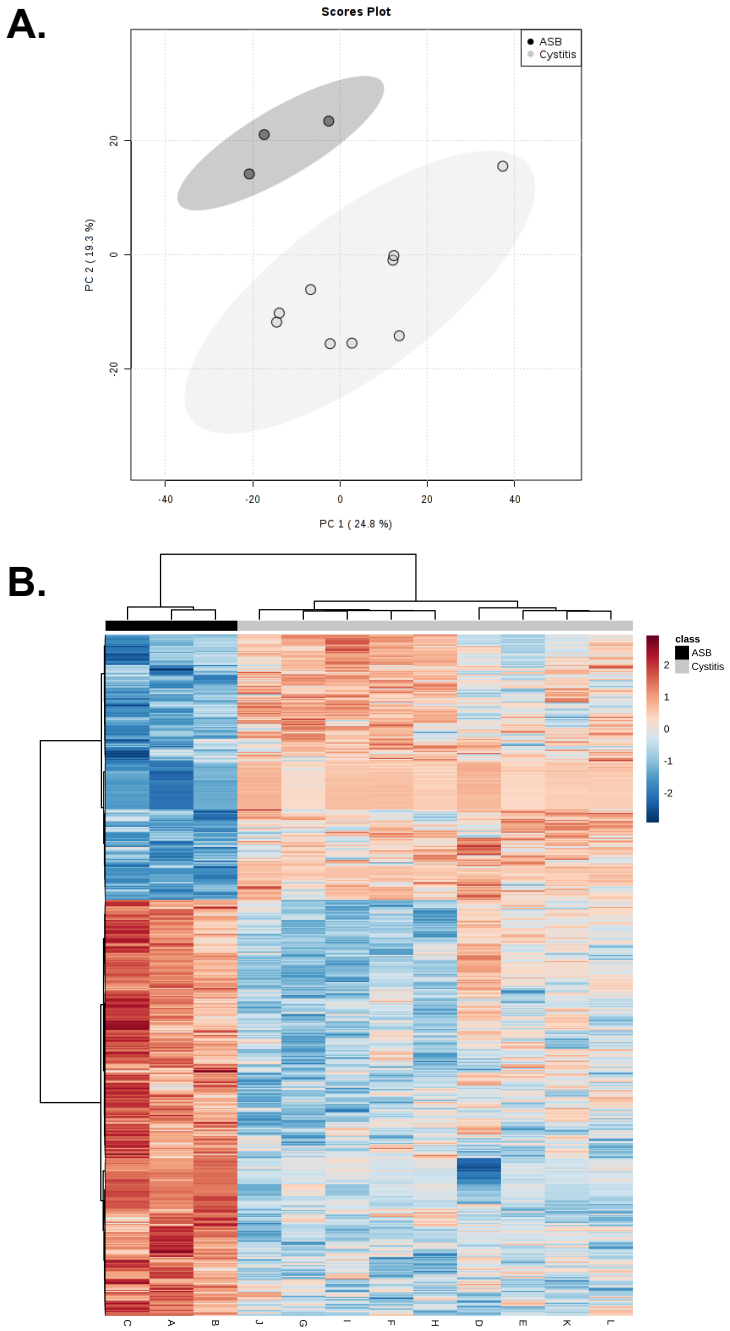

Figure 34. Metabolic differences between asymptomatic and symptomatic urinary tract *E. coli* isolates. A. PCA plot uses abundance levels for all metabolite species within a sample (shown as individual data points) to determine the principle axes of abundance variation. **B.** heat map shows significant metabolites by q-value<0.05. Red color indicates higher abundance while blue indicates low abundance. A-C correspond to ASB, while D-L correspond to cystitis. For both **A-B**, chemometrics and supervised hierarchical cluster analyses were performed on peak intensity values using the MetaboAnalyst software to generate heat maps. Log transformation and Pareto scaling were performed to normalize the data.

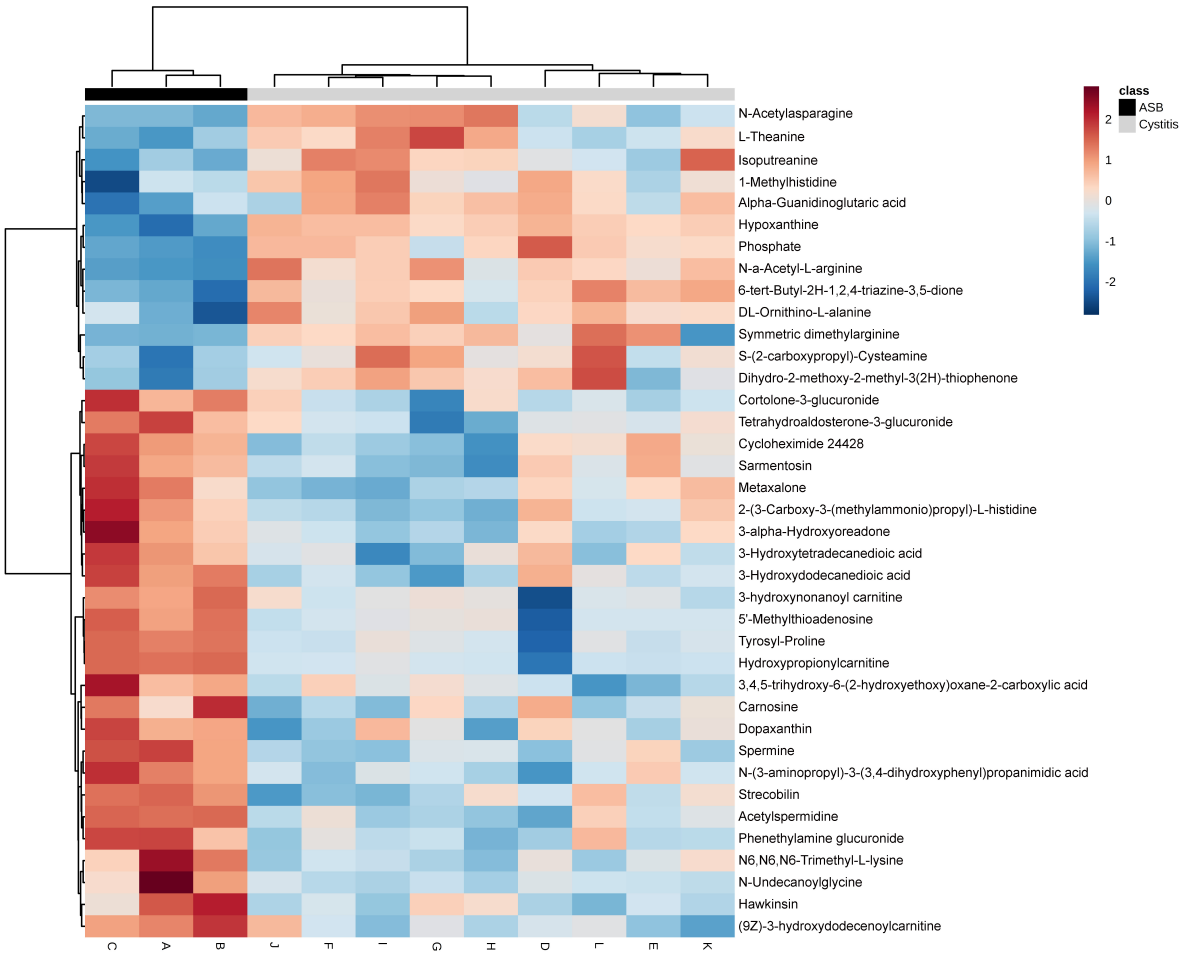

Figure 35. ASB isolates display metabolic differences compared to cystitis isolates. Heat map shows metabolites with level 1 and 2 confidence. Red color indicates higher abundance while blue indicates low abundance. A-C correspond to ASB, while D-L correspond to cystitis. Chemometrics and supervised hierarchical cluster analyses were performed on peak intensity values using the MetaboAnalyst software to generate heat maps. Log transformation and Pareto scaling were performed to normalize the data.

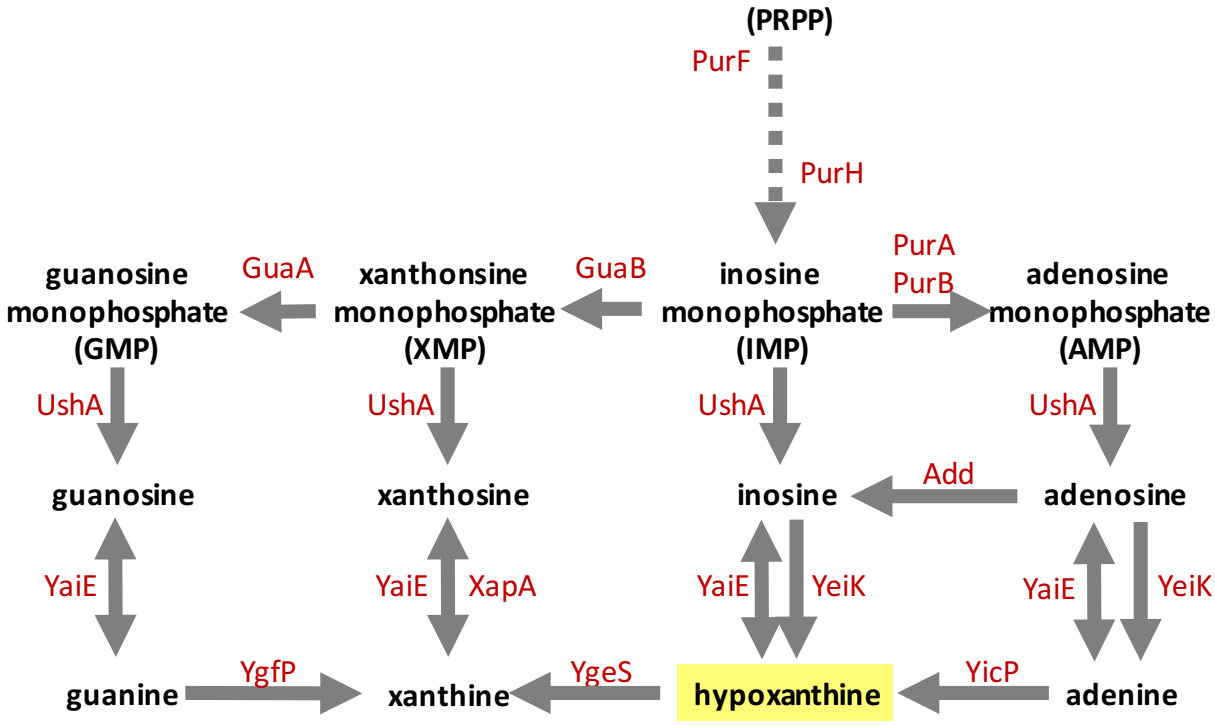

Figure 36. Hypoxanthine in the *de novo* purine metabolism pathway. Schematic shows the enzymes (red) and metabolites (black) near hypoxanthine (yellow background) in *de novo* purine metabolism in *E. coli* isolate UTI89. This schematic has been adapted from KEGG pathway analysis.

CHAPTER V

CONCLUSIONS AND FUTURE DIRECTIONS

The studies in this thesis highlight the need for improved diagnostics and treatment for UTIs. UTIs are a very common infection with a vast array of clinical diagnoses. Though several factors can compound treatment of UTIs, biofilm formation by UPEC contributes to infection persistence and possibly recurrent infections. **Chapters II** and **III** show that UPEC biofilm formation is optimal under bladder-like oxygen conditions and that cytochrome *bd* is requisite for bladder infection and the formation of architecturally complex biofilms with the ability to exclude antibiotics. A deeper understanding of how biofilms are formed at the molecular level is key to designing effective therapeutics. Another issue plaguing clinicians and basic scientists alike is the inability to differentiate asymptomatic from symptomatic UTIs. **Chapter IV** emphasizes the variability in phenotypic characteristics among urine-associated *E. coli* isolates and lays the foundation for defining a metabolic signature that may serve a diagnostic purpose in the future. Utilizing technologies readily available to diagnostic laboratories, such as mass spectrometry and genomic sequencing, to identify asymptomatic from symptomatic infections will cut down on the number of antibiotics prescribed for UTI and, in turn, slow down the rising antibiotic resistance rates. This chapter details experiments that are ongoing, as well as future directions.

Determine the extent to which oxygen concentration affects type 1 pili biogenesis

Chapter II shows that biofilm formation levels vary depending upon the oxygen concentration, with the lowest biofilm abundance during growth in an anoxic

environment. Previous work shows that type 1 pili— which mediate adherence and initiate biofilm formation— have decreased expression under anoxic conditions (213). I began a series of transmission electron microscopy experiments imaging cells grown under atmospheric or anoxic conditions. Preliminary images suggest that though there is a decrease in pili abundance under anoxia compared to atmospheric conditions, there are still pili on the surface (**Figure 37A**). Furthermore, I have tested FimA expression under decreasing oxygen conditions and see variable levels (**Figure 37B**) that do not correlate with biofilm abundance measured in **Figure 18**. Previous work has shown that S pili, another CUP pili encoded by UPEC, are expressed when type 1 pili expression is decreased, especially under anoxic conditions (210, 213, 231, 274). To truly monitor the number of type 1 pili on the surface on UPEC under different oxygen conditions, immuno-gold labeling of Fim with subsequent transmission electron microscopy needs to be performed to enumerate type 1 pili.

If there are altered levels of type 1 pili under the different oxygen conditions, there may be a defect at one of the checkpoints of type 1 pilus transport or assembly. The first checkpoint that could be impeded is the energy dependent translocation of pilus subunits. To evaluate this possibility, UPEC cultures can be grown under decreasing oxygen conditions and subsequently fractionated to determine if the localization of FimA is in the cytoplasmic, periplasmic, or membrane-associated. Another possibility is that the Fim protein-protein interactions are altered under oxygen replete conditions. These interactions, namely the FimA interaction with the chaperone and usher subunits, FimC and FimD respectively, can be teased apart *in vitro* with

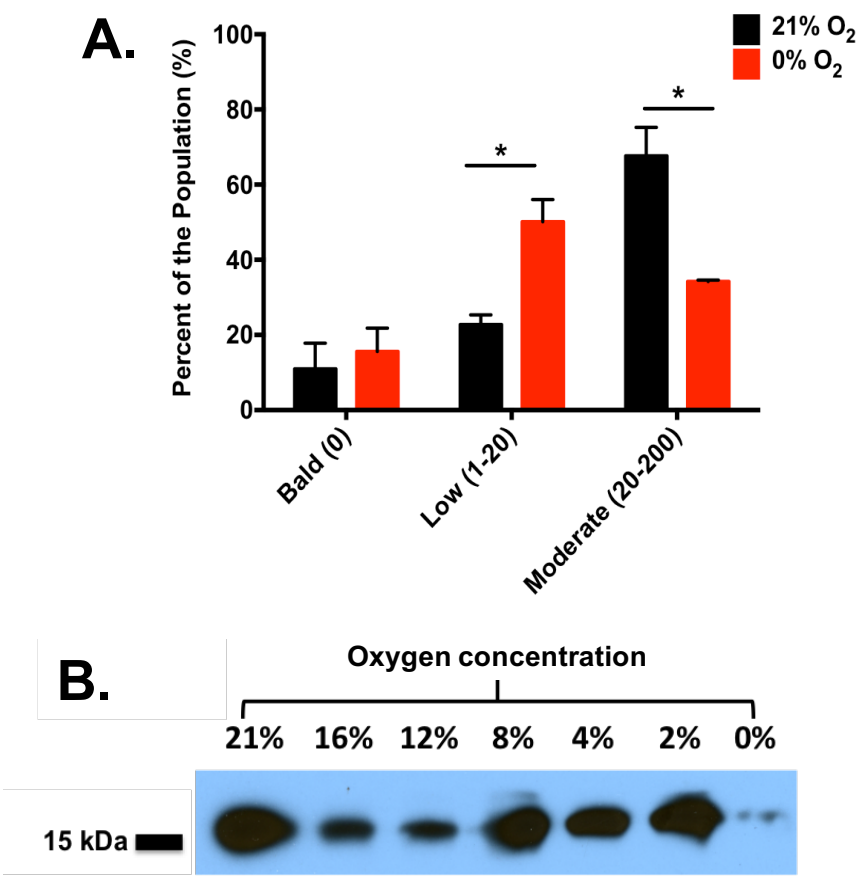

Figure 37. Type 1 pili levels vary with oxygen concentration. A. Graph depicts percent of population expressing no pili (bald), low pili (1-20) and moderate pili (20-200). Bacterial cultures were grown under atmospheric or anoxic conditions for 48 hours. After 48 hours, cultures were normalized and prepped for transmission electron microscopy. There were 229 cells grown under 21% oxygen and 227 cells grown under 0% oxygen counted. Statistical analysis was performed with 2-way ANOVA comparing values of 21% to 0% within each piliation classification. * $p < 0.05$. **B.** Immunoblot probing for the major subunit of FimA from cultures grown statically for 48 hours at room temperature under decreasing oxygen conditions. Blot represents one biological replicate.

purified protein using bio-layer interferometry in collaboration with the Thanassi group at Stony Brook University.

A third checkpoint is that type 1 pili may be assembled but not anchored to the cell surface. In P pili, there is a specific terminator protein responsible for interacting with the last major subunit to terminate pilus growth (100), but no such protein in type 1 pili has been identified. Since the only uncharacterized gene in the type 1 operon is *fimI*, I hypothesize that FimI is contributing to pilus anchoring to the outer membrane and is impaired under anoxia. Experiments to test this hypothesis first include genetic construction of a non-polar *fimI* deletion following recently published methods (275, 276), as well as an over-expression *fimI* construct, followed by growth and biofilm formation assays. To date, an over-expression candidate has been confirmed by sequencing, but has not been functionally tested for expression levels of *fimI* (cataloged in Hadjifrangiskou lab strain database). Intriguingly, FimI contains an RxxxR motif near the C-terminus. Work in *P. aeruginosa* has identified that an RxxxR motif binds c-di-GMP to control the length of type IV pili (277). Levels of c-di-GMP within the bacterial cell are critical for dictating the switch from a motile, planktonic state to a sessile, biofilm state (77, 80, 165). Site-directed mutagenesis to mutate the RxxxR motif of FimI by changing the five amino acids to alanine individually and in combination should be performed as previously described (278), followed by monitoring biofilm formation of each mutant. If biofilm is altered, transmission electron microscopy with immune-gold labeling should be performed to visualize and characterize pili on the cell surface. I predict that if FimI plays a role in terminating the length of type 1 pili, c-di-GMP levels may be implicated and affected by anoxia (c-di-GMP measurements described in next

section). In that case, the deletion strain will exhibit long pili and the overexpression construct will have shortened pili in comparison to the wild-type strain. If the RxxxR motif is involved, the site-directed mutants will have the same effect on pili length as the *fimI* deletion strain.

Elucidate cytochrome bd regulation of biofilm formation in response to oxygen availability

Each cytochrome oxidase appears to contribute to biofilm formation in some way due to subtle differences observed when compared to the parent strain. The creation of mutants harboring only one cytochrome oxidase will allow these roles to be interrogated. Further characterization of cytochrome bd_2 and cytochrome *bo* and their role in biofilm architecture is of interest in future studies. For example, when scraping colony biofilms from the agar for RNA extraction and other analyses, the cytochrome bd_2 mutant colony biofilms were sticky compared to the other strains. To get a snapshot into what appendages the individual cells within the colony biofilm are decorated with, center and periphery portions of colony biofilms were subjected to transmission electron microscopy. Preliminary counts of two biological replicates show that majority of the cells are bald (**Table 4**). Upon construction of mutant strains harboring only one terminal oxidase (UTI89Δ*cydAB*Δ*appBC*, UTI89Δ*cydAB*Δ*cyoAB*, and UTI89Δ*cyoAB*Δ*appBC*), these microscopy experiments should be repeated.

However, since cytochrome *bd* is the most implicated quinol oxidase in UPEC pathogenesis, teasing apart the regulation can lead to new therapeutic targets. However, unlike the work outlined in **Chapter IV**, my first cytochrome oxidase studies

Sample	Total # of cells	# Bald	# Pillated	# Flagellated	% Bald	% Pillated	% Flagellated
UTI89 C	307	260	30	19	84.69%	9.77%	6.19%
UTI89 P	322	313	6	3	97.20%	1.86%	0.93%
Δ*cydAB* C	332	331	1	0	99.70%	0.30%	0.00%
Δ*cydAB* P	331	317	9	5	95.77%	2.72%	1.51%
Δ*appBC* C	287	260	20	7	90.59%	6.97%	2.44%
Δ*appBC* P	331	322	5	4	97.28%	1.51%	1.21%

Table 4. Transmission electron microscopy reveals pili and flagella levels in cytochrome oxidase *bd* and *bd*$_2$ mutants. Table depicts total number of cells counted, as well as the number of cells with neither pili nor flagella (bald), flagella, or pili. Percent of population that are bald, piliated, or flagellated is also shown. Colony biofilms were grown on YESCA agar for 11 days before extraction of center (C) and periphery (P).

were in planktonic culture. It is important to note that expression patterns, as well as other factors, may change under different growth conditions. To ensure that cytochrome *bd* was indeed the highest quinol oxidase expressed under hypoxic conditions in the planktonic state, cytochrome oxidase expression of bacteria grown in the planktonic state under decreasing oxygen conditions was tested. First, RNA was extracted from 4mL of planktonic cultures grown statically for 48 hours under either 21%, 12%, 8%, or 4% oxygen using the RNeasy kit (Qiagen). A total of 5µg of RNA was DNase treated using Turbo DNase I (Invitrogen). Removal of DNA was validated by PCR. One microgram of DNase-treated RNA was reverse-transcribed using random hexamers (Invitrogen) and SuperScript III Reverse Transcriptase (Invitrogen). Resulting complementary (c) DNA was quantified and diluted to 100 ng/µL for subsequent quantitative polymerase chain reaction (qPCR) analysis. Quantitative (q) PCR was performed TaqMan MGB chemistry with the primers and probes listed in **Table 5**. A StepOne Plus Real-Time Instrument was used to perform all reactions. All reactions were performed in triplicate with four different cDNA concentrations (100, 50, 25, or 12.5 ng per reaction). Relative fold change in transcript abundance was determined using the log fold-change ($\Delta\Delta C_T$) method (279) with target transcripts normalized to *gyrB* abundance from a total of at least 3 biological replicates. **Figure 38A** shows that *cydA* is expressed at higher levels as oxygen concentration decreases and that *cydA* is the most abundant transcript of the three quinol oxidases.

In addition to functioning as a quinol oxidase, cytochrome *bd* also plays a role in detoxifying nitric oxide (280, 281). Furthermore, nitric oxide has also been shown to

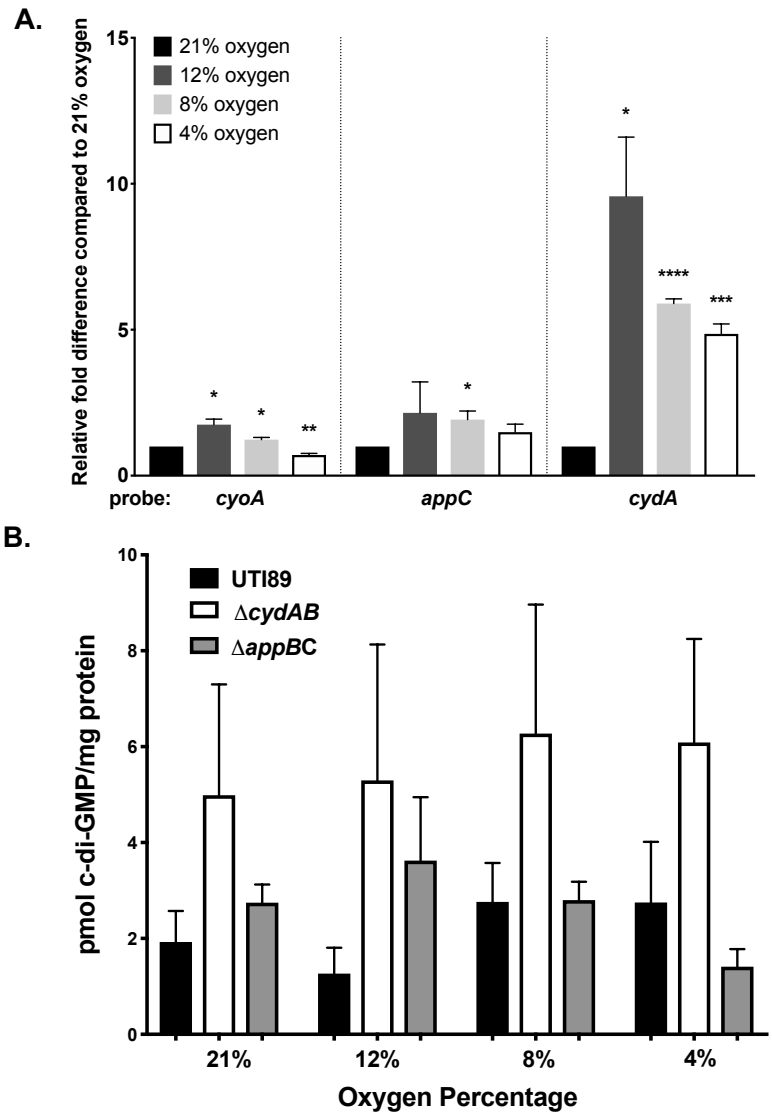

Figure 38. Expression of cytochrome oxidases and c-di-GMP levels under decreasing oxygen. A. Relative abundance of each transcript under decreasing oxygen as compared to *gyrB*. Data are presented as mean ± SEM. All data are representative of three biological replicates. **B.** c-di-GMP levels under decreasing oxygen concentrations in the parent and cytochrome *bd* oxidases are depicted in graph as picomoles of c-di-GMP per milligrams of protein. Data are representative of three replicates. Data are not significant by Kruskal-Wallace. * $p < 0.05$, ** $p < 0.01$, *** $p < 0.001$, **** $p < 0.0001$.

Primer/Probe	Sequence (5' → 3')	Purpose
cyoA_Fwd	CAATGCCCTGTTCCGGGTAGATG	qPCR
cyoA_Rev	ACGGTACCTATCTTAATCATCATCTTCC	qPCR
cyoA probe	NED-TCGTCGTGTGCCAGCGGCTTG	qPCR
appC_Fwd	CGATGTCGCATTACGCTCG	qPCR
appC_Rev	GGTGCAGGTTCTGTTTGCCACT	qPCR
appC probe	NED-CTGCGTATGAAGTCGCGCAAG	qPCR
cydA_Fwd	GTGGCTACCGGTCTGACCATG	qPCR
cydA_Rev	CCAACCGAAGAAGAACAGACCTAC	qPCR
cydA probe	FAM-CGCTGGCAATCGAAGGTCTGATG	qPCR

Table 5. Primers and probes used in qPCR in Figure 38A.

enhance the function of phosphodiesterases (PDEs) that break down c-di-GMP and promote dispersal of the biofilm (282, 283). This suggests that when c-di-GMP levels are high, nitric oxide levels will be low, and the bacteria are protected in the biofilm. However, when nitric oxide levels are high, the bacteria are signaled to disperse from the biofilm in attempts to avoid the nitric oxide stress. I hypothesize that c-di-GMP levels will be higher under low oxygen conditions when cytochrome *bd* is functioning as the primary quinol oxidase. In collaboration with the Yildiz group at University of California Santa Cruz, I preliminarily measured c-di-GMP levels from planktonic cultures using their previously published methods (**Figure 38B** and (284)). These results preliminarily show that c-di-GMP levels are increased in the absence of cytochrome *bd*, but need to be repeated for statistical robustness. In parallel, c-di-GMP measurements will be taken from colony biofilms and c-di-GMP levels monitored over time, especially in the early stages (0-72 hour) of biofilm formation.

Upstream regulators of cytochrome *bd* including ArcAB, H-NS, and FNR (285-287). Under anoxic conditions, FNR represses *cydABX* transcription. Under hypoxic conditions, ArcA/B activates *cydABX* transcription, while H-NS represses *cydABX* transcription under aerobic conditions (285-287). Importantly, loss of either *hns* or *fnr* results in ArcA/B controlling *cydABX* regardless of the oxygen conditions, as it is the master regulator of *cydABX* (285). These *cydABX* regulators are likely to play a role in the biofilm defect observed in the *cydAB* mutant. Since Dr. Hadjifrangiskou specializes in bacterial signaling, our lab has both *fnr* and *arcA/B* mutants in strain UTI89. I tested colony biofilm formation and motility of these two mutants under ambient oxygen (**Figure 39**)**.** Though the *fnr* mutant has an intermediate motility, it forms colony biofilm

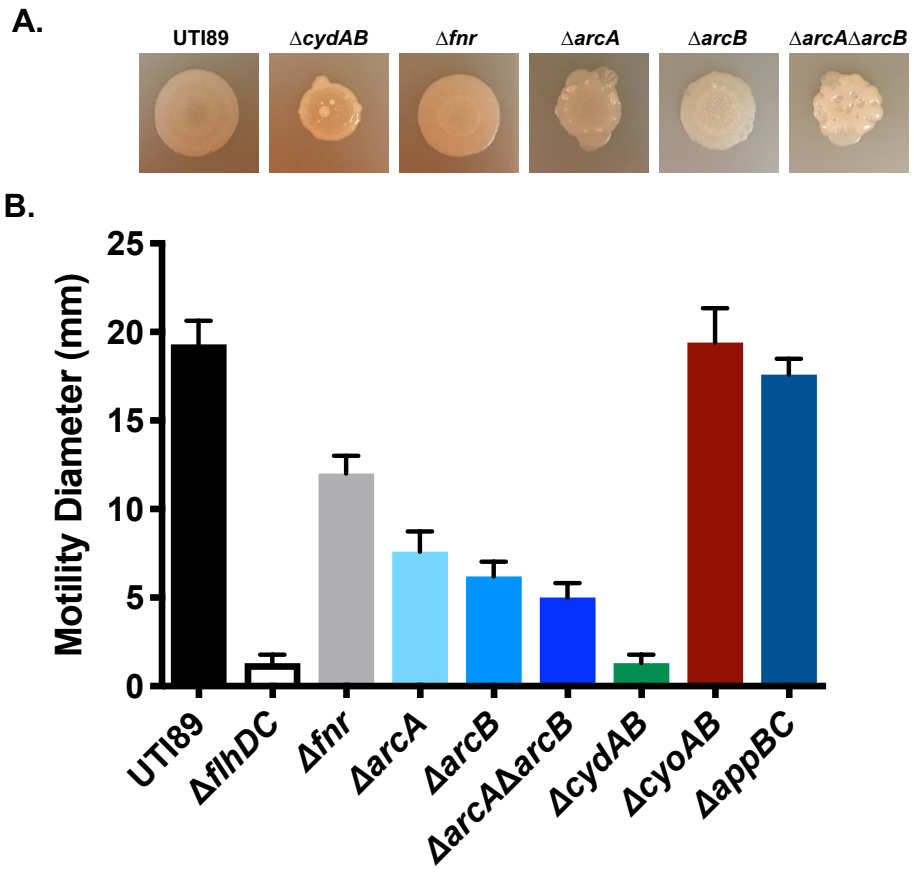

Figure 39. *arcA/B* deletion phenotype mimics cytochrome *bd* mutant. A. Images are representative day 11 colony biofilms grown on YESCA plates. Data is representative of at least 3 biological replicates. **B.** Graph shows motility of parent and mutant strains. Data is representative of at least 3 technical replicates.

similar to the parent strain. However, UTI89Δ*arcA*Δ*arcB* mutant displays a similar phenotypic defect as the cytochrome *bd* mutant. Furthermore, the *arcA/B* mutant displays decreased motility. The motility assay must be repeated, but preliminary results suggest that ArcAB regulates the ability of cytochrome *bd* to form biofilm. Future work should be to create a *hns* mutant and test it for its effect on biofilm formation and motility. In addition, the entire mutant panel (Δ*cydAB*, Δ*arcA*Δ*arcB*, Δ*fnr*, and Δ*hns*) should be tested for biofilm formation under hypoxic and anoxic conditions.

In addition to testing the known regulators of *cydABX*, subpopulations distinct from the parent population were observed in the *cydAB* colony biofilms after the third day of growth, and the genetic differences in these subpopulations should be investigated. These apparent spontaneous suppressor mutations are especially apparent on YESCA-CR plates, with white, mucoid subpopulations growing on top of areas that took up CR dye and were more rugose. **Figure 40** shows a representative comparison of UTI89 parent and Δ*cydAB* grown on YESCA-CR over time. Genomic DNA from the subpopulations were isolated from 20 different mutant colonies and sent for whole genome sequencing (WGS). The resulting genomic data can be mined to identify single nucleotide polymorphisms as well as insertions or deletions. Results of the identified genes with mutations can be further studied to elucidate why such mutations may arise. For example, without the cytochrome *bd* gene, these bacteria may be in a permanent state of stress response and alter other genes to help produce enough energy and resources to survive. Such genes that may be implicated include the regulators of *cydABX* and the master regulator of stress response *rpoS*, as well as *oxyR* and *soxR* that are involved with response to oxidative stress. Additional genes

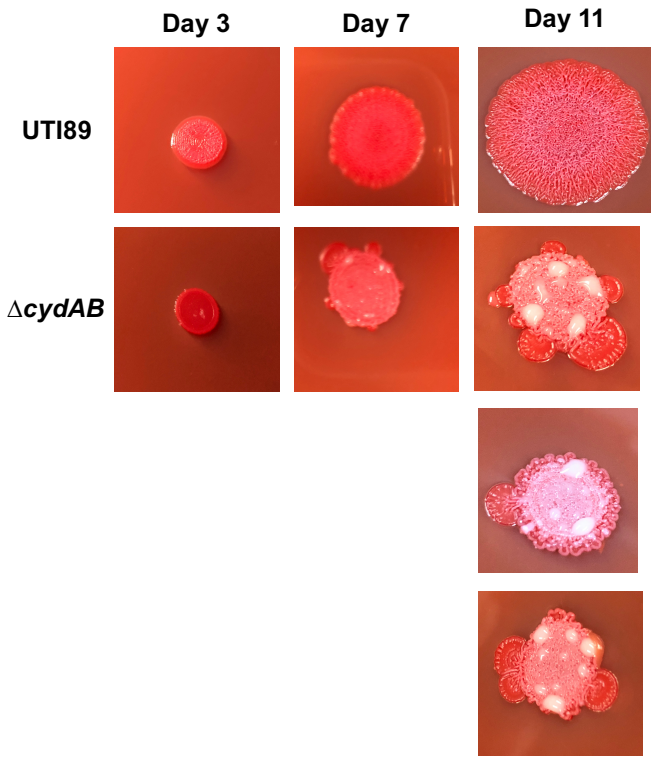

Figure 40. Spontaneous suppressor mutants arise in mature cytochrome *bd* mutant colony biofilms. Images show colony biofilms grown on YESCA-CR agar over time. At day 7, the cytochrome oxidase mutant displays subpopulations. By day 11, more subpopulations have emerged, including some that no longer uptake CR dye.

that may be implicated in these subpopulations are those involved in ECM production, including PDEs and diguanylate cyclases that control c-di-GMP levels, the master regulator of curli production *csgD*, and cellulose production *bcsA* and *bcsB* that important to biofilm formation and shown to be altered in response to the switch between motile and biofilm states (75).

Target cytochrome bd for therapeutics

Cytochrome *bd* deletion mutant disrupts biofilm architecture and in turn sensitizes the biofilm to antibiotics, making cytochrome oxidase an ideal therapeutic target. Naturally occurring inhibitors against cytochrome oxidases *bo* and *bd* have been discovered (288), and three of these compounds, including Ilicicolin ß (LL-Z1272ß), have been synthesized by the Vanderbilt Institute for Chemical Biology. We hypothesize that the inhibitors will be most potent in combination with antibiotics. Others in the lab are working to characterize these inhibitors, but we preliminarily tested Ilicicolin ß in combination with trimethoprim/sulfamethoxazole, an antibiotic frequently prescribed for UTIs in a murine model (**Figure 41**). Initial results suggest that the inhibitor in combination with antibiotic decreases colonization of the kidney in more mice in the UTI89+Combo than the UTI89+antibiotic alone. Mice were infected with bacteria in the presence of PBS vehicle, Ilicicolin ß inhibitor (100μM), antibiotics (54μg/mL trimethoprim, 270μg/mL sulfamethoxazole), or combination of antibiotics and inhibitor. Mice treated with inhibitor, antibiotic, or combination were given antibiotic added to water at 24 hours post infection for 48 hours. At 72 hours post infection, mice were sacrificed and bladders and kidneys were harvested and homogenized for CFU

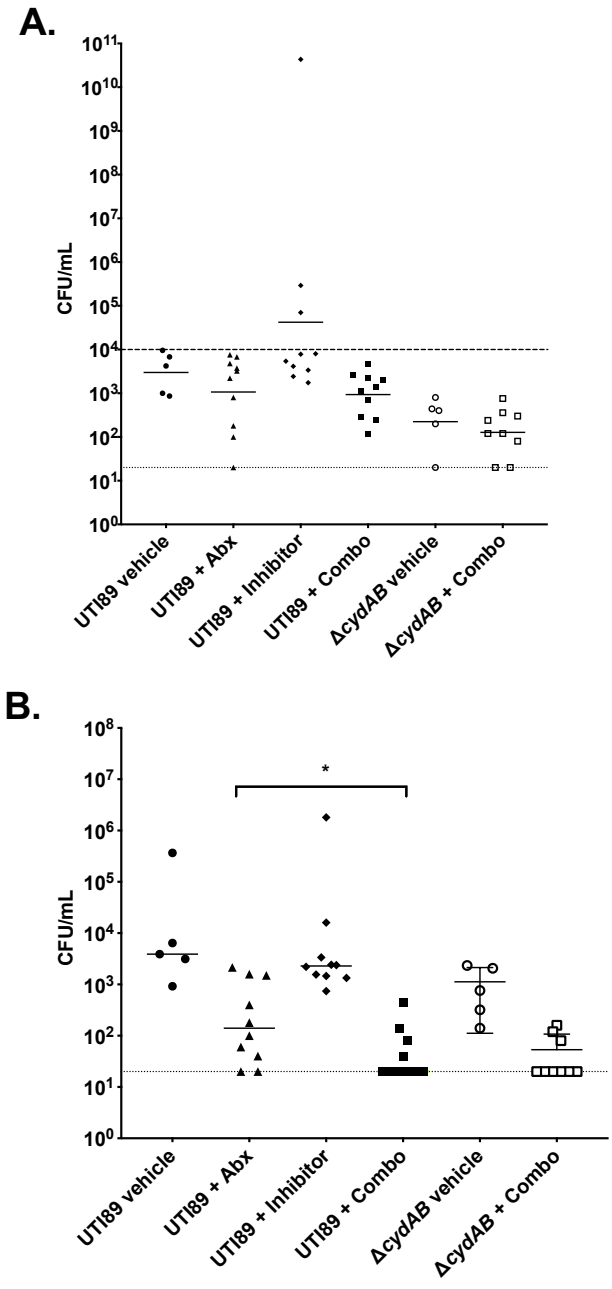

Figure 41. Bladder and kidney CFU of mice treated with cytochrome inhibitor and/or antibiotics. A. Bladder titers were obtained from mice infected with UTI89 or Δ*cydAB* and one of the following: PBS vehicle, antibiotic alone, inhibitor alone, or a combination of antibiotic and inhibitor. **B.** Kidney titers were obtained from mice infected with UTI89 or Δ*cydAB* and one of the following: PBS vehicle, antibiotic alone, inhibitor alone, or a combination of antibiotic and inhibitor. Each point represents a mouse. Statistical analysis was performed in GraphPad Prism using a two-tailed Mann-Whitney test. Line represents geometric mean. * $p < 0.05$.

enumeration. After biochemical characterization and optimal concentrations are determined through *in vitro* models such as colony biofilms and bladder cell culture, the inhibitor and antibiotic combination can be tested in both acute and chronic murine models.

One of the most feasible applications of this family of inhibitor may be in catheter-associated UTI. As biochemical characterization of the inhibitors is continued, a flow system catheter model should be optimized utilizing expertise of and previous studies by the Stewart and James labs at Montana State University Center for Biofilm Engineering (289). Efficacy of the inhibitors should be tested on catheters with preformed biofilms with inhibitor and antibiotic dissolved in urine, as well as catheters pre-coated with inhibitor, biofilm formed and then treated with antibiotic. If any of the applications of the inhibitors proves successful both *in vitro* and *in vivo*, the inhibitors should be considered for clinical trials.

Identify other oxygen-dependent regulators of biofilm formation

To find additional oxygen-dependent regulators of biofilm formation, a transposon library with 6x coverage in UTI89 was created. The library creation and screening is detailed in **Appendix A**. Biofilm formation by 96-well crystal violet assay was tested under 21%, 4%, and 0% oxygen for 2,208 mutants (23 96-well plates) to date. Of these, 57 mutants of interest arose with increased biofilm formation under at least one oxygen concentration tested (**Table 6**). Of these, only transposon mutant Tn 11-B5 has undergone secondary crystal violet biofilm screening at 21% and 4% oxygen and been identified as a transposon insertion in *clpX* (**Figure 42A-B**). Furthermore, confocal laser

Tn Plate #	Position #	21% oxygen	p-value	4% oxygen	p-value	0% oxygen
1	D9	+	0.0098	ns		
1	D10	+	0.001	ns		
1	F8	ns		+	<.0001	
5	A2	ns		+	<.0001	
5	A4	ns		+	0.0074	
5	B1	ns		+	<.0001	
6	A1	ns		ns		+
7	A3	+	0.0093			
8	A1	+	0.0397			
8	H11	+	<.0001			
9	G12	+	0.0042	ns		
11	B5	+	<.0001	+	<.0001	
12	E3	ns		+	<.0001	
12	E11	ns		+	<.0001	
15	A7	ns		+	0.0064	
15	G12	ns		+	0.0012	
16	C1	ns		+	<.0001	
16	E1	ns		+	0.004	
16	H12	+	0.0032	ns		
17	B7	+	0.0025	ns		
17	C12	+	<.0001	ns		
17	D12	+	0.0096	ns		
17	H3	+	<.0001	ns		
17	H9	+	0.0034	ns		
18	D3	+	<.0001	+	<.0001	
22	H6	+	<.0001			
23	B9	+	0.0274			
23	C12	+	<.0001			
23	D12	+	0.0245			
23	E11	+	0.0053			
23	F11	+	0.0069			
23	G12	+	<.0001			
23	H8	+	<.0001			
23	H9	+	0.0025			
23	H10	+	0.0014			
23	H11	+	0.0475			
23	H12	+	<.0001			
8	B5	+	<.0001			
8	B7			+	<.0001	
8	B9	+	0.0013			
8	B11	+	<.0001			
8	B12	+	<.0001	+	<.0001	
8	C12	+	0.0079			
8	D3	+	<.0001			
8	D4	+	<.0001			
8	D6	+	0.0053			
8	D10	+	<.0001			
8	D11	+	<.0001			
8	D12	+	<.0001	+	0.0007	
8	E2	+	<.0001			
8	E11	+	<.0001			
8	E12	+	<.0001			
8	F11	+	<.0001			
8	G6	+	0.04			
8	G8	+	<.0001			
8	G10	+	0.0017			
8	H12	+	<.0001	+	<.0001	

Table 6. Transposon mutants of interest for biofilm formation by p-value < 0.05. Statistical significance determined by one-way ANOVA compared to UTI89 *HK::kan*^{r}. Colors denote the following: blue- increased at 21% oxygen, purple- increased at 4% oxygen, orange- increased at 0% oxygen, green- increased under both 21% and 4% oxygen.

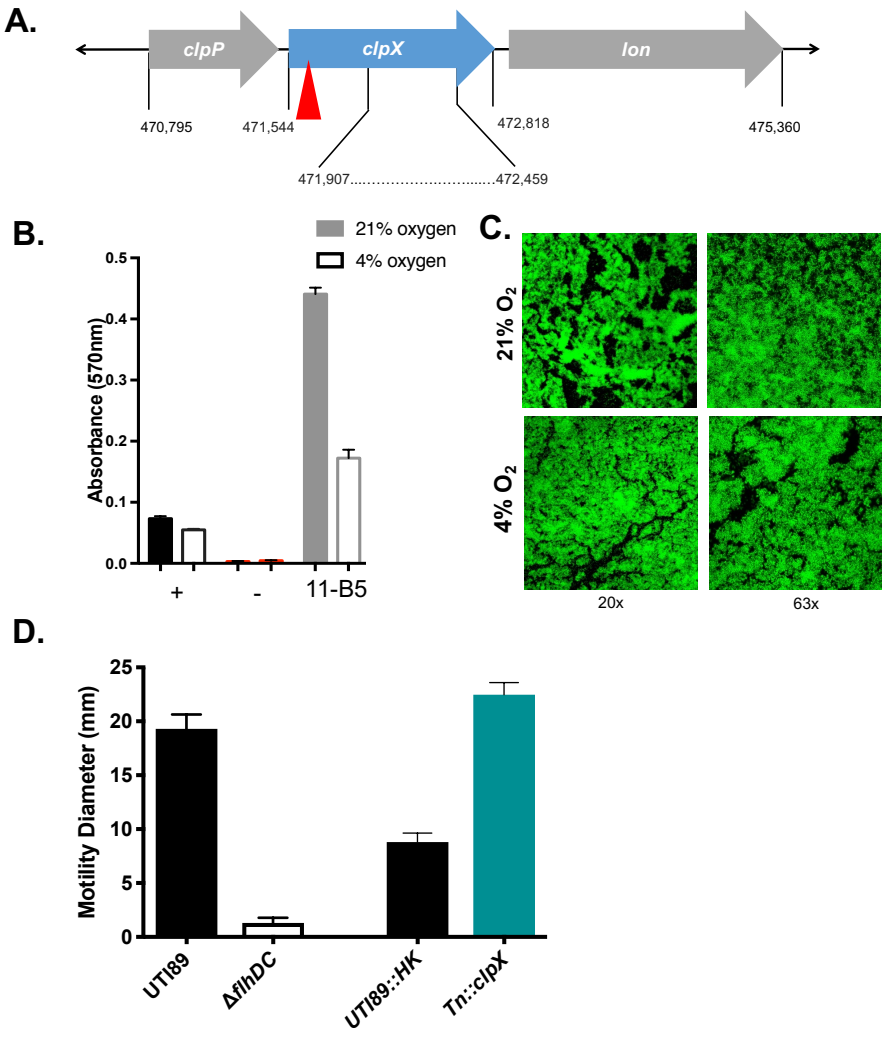

Figure 42. Transposon screen identified *clpX* mutant exhibits increased biofilm formation. A. Transposon insertion mapped to *clpX* as described in **Appendix A. B.** Secondary 96-well crystal violet biofilm assay of *Tn::clpX*. +, positive control UTI89 HK::*kan*^{r} ; -, negative control Δ*fimA-H::kan*^{r}. **C.** Representative confocal laser scanning microscopy images of *Tn::clpX* biofilms grown on PVC slides grown at 21% or 4% oxygen as described in **Chapter III.** **D.** Motility assay shows *Tn::clpX* motility as described in **Chapter IV.**

scanning microscopy of *Tn::clpX* to look at biofilm at the microscopic level was performed, and data show areas with tall peaks are evident, especially under atmospheric conditions (**Figure 42C**). ClpX binds and unfolds substrates as part of the ClpXP ATP-dependent protease and has been shown to increase biofilm formation in K12 *E. coli*, but the mechanism is unknown (290, 291). Intriguingly, ClpXP can inhibit sigma factor S (*rpoS*), which acts as the master regulator of stress response in *E. coli*, as well as inhibit flagella to disrupt motility (75). The *Tn::clpX* does not display altered motility compared to wild-type UTI89 under the conditions tested (**Figure 42D**). Future work should include further characterization of the role of *clpX* in the sigma factor S stress response pathway that regulates curli and cellulose, major constituents of the biofilm ECM (75).

Though only one transposon insertion mutant implicated in biofilm formation has been identified to date, this tool shows the power of identifying oxygen-dependent factors involved in biofilm formation. Several known factors of biofilm formation will surface in future work with the transposon library, such as genes involved in the production and regulation of ECM components, however new factors may be identified as well. Another avenue of this biofilm screen is to identify transposon mutants that form biofilm under anoxic conditions to identify factors that may promote surface-attachment and biofilm formation in an anoxic niche such as the gut.

Develop diagnostic assay to differentiate asymptomatic from symptomatic UTI

Chapter IV highlights exciting preliminary data showing that metabolic differences exist between asymptomatic and symptomatic urine-associated *E. coli*

isolates. An improved diagnostic approach for distinguishing ASB from cystitis would be ground-breaking, since current methods rely on patient symptoms and the presence of bacteria in the urine. Future work will be two-fold: (1) understand the biological role of each pathway identified and (2) identify and validate a metabolic profile to create a diagnostic test that can be used in the clinical microbiology labs. The biological role of identified metabolic pathways can be studied through genetic manipulation of the bacterial strains and studied both *in vitro* and *in vivo* as detailed in **Chapter IV**. As the pathways are identified, urine specimens can be collected for targeted mass spectrometry against specific metabolites to validate these initial findings as described in **Chapter IV**.

In addition to the metabolic inventory shedding light on differences between asymptomatic and symptomatic isolates, I hypothesize that genetic differences are driving the metabolic alterations in the asymptomatic strains compared to the symptomatic strains. To address this, we have isolated genomic DNA from 50 select isolates and collected whole genome sequences (WGS) (**Table 7**). Genomic DNA was extracted using the UltraClean Microbial DNA Isolation Kit (MOBIO) in accordance with the manufacturer's protocol from 5 mL of overnight culture. DNA concentrations were quantified using NanoDrop 200C Spectrophotometer (ThermoScientific). Samples were subjected to WGS on Illumina NovaSeq6000 by VUMC Vanderbilt Technologies for Advanced Genomics (VANTAGE). Data will be mined for single nucleotide polymorphisms (SNPs) in pathways that are identified as altered in the metabolomics data, as well as to compare putative virulence factors. Ideally, there will be repeat changes across several ASB strains and different repeat changes in the cystitis strains.

The overarching goal of this is to overlay the genetic information with metabolic information to identify the strongest predictive signature to differentiate asymptomatic-causing from symptomatic-causing isolates. If this is possible, it will change clinical diagnostics for UTI, overcoming a challenge that has been present for several decades.

VUTI isolate	Associated Infectio
115	Pyleonephritis
118	ASB
126	Cystitis
134	Cystitis
135	Cystitis
139	ASB
142	ASB
146	Cystitis
150	Pyleonephritis
159	Bacteremia
166	ASB
167	ASB
169	Pyleonephritis
170	ASB
174	Cystitis
180	CYstitis
182	Cystitis
191	Bacteremia
199	Pyleonephritis
202	Cystitis
204	Cystitis
205	Bacteremia
220	ASB
222	Pyleonephritis
223	Cystitis
226	ASB
229	Pyleonephritis
244	Cystitis
245	ASB
259	ASB
263	Cystitis
265	Cystitis
279	ASB
282	Cystitis
283	Unclear
284	ASB
290	Cystitis
295	ASB
300	Cystitis
308	Pyleonephritis
320	Cystitis
325	Cystitis
338	Cystitis
349	Cystitis
364	Cystitis
366	Cystitis
367	Cystitis
397	Pyleonephritis
410	Cystitis
412	Cystitis

Table 7. List of VUTI isolates sequenced.

APPENDIX A

UTI89 TRANSPOSON LIBRARY AND SUBSQUENT SCREENING

UTI89 Transposon Library Construction & Storage

Super-electro-competent cell preparation and subsequent transposon mutagenesis

Super-electro-competent cells were prepared as previously described (212). Briefly, an overnight culture of UTI89 in no-salt LB grown at 37 °C shaking was diluted to OD_{600} = 0.05 in 10 mL no-salt LB and incubated at 37 °C shaking until reaching the exponential growth phase (OD_{600} = 0.3-0.6). This culture was again diluted to OD_{600} = 0.05 in 50 mL no-salt LB in a 250-mL flask and incubated under conditions described above until OD_{600} = 0.3-0.6. The flask was chilled in a sodium chloride ice bath for 30 minutes on a rocker. Chilled cells were transferred to a 50-mL conical tube and centrifuged at 4,000 RPM for 7 minutes at 4 °C (the conditions for all subsequent centrifugations in this protocol). The cell pellet was re-suspended in 50 mL of chilled 20% 3-n-morpholinopropane-1-sulfonic acid-glycerol (MOPS-glycerol) buffer. The suspension was centrifuged and the resulting pellet was re-suspended in 25 mL chilled 10% glycerol. Cells were centrifuged and the pellet was re-suspended in 12.5 mL MOPS-glycerol. The suspension was centrifuged and the pellet was re-suspended in 300µL of 10% glycerol. Competent cells were stored at -80°C in 50 µL aliquots.

The schematic in **Figure 43A** depicts the steps transposon library construction. One aliquot of super-electro-competent cells was transformed with 66 ng of the EZ-Tn5™ <R6Kγ*ori*/KAN-2>Tnp Transposome™ (Epicentre) according to the manufacturer's instructions. Electroporated cells were recovered in 1 mL of super optimal broth with catabolite repression (SOC: 0.5% yeast extract, 2% tryptone, 10 mM

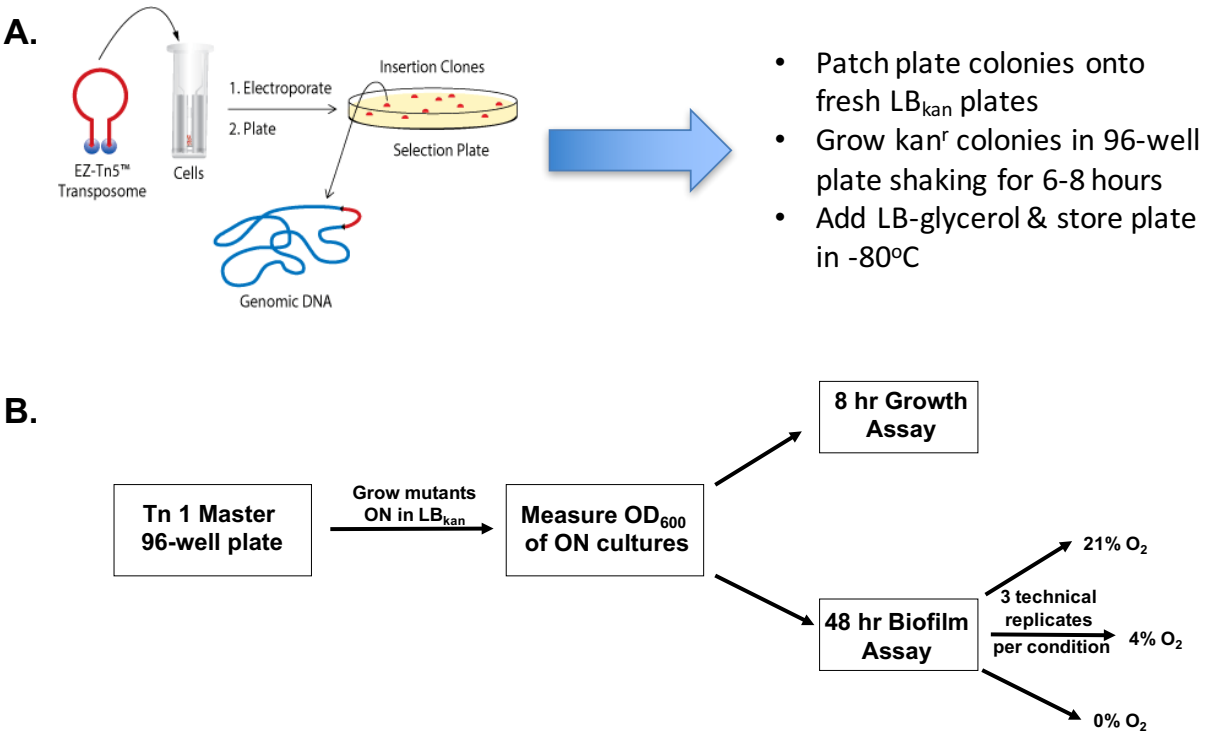

Figure 43. Transposon library workflow. A. Pictorially describes transposon insertion and selecting for transposon mutants (insertion clones), as well as storing of the library. Schematic from http://www.epibio.com/applications/tn5-transposon-mutagenesis/introduction -to-ez-tn5-transposomes-and-in-vivo-transposomics. **B.** After construction, each 96-well plate will be screened for end-point optical density from overnight growth, growth by optical density over 8 hours, 48 hours biofilm assays, as well as phenotypic characteristics on agar plates.

sodium chloride, 2.5 mM potassium chloride, 10 mM magnesium chloride, 10 mM magnesium sulfate, and 20 mM glucose) at 37°C shaking for 60 minutes. The culture was diluted 1:10,000 and plated in 100 μl aliquots on LB agar plates supplemented with kanamycin (kan, final concentration = 50 μg/mL) to select for transposon-containing mutants. Plates were incubated overnight at 30°C for about 18 hours. Transformants were patch plated onto LB+kan plates to confirm transposon incorporation. Each patch was then inoculated into 100μL of LB+kan in a single well of a 96-well plate and grown at 37°C for 6-8 hours in 96-well plates. At this point, LB-glycerol was added to each well of the 96-well plate to create freezer stocks. Each plate was sealed with sterile sealing films and stored at -80°C. I stored 320 96-well plates of transposon mutants, which, once growth defects are subtracted, is roughly 30,000 transposon mutants. Since the UTI89 genome contains about 5,500 genes, this represents 6x coverage of the genome.

Transposon library screening

The schematic in **Figure 43B** outlines the assays performed to each 96-well transposon plate.

Overnight culture

Each transposon (Tn) 96-well plate freezer stock is used to inoculate 100uL of LB+kan in a fresh 96-well plate via 96-well replicator. These overnight cultures are grown at 37 °C shaking for roughly 16 hours. The OD_{600} of the overnight cultures is measured and recorded to determine any growth defects. The following overnight

cultures used as controls should also be set up in 5 mL LB+kan: UTI89 HK::*kan*^{r} ; UTI89 Δ*fimA-H::kan*^{r}; MC1061/pANT4; MG1655/pANT4.

Growth curve

A 96-well flat bottom plate with 100 µL of LB +Kan is prepped for the growth curve. Using the 12-well multichannel pipet multi-channel pipet, 5µL of each overnight culture are used to seed the same well coordinates as in the overnight cultures for 8-hour growth curves to detect growth defects using Molecular Devices Spectramax plate reader (set to incubate at 37 °C shaking and measure OD_{600} at 15-minute intervals). Screenshot of the growth curve is taken and OD_{600} over time exported.

Biofilm formation 96-well crystal violet assay

Twelve 96-well round bottom PVC plates with 100 µL of LB +Kan are prepped for the growth curve. Using the 12-well multichannel pipet multi-channel pipet, 5µL of each overnight culture are used to seed the same well coordinates as in the overnight cultures in 9 of the 12 plates. The remaining 3 plates are control plates with the following layout: columns 1 and 12 blank media, columns 2-6 UTI89 Δ*fimA-H::kan*^{r} (negative control), columns 7-11 UTI89 HK::*kan*^{r} (positive control). Four (3 Tn, 1 control) plates are then placed at either 21%, 4%, or 0% oxygen for 48 hours. At the 48 hour time point, image one control plate and one Tn plate from each oxygen concentration to visualize any growth defects. Then, rinse and stain biofilms with crystal violet as previously described (292). Image one Tn plate and one control plate from each oxygen condition after crystal violet staining. Disrupt crystal violet stain by adding 150 µL of

acetic acid to each well and transfer 100 µL to a new flat-bottom 96-well plate. Read the absorbance at 570nm of each plate and record. The absorbance values are averaged for each Tn mutant under each oxygen condition and graphed against the positive and negative controls to identify mutants that alter biofilm formation in response to oxygen.

Phenotypic agar plates

Using a 96-well replicator, different types agar plates were spotted with the transposon mutants, incubated overnight at 37 °C and imaged the next day. When spotting the plates, insert 96-well replicator into the overnight plate and gently swirl in wells. Then, carefully place on the agar plates and let sit for a few seconds before removing. It is important to touch down straight and pick up straight in order to keep strains separated. Lastly, ensure that cultures are fully dry on the plates before placing the plates upside down to incubate overnight. Controls were also plated at the bottom of each agar plate. First, LB+Kan serves as a growth control and includes positive and negative controls (UTI89 HK::*kan*^{r} and Δ*fimA-H::kan*^{r}, respectively). YESCA+Kan and YESCA-CR+Kan plates are proxies for cellulose and curli production that contribute to the extracellular matrix of biofilms and include positive and negative controls (UTI89 HK::*kan*^{r} and Δ*fimA-H::kan*^{r}, respectively). Mutants that do not uptake the CR dye are of particular interest.

Lastly, MacConkey+Kan, LB +Kan +X-gal, and LB +Kan +X-gal +Glucose are assessing metabolic activities of the Tn mutants. Another project in the lab is studying the difference between pathogens and non-pathogens in glucose utilization. This can be monitored by the activity of the *lac* operon, which can be monitored using a blue/white

screen. Against dogma, pathogens do not preferentially utilize glucose, which results in blue colonies in the presence of X-gal, even when glucose is present. This screen can help to identify genes that may be responsible for this phenomenon in pathogens. UTI89 HK::*kan*^{r} displays blue colonies in both LB +Kan +X-gal and LB +Kan +X-gal +glucose, while the non-pathogen MG1655/pANT4 is blue on X-gal and white X-gal +glucose in. The non-pathogen MC1061/pANT4 does not have a functional *lac* operon, so it appears white on both plates. Tn mutants that follow the MG1655 phenotype are of interest. MacConkey agar remains pink when lactose is fermented and turns yellow when lactose is not fermented. *E. coli* normally ferments lactose, so non-fermenters are of interest.

Agar Recipes for Transposon Library Screen

All recipes below are for 0.5L total volume and are to be poured in 100mmx15mm petri dishes to allow use of the 96-well microplate replicator.

LB + Kan Agar

- 12.5 g LB powder
- 7.5 g agar
- 500 mL water
- Autoclave
- Before pouring plates, add 0.5 mL Kan stock solution (50 mg/mL stock)

LB + Kan + X-gal Agar

- 12.5 g LB powder
- 7.5 g agar
- 500 mL water
- Autoclave
- Before pouring plates, add 0.5 mL Kan stock solution (50 mg/mL stock), 0.5 mL X-gal stock solution (20 mg/mL X-gal in dimethylformamide stock)

LB + Kan + X-gal + glucose Agar

- 12.5 g LB powder

- 7.5 g agar
- 500 mL water
- Autoclave
- Before pouring plates, add 0.5 mL Kan stock solution (50 mg/mL stock), 0.5 mL X-gal stock solution (20 mg/mL X-gal in dimethylformamide stock), 5 mL glucose stock solution (2M stock)

MacConkey agar Agar

- 25 g MacConkey agar mix
- 500 mL H2O
- Autoclave
- Before pouring plates, add 0.5 mL Kan stock solution (50 mg/mL stock)

1.2x YESCA Agar

- 6 g Casamino acids
- 0.6 g Yeast Extract
- 11 g agar
- 500 mL water
- Autoclave
- Before pouring plates, add 0.5 mL Kan stock solution (50 mg/mL stock)

1.2x YESCA-CR Agar

- 6 g Casamino acids
- 0.6 g Yeast Extract
- 11 g agar
- 500 mL water
- Autoclave
- Before pouring plates, Add 750 µL Congo Red Dye stock solution (40 mg/mL stock), 5 µL of Bromophenol Blue stock solution (10 mg/mL stock), 0.5 mL Kan stock solution (50 mg/mL stock)

Screening Results

To date, 2,208 mutants (23 96-well plates) have been screened. Of these 2,208 mutants, 62 have been removed from downstream analyses due to growth defects. Each plate has an “Info sheet” with all corresponding optical density reads, agar plate images, and CV biofilm formation images and graphs. Tn plate 4 info is below:

UTI89 – Tn Plate 4

1. Growth Defects

a) Overnight OD_{600}

	1	2	3	4	5	6	7	8	9	10	11	12
A	1.093	1.0029	1.113	1.1632	1.2371	1.0533	1.1235	1.1065	1.1103	1.0092	1.1144	0.0837
B	1.1881	1.1408	1.1323	1.3167	1.2423	1.2263	1.2257	1.2648	1.1324	1.1418	1.0845	1.0896
C	1.1572	1.1274	1.1697	1.0926	1.2096	1.1652	1.1725	1.2423	1.2298	1.1994	1.1235	1.0562
D	0.9154	1.1606	1.188	1.1549	1.1982	1.1913	1.183	1.2928	1.2144	1.1681	1.1082	1.0995
E	0.924	0.895	0.0879	1.1521	1.1635	1.1614	1.24	1.2051	1.1313	1.2083	1.1831	1.1911
F	0.0744	1.1566	1.0833	1.1271	1.0768	1.2003	1.2513	1.2123	1.1862	1.1343	1.1422	1.2067
G	1.2492	1.2308	1.1981	1.2275	1.1953	1.2382	1.2634	1.2722	1.2558	1.2775	1.2932	1.1929
H	1.2201	1.1302	1.1444	1.2965	1.2645	1.2743	1.2522	1.3168	1.3065	1.2632	1.2046	1.2128

- F1, E3, and A12 exhibited extreme growth defects

b) Growth Curves

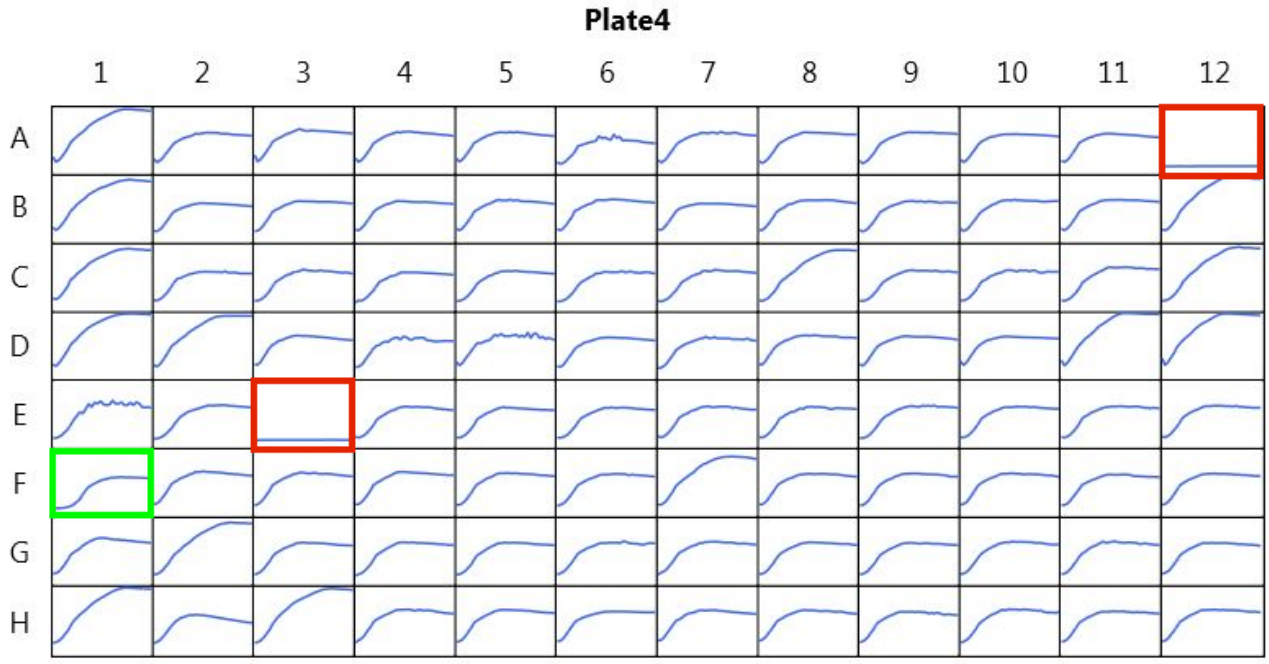

- E3 and A12 exhibited extreme growth defects
- F1 exhibited growth in the 8 hour growth curve but not in the overnight culture

2) Biofilm Characteristics in LB (surface-associated)

*These images are a representative of 3 replicates at each oxygen condition.

21% oxygen growth after 48 hours:

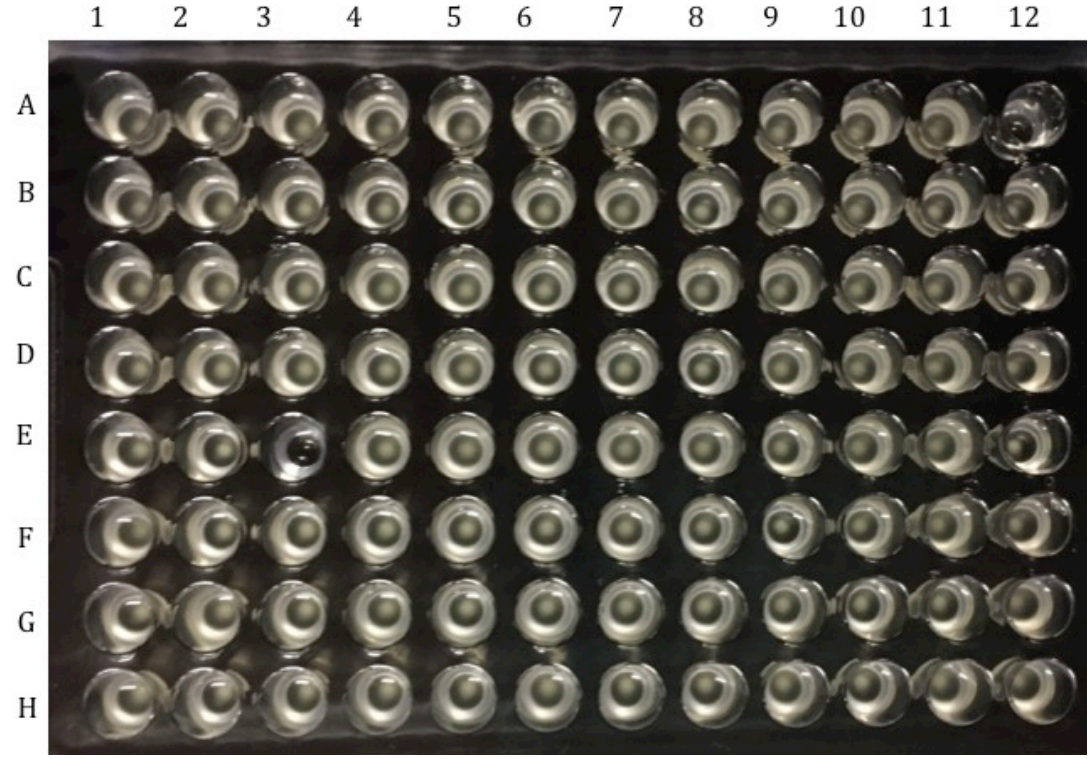

- No notes

21% oxygen CV stain:

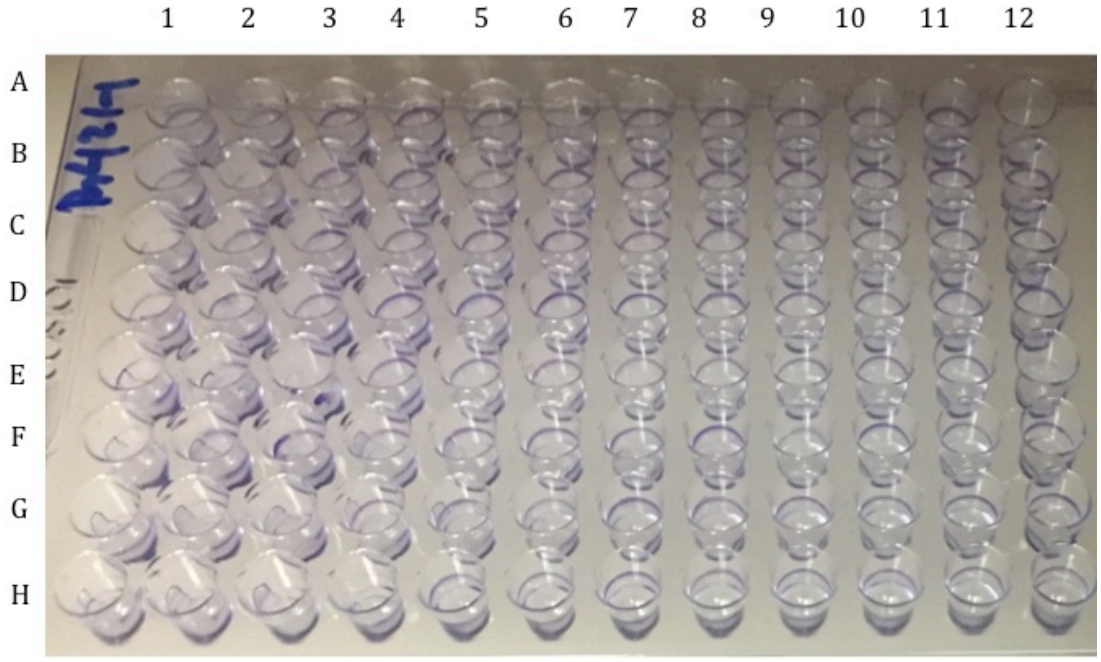

- No notes

4% oxygen growth after 48 hours:

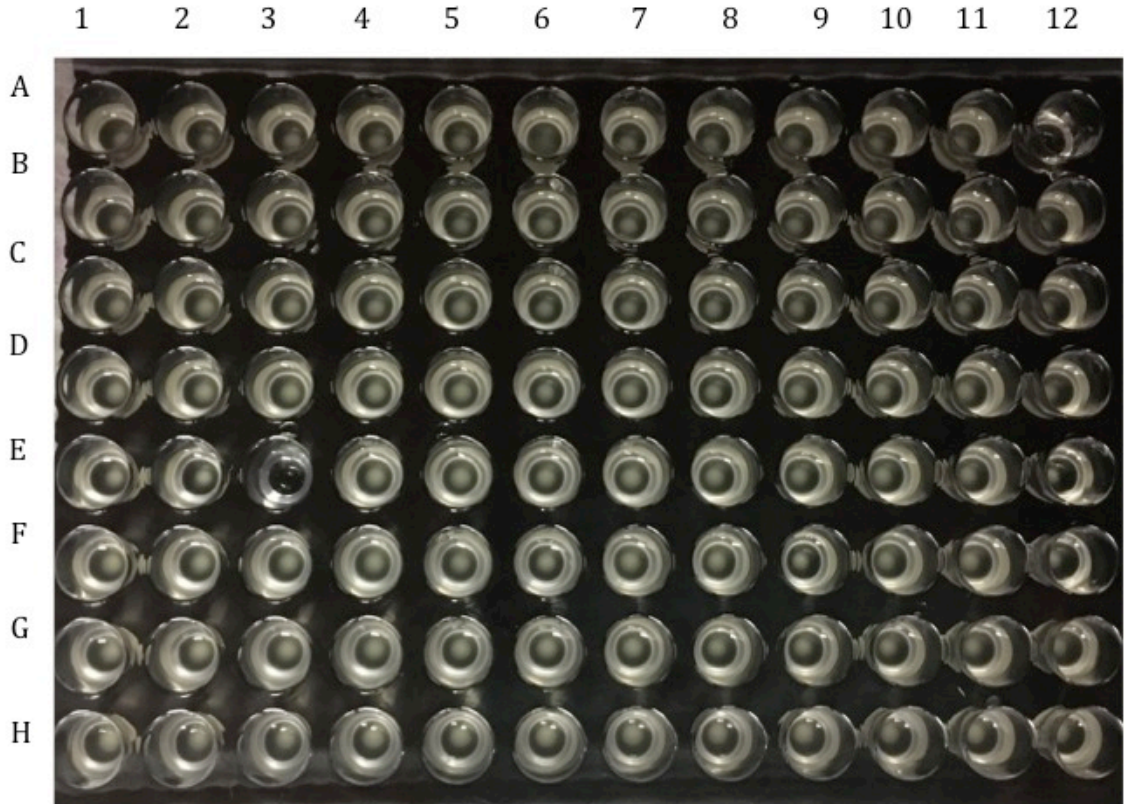

- No notes

4% oxygen CV stain:

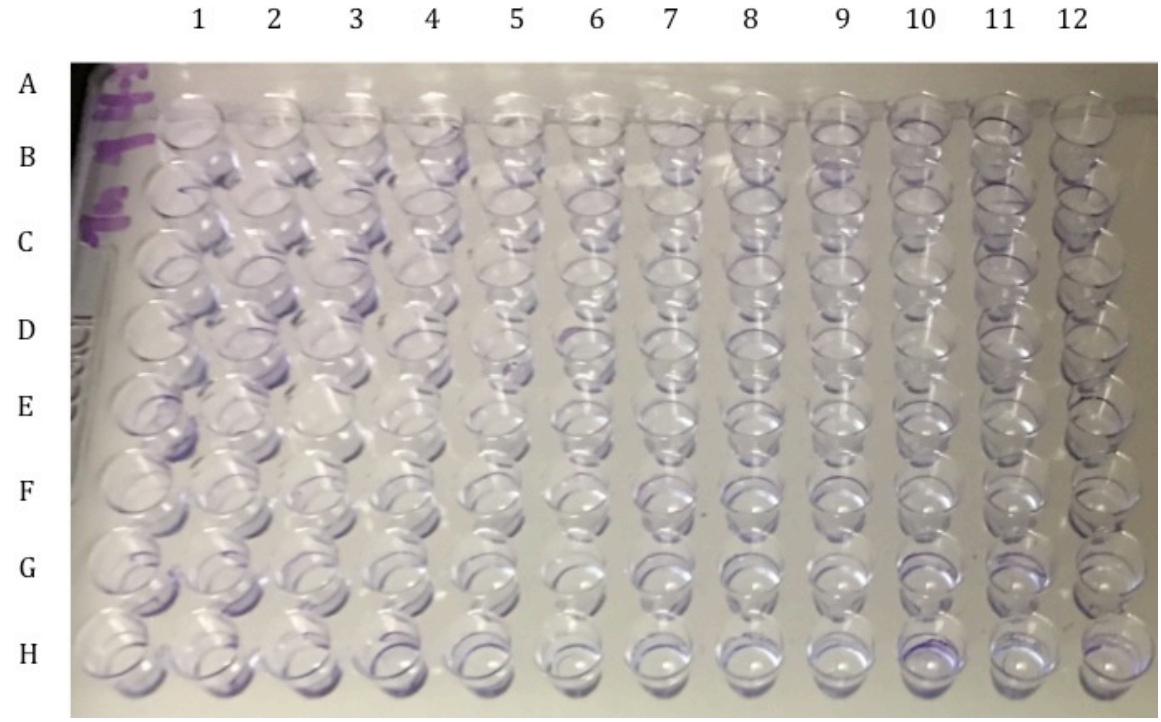

- No notes

0% oxygen growth after 48 hours:

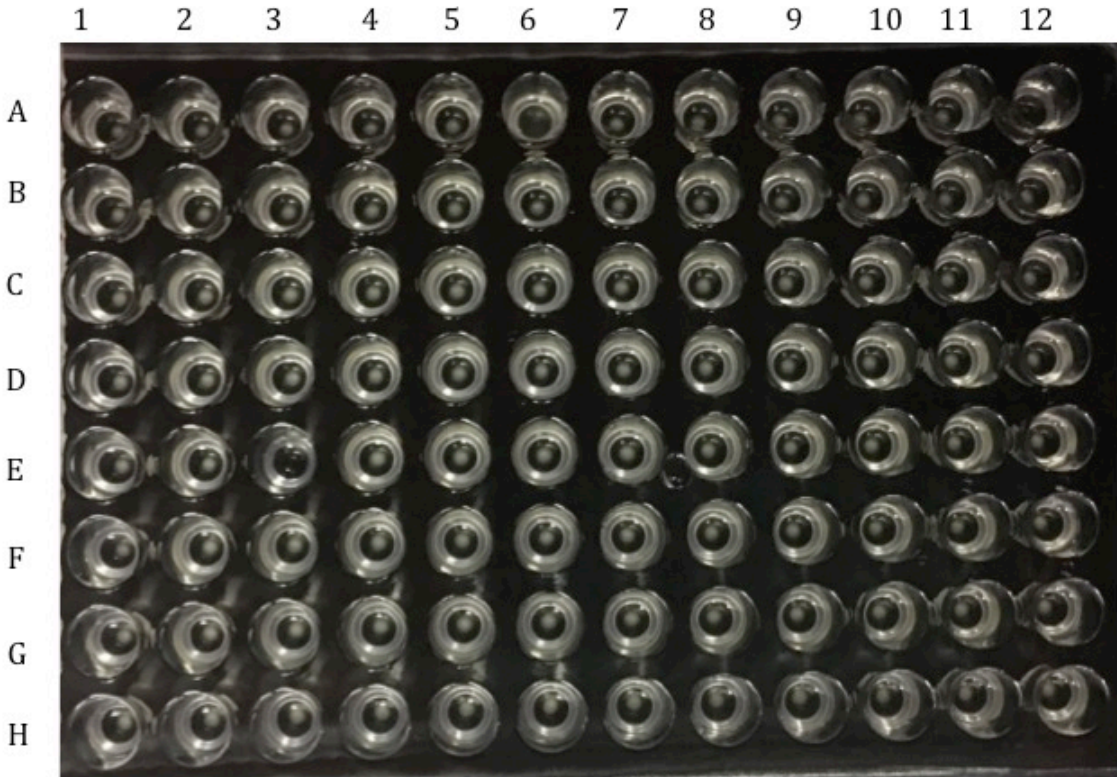

- No Notes

0% oxygen CV stain:

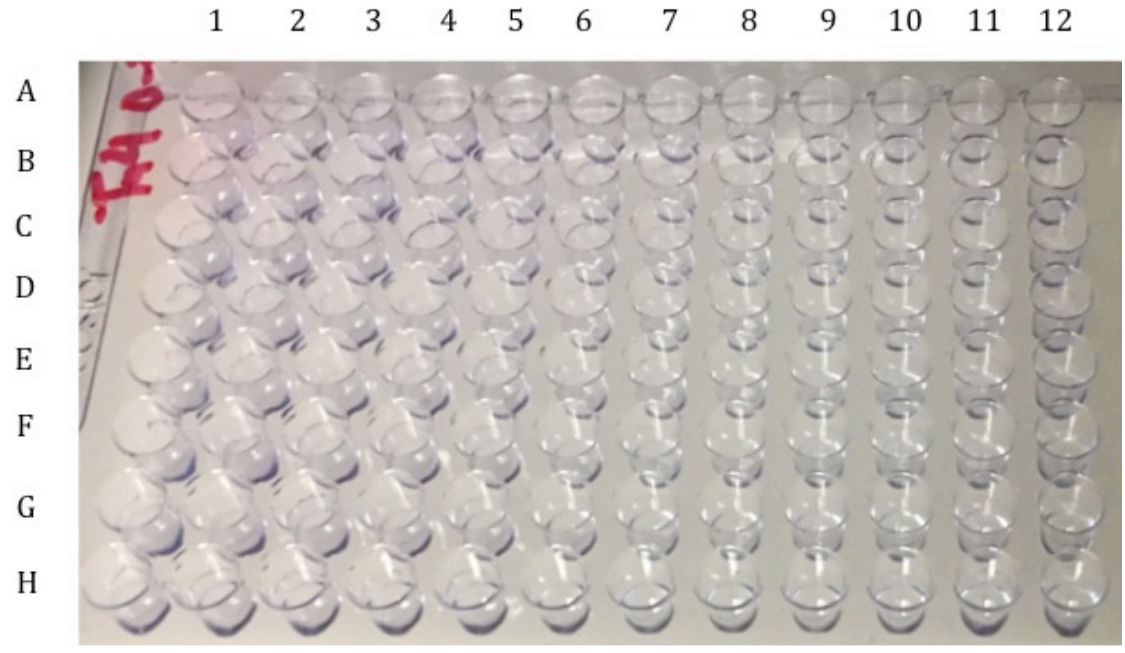

- No notes

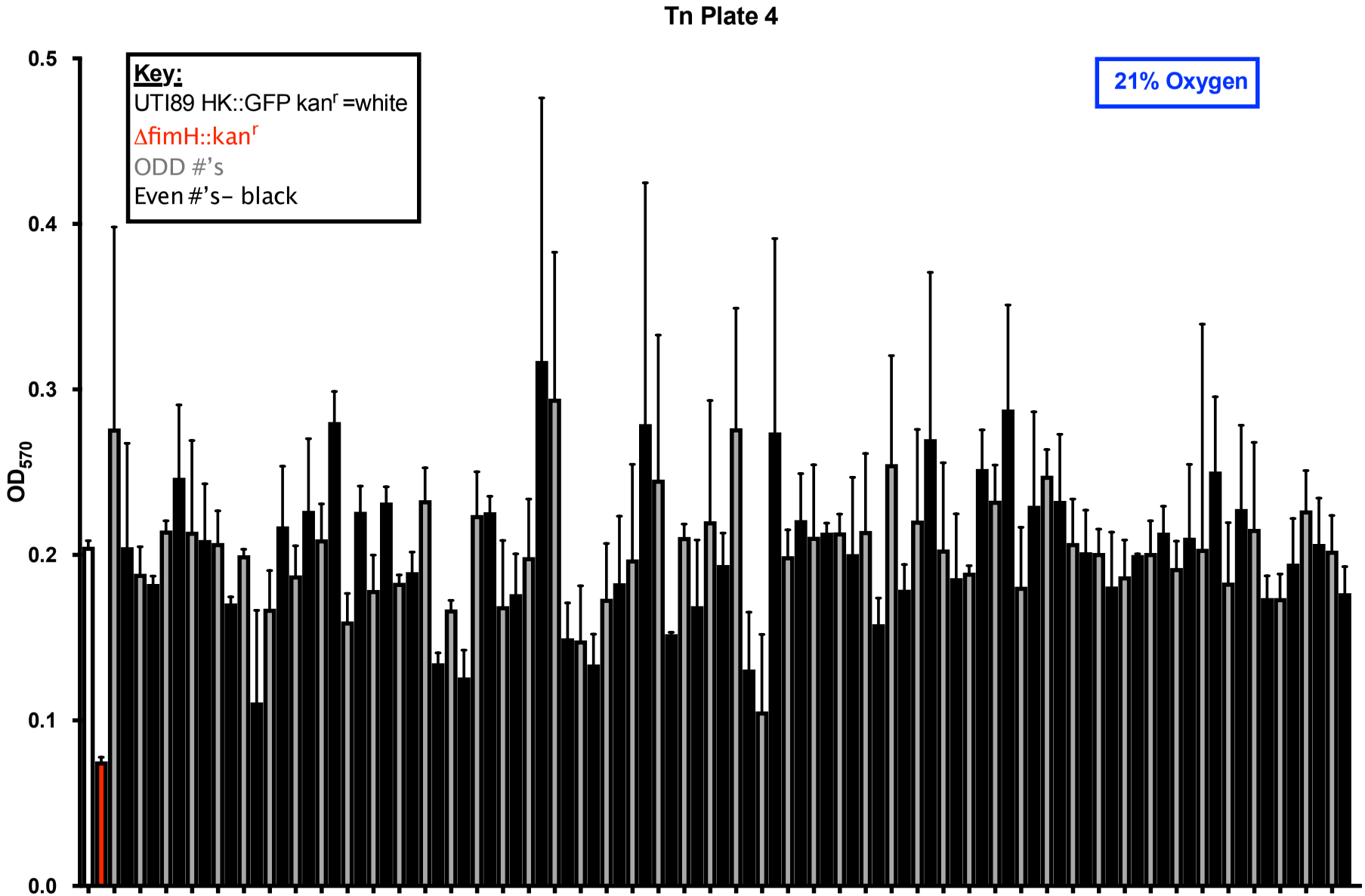
Tn Plate 4
Key:
UTI89 HK::GFP kan^r =white
ΔfimH::kan^r
ODD #'s
Even #'s- black
21% Oxygen
OD$_{570}$
0.5
0.4
0.3
0.2
0.1
0.0

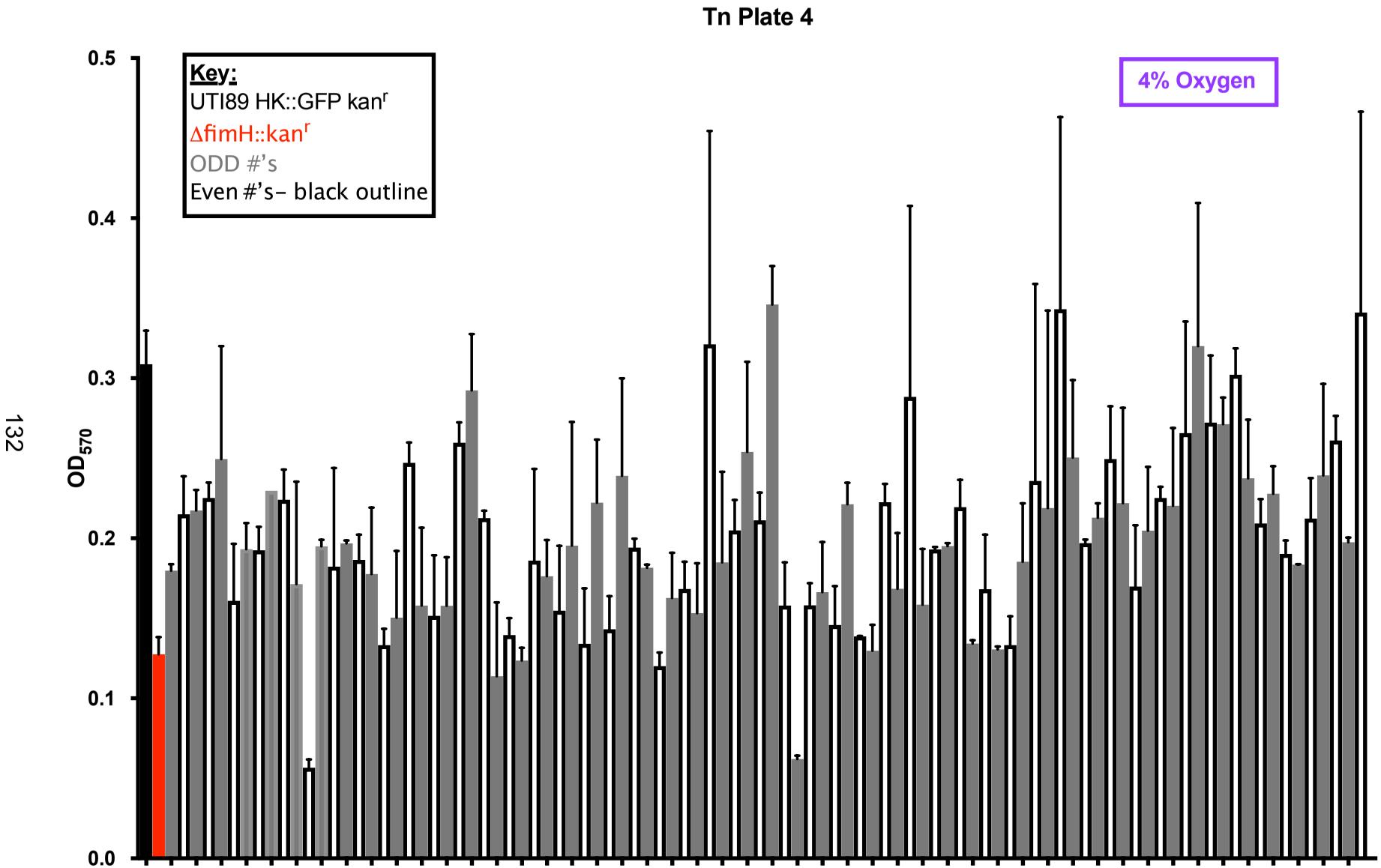
Tn Plate 4
Key:
UTI89 HK::GFP kanr
ΔfimH::kanr
ODD #'s
Even #'s- black outline
4% Oxygen
OD570
0.5
0.4
0.3
0.2
0.1
0.0

3) Colony Morphology and Properties

LB+ Kan:

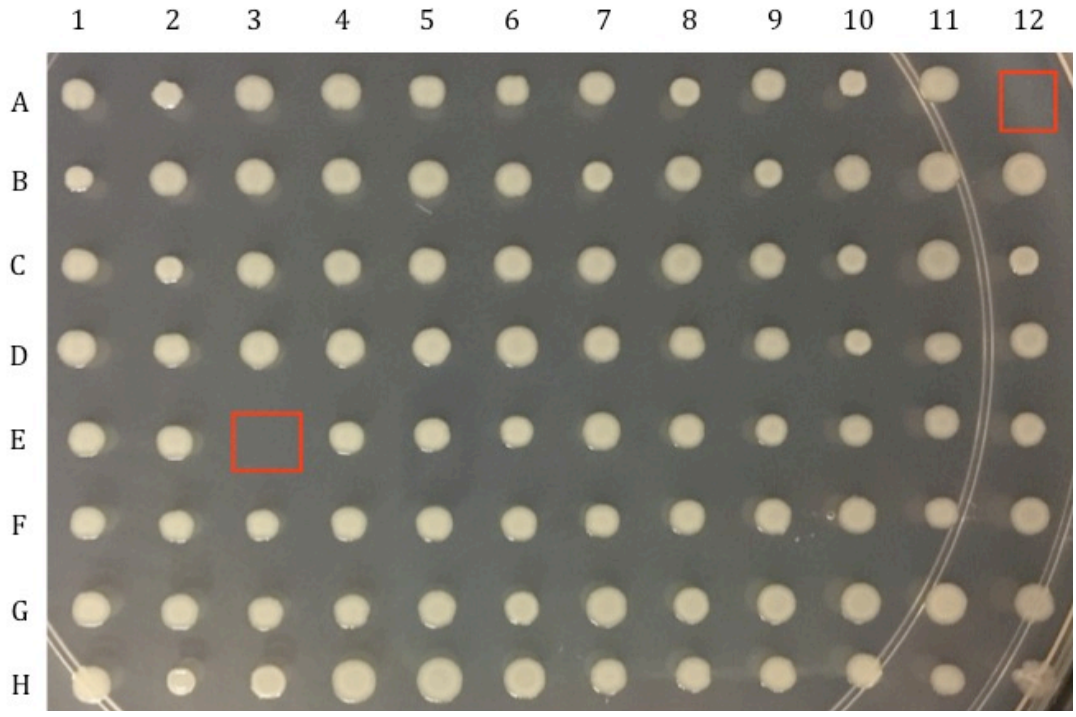

- E3 and A12 have growth defects

LB+ Kan + X-gal:

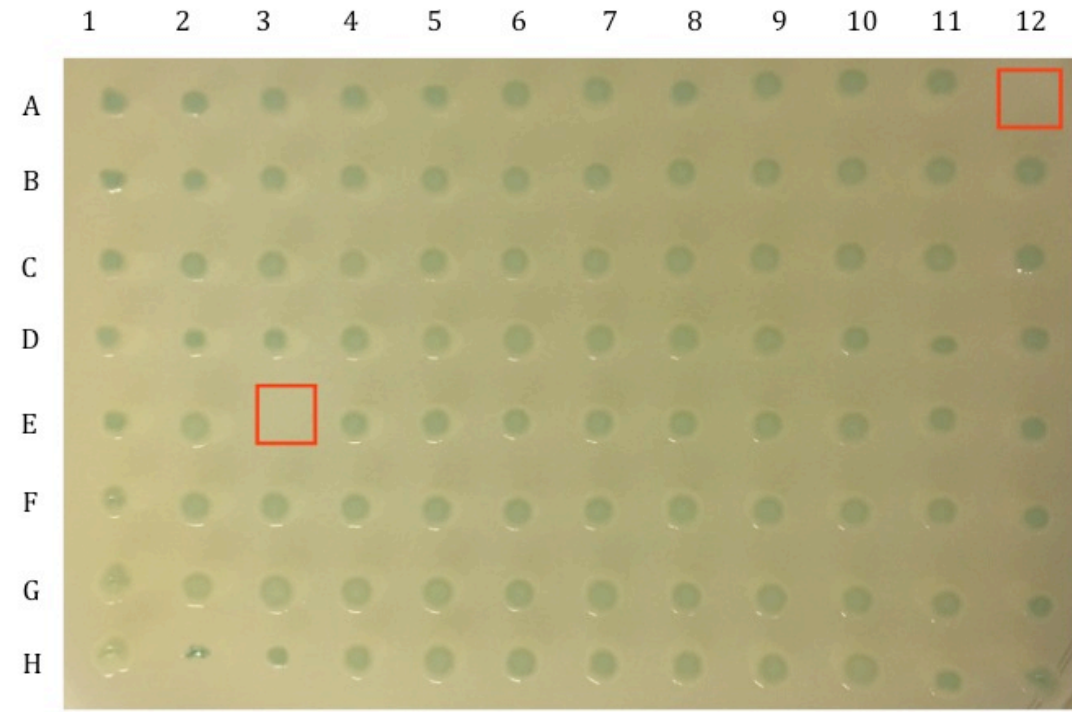

- E3 and A12 have growth defects

LB +Kan +X-gal +glu:

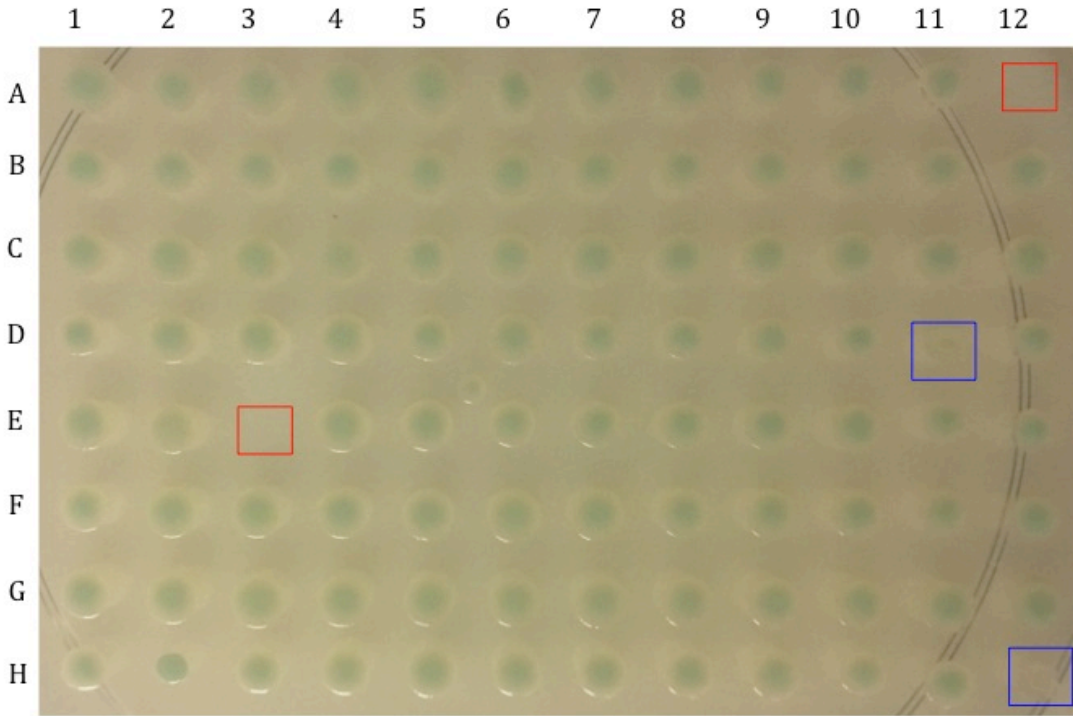

- E3 and A12 have growth defects
- D11 and H12 exhibit the white colony phenotype

MacConkey:

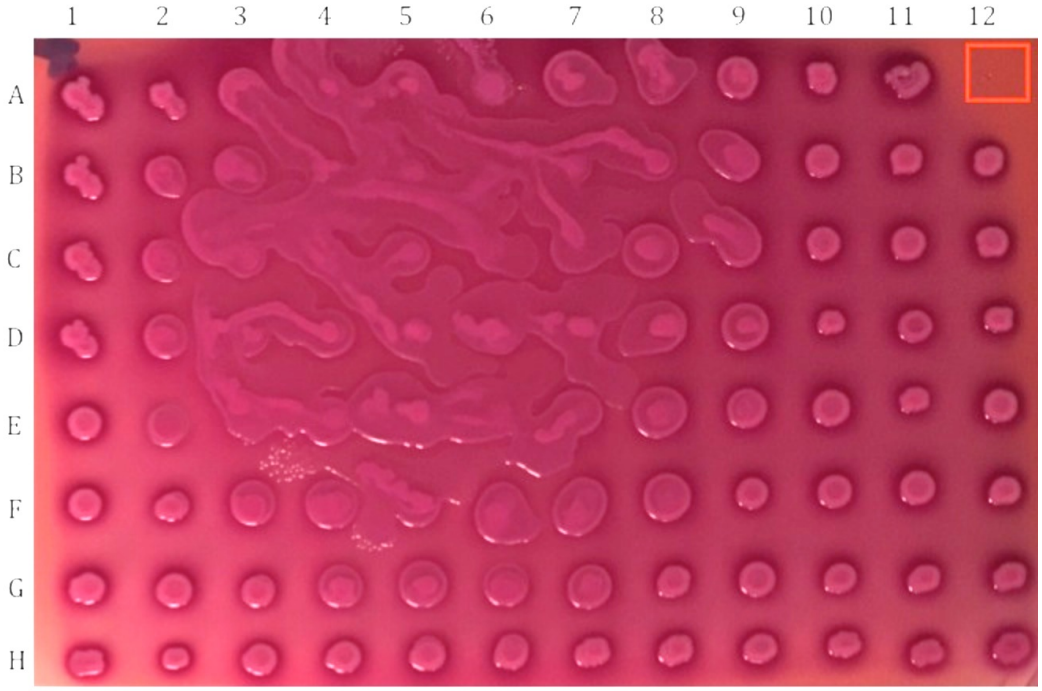

- Must repeat-smear renders E3 growth defect indeterminate
- A12 has a growth defect

YESCA

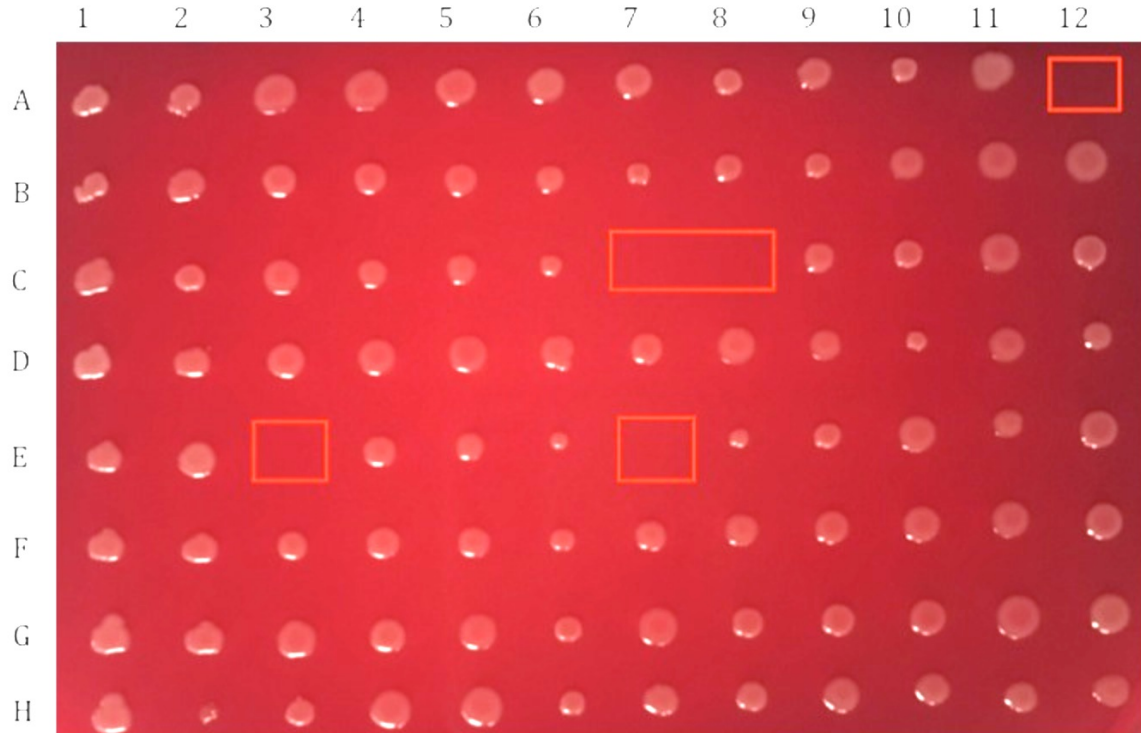

- E3, C7, C8, E7 and A12 have growth defects

YESCA +CR:

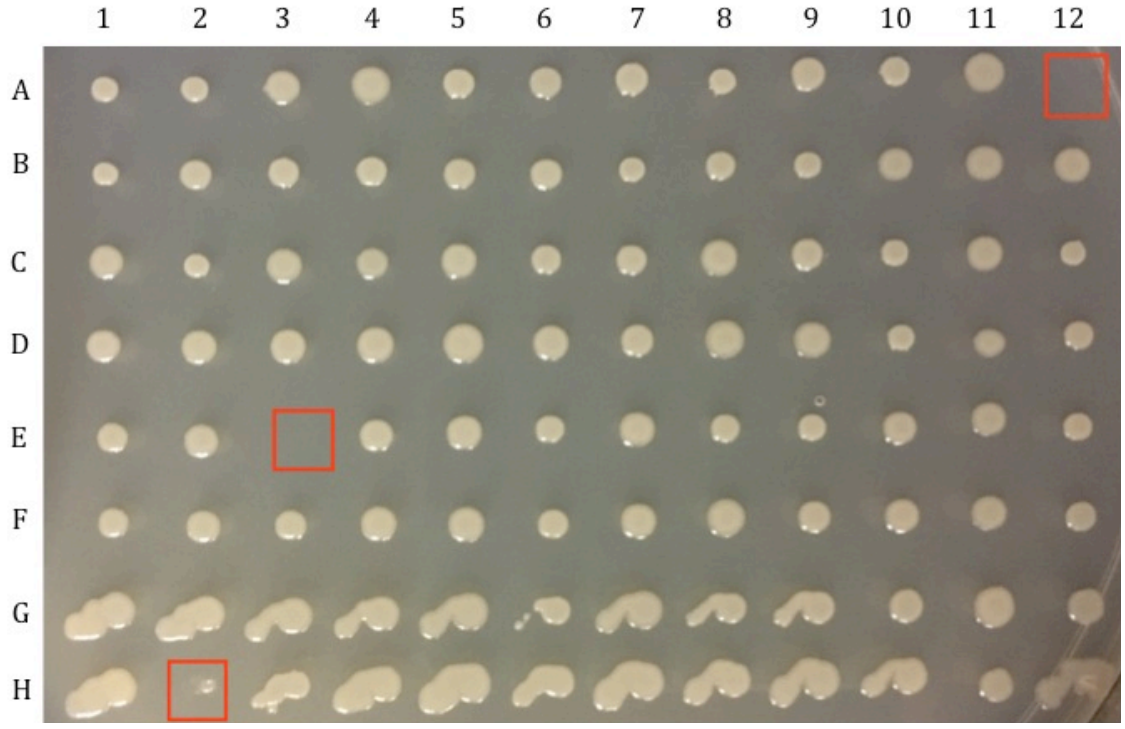

- A12, E3, and H2 exhibit growth defects

Tn plate 4 Summary:

- E3 and A12 exhibited extreme growth defects on all media
    - Exception: E3 growth not visible on MacConkey
- F1 exhibited growth in the 8 hour growth curve but not in the overnight culture
- C7, C8, and E7 exhibit growth defects on YESCA + CR
- H2 exhibits a growth defect on YESCA
- D11 and H12 exhibit the white colony phenotype on X-gal + glucose media

Biofilm formation assay & secondary screening

Upon first pass, statistical significance of 96-well biofilms was determined by one-way ANOVA compared to UTI89 *HK::kan*^{r}. Of the 2,208 mutants screened, 57 of these are mutants of interest (**Table 5**), corresponding to a 2.58% hit rate. To date, Tn 11-B5 has been screened a second time for biofilm formation at both 21% and 4% (**Figure 42B**). Tn 11-B5 has been subjected to genomic DNA extraction and subsequent sequencing to identify the disrupted gene(s).

In collaboration with the High-Throughput Screening (HTS) Facility, namely Paige Vinson and Chris Farmer, WaveGuide software has been adapted to analyze biofilm absorbance data. This protocol can be found in the Transposon library binder, as well as on the Hadjifrangiskou lab server under "UTI89 Transposon Library->WaveGuide".

Identification of genes disrupted by transposon insertion

Genomic DNA was extracted using the MOBio UltraClean Microbial DNA Isolation Kit following the manufacturer's protocol and quantified. To map the transposon insertion, a three-step PCR protocol was used to identify the transposon insertion loci (212, 293). Briefly, Inv-2 primer was utilized for amplification. An annealing temperature of 54°C was utilized for the first and third rounds of replication. PCR

products were prepped and sent for sequencing by GeneWiz according to the company's guidelines. Sequences were analyzed using the KAN-2 primers provided by the transposon kit and were mapped using BLAST (NCBI). **Figure 42A** shows the identification of Tn 11-B5, an insertion in *clpX*.

APPENDIX B

VANDERBILT URINARY TRACT ISOLATE DATABASE

In accordance with IRB #151465, *E. coli* positive urinary tract cultures and patient data from the electronic medical records were collected from the Vanderbilt University Medical Center by Dr. Jonathan Schmitz. Undergraduate students Madison Fitzgerald and Emily Apple were instrumental in preserving isolates and organizing de-identified patient data, respectively. The following criteria pertaining to urinary tract infections were recorded for each isolate: sex, age range, collection setting, recent indwelling urinary catheter, pregnancy, diabetes, structural or functional urinary tract abnormality, immunocompromised, associated infection.

Table key:

	No information/ incorrect collection
Orange Text	Unclear from electronic medical record
-	Not applicable

VUTI Strain	Sex	Age	Collection Setting	Collection Method	Recent Urinary Catheter	Pregnant	Diabetes	ASB	Urinary Tract Abnormality	Abnormality Type	Immuno-compromised	Immuno-compromise Type	Associated Infections	Notes
113	F	18-35	Outpatient	Clean Catch	N	N	N	N	N	-	N	-	Cystitis	-
114	F	18-35	Outpatient	Clean Catch	N	Y	N	Y	N	-	N	-	ASB	-
115	F	18-35	Outpatient	Clean Catch	N	N	N	N	N	-	N	-	Pyelonephritis	Clinical Suspicion of Pyelonephritis
116	F	71-80	Outpatient	Clean Catch	N	N	N	N	Y	H/O Urinary Incontinence	N	-	Cystitis	-
117	F	18-35	Outpatient	Clean Catch	N	N	N	N	N	-	N	-	Cystitis	-
118	F	51-60	Outpatient	Clean Catch	N	N	Y	N	N	-	N	-	ASB	-
119	F	71-80	Outpatient	Clean Catch	N	N	N	N	Y	Stress incontinence (utero vaginal prolapse)	N	-	Cystitis	-
120	F	36-50	ED	Clean Catch	N	N	Y	N	N	-	N	-	Cystitis	-
121	F	18-35	Outpatient	Clean Catch	N	Y	N	Y	N	-	N	-	ASB	-
122	F	61-70	Outpatient	Clean Catch	N	N	N	Y	Y	Bilateral urethral reflux, past recurrent UTI	N	-	ASB	-
123	F	61-70	Outpatient	Clean Catch	N	N	Y	N	Y	Urge/stress incontinence, recurrent UTI	N	-	Cystitis	-
124	M	61-70	ED	Clean Catch	N	N	N	N	Y	BPH; urinary retention; hydronephrosis	Y	Recent chemo for SCLC	Cystitis	-
125	F	18-35	Outpatient	Clean Catch	N	N	N	N	N	-	N	-	Cystitis	-
126	F	18-35	Outpatient	Clean Catch	N	N	N	N	N	-	N	-	Cystitis	-
127	F	51-60	ED	Clean Catch	N	N	Y	Y	N	-	N	-	ASB	-

128	F	71-80	Outpatient	Clean Catch		N	Y	N	N	-	N	-	Cystitis	-
129	F	18-35	Outpatient	Clean Catch	N	N	N	N	N	-	N	-	Cystitis	-
130	M	71-80	Outpatient	Clean Catch	N	N	N	N	Y	CIS of bladder; recent BCG infusion	Y	ESRD with HAD/ chemot herapy	Cystitis	-
131	F	61-70	Outpatient	Clean Catch	N	N	N	N	Y	Ureteral reflux; recurrent UTI; incomplete emptying of bladder	N	-	Cystitis	-
132	F	61-70	Outpatient	Clean Catch	N	N	Y	Y	N	-	N	-	ASB	+ for pyuria
133	F	36-50	ED	Clean Catch	N		Y	Y	N	-	N	-	ASB	-
134	F	61-70	Outpatient	Clean Catch	N	N	N	N	Y	Recurrent UTI	N	-	Cystitis	-
135	F	51-60	Outpatient	Clean Catch	N	N	N	N	N	-	N	-	Cystitis	-
136	F	61-70	Outpatient	Clean Catch	N	N	Y	N	Y	Stress incontinence	N	-	Pyelonephritis	Pyelonephritis questionable
137	F	61-70	Outpatient	Clean Catch	N	N	N	Y	Y	Recurrent UTI; urge; incontinence; ureteral injury 2/2 prior hysterectomy	N	-	ASB	-
138	M	18-35	Outpatient	Clean Catch	N	N	Y	N	Y	Bilateral hydronephrosis; obstructive nephropathy; CRD (in c/o genetic syndrome)	N	-	Cystitis	-
139	F	36-50	Outpatient	Clean Catch	N	N	N	Y	N	-	N	-	ASB	-
140	F	61-70	Inpatient	Clean Catch	?	N		Y	Y	urinary incontinence; h/o urinary retention; Foley	Y	moribund post-surgical patient	ASB	malodor
141	M	81+	Outpatient	Clean Catch	N	N	N	N	Y	H/O Urinary retention; unspecified prostate problems	N	-	Cystitis	-

142	F	71-80	ED	Clean Catch	N	N	N	Y	N	-	N	-	ASB	-
143	F	51-60	Outpatient	Clean Catch	N	N	N	N	Y	H/O stress incontinence; pelvic relaxation	N	-	Cystitis	-
144	F	71-80	Outpatient	Clean Catch	N	N	N	?	Y	mixed incontinence	N	-	Unclear	no specific SIRS criteria or urinary complaints, but general sense of unwell/nausea in c/o recent med changes
145	F	18-35	Outpatient	Clean Catch	N	N	N	N	N	-	N	-	Cystitis	-
146	F	36-50	ED	Foley	Y	N	N	N	Y	Quadriplegic/ incontinent to urine	N	-	Cystitis	Symptoms (SIRS criteria) predate Foley placement
147	F	36-50	ED	Clean Catch	N	N	N	N	Y	obstructive nephrolithiasis	N	-	Pyelonephritis	-
148	F	18-35	ED	Straight Catheter	N	Y	N	N	Y	Recurrent UTI (multiple different organisms)	N	-	Cystitis	-
149	F	61-70	Outpatient	Clean Catch	N	N	N	N	Y	urinary incontinence/ recurrent UTI	N	-	Cystitis	-
150	F	51-60	ED	Clean Catch	N	N	N	N	N	-	N	-	Pyelonephritis	Questionable
151	F	18-35	Outpatient	Clean Catch	N	N	N	Y	N	-	N	-	ASB	Recent postpartum
152	F	51-60	Outpatient	Clean Catch	N	N	N	N	N	-	N	-	Cystitis	-
153	F	71-80	ED	Clean Catch	N	N	N	Y	N	-	N	-	ASB	Strain incorrectly included; only 50-100K *E. coli*; < 10k α-strep
154	F	18-35	ED	Clean Catch	N	N	N	N	Y	solitary kidney; S/P nephrectomy due to extensive nephrolithiasis & parenchymal disease			Pyelonephritis	-
155	F	71-80	Outpatient	Clean Catch		N	N		Y	Bladder suspension surgery; recurrent UTI	N	-	Unclear	-

156	F	61-70	Outpatient	Clean Catch	N	N	N	Y	Y	Urinary retention; urge incontinence; MS	N	-	ASB	-
157	F	18-35	Outpatient	Clean Catch		N	N	N	Y	Nephrolithiasis	N	-	Cystitis	-
158	M	71-80	Outpatient	Clean Catch	N	N	Y	Y	Y	H/o prostate cancer; S/P radiation	N	-	ASB	-
159	M	61-70	ED	Ileal conduit		N	Y	N	Y	Ileal conduit; S/P cystectomy for bladder cancer; S/P proctectomy for prostate cancer	N	-	Pyelonephritis Bacteremia	Pyelonephritis that lead to bacteremia
160	F	36-50	Outpatient	Clean Catch		N	N	N	N	-	N	-	Pyelonephritis	-
161	F	18-35	Outpatient	Clean Catch	N	N	N	Y	N	-	N	-	ASB	Kidney donor urine screen
162	F	18-35	Inpatient	Clean Catch	N	N		?	N	-	N	-	Unclear	Immediate Postpartum
163	F	36-50	Outpatient	Clean Catch	N	N	N	N	N	-	N	-	Cystitis	-
164	F	18-35	Outpatient	Clean Catch	N	N	N	N	N	-	N	-	Cystitis	-
165	F	81+	Inpatient	Clean Catch	N	N	N	N	Y	Recurrent UTI	N	-	Cystitis	-
166	M	36-50	ED	Straight Catheter	N	N	Y	Y	Y	Paraplegic requiring straight catheter to void	N	-	ASB	-
167	F	51-60	ED	Clean Catch	N	N	N	Y	N	-	N	-	ASB	-
168	F	36-50	Outpatient	Clean Catch	N	N	N	N	N	-	N	-	Cystitis	-
169	F	36-50	Outpatient	Clean Catch	N	N	N	N	N	-	Y	α-TNF therapy for RA	Pyelonephritis	Questionable
170	F	36-50	ED	Clean Catch	N	N	N	Y	N	-	N	-	ASB	-
171	F	51-60	Outpatient	Clean Catch	N	N	N	N	Y	Recurrent UTI	N	-	Cystitis	-
172	F	18-35	Outpatient	Clean Catch	N	N	N	N	N	-	N	-	Cystitis	-
173	F	18-35	Outpatient	Clean Catch	N	N	N	N	Y	Recurrent UTI	N	-	Cystitis	-

174	F	51-60	Inpatient	Foley	Y	N	N	N	N	-	N	-	Cystitis	-
175	F	61-70	Outpatient	Clean Catch	N	N	N	N	N	-	N	-	Cystitis	-
176	F	71-80	Outpatient	Clean Catch	N	N	N	Y	Y	Recurrent UTI	N	-	ASB	-
177	M	51-60	ED	Clean Catch	N	N	N	Y	N	-	N	-	ASB	-
178	M	51-60	Outpatient	Straight Catheter	N	N	N	Y	Y	Paraplegic; neurogenic bladder; recurrent UTI	N	-	ASB	-
179	F	71-80	ED	Clean Catch	N	N	Y	Y	N	-	N	-	ASB	-
180	F	36-50	Outpatient	Clean Catch	N	N	N	N	N	-	N	-	Cystitis	-
181	F	61-70	Outpatient	Clean Catch	N	N	N	N	Y	Hemiparesis (cut); recurrent UTI; incontinence	N	-	Cystitis	-
182	F	36-50	Outpatient	Clean Catch	N	N	N	N	N	-	N	-	Cystitis	-
183	F	51-60	ED	Clean Catch	N	N	N	Y	N	-	N	-	ASB	-
184	M	36-50	Outpatient	Clean Catch	N	N	N	N	N	-	N	-	Cystitis	-
185	F	36-50	Outpatient	Clean Catch	N	N	N	N	Y	Renal transplant recipient (SLE); recurrent UTI	Y	rejection Rx (prednisone, cellcept, tacrolimus)	Cystitis	-
186	M	81 +	Outpatient	Clean Catch	N	N	Y	N	Y	S/P prostatectomy	N	-	Cystitis	-
187	F	71-80	Outpatient	Clean Catch	N	N	Y	N	N	-	N	-	Cystitis	-
188	F	18-35	Outpatient	Clean Catch	N	N	N	N	N	-	N	-	Cystitis	-
189	F	71-80	ED	Clean Catch	N	N	N	N	Y	urinary incontinence; recurrent UTI	N	-	Cystitis	-
190	F	71-80	Inpatient	Clean Catch	N	N	N	Y	N	-	N	-	ASB	-
191	M	51-60	Inpatient	Clean Catch	N	N	N	N	Y	Pelvic fracture; polytrauma S/p MVC	N	-	Bacteremia	-

192	F	36-50	Outpatient	Clean Catch	N	N	N	Y	Y	Renal transplant; patient S/P FSGS; solitary kidney	Y	transplant RX (prednisone, cellcept, tacrolimus)	ASB	-
193	F	18-35	Outpatient	Clean Catch	N	N	N	N	N	-	N	-	Cystitis	-
194	F	18-35	Outpatient	Clean Catch	N	N	N	N	N	-	N	-	Cystitis	-
195	F	81+		Clean Catch	N	N	N	Y	N	-	Y	Chemo for DLBCL	ASB	-
196	F	18-35	Outpatient	Clean Catch	N	N	N	N	Y	Stress incontinence; recurrent UTI	N	-	Cystitis	-
197	F	51-60	Outpatient	Clean Catch	N	N	N		Y	Incontinence; recurrent UTI	N	-	Unclear	-
198	F	18-35	Outpatient	Clean Catch	N	N	N	N	N	-	N	-	Cystitis	-
199	F	18-35	Outpatient	Clean Catch	N	N	N	N	N	-	N	-	Pyelonephritis	-
200	M	61-70	Outpatient	Clean Catch	N	N	N	N	Y	BPH; urinary retention	N	-	Cystitis	-
201	F	51-60	Outpatient	Clean Catch	N	N	Y	N	Y	Recurrent UTI; neurogenic bladder (S/P T12 injury)	N	-	Cystitis	-
202	F	51-60	Inpatient	Foley	Y	N	N	N	Y	Neurogenic bladder; 2/2 MS	N	-	Cystitis	-
203	M	36-50	Inpatient	Straight Catheter	N	N	N	N	Y	quadraplegia w/ neurogenic bladder	N	-	Cystitis	-
204	F	51-60	ED	Clean Catch	N	N	N	N	N	-	N	-	Cystitis	-
205	F	61-70	ED	Clean Catch	N	N	Y	N	Y	S/P renal transplant; recurrent UTI (multiple organisms)	Y	rejection Rx (prednisone, prograf, mycophen)	Bacteremia	-
206	M	61-70	Outpatient	Clean Catch	N	N	N	N	Y	Possible BPH	N	-	Cystitis	-
207	F	36-50	Outpatient	Clean Catch	N	N	N	N	N	-	N	-	Cystitis	-

208	F	51-60	ED	Clean Catch	N	N	N	N	N	-	Y	Myesthenia gravis w/ prednisone + PLEX	Cystitis	-
209														Collected in error; isolate does not meet inclusion criteria
210	M	51-60	Inpatient	Clean Catch	N	N	N	N	Y	S/P MVC w/ pelvic trauma	N	-	Cystitis	-
211	F	61-70	Outpatient	Clean Catch	N	N	Y	N	N	-	N	-	Cystitis	-
212	F	51-60	Outpatient	Clean Catch	N	N	N	?	Y	ureteral stent post nephrolithiasis	N	-	Unclear	-
213	F	71-80	Outpatient	Clean Catch	N	N	N	N	N	-	N	-	Cystitis	-
214	F	18-35	ED	Clean Catch	N	N	N	N	N	-	Y	Methotrexate + αIL6 for RA	Pyelonephritis	-
215	F	61-70	Outpatient	Clean Catch	N	N	N	N	N	-	N	-	Cystitis	-
216	M	71-80	Outpatient	Clean Catch	N	N	N	N	Y	BPH/Urinary retention	N	-	Cystitis	-
217	F	18-35	Outpatient	Clean Catch	N	N	N	N	N	-	N	-	Cystitis	-
218	F	71-80	Outpatient	Clean Catch	N	N	Y	Y	Y	H/O urinary retention	Y	Mycophenolate mofetil (myesthenia gravis)	ASB	-
219	F	18-35	ED	Clean Catch	N	N	N	Y	N	-	N	-	ASB	-
220	F	18-35	ED	Clean Catch	N	N	N	Y	Y	Recurrent UTI	N	-	ASB	-
221	F	71-80	Outpatient	Clean Catch	N	N	N	N	Y	Recurrent UTI, R nephrectomy (+), multiple bladder surgeries, exposed pelvic mesh	N	-	Cystitis	-

222	F	36-50	ED	Clean Catch	N	N	N	N	N	-	N	-	Pyelonephritis	-
223	F	18-35	Outpatient	Clean Catch	N	N	N	N	N	-	N	-	Cystitis	-
224	F	36-50	Outpatient	Clean Catch	N	N	N	N	N	-	N	-	Cystitis	-
225	F	18-35	Outpatient	Clean Catch	N	N	N		Y	Recurrent UTI	N	-	Unclear	-
226	F	51-60	Outpatient	Clean Catch	N	N	Y	Y	Y	Renal transplant recipient (membranous GN)	Y	Rejection Rx (prograf t, MM, prednis one)	ASB	-
227	F	18-35	Outpatient	Clean Catch	N	Y	N	Y	N	-	N	-	ASB	-
228	F	61-70	Outpatient	Clean Catch		N	N	N	Y	Urge incontinence, pelvic sling, chronic interstitial cystitis	N	-	Cystitis	-
229	F	36-50	Outpatient	Clean Catch	N	N	N	N	N	-	N	-	Pyelonephritis	-
230	F	61-70	Outpatient	Clean Catch	N	N	N	N	N	-	N	-	Cystitis	-
231	F	71-80	ED	Clean Catch	N	N	N	Y	N	-	N	-	ASB	-
232	F	51-60	Outpatient	Clean Catch	N	N	N	N	N	-	N	-	Cystitis	-
233	F	18-36	Outpatient	Clean Catch	N	Y	N	N	N	-	N	-	Cystitis	-
234	F	18-35	Outpatient	Clean Catch	N	N	N	N	Y	Recurrent UTI	N	-	Cystitis	-
235	F	36-50	Outpatient	Clean Catch	N	Y	N	Y	N	-	N	-	ASB	-
236	F	61-70	Outpatient	Clean Catch	N	N	N	N	N	-	N	-	Cystitis	-
237	F	71-80	Outpatient	Clean Catch	N	N	N	N	N	-	N	-	Cystitis	-
238	F	71-80	Outpatient	Clean Catch	N	N	N	N	Y	Recurrent UTI	N	-	Cystitis	-
239	F	18-35	Inpatient	Clean Catch	N	N	N	N	N	-	N	-	Cystitis	-
240	M	61-70	Outpatient	Clean Catch	N	N	N	?	Y	Recent prostatectomy (Prostate Ca)	N	-	Unclear	-

241	F	71-80	Outpatient	Clean Catch	N	N	N	Y	Y	Urge incontinence, bladder prolapse s/p sling, recurrent UTI (multiple organisms)	N	-	ASB	-
242	F	61-70	Outpatient	Clean Catch	N	N	N		Y	Recurrent UTI, stress incontinence	N	-	Unclear	-
243	F	51-60	Outpatient	Clean Catch	N	N	N	Y	Y	Renal transplant, urge incontinence	Y	transplant RX (prednisone, tacrolimus)	ASB	-
244	F	61-70	Outpatient	Clean Catch	N	N	N	N	N	-	N	-	Cystitis	-
245	F	81 +	Outpatient	Straight Catheter	N	N	Y	Y	Y	Recurrent UTI (multiple different organisms), incontinence	N	-	ASB	Currently asymptomatic
246	F	18-35	Outpatient	Clean Catch	N	Y	N	Y	N	-	N	-	ASB	-
247	F	51-60	Inpatient	Clean Catch	N	N	Y	?	N	-	N	-	Unclear	-
248	F	18-35	Outpatient	Clean Catch	N	Y	N	N	N	-	N	-	Cystitis	-
249	F	71-80	Outpatient	Clean Catch	N	N	N	N	N	-	N	-	Cystitis	-
250	F	18-35	Outpatient	Clean Catch	N	N	N	N	Y	Questionable recurrent UTI (urogyn eval unremarkable)	N	-	Cystitis	-
251	F	18-35	Inpatient	Clean Catch	N	N	N	N	N	-	N	-	Pyelonephritis Bacteremia	Postpartum; Pyelonephritis that lead to bacteremia
252	F	61-70	Outpatient	Clean Catch	N	N	N	N	Y	Recurrent UTI; incontinence; incomplete emptying	N	-	Cystitis	-
253	F	61-70	Outpatient	Straight Catheter	N	N	N	Y	Y	urinary incontinence; staghorn calculi	N	-	ASB	-
254	F	61-70	Outpatient	Clean Catch	N	N	N	N	Y	Recurrent UTI	N	-	Cystitis	-

255	M	61-70	Outpatient	Unclear	N	N	N	Y	Y	Bladder lesion of unclear neoplasticity	N	-	ASB	-
256	F	71-80	Outpatient	Clean Catch	N	N	N	N	N	-	N	-	Cystitis	-
257	F	61-70	Outpatient	Clean Catch	N	N	Y	Y	Y	Recurrent UTI; Ureteral Reflux; Urge incontinence	N	-	ASB	Currently asymptomatic
258	F	36-50	Outpatient	Clean Catch	N	Y	N	?	N	-	N	-	Unclear	-
259	F	61-70	Outpatient	Clean Catch	N	N	N	Y	N	-	N	-	ASB	-
260	F	61-70	Outpatient	Clean Catch	N	N	N	N	Y	Recent bladder sling operation	N	-	Cystitis	-
261	F	61-70	Outpatient	Clean Catch	N	N	N	N	Y	S/P bladder sling	N	-	Cystitis	-
262	M	71-80	Outpatient	Clean Catch		N	Y	Y	Y	TS cell carcinoma of bladder, radical right nephrectomy, urinary retention, BPH	N	-	ASB	-
263	F	71-80	Outpatient	Clean Catch	N	N	N	N	N	-	N	-	Cystitis	-
264	F	18-35	Outpatient	Clean Catch	N	N	N	N	N	-	N	-	Cystitis	Recent postpartum
265	F	61-70	Outpatient	Clean Catch	N	N	N	N	N	-	N	-	Cystitis	-
266	F	18-35	ED	Clean Catch	N	N	N	N	N	-	N	-	Cystitis	-
267	F	51-60	Outpatient	Clean Catch	N	N	Y	Y	Y	S/p tacked bladder of stress incontinence; recurrent UTI in past; nephrolithiasis ?	N	-	ASB	Not currently symptomatic
268	F	36-50												No EMR record
269	F	36-50	Outpatient	Clean Catch	N	N	N	Y	N	-	N	-	ASB	-
270	F	36-50	Outpatient	Clean Catch	N	N	N	N	N	-	N	-	Cystitis	-

271	F	51-60	Outpatient	Straight Catheter	N	N	N	Y	Y	Radical cystectomy w/ Indiana pouch (bladder cancer); nephrolithiasis, recurrent UTI	N	-	ASB	Not currently symptomatic
272	F	81+	Outpatient	Clean Catch	N	N	N	N	N	-	N	-	Cystitis	-
273	F	36-50	Outpatient	Clean Catch	N	N	N	Y	Y	Bilateral uteral stents; Hartman pouch w/ cystic fistula; recurrent UTI	N	-	ASB	-
274	F	18-35	Outpatient	Clean Catch	N	N	N	Y	Y	S/P renal transplant (genetic syndrome)	Y	α-rejection Rx (cellcept, prednisone, prograf)	ASB	-
275	F	18-35	Outpatient	Clean Catch	N	N	N	N	N	-	N	-	Cystitis	-
276	F	71-80	Outpatient	Clean Catch	N	N	Y	Y	Y	Bladder carcinoma; s/p renal transplant (diabetic nephropathy), recurrent UTI	Y	α-rejection Rx (prednisone, tacrolimus)	ASB	-
277	F	61-70	ED	Foley	Y	N	N	?	Y	Neurologically devastated (CVA)	N	-	Unclear	high clinical suspicion of UTI from urinalysis but patient unable to convey symptoms
278	F	81+	Outpatient	Clean Catch	N	N	N	Y	Y	S/P bladder repair surgery (unclear reason)	N	-	ASB	-
279	F	61-70	Outpatient	Clean Catch	N	N	Y	Y	N	-	N	-	ASB	-
280	F	36-50	ED	Clean Catch	N	N	N	Y	N	-	N	-	ASB	-
281	M	18-35	Inpatient	Straight Catheter	N	N	N	N	Y	Paraplegia w/ neurogenic bladder	N	-	Cystitis	-

282	F	36-50	Outpatient	Clean Catch	N	N	N	N	Y	Mixed incontinence; recurrent UTI	N	-	Cystitis	-
283	F	61-70	Outpatient	Clean Catch	N	N	Y	?	Y		N	-	Unclear	-
284	F	51-60	ED	Foley	Y	N	Y	Y	N	-	N	-	ASB	-
285	F	81 +	ED	Clean Catch	N	N	N	Y	N	-	N	-	ASB	-
286	F	51-60	Outpatient	Clean Catch	N	N	N	N	N	-	N	-	Cystitis	-
287	F	61-70	Outpatient	Clean Catch	N	N	N	N	N	-	Y	methotrexate for RA	Cystitis	-
288	F	51-60	Outpatient	Clean Catch	N	N	N	N	N	-	N	-	Cystitis	-
289	F	51-60	Outpatient	Clean Catch	N	N	N	Y	Y	Urinary tract reconstruction; solitary kidney w/ hydronephrosis; urinary retention; recurrent UTI	N	-	ASB	-
290	F	51-60	Outpatient	Clean Catch		N	N	N	N	-	N	-	Cystitis	-
291	M	71-80	Outpatient	Clean Catch	N	N	N	Y	Y	Bladder cancer; hydronephrosis; ureteral stent; recurrent UTI	N	-	ASB	-
292	F	18-35	Outpatient	Clean Catch	N	Y	N	Y	N	-	N	-	ASB	-
293	M	61-70	Outpatient	Clean Catch	N	N	N	N	N	-	N	-	Cystitis	-
294	F	81 +	Outpatient	Straight Catheter	N	N	N	N	Y	Bladder cancer s/p resection; L ureteral stricture w/ stent; incontinence	N	-	Cystitis	-
295	F	61-70	Inpatient	Clean Catch	N	N	Y	Y	N	-	N	-	ASB	-
296	F	61-70	Outpatient	Clean Catch	N	N	Y	N	Y	Urinary incontinence	N	-	Cystitis	-
297	M	61-70	Outpatient	Clean Catch	N	N	N	N	N	-	N	-	Cystitis	-

298	F	81 +	ED	Unclear	N	N	N	Y	N	-	N	-	ASB	-
299	F	61-70	ED	Clean Catch	N	N	Y	Y	Y	"Bladder muscle dysfunction"	N	-	ASB	-
300	F	71-80	Outpatient	Clean Catch	N	N	N	N	N	-	N	-	Cystitis	-
301	F	61-70	Outpatient	Clean Catch		N	Y	N	Y	Mix urinary incontinence s/p retropubic sling; urinary retention	N	-	Cystitis	-
302	F	18-35	ED	Clean Catch	N	N	N	Y	N	-	N	-	ASB	-
303	F	36-50	Outpatient	Unclear	N	N	N	N	Y	-	Y	α-rejection Rx; current chemotherapy for cervical cancer	Cystitis	-
304	F	18-35	ED	Clean Catch	N	Y	N	N	N	-	N	-	Cystitis	-
305	M	61-70	ED	Foley	N	N	N	N	Y	Radical prostatectomy (post-prostate ca)	N	-	Cystitis	Foley inserted at presentation
306	M	51-60	Outpatient	Clean Catch	N	N	N	N	N	-	N	-	Cystitis	-
307	F	61-70	Outpatient	Clean Catch	N	N	N	N	N	-	N	-	Cystitis	-
308	F	36-50	ED	Clean Catch	N	N	N	N	N	-	N	-	Pyelonephritis	-
309	F	36-50	Outpatient	Clean Catch	N	N	Y	N	N	-	N	-	Pyelonephritis	-
310	F	61-70	Outpatient	Clean Catch	N	N	Y	N	Y	Recurrent UTI	Y	Chemotherapy (endometrial cancer)	Cystitis	-
311	M	51-60	ED	Clean Catch	N	N	Y	N	Y	BPH	N	-	Pyelonephritis	-
312	F	18-35	Outpatient	Clean Catch	N	N	N	N	N	-	N	-	Cystitis	-
313	F	51-60	ED	Clean Catch	N	N	N	Y	N	-	N	-	ASB	-

314	F	18-35	ED	Clean Catch	N	N	N	N	N	-	N	-	Cystitis	-
315	F	18-35	ED	Straight Catheter	N	N	N	Y	Y	Paraplegic w/ neurogenic bladder	N	-	ASB	-
316	F	36-50	Outpatient	Clean Catch	N	N	N	N	N	-	N	-	Cystitis	-
317	F	51-60	Outpatient	Clean Catch	N	N	N	N	N	-	N	-	Cystitis	-
318	F	81 +	ED	Unclear	N	N	N	Y	N	-	N	-	ASB	-
319	F	18-35	Outpatient	Clean Catch	N	Y	N	Y	N	-	N	-	ASB	-
320	F	81 +	ED	Clean Catch	N	N	Y	N	N	-	N	-	Cystitis	-
321	F	71-80	Outpatient	Clean Catch	N	N	N	N	Y	Recurrent UTI	N	-	Cystitis	-
322	F	61-70	Outpatient	Unclear	N	N	N	N	Y	Urge, incontinence	Y	Chemotherapy for renal cell carcinoma	Cystitis	-
323	F	18-35	ED	Straight Catheter	N	N	N	?	Y	Neurogenic bladder (spina bifida)	N	-	Unclear	Patient nonverbal; SIRS criteria attributable to multiple potential etiologies
324	F	18-35	ED	Unclear	N	N	N	Y	N	-	N	-	ASB	-
325	F	71-80	ED	Straight Catheter	N	N	N	N	N	-	N	-	Cystitis	-
326	F	71-80	ED	Clean Catch	N	N	Y	Y	Y	H/O recurrent UTI	N	-	ASB	-
327	F	81 +	Outpatient	Clean Catch	N	N	N	N	Y	H/O recurrent UTI w/ multiple organisms	N	-	Cystitis	-
328	F	36-50	ED	Clean Catch	N	N	N	Y	Y	R nephrectomy	N	-	ASB	-
329	M	51-60	Outpatient	Clean Catch	N	N	N	N	Y	BPH w/ outflow obstruction; recurrent UTI	N	-	Cystitis	-
330	M	61-70	Outpatient	Straight Catheter	N	N	N	?	Y	paraplegic w/ urinary retention	N	-	Unclear	-
331	F	36-50	Outpatient	Clean Catch	N	N	N	?	Y	Recurrent UTI	N	-	Unclear	Urinary malodor w/o overt symptoms

332	F	36-50	Outpatient	Clean Catch	N	N	N	Y	Y	S/P renal transplant	Y	α-rejection Rx (prograf MMF, prednisone)	ASB	-
333	F	18-35	ED	Clean Catch	N	N	N	N	N	-	N	-	Cystitis	-
334	F	61-70	Outpatient	Clean Catch	N	N	N	Y	Y	mixed incontinence; h/o bladder spasm	N	-	ASB	-
335	F	51-60	Outpatient	Clean Catch	N	N	N	N	N	-	N	-	Cystitis	-
336	F	71-80	Outpatient	Clean Catch	N	N	N	Y	Y	Mixed incontinence (s/p sling); recurrent UTI	N	-	ASB	Included in error; also had 50-100K GBS
337	F	71-80	Outpatient	Clean Catch	N	N	N	N	N	-	N	-	Cystitis	-
338	F	51-60	Outpatient	Clean Catch	N	N	N	N	Y	Recurrent UTI	N	-	Cystitis	-
339	M	61-70	Outpatient	Clean Catch	N	N	N	N	N	-	N	-	Cystitis	-
340	F	71-80	Outpatient	Clean Catch	N	N	N	N	Y	Recurrent UTI	Y	Methotrexate + prednisone for RA	Cystitis	-
341	F	36-50	Inpatient	Clean Catch	N	N	N	N	Y	Recurrent UTI; MS; urinary retention	N	-	Pyelonephritis	-
342	F	18-35	Outpatient	Clean Catch	N	N	N	N	N	-	N	-	Unclear	Positive for urinary malodor
343	F	18-35	Outpatient	Clean Catch	N	N	N	N	Y	Mixed incontinence; recurrent UTI	N	-	Cystitis	-
344	F	18-35	Outpatient	Clean Catch	N	Y	N	Y	N	-	N	-	ASB	-
345	F	51-60	Outpatient	Clean Catch	N	N	N	N	N	-	Y	Radiation for metastatic ovarian cancer	Cystitis	-
346	F	71-80	Outpatient	Clean Catch	N	N	N	N	Y	Incontinence; recurrent UTI	N	-	Cystitis	-

347	F	81 +	Outpatient	Clean Catch	N	N	N	N	Y	Recurrent UTI	N	-	Cystitis	-
348	F	36-50	Outpatient	Clean Catch	N	N	N	N	Y	Post-surgical urinary retention	N	-	Cystitis	-
349	M	81 +	Outpatient	Clean Catch	N	N	Y	N	Y	Urethral sling; prostate adenocarcinoma (s/p resection); urinary retention; artificial urinary sphincter	N	-	Cystitis	-
350	F	81 +	ED	Unclear	N	N	Y	Y	Y	Urinary incontinence	N	-	ASB	-
351	F	81 +	ED	Clean Catch	N	N	N	Y	N	-	N	-	ASB	-
352	F	61-70	Outpatient	Unclear	N	N	N	Y	Y	S/P cystocele repair w/ sling	N	-	ASB	-
353	F	71-80	Outpatient	Clean Catch	N	N	N	N	N	-	N	-	Cystitis	-
354	F	81 +	Outpatient	Clean Catch	N	N	N	N	Y	Urethral stricture (s/p dilation)	N	-	Cystitis	-
355	F	61-70	Outpatient	Clean Catch	N	N	Y	N	N	-	N	-	Cystitis	-
356	F	71-80	Inpatient	Straight Catheter	N	N	N	N	Y	Neurogenic bladder	N	-	Cystitis	-
357	F	18-35	Outpatient	Clean Catch	N	Y	N	Y	N	-	N	-	ASB	-
358	F	51-60	ED	Clean Catch	N	N	N	N	Y	Right UPJO; hydronephrosis	N	-	Pyelonephritis	-
359	F	36-50	Inpatient	Clean Catch	N	N	N	Y	N	-	N	-	ASB	-
360	M	61-70	Outpatient	Straight Catheter	N	N	N	N	Y	Prostatic hypertrophy w/ high retention	N	-	Cystitis	-
361	F	71-80	ED	Clean Catch	N	N	N	N	N	-	N	-	Cystitis	-
362	F	18-35	ED	Clean Catch	N	N	N	N	N	-	N	-	Cystitis	-
363	F	18-35	Outpatient	Clean Catch	N	Y	N	?	Y	Recurrent UTI	N	-	Unclear	Unclear if currently symptomatic
364	M	61-70	ED	Clean Catch	N	N	Y	N	N	-	N	-	Cystitis	-

365	F	18-35	Outpatient	Clean Catch	N	N	N	N	N	-	N	-	Cystitis	-
366	F	36-50	Outpatient	Clean Catch	N	N	N	N	N	-	N	-	Cystitis	-
367	F	71-80	Outpatient	Unclear	N	N	N	N	Y	Neurogenic bladder	N	-	Cystitis	Patient occasionally self-catheterizes, but not clear how this was collected
368	F	51-60	Outpatient	Clean Catch	N	N	Y	N	N	-	N	-	Cystitis	-
369	F	81 +	ED	Unclear	N	N	Y	Y	Y	Incontinence; S/P L nephrectomy (renal cancer)	N	-	ASB	-
370	F	61-70	Outpatient	Clean Catch	N	N	N	N	Y	Recurrent UTI	N	-	Cystitis	-
371	F	36-50	Outpatient	Clean Catch	N	N	N	N	N	-	N	-	Cystitis	-
372	F	18-35	ED	Unclear	N	N	N	Y	N	-	N	-	ASB	-
373	F	71-80	Outpatient	Clean Catch	N	N	Y	N	N	-	N	-	Cystitis	-
374	F	18-35	Outpatient	Clean Catch	N	N	N	N	N	-	N	-	Cystitis	-
375	F	61-70	Outpatient	Clean Catch	N	N	Y	Y	Y	Recurrent UTI	N	-	ASB	Currently asymptomatic
376	M	61-70	Outpatient	Clean Catch	N	N	Y	N	Y	Prostate carcinoma	N	-	Cystitis	-
377	F	51-60	Outpatient	Clean Catch	N	N	N	N	Y	Recurrent UTI post-hysterectomy; incontinence; s/p cervical radiation (carcinoma)	N	-	Cystitis	-
378	F	18-35	Outpatient	Clean Catch	N	N	N	N	Y	Recurrent UTI (multiple organisms); unclear predisposition	N	-	Cystitis	-
379	F	51-60	Outpatient	Straight Catheter	N	N	Y	N	Y	Mixed incontinence; neuromuscular bladder dysfunction: MS	N	-	Cystitis	-
380	F	61-70	Outpatient	Clean Catch	N	N	N	N	N	-	N	-	Cystitis	-

381	M	51-60	ED	Unclear	N	N	N	N	N	-	N	-	Bacteremia	-
382	F	81+	Outpatient	Clean Catch	N	N	N	N	N	-	N	-	Cystitis	-
383	M	18-35	Outpatient	Straight Catheter	N	N	N	N	Y	MS w/ neurogenic bladder	N	-	Cystitis	-
384	F	71-80	Inpatient	During cystoscopy/ stenting procedure	N	N	N	Y	Y	Obstructing uteral stone	N	-	ASB	-
385	F	61-70	ED	Unclear	?	N	N	N	N	-	N	-	Bacteremia	Transfer from OSH
386	F	36-50	ED	Clean Catch	N	N	N	N	N	-	N	-	Cystitis	-
387	F	81+	Outpatient	Clean Catch	N	N		N	N	-	N	-	Cystitis	-
388	F	36-50	ED	Clean Catch	N	N	N	Y	N	-	N	-	ASB	-
389	F	18-35	Outpatient	Clean Catch	N	N	N	N	N	-	N	-	Cystitis	-
390	F	18-35	Outpatient	Clean Catch	N	N	N	N	N	-	N	-	Cystitis	-
391	F	18-35	ED	Clean Catch	N	N	N	?	N	-	N	-	Unclear	Recent postpartum
392	F	51-60	Outpatient	Straight Catheter	N	N	N	N	Y	Incomplete emptying w/ bladder spasms; S/P intravesical botox	N	-	Cystitis	-
393	M	61-70	Outpatient	Clean Catch	N	N	N	N	N	-	N	-	Cystitis	-
394	M	71-80	Inpatient	Foley	Y	N	N	?	N	-	N	-	Unclear	Catheter placed very recently before collection for PEA; unable to assess for asymptomatic bacteriuria (patient moribund/nonverbal)
395	F	36-50	ED	Clean Catch	N	N	N	Y	N	-	N	-	ASB	-
396	F	36-50	Inpatient	Clean Catch	N	N	Y	Y	N	-	N	-	ASB	-
397	F	18-35	ED	Clean Catch	N	N	N	N	N	-	N	-	Pyelonephritis	-

398	F	18-35	ED	Clean Catch	N	N	N	Y	N	-	N	-	ASB	-
399	F	36-50	ED	Clean Catch	N	N	N	Y	N	-	Y	HIV+	ASB	-
400	F	71-80	Outpatient	Clean Catch	N	N	Y	N	Y	Urinary retention; recurrent UTI	N	-	Cystitis	-
401	F	71-80	Outpatient	Clean Catch	N	N	Y	N	Y	Recurrent UTI	N	-	Cystitis	-
402	M	71-80	ED	Clean Catch	N	N	N	N	Y	Recurrent UTI	N	-	Pyelonephritis	-
403	F	61-70	Outpatient	Clean Catch	N	N	N	N	N	-	N	-	Cystitis	-
404	F	36-50	Outpatient	Clean Catch	N	N	N	N	N	-	N	-	Cystitis	-
405	F	18-35	Outpatient	Clean Catch	N	N	N	N	N	-	N	-	Cystitis	-
406	F	81 +	ED	Clean Catch	N	N	N	Y	N	-	N	-	ASB	-
407	F	51-60	ED	Clean Catch	N	N	N	N	N	-	N	-	Cystitis	-
408	F	36-50	Inpatient	Foley	Y	N	Y	N	N	-	Y	Moribund ICU patient	Cystitis	-
409	F	36-50	Outpatient	Clean Catch	N	N	N	N	N	-	N	-	Cystitis	-
410	M	71-80	ED	Unclear	N	N	N	N	Y	Paraplegic (S/P AAA rupture)	N	-	Cystitis	probable straight catheter, but not documented as such explicitly
411	F	71-80	Outpatient	Clean Catch	N	N	Y	N	Y	Urinary incontinence; nephrolithiasis	N	-	Cystitis	-
412	F	51-60	Outpatient	Clean Catch	N	N	N	N	N	-	N	-	Cystitis	-
413	F	36-50	Outpatient	Clean Catch	N	N	N	N	N	-	N	-	Cystitis	-
414	F	51-60	Outpatient	Clean Catch	N	N	N	Y	N	-	N	-	ASB	-
415	M	71-60	Outpatient	Clean Catch	N	N	N	Y	Y	Recurrent UTI; renal transplant; neurogenic bladder; urinary retention	Y	α-rejection Rx (prednisone, tacrolimus)	ASB	-

APPENDIX C

VANDERBILT URINARY TRACT ISOLATE BIOFILM FORMATION

Biofilm formation was tested under atmospheric (21%) and hypoxic (4%) oxygen for each of the 300 isolates by a 96-well crystal violet assay. A waterfall plot of biofilm formation under each oxygen condition is presented on the following pages. UTI89 (positive control) and UTI89Δ*fimA-H* (negative control) are included on each graph. Each bar represents the mean of at least 3 biological replicates with at least 8 technical replicates. Error bars show the standard error of the mean.

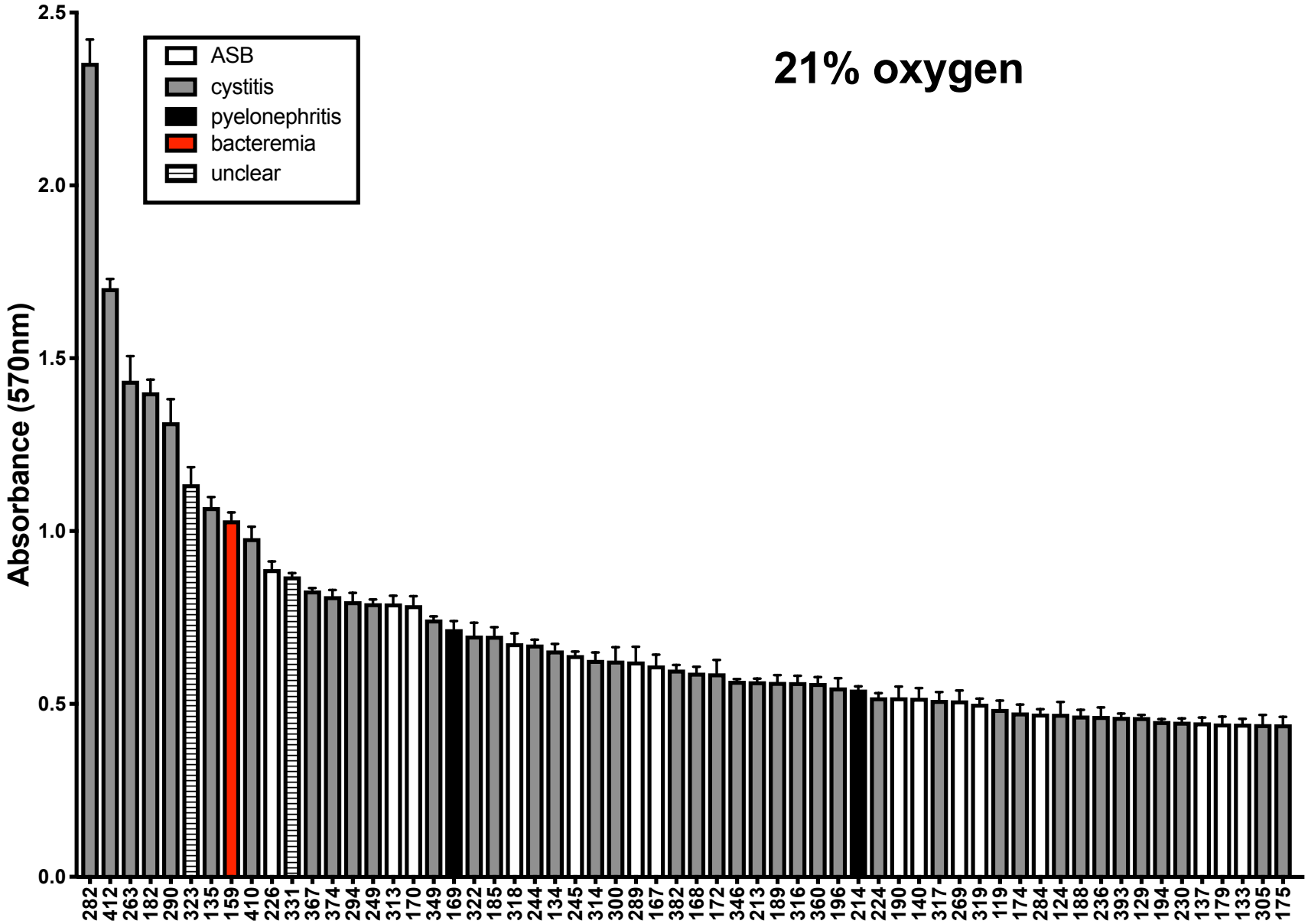
21% oxygen
ASB
cystitis
pyelonephritis
bacteremia
unclear
Absorbance (570nm)
2.5
2.0
1.5
1.0
0.5
0.0
282 412 263 182 290 323 135 159 410 226 331 367 374 294 249 313 170 349 169 322 185 318 244 134 245 314 300 289 167 382 168 172 346 213 189 316 360 196 214 224 190 140 317 269 319 119 174 284 124 188 236 393 129 194 230 137 179 133 305 175

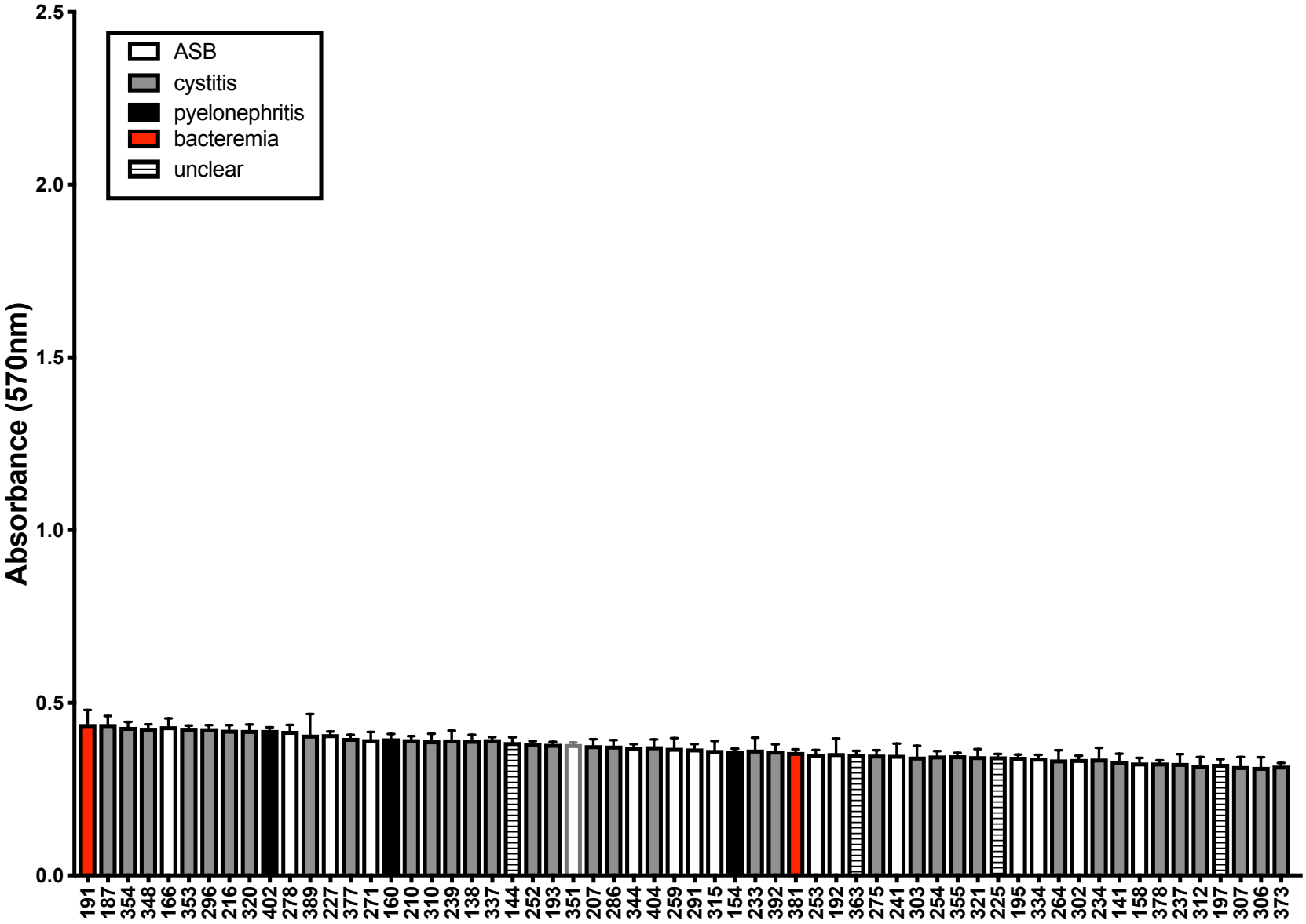
ASB
cystitis
pyelonephritis
bacteremia
unclear
Absorbance (570nm)
2.5
2.0
1.5
1.0
0.5
0.0
191 187 354 348 166 353 296 216 320 402 278 389 227 377 271 160 210 310 239 138 337 144 252 193 351 207 286 344 404 259 291 315 154 233 392 381 253 192 363 275 241 303 254 355 321 225 195 334 264 302 234 141 158 378 237 312 197 307 306 373

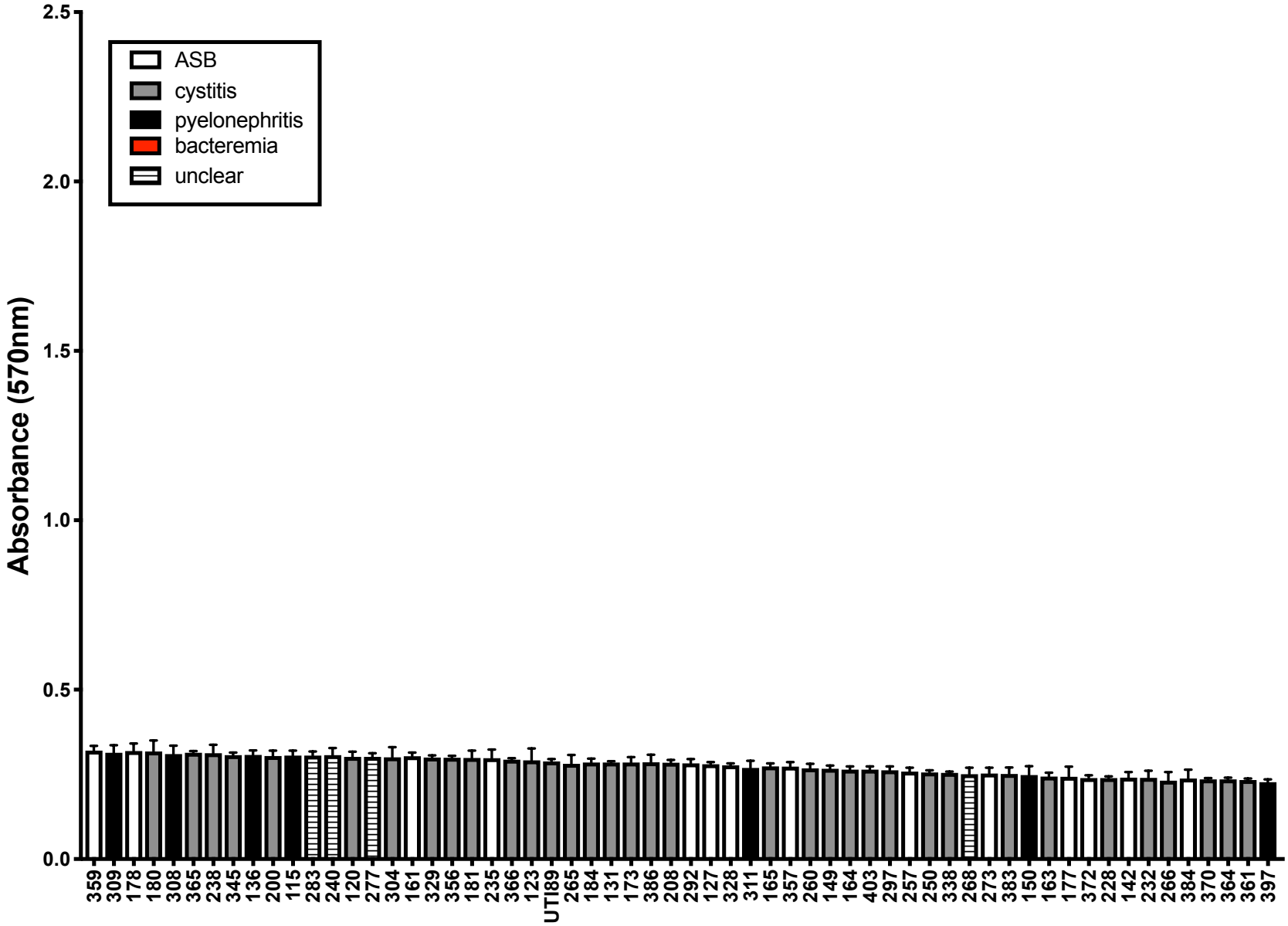
ASB
cystitis
pyelonephritis
bacteremia
unclear
Absorbance (570nm)
2.5
2.0
1.5
1.0
0.5
0.0
359 309 178 180 308 365 238 345 136 200 115 283 240 120 277 304 161 329 356 181 235 366 123 UTI89 265 184 131 173 386 208 292 127 328 311 165 357 260 149 164 403 297 257 250 338 268 273 383 150 163 177 372 228 142 232 266 384 370 364 361 397

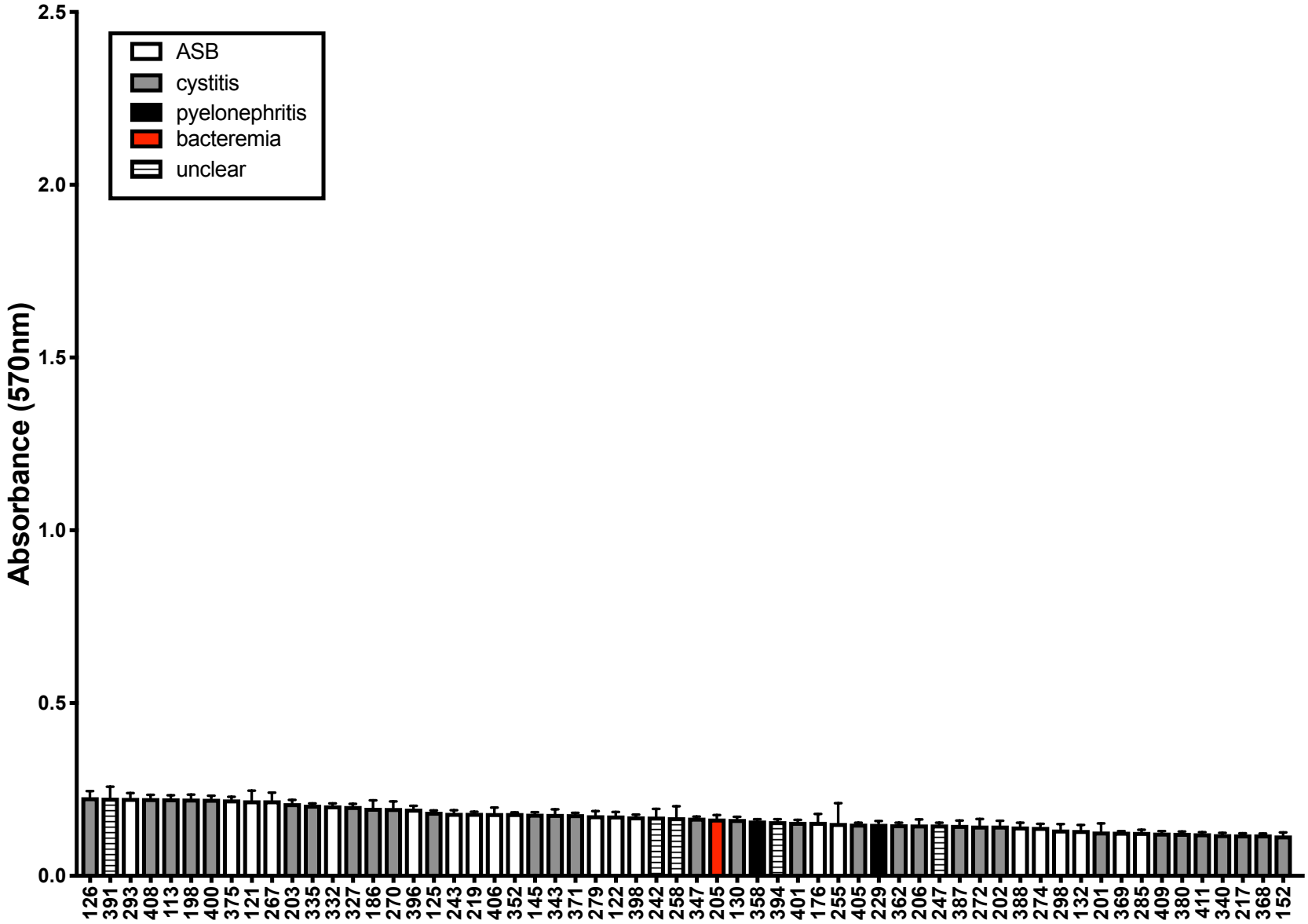
ASB
cystitis
pyelonephritis
bacteremia
unclear
Absorbance (570nm)
2.5
2.0
1.5
1.0
0.5
0.0
126 391 293 408 113 198 400 375 121 267 203 335 332 327 186 270 396 125 243 219 406 352 145 343 371 279 122 398 242 258 347 205 130 358 394 401 176 255 405 229 362 206 247 387 272 202 388 274 298 132 201 369 285 409 380 411 340 217 368 152

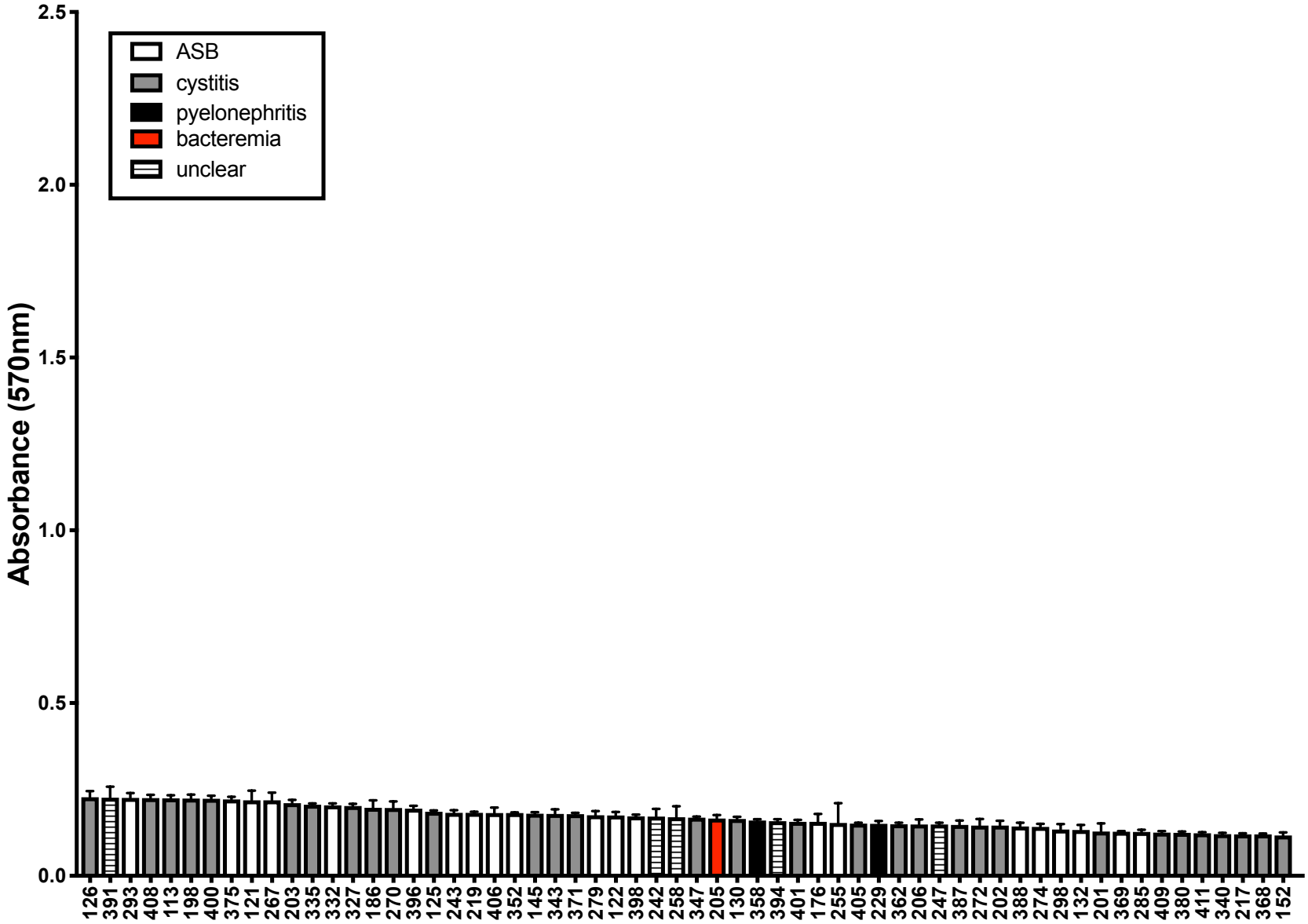
ASB
cystitis
pyelonephritis
bacteremia
unclear
Absorbance (570nm)
2.5
2.0
1.5
1.0
0.5
0.0
126 391 293 408 113 198 400 375 121 267 203 335 332 327 186 270 396 125 243 219 406 352 145 343 371 279 122 398 242 258 347 205 130 358 394 401 176 255 405 229 362 206 247 387 272 202 388 274 298 132 201 369 285 409 380 411 340 217 368 152

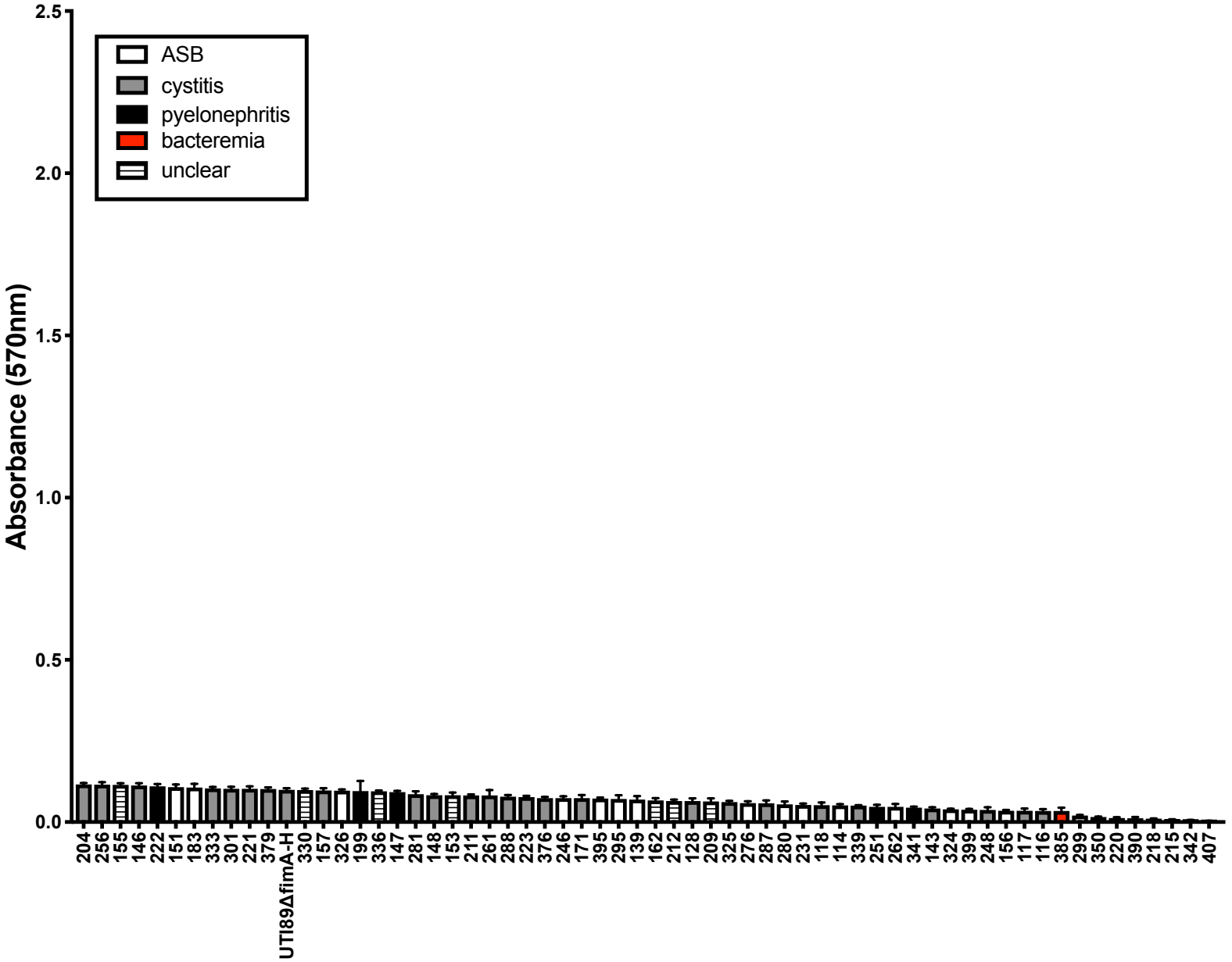
ASB
cystitis
pyelonephritis
bacteremia
unclear
Absorbance (570nm)
2.5
2.0
1.5
1.0
0.5
0.0
204
256
155
146
222
151
183
333
301
221
379
UTI89ΔfimA-H
330
157
326
199
336
147
281
148
153
211
261
288
223
376
246
171
395
295
139
162
212
128
209
325
276
287
280
231
118
114
339
251
262
341
143
324
399
248
156
117
116
385
299
350
220
390
218
215
342
407

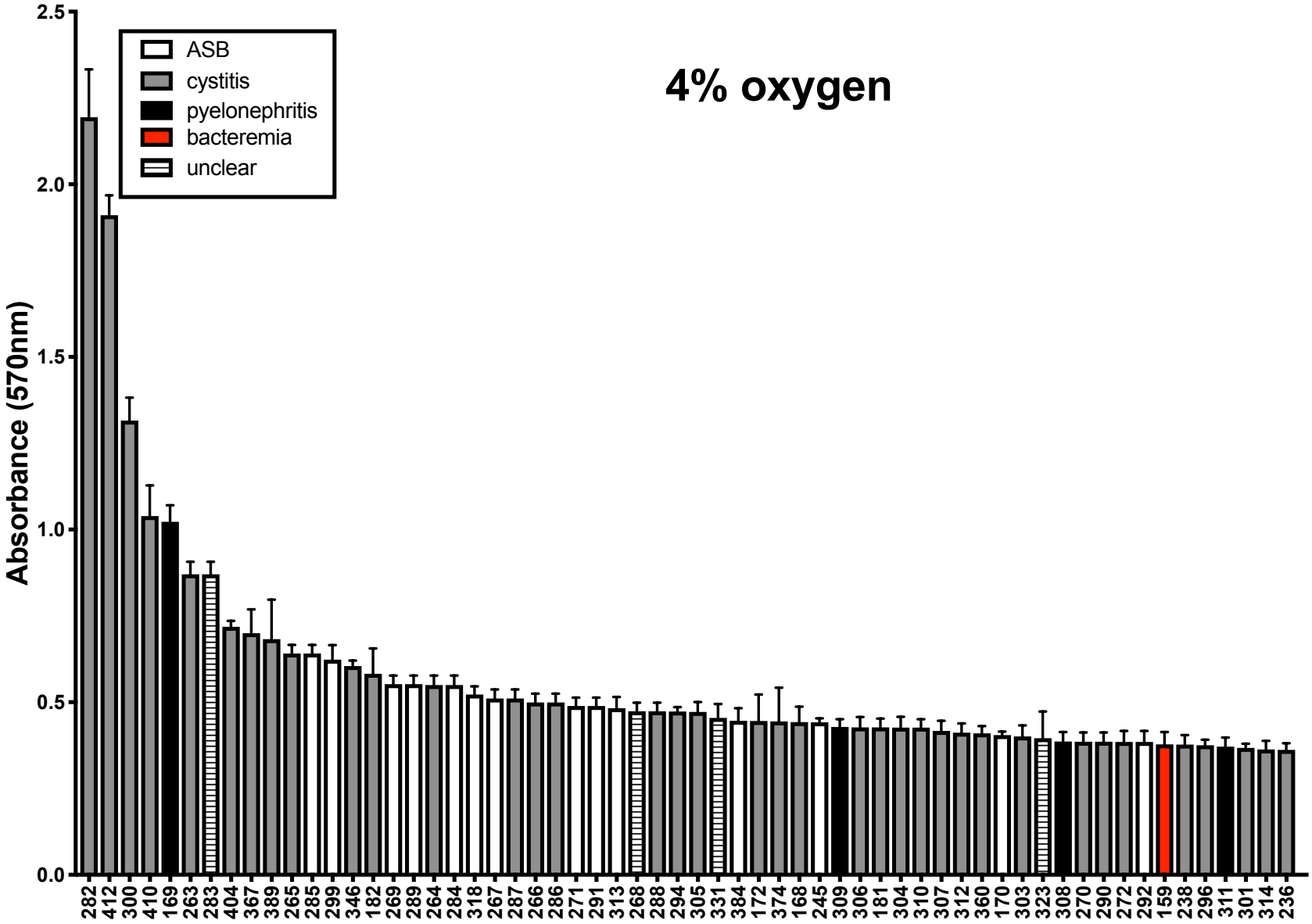
4% oxygen
ASB
cystitis
pyelonephritis
bacteremia
unclear
Absorbance (570nm)
2.5
2.0
1.5
1.0
0.5
0.0
282 412 300 410 169 263 283 404 367 389 265 285 299 346 182 269 289 264 284 318 267 287 266 286 271 291 313 268 288 294 305 331 384 172 374 168 245 309 306 181 304 310 307 312 360 170 303 323 308 270 290 272 292 159 238 296 311 301 314 236

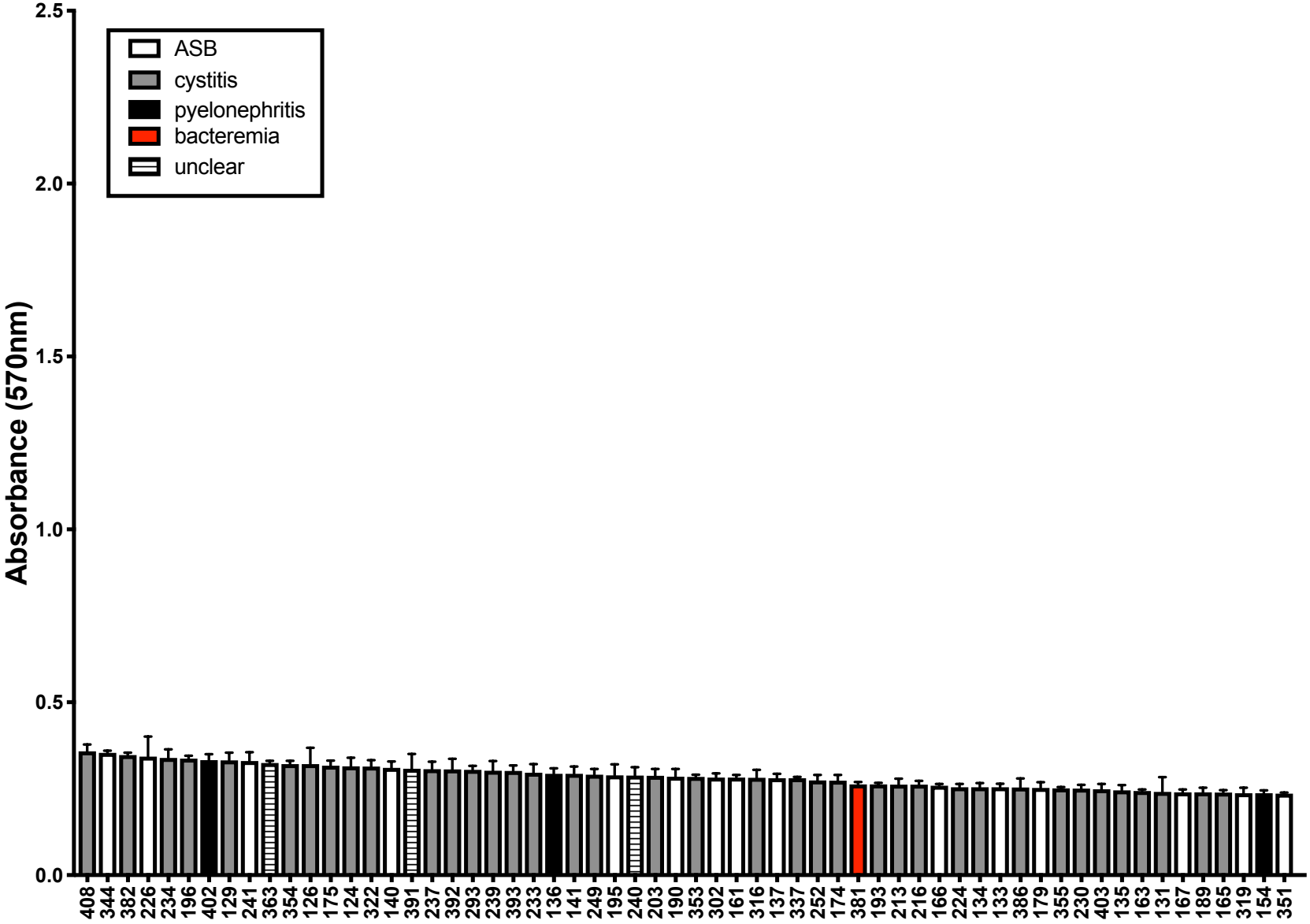
ASB
cystitis
pyelonephritis
bacteremia
unclear
Absorbance (570nm)
2.5
2.0
1.5
1.0
0.5
0.0
408 344 382 226 234 196 402 129 241 363 354 126 175 124 322 140 391 237 392 293 239 393 233 136 141 249 195 240 203 190 353 302 161 316 137 337 252 174 381 193 213 216 166 224 134 133 386 179 355 230 403 135 163 131 167 189 165 319 154 351

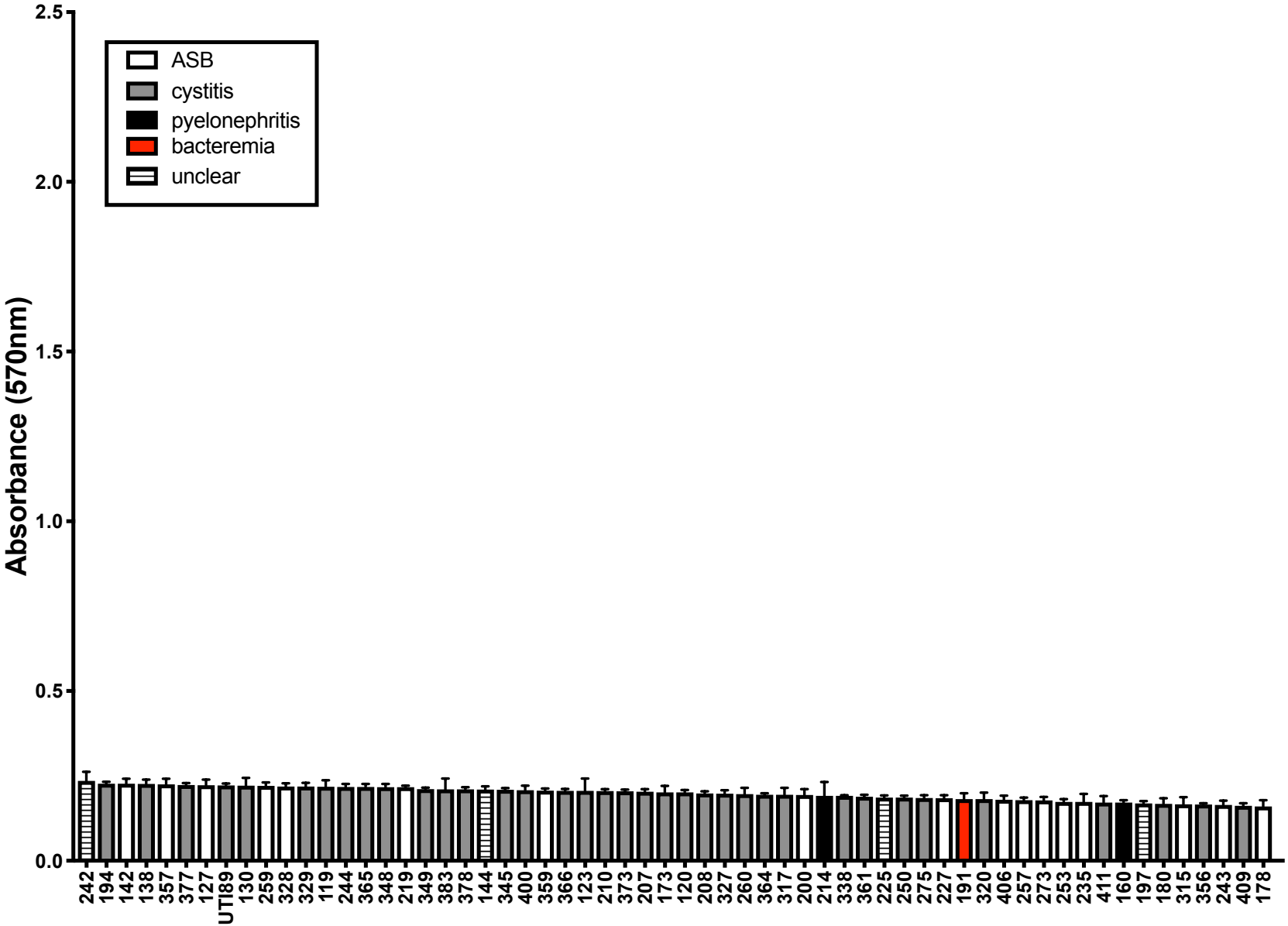
ASB
cystitis
pyelonephritis
bacteremia
unclear
Absorbance (570nm)
2.5
2.0
1.5
1.0
0.5
0.0
242 194 142 138 357 377 127 UTI89 130 259 328 329 119 244 365 348 219 349 383 378 144 345 400 359 366 123 210 373 207 173 120 208 327 260 364 317 200 214 338 361 225 250 275 227 191 320 406 257 273 253 235 411 160 197 180 315 356 243 409 178

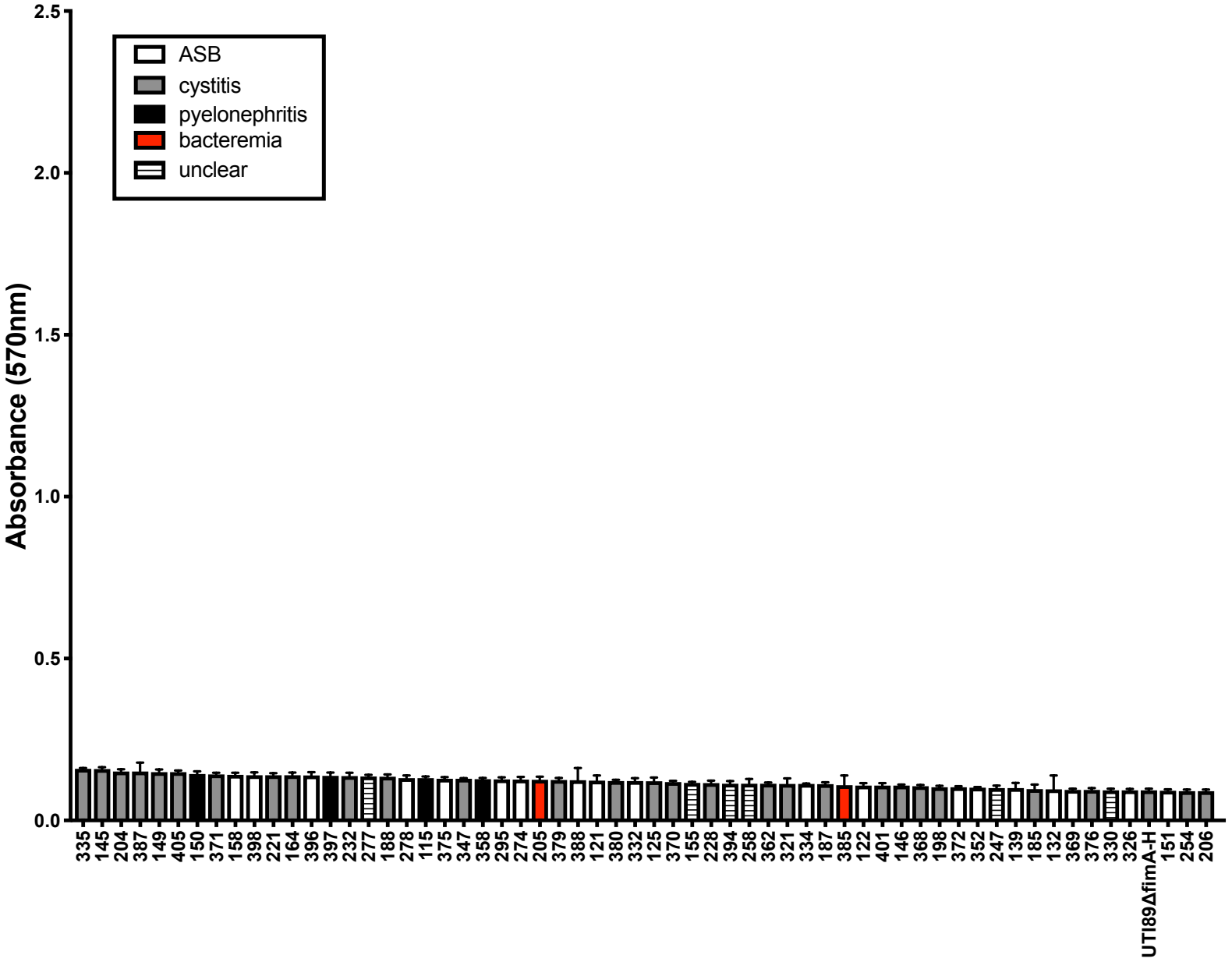
ASB
cystitis
pyelonephritis
bacteremia
unclear
Absorbance (570nm)
2.5
2.0
1.5
1.0
0.5
0.0
335 145 204 387 149 405 150 371 158 398 221 164 396 397 232 277 188 278 115 375 347 358 295 274 205 379 388 121 380 332 125 370 155 228 394 258 362 321 334 187 385 122 401 146 368 198 372 352 247 139 185 132 369 376 330 326 UTI89ΔfimA-H 151 254 206

APPENDIX D

METABOLITE CANDIDATE IDENTIFICATION

Table key:

	Level 1 & 2 confidence
	Level 3 confidence
	Level 3b confidence

Compound	Description	Formula	Score	Fragmentation Score	Mass Error (ppm)	m/z	Charge	Retention time (min)	Chromatographic peak width (min)	Anova (p)	q Value	Max Fold Change	L 1	L 2	L 3	L 3 b	# of IDS	Highest Mean	Lowest Mean
0.91_169.0852n	1-Methylhistidine	C7H11N3O2	50.1	59.3	0.63	170.09	1	0.91	0.17	0.015	0.110	-1.03	x				8	Cystitis	ASB
0.90_203.2232m/z	Spermine	C10H26N4	38.3	0	0.96	203.22	1	0.90	0.07	0.000	0.005	2.42	x				7	ASB	Cystitis
0.94_188.1526n	N6,N6,N6-Trimethyl-L-lysine	C9H20N2O2	45.3	37.3	0.64	189.16	1	0.94	0.17	0.001	0.024	1.07	x				4	ASB	Cystitis
1.24_174.0642n	N-Acetylasparagine	C6H10N2O4	44.6	31	0.87	197.05	1	1.24	0.12	0.012	0.098	-1.18	x				3	Cystitis	ASB
1.53_170.0925m/z	6-tert-Butyl-2H-1,2,4-triazine-3,5-dione	C7H11N3O2	51.7	65.2	0.43	170.09	1	1.53	0.37	0.000	0.003	-1.19		x			8	Cystitis	ASB
1.35_190.0823m/z	.alpha.-Guanidinoglutaric acid	C6H11N3O4	44.7	29.1	0.36	190.08	1	1.35	0.12	0.004	0.060	-1.09		x			4	Cystitis	ASB
10.11_282.1700m/z	Cycloheximide 24428	C15H23NO4	52	63.8	0.05	282.17	1	10.11	0.19	0.009	0.088	1.10		x			6	ASB	Cystitis
0.90_227.1146m/z	Carnosine	C9H14N4O3	46.7	45.9	3.27	227.11	1	0.90	0.07	0.009	0.086	1.09		x			21	ASB	Cystitis
0.87_101.0252m/z	Hypoxanthine	C5H4N4O	29.4	6.85	4.24	101.03	1	0.87	0.16	0.000	0.000	-3.08		x			14	Cystitis	ASB
9.26_274.1781n	3-Hydroxytetradecanedioic acid	C14H26O5	48.4	48.1	0.12	239.16	1	9.26	0.30	0.009	0.088	1.04		x			2	ASB	Cystitis
6.69_246.1468n	3-Hydroxydodecanedioic acid	C12H22O5	44.2	23.4	0.25	247.15	1	6.69	0.22	0.001	0.026	1.04		x			3	ASB	Cystitis
3.96_280.0850m/z	5'-Methylthioadenosine	C11H15N5O3S	36.7	0	-4.37	280.08	1	3.96	0.10	0.002	0.044	1.41		x			9	ASB	Cystitis
0.87_188.1759m/z	Acetylspermidine	C9H21N3O	45.6	34.8	0.63	188.18	1	0.87	0.10	0.000	0.006	1.19		x			7	ASB	Cystitis
0.94_142.9482m/z	Phosphate	H3O4P	42.8	17	1.53	142.95	1	0.94	0.25	0.000	0.005	-1.44		x			5	Cystitis	ASB
1.73_164.0740m/z	S-(2-carboxypropyl)-Cysteamine	C6H13NO2S	53.3	78.1	0.24	164.07	1	1.73	0.28	0.011	0.095	-1.03		x			4	Cystitis	ASB
3.14_292.0849m/z	Hawkinsin	C11H17NO6S	51.4	66.8	-0.07	292.08	1	3.14	0.14	0.003	0.049	1.05		x			3	ASB	Cystitis
1.00_225.1322m/z	Symmetric dimethylarginine	C8H18N4O2	39.5	0	-0.19	225.13	1	1.00	0.05	0.012	0.098	-1.21		x			13	Cystitis	ASB
1.80_217.1297m/z	N-a-Acetyl-L-arginine	C8H16N4O3	38.5	0	0.74	217.13	1	1.80	0.09	0.000	0.002	-1.40		x			2	Cystitis	ASB
1.15_143.1180m/z	Isoputreanine	C7H16N2O2	51.4	66.3	0.73	143.12	1	1.15	0.21	0.008	0.081	-1.06		x			3	Cystitis	ASB
10.37_542.2730n	Cortolone-3-glucuronide	C27H42O11	54.8	81.4	0.52	525.27	1	10.37	0.15	0.002	0.039	1.08		x			1	ASB	Cystitis
7.75_280.1180m/z	Phenethylamine glucuronide	C14H19NO6	52.1	63.2	0.07	280.12	1	7.75	0.21	0.001	0.022	1.03		x			2	ASB	Cystitis
10.04_540.2575n	Tetrahydroaldosterone-3-glucuronide	C27H40O11	51.8	66.6	0.81	523.25	1	10.04	0.09	0.005	0.060	1.10		x			2	ASB	Cystitis
10.64_254.1387m/z	2-(3-Carboxy-3-(methylammonio)propyl)-L-histidine	C11H19N4O4+	46.3	50.3	4.84	254.14	1	10.64	0.22	0.008	0.081	1.05		x			4	ASB	Cystitis
3.09_390.1062n	Dopaxanthin	C18H18N2O8	44.1	25.2	-0.23	391.11	1	3.09	0.17	0.010	0.090	1.06		x			4	ASB	Cystitis
12.33_243.1835n	N-Undecanoylglycine	C13H25NO3	46.3	35.1	0.35	244.19	1	12.33	0.12	0.002	0.036	1.80		x			1	ASB	Cystitis
8.40_222.1126m/z	Metaxalone	C12H15NO3	49.2	50.4	0.52	222.11	1	8.40	0.14	0.010	0.089	1.06		x			16	ASB	Cystitis

7.18_279.1340m/z	Tyrosyl-Proline	C14H18N2O4	48.3	45.7	0.33	279.13	1	7.18	0.12	0.001	0.027	1.60		x			81	ASB	Cystitis
1.34_219.1220n	DL-Ornithino-L-alanine	C8H17N3O4	46.9	44.7	0.50	202.12	1	1.34	0.15	0.003	0.050	-1.42		x			1	Cystitis	ASB
10.07_240.0867m/z	Sarmentosin	C11H17NO7	41.7	12.1	0.12	240.09	1	10.07	0.13	0.012	0.099	1.08		x			3	ASB	Cystitis
5.78_175.1079m/z	L-Theanine	C7H14N2O3	41.7	17.8	0.83	175.11	1	5.78	0.13	0.010	0.091	-1.06		x			17	Cystitis	ASB
8.58_253.1436m/z	3alpha-Hydroxyoreadone	C14H20O4	52.7	68.1	0.46	253.14	1	8.58	0.33	0.003	0.049	1.05		x			3	ASB	Cystitis
1.73_147.0475m/z	Dihydro-2-methoxy-2-methyl-3(2H)-thiophenone	C6H10O2S	50	61.6	0.44	147.05	1	1.73	0.27	0.009	0.087	-1.03		x			1	Cystitis	ASB
11.12_300.2169m/z	3-hydroxynonanoyl carnitine	C16H31NO5	49	48.4	-0.03	300.22	1	11.12	0.69	0.009	0.086	1.04		x			1	ASB	Cystitis
3.93_221.0657m/z	3,4,5-trihydroxy-6-(2-hydroxyethoxy)oxane-2-carboxylic acid	C8H14O8	51.7	62.9	0.50	221.07	1	3.93	0.12	0.004	0.054	1.04		x			12	ASB	Cystitis
8.47_239.1391m/z	N-(3-aminopropyl)-3-(3,4-dihydroxyphenyl)propanimidic acid	C12H18N2O3	47.1	39.2	0.29	239.14	1	8.47	0.15	0.001	0.019	1.04		x			20	ASB	Cystitis
10.39_595.3493m/z	(-)-Stercobilin	C33H46N4O6	47.4	45.9	0.53	595.35	1	10.39	0.15	0.002	0.039	1.12		x			7	ASB	Cystitis
11.18_358.2587m/z	(9Z)-3-hydroxydodecenoylcarnitine	C19H35NO5	43.4	22.1	-0.23	358.26	1	11.18	0.18	0.001	0.027	1.03		x			1	ASB	Cystitis
5.19_234.1337m/z	Hydroxypropionylcarnitine	C10H19NO5	46.3	33.9	0.37	234.13	1	5.19	0.13	0.000	0.006	1.66		x			1	ASB	Cystitis
1.00_137.0710m/z	1-METHYLNICOTINAMIDE-103	C7H8N2O	53.5	70.6	0.88	137.07	1	1.00	0.13	0.004	0.058	-1.10			x		24	Cystitis	ASB
10.62_271.2056m/z	5-Androsten-3.beta.-ol-17-one	C19H28O2	57.6	92.5	-0.20	271.21	1	10.62	0.13	0.003	0.049	1.07			x		42	ASB	Cystitis
2.47_276.0173m/z	Benzophenone, 2-amino-5-chloro-	C13H10ClNO	33.2	0	4.44	276.02	1	2.47	0.18	0.000	0.007	1.06			x		1	ASB	Cystitis
6.40_414.2465n	Nonaethylene glycol	C18H38O10	39.9	4.6	0.07	415.25	1	6.40	0.12	0.002	0.042	-1.06			x		1	Cystitis	ASB
1.41_224.1129m/z	N-Acetyl-D-galactosaminitol	C8H17NO6	38.1	0	0.30	224.11	1	1.41	0.07	0.004	0.054	1.53			x		1	ASB	Cystitis
23.22_530.4008n	Didodecyl 3,3'-thiodipropionate oxide	C30H58O5S	38.7	3.74	0.57	553.39	1	23.22	0.80	0.007	0.076	-1.13			x		1	Cystitis	ASB
8.90_350.1597m/z	(-)-N6-(2-Phenylisopropyl)adenosine	C19H23N5O4	37.8	0	-3.73	350.16	1	8.90	0.11	0.004	0.058	1.03			x		1	ASB	Cystitis
3.25_256.1009m/z	L-NG-Nitroarginine methyl ester	C7H15N5O4	38.9	0	-3.28	256.10	1	3.25	0.33	0.002	0.044	1.04			x		4	ASB	Cystitis
7.39_216.0999n	3-Oxo-1,8-octanedicarboxylic acid	C10H16O5	44.9	29.5	0.59	199.10	1	7.39	0.95	0.007	0.077	1.02			x		1	ASB	Cystitis
6.20_318.1371m/z	Triticonazole	C17H20ClN3O	33.9	0	1.13	318.14	1	6.20	0.13	0.011	0.093	1.03			x		1	ASB	Cystitis
3.32_214.1268m/z	Dipropylenetriamine NONOate	C6H17N5O2	38.6	0	-3.36	214.13	1	3.32	0.16	0.002	0.035	1.09			x		2	ASB	Cystitis
13.34_301.1547m/z	Carbobenzyloxyglycyl-L-norleucine methyl ester	C17H24N2O5	39.2	0	-0.01	301.15	1	13.34	0.13	0.005	0.066	1.02			x		1	ASB	Cystitis
3.98_286.0579m/z	Ethanesulfonic acid	C12H19NO5S2	34.7	0	3.88	286.06	1	3.98	0.20	0.007	0.078	1.05			x		1	ASB	Cystitis
4.44_292.1213m/z	2-(2-(1-Hexyl-4(1H)-pyridinylidene)ethylidene)malononitrile	C16H19N3	38	0	1.13	292.12	1	4.44	0.11	0.001	0.034	1.07			x		1	ASB	Cystitis
10.67_325.0182m/z	4-[[4-(4-Chlorophenyl)-2-thiazolyl]amino]phenol	C15H11ClN2OS	32.9	0	3.03	325.02	1	10.67	0.09	0.003	0.052	1.06			x		1	ASB	Cystitis
4.56_545.1505m/z	(+)-Nutlin-3	C30H30Cl2N4O4	29.8	0	-0.09	545.15	1	4.56	0.12	0.008	0.084	1.07			x		4	ASB	Cystitis
24.09_113.0167m/z	AG-82 21779	C10H6N2O3	36.8	0	-4.45	113.02	2	24.09	0.60	0.003	0.049	-1.05			x		3	Cystitis	ASB

9.00_282.1529m/z	AGC 22132	C15H25NO3S	35.7	0	2.39	282.15	1	9.00	0.18	0.010	0.091	1.06			x		5	ASB	Cystitis
8.58_306.1911m/z	Amiprilose 17665	C14H27NO6	39.3	0.332	-0.03	306.19	1	8.58	0.25	0.003	0.049	1.07			x		5	ASB	Cystitis
6.52_440.2104m/z	N-Ethyl-D-clindamycin	C19H34ClDN2O5S	33.4	0	2.98	440.21	1	6.52	0.09	0.003	0.050	-1.08			x		1	Cystitis	ASB
8.76_251.1310m/z	DMABA-d6 NHS ester 29004	C13H8D6N2O4	36.8	0	4.67	251.13	1	8.76	0.14	0.005	0.064	1.07			x		3	ASB	Cystitis
8.20_462.2335m/z	Glu-Trp-Lys	C22H31N5O6	52.6	74.1	-2.64	462.23	1	8.20	0.15	0.001	0.023	-1.14			x		5	Cystitis	ASB
5.96_388.2540m/z	Gln Lys Leu 3540	C17H33N5O5	51	65	-3.78	388.25	1	5.96	0.27	0.009	0.086	1.03			x		29	ASB	Cystitis
9.87_363.2165m/z	Cortisol	C21H30O5	49	50.2	-0.33	363.22	1	9.87	0.11	0.007	0.078	1.09			x		39	ASB	Cystitis
1.34_130.0864m/z	Pipecolic acid	C6H11NO2	39.4	0	0.77	130.09	1	1.34	0.12	0.004	0.058	-1.12			x		42	Cystitis	ASB
0.91_90.9768m/z	Formic acid	CH2O2	39.2	0	2.40	90.98	1	0.91	0.08	0.003	0.049	1.11			x		3	ASB	Cystitis
0.91_178.0588m/z	L-Histidine	C6H9N3O2	46.6	41.6	0.88	178.06	1	0.91	0.11	0.000	0.002	1.14			x		9	ASB	Cystitis
3.97_171.1129m/z	N6-Acetyl-L-lysine	C8H16N2O3	47.2	38.9	0.38	171.11	1	3.97	0.12	0.009	0.088	1.03			x		38	ASB	Cystitis
7.37_208.0969m/z	N-Acetyl-L-phenylalanine	C11H13NO3	47.7	42.4	0.61	208.10	1	7.37	0.89	0.000	0.005	1.03			x		23	ASB	Cystitis
8.41_231.1592m/z	Dodecanedioic acid	C12H22O4	44	23.5	0.51	231.16	1	8.41	0.12	0.010	0.091	1.04			x		10	ASB	Cystitis
0.87_156.0142m/z	Cytosine	C4H5N3O	38.8	0	-1.80	156.01	1	0.87	0.11	0.000	0.000	-4.31			x		8	Cystitis	ASB
1.35_146.0692n	L-Glutamine	C5H10N2O3	38.7	0	0.63	169.06	1	1.35	0.08	0.003	0.048	1.12			x		14	ASB	Cystitis
5.54_263.1028m/z	Aspartylphenylalanine	C13H16N2O5	51.6	62.8	0.43	263.10	1	5.54	0.13	0.000	0.002	-1.09			x		31	Cystitis	ASB
12.92_412.3058m/z	Hexadecanedioic acid mono-L-carnitine ester	C23H43NO6	39	0.484	0.04	412.31	1	12.92	0.14	0.000	0.015	1.06			x		4	ASB	Cystitis
3.34_266.0329m/z	N-Acetylglucosamine 6-sulfate	C8H15NO9S	41	13.6	0.07	266.03	1	3.34	0.22	0.002	0.036	1.09			x		6	ASB	Cystitis
1.00_137.0477n	Trigonelline	C7H7NO2	51.8	64.1	0.42	160.04	1	1.00	0.21	0.010	0.090	-1.03			x		32	Cystitis	ASB
10.04_364.2249n	Tetrahydrocortisone	C21H32O5	53	68.8	-0.10	365.23	1	10.04	0.22	0.005	0.065	1.10			x		17	ASB	Cystitis
7.59_424.1746m/z	5-Methyltetrahydrofolic acid	C20H25N7O6	40.1	23.1	3.90	424.17	1	7.59	0.36	0.000	0.014	1.03			x		21	ASB	Cystitis
1.54_147.0765m/z	Ureidoisobutyric acid	C5H10N2O3	35	0	0.57	147.08	1	1.54	0.47	0.008	0.082	1.03			x		14	ASB	Cystitis
2.38_232.0275m/z	Norepinephrine sulfate	C8H11NO6S	44.8	33.4	0.31	232.03	1	2.38	0.12	0.012	0.097	1.05			x		3	ASB	Cystitis
0.87_103.1230m/z	Cadaverine	C5H14N2	43.4	24.1	0.67	103.12	1	0.87	0.11	0.011	0.092	-1.45			x		8	Cystitis	ASB
11.64_528.2629m/z	N-[(3a,5b,7a,12a)-3,7-dihydroxy-24-oxo-12-(sulfooxy)cholan-24-yl]-Glycine	C26H43NO9S	45.2	44.3	0.56	528.26	1	11.64	0.14	0.010	0.092	1.07			x		4	ASB	Cystitis
1.34_112.0394m/z	O-Acetylserine	C5H9NO4	49.8	51.9	0.31	112.04	1	1.34	0.44	0.001	0.016	-1.11			x		65	Cystitis	ASB
3.15_157.0497m/z	Quinic acid	C7H12O6	50.2	55.6	0.77	157.05	1	3.15	0.14	0.004	0.059	1.06			x		29	ASB	Cystitis
10.54_188.0707m/z	5-Methoxyindoleacetate	C11H11NO3	54.7	86.4	0.49	188.07	1	10.54	0.20	0.003	0.046	1.46			x		55	ASB	Cystitis
10.35_591.3181m/z	D-Urobilinogen	C33H42N4O6	45.8	38.6	0.64	591.32	1	10.35	0.14	0.012	0.099	1.11			x		3	ASB	Cystitis

6.56_200.0919m/z	Putreanine	C7H17N2O2+	50.3	54.7	-1.88	200.09	1	6.56	0.14	0.011	0.092	1.06			x		5	ASB	Cystitis
9.58_301.2162m/z	15-HEPE	C20H30O3	55.2	80.4	-0.11	301.22	1	9.58	0.13	0.004	0.056	1.06			x		366	ASB	Cystitis
24.09_111.0203m/z	Imidazole acetol-phosphate	C6H9N2O5P	37.9	0	4.87	111.02	2	24.09	1.10	0.008	0.082	-1.03			x		1	Cystitis	ASB
6.77_364.1965m/z	Isopentenyladenine-9-N-glucoside	C17H25N5O4	37.4	0	-3.85	364.20	1	6.77	0.09	0.005	0.064	1.08			x		1	ASB	Cystitis
11.22_313.2122m/z	Oseltamivir	C16H28N2O4	41.6	12.5	-0.08	313.21	1	11.22	0.18	0.002	0.039	1.07			x		62	ASB	Cystitis
25.83_199.9881m/z	Pamidronate	C3H11NO7P2	38.5	0	3.90	199.99	1	25.83	2.75	0.007	0.078	1.16			x		2	ASB	Cystitis
1.31_243.1704m/z	Carisoprodol	C12H24N2O4	38	0	0.21	243.17	1	1.31	0.07	0.001	0.016	-1.28			x		15	Cystitis	ASB
12.35_326.2325m/z	Bisoprolol	C18H31NO4	42.1	16.2	-0.17	326.23	1	12.35	0.17	0.011	0.094	1.04			x		13	ASB	Cystitis
12.14_224.1282m/z	Cerulenin	C12H17NO3	41.8	22.3	0.30	224.13	1	12.14	0.24	0.005	0.065	1.03			x		15	ASB	Cystitis
2.74_248.0587m/z	Proflavine	C13H11N3	37.8	0	1.40	248.06	1	2.74	0.14	0.010	0.088	-1.05			x		2	Cystitis	ASB
6.50_223.1442m/z	Pirbuterol	C12H20N2O3	42.3	16	0.29	223.14	1	6.50	0.09	0.007	0.074	-1.04			x		3	Cystitis	ASB
2.50_295.0860m/z	Sulfacytine	C12H14N4O3S	38.5	1.98	0.05	295.09	1	2.50	0.22	0.001	0.030	1.04			x		3	ASB	Cystitis
4.75_226.1318n	Amobarbital	C11H18N2O3	40.3	9.63	0.20	265.10	1	4.75	0.31	0.007	0.077	1.06			x		9	ASB	Cystitis
7.42_246.1337m/z	Neostigmine	C12H19N2O2+	39.1	2.05	-0.72	246.13	1	7.42	0.20	0.001	0.029	1.06			x		1	ASB	Cystitis
11.06_298.1650m/z	Alizapride	C16H21N5O2	38	0	-4.05	298.16	1	11.06	0.16	0.006	0.072	1.09			x		1	ASB	Cystitis
3.39_250.1286m/z	Voglibose	C10H21NO7	39.2	0	0.20	250.13	1	3.39	0.13	0.009	0.086	1.07			x		1	ASB	Cystitis
5.56_185.1286m/z	Alanyl-Isoleucine	C9H18N2O3	44.1	25.9	0.69	185.13	1	5.56	0.12	0.001	0.032	-1.15			x		26	Cystitis	ASB
1.71_254.1611m/z	Arginyl-Proline	C11H21N5O3	49.2	59.4	-0.12	254.16	1	1.71	0.17	0.005	0.065	-1.06			x		4	Cystitis	ASB
3.32_213.1235m/z	Hydroxyprolyl-Valine	C10H18N2O4	48.4	54.1	0.38	213.12	1	3.32	0.16	0.012	0.098	1.06			x		8	ASB	Cystitis
5.10_209.1285m/z	Isoleucyl-Hydroxyproline	C11H20N2O4	45.3	30.6	0.33	209.13	1	5.10	0.16	0.001	0.022	-1.05			x		17	Cystitis	ASB
1.05_141.0659m/z	Threoninyl-Glycine	C6H12N2O4	53.8	72.8	0.34	141.07	1	1.05	0.39	0.000	0.012	-1.08			x		26	Cystitis	ASB
5.46_181.0972m/z	Threoninyl-Proline	C9H16N2O4	46.1	37.4	0.17	181.10	1	5.46	0.11	0.012	0.099	1.07			x		21	ASB	Cystitis
2.75_221.0921m/z	Tyrosyl-Glycine	C11H14N2O4	53.1	72.2	0.34	221.09	1	2.75	0.28	0.000	0.000	-1.46			x		38	Cystitis	ASB
4.82_199.1442m/z	Valyl-Valine	C10H20N2O3	38.8	0	0.59	199.14	1	4.82	0.11	0.000	0.000	1.68			x		5	ASB	Cystitis
1.10_174.0874m/z	4-Hydroxycitrulline	C6H13N3O4	48.1	47.1	0.69	174.09	1	1.10	0.17	0.002	0.042	-1.31			x		2	Cystitis	ASB
11.95_195.1381m/z	Cucurbic acid	C12H20O3	48.6	47	0.75	195.14	1	11.95	0.20	0.004	0.058	1.03			x		56	ASB	Cystitis
1.33_141.0790n	L-Hypoglycin A	C7H11NO2	42.7	17.8	0.27	164.07	1	1.33	0.15	0.000	0.000	-1.25			x		7	Cystitis	ASB
2.65_162.0584m/z	(R)C(R)S-S-Propylcysteine sulfoxide	C6H13NO3S	40.7	9.03	0.45	162.06	1	2.65	0.21	0.008	0.081	1.06			x		14	ASB	Cystitis
1.69_237.0870m/z	L-Agaridoxin	C11H14N2O5	54.2	73.9	0.11	237.09	1	1.69	0.14	0.005	0.062	1.04			x		37	ASB	Cystitis

19.28_425.2873m/z	Sorbitan palmitate	C22H42O6	39.1	0.0759	-0.09	425.29	1	19.28	0.14	0.011	0.096	-1.19			x		4	Cystitis	ASB
0.88_325.0887m/z	Kuwanon L	C35H30O11	37.3	0.054	3.40	325.09	2	0.88	0.07	0.000	0.000	-2.11			x		1	Cystitis	ASB
9.81_230.1520n	Talaromycin A	C12H22O4	48.3	46	0.74	195.14	1	9.81	0.29	0.004	0.054	1.06			x		8	ASB	Cystitis
1.06_143.0947n	L-2-Amino-3-methylenehexanoic acid	C7H13NO2	45.6	36.2	0.61	144.10	1	1.06	0.37	0.008	0.081	-1.05			x		8	Cystitis	ASB
10.50_214.1206n	alpha-Carboxy-delta-decalactone	C11H18O4	47.7	42.5	0.56	215.13	1	10.50	0.17	0.004	0.059	1.07			x		3	ASB	Cystitis
3.44_129.0547m/z	Osmundalactone	C6H8O3	51.9	62.2	0.32	129.05	1	3.44	0.46	0.005	0.064	-1.17			x		85	Cystitis	ASB
5.67_262.0954n	L-cis-Cyclo(aspartylphenylalanyl)	C13H14N2O4	45.2	40.2	0.13	263.10	1	5.67	0.22	0.000	0.006	-1.06			x		3	Cystitis	ASB
3.39_232.0948n	Glycerol 1-propanoate diacetate	C10H16O6	42.3	13.8	0.65	215.09	1	3.39	0.21	0.002	0.039	1.08			x		1	ASB	Cystitis
9.25_229.1435m/z	Hexyl glucoside	C12H24O6	48.4	46.7	0.43	229.14	1	9.25	0.32	0.002	0.036	1.07			x		19	ASB	Cystitis
7.41_245.1385m/z	Phaseolic acid	C12H22O6	46	36	0.39	245.14	1	7.41	0.17	0.012	0.097	1.07			x		12	ASB	Cystitis
3.41_332.1339m/z	Casuarine 6-alpha-D-glucoside	C14H25NO10	45.2	31.1	-0.21	332.13	1	3.41	0.15	0.011	0.092	1.09			x		30	ASB	Cystitis
24.09_114.0166m/z	Sinalexin	C10H8N2OS	37.4	8.3	4.79	114.02	2	24.09	0.39	0.002	0.044	-1.05			x		1	Cystitis	ASB
7.92_394.1643m/z	N-[2-(3,4-Dimethoxyphenyl)ethyl]-3,4-dimethoxycinnamic acid amide	C21H25NO5	38.3	3.67	4.95	394.16	1	7.92	0.34	0.002	0.042	1.05			x		2	ASB	Cystitis
8.22_244.1312n	Polyethylene, oxidized	C12H20O5	47.5	41.5	0.54	245.14	1	8.22	0.14	0.002	0.046	1.04			x		1	ASB	Cystitis
8.03_166.0323m/z	4-Hydroxybenzyl isothiocyanate	C8H7NOS	38.3	0	0.88	166.03	1	8.03	0.12	0.007	0.078	-1.18			x		1	Cystitis	ASB
0.90_316.9776m/z	Menadiol disulfate	C11H10O8S2	36.8	0	-2.51	316.98	1	0.90	0.05	0.000	0.000	-27.15			x		1	Cystitis	ASB
6.59_261.1333m/z	Glycerol tripropanoate	C12H20O6	43.4	19.1	0.16	261.13	1	6.59	0.19	0.001	0.026	1.04			x		12	ASB	Cystitis
24.80_208.0394m/z	5-(2-Hydroxyethyl)-4-methylthiazole acetate	C8H11NO2S	38.7	6.76	-4.47	208.04	1	24.80	1.62	0.008	0.084	1.10			x		1	ASB	Cystitis
7.05_480.1867m/z	Cadabicine	C25H29N3O4	38.5	1.32	-0.58	480.19	1	7.05	0.10	0.008	0.082	-1.06			x		1	Cystitis	ASB
7.51_114.0373m/z	4-Isothiocyanato-1-butene	C5H7NS	41	16.8	1.05	114.04	1	7.51	0.22	0.005	0.062	-1.22			x		19	Cystitis	ASB
11.30_312.1441m/z	Domoic acid	C15H21NO6	45.6	32.2	-0.24	312.14	1	11.30	0.14	0.003	0.049	1.05			x		12	ASB	Cystitis
3.17_200.0918m/z	2-Acetyl-1,5,6,7-tetrahydro-6-hydroxy-7-(hydroxymethyl)-4H-azepine-4-one	C9H13NO4	53.8	72.7	0.52	200.09	1	3.17	0.41	0.003	0.051	1.05			x		5	ASB	Cystitis
2.46_293.0437m/z	Aurantricholide B	C17H10O6	37.7	2.99	-2.42	293.04	1	2.46	0.15	0.001	0.033	1.08			x		31	ASB	Cystitis
9.68_496.2310n	Glaucarubin	C25H36O10	39.7	4.42	0.28	497.24	1	9.68	0.18	0.012	0.098	1.05			x		4	ASB	Cystitis
3.02_233.0900n	Hirsutin	C10H19NOS2	36.7	0	-3.53	234.10	1	3.02	0.24	0.006	0.072	1.02			x		2	ASB	Cystitis
17.05_194.1672n	7,8-Dehydro-3,4-dihydro-beta-ionol	C13H22O	45.3	29	0.58	195.17	1	17.05	0.16	0.008	0.081	-1.11			x		14	Cystitis	ASB
11.23_227.1642m/z	Riesling acetal	C13H22O3	49.3	49.7	0.15	227.16	1	11.23	0.11	0.010	0.090	1.41			x		14	ASB	Cystitis
8.33_380.1471n	(S)-Bitalin A 12-glucoside	C19H24O8	44.8	29.6	-0.17	363.14	1	8.33	0.40	0.004	0.054	1.04			x		5	ASB	Cystitis
23.37_569.3849m/z	33-Deoxy-33-hydroperoxyfurohyperforin	C35H52O6	37.3	0.169	2.21	569.38	1	23.37	0.23	0.003	0.051	-1.08			x		7	Cystitis	ASB

1.33_142.0864m/z	Medicanine	C7H13NO3	50.3	54.5	0.71	142.09	1	1.33	0.77	0.000	0.000	-1.26			x		30	Cystitis	ASB
2.14_305.1131m/z	L-N-(1H-Indol-3-ylacetyl)glutamic acid	C15H16N2O5	39	0	-0.41	305.11	1	2.14	0.15	0.000	0.015	3.08			x		34	ASB	Cystitis
9.28_184.1101n	(4S,8R)-8,9-Dihydroxy-p-menth-1(6)-en-2-one	C10H16O3	49.8	53.3	0.81	185.12	1	9.28	0.21	0.009	0.086	1.07			x		11	ASB	Cystitis
12.76_507.3070m/z	21-Hydroxyisoglabrolide	C30H44O5	52.7	71.8	-2.16	507.31	1	12.76	0.10	0.003	0.049	-1.14			x		31	Cystitis	ASB
1.61_164.1071m/z	2-(5-Methyl-2-furanyl)-3-piperidinol	C10H15NO2	44	25.3	0.79	164.11	1	1.61	0.15	0.000	0.000	-1.47			x		40	Cystitis	ASB
8.06_152.0838n	4-Ethyl-2-methoxyphenol	C9H12O2	48.2	43.4	0.48	153.09	1	8.06	0.20	0.011	0.094	1.05			x		19	ASB	Cystitis
5.95_391.1135m/z	8-Hydroxy-3',4',5',7-tetramethoxyflavan	C19H22O6	40.7	11.1	1.96	391.11	1	5.95	0.09	0.009	0.086	1.12			x		96	ASB	Cystitis
6.37_152.0166m/z	4-Thiocyanatophenol	C7H5NOS	37.4	0.288	0.68	152.02	1	6.37	0.14	0.000	0.002	-1.67			x		4	Cystitis	ASB
5.45_562.1770m/z	Pulcherosine	C27H29N3O9	39.1	12.7	-4.79	562.18	1	5.45	0.10	0.010	0.092	1.19			x		1	ASB	Cystitis
7.78_225.0426m/z	1-Methoxy-1H-indole-3-acetonitrile	C11H10N2O	39	0	0.84	225.04	1	7.78	0.11	0.003	0.049	1.09			x		7	ASB	Cystitis
0.93_194.0328m/z	Phosphocreatinine	C4H8N3O4P	38.9	0	1.54	194.03	1	0.93	0.12	0.006	0.072	1.10			x		16	ASB	Cystitis
2.34_160.0758m/z	N-Acetyldopamine	C10H13NO3	41.3	11	0.53	160.08	1	2.34	0.29	0.008	0.082	-1.04			x		32	Cystitis	ASB
3.41_148.0737n	(2-Methoxyethoxy)propanoic acid	C6H12O4	42.7	19	0.75	171.06	1	3.41	0.25	0.010	0.090	1.05			x		10	ASB	Cystitis
6.58_246.1530m/z	S-3-oxodecanoyl cysteamine	C12H23NO2S	37.2	0	3.06	246.15	1	6.58	0.21	0.001	0.027	1.04			x		1	ASB	Cystitis
12.33_299.1965m/z	Diphthamide	C13H24N5O3+	44	27.9	4.44	299.20	1	12.33	0.14	0.001	0.034	1.04			x		77	ASB	Cystitis
13.09_268.1544m/z	N-Monodesmethyl-rizatriptan	C15H19N5O	39.9	9.54	-4.60	268.15	1	13.09	0.14	0.000	0.001	1.94			x		8	ASB	Cystitis
12.98_254.1751m/z	3-hydroxyhexanoyl carnitine	C14H27NO5	43.1	18.5	0.02	254.18	1	12.98	0.13	0.000	0.002	1.86			x		2	ASB	Cystitis
16.96_356.2794m/z	3-hydroxytridecanoyl carnitine	C20H39NO5	39.6	3.09	-0.24	356.28	1	16.96	0.11	0.013	0.100	1.06			x		1	ASB	Cystitis
1.33_160.0969m/z	Methyl 5-(hydroxymethyl)pyrrolidine-3-carboxylate	C7H13NO3	50.6	58.9	0.63	160.10	1	1.33	0.27	0.002	0.041	-1.16			x		26	Cystitis	ASB
2.28_173.0810m/z	6-(2-Hydroxyethoxy)-6-oxohexanoic acid	C8H14O5	49	49.7	0.75	173.08	1	2.28	0.29	0.001	0.034	1.05			x		18	ASB	Cystitis
3.45_499.1561m/z	alpha-CEHC glucuronide	C22H30O10	40	9.35	2.21	499.16	1	3.45	0.11	0.007	0.077	-1.30			x		19	Cystitis	ASB
1.18_203.0794n	N-acetyl-L-2-aminoadipate(2-)	C8H13NO5	34.8	0	0.14	242.04	1	1.18	0.15	0.010	0.091	-1.11			x		2	Cystitis	ASB
10.11_264.1362n	3-[4-hydroxy-2-methoxy-3-(3-methylbut-2-en-1-yl)phenyl]propanoic acid	C15H20O4	49.5	50.3	0.22	247.13	1	10.11	0.22	0.010	0.090	1.05			x		48	ASB	Cystitis
4.23_169.0860m/z	4-ethyl-6-methoxybenzene-1,3-diol	C9H12O3	47.7	45.2	0.51	169.09	1	4.23	0.18	0.000	0.006	-1.26			x		26	Cystitis	ASB
3.75_195.0654m/z	3-(3,4-dihydroxy-5-methoxyphenyl)propanoic acid	C10H12O5	53.2	78.6	0.82	195.07	1	3.75	0.16	0.001	0.029	1.06			x		79	ASB	Cystitis
5.99_239.0551m/z	3-(7-hydroxy-6-methoxy-2H-1,3-benzodioxol-5-yl)prop-2-enoic acid	C11H10O6	44.9	28	0.26	239.06	1	5.99	0.11	0.011	0.096	-1.06			x		10	Cystitis	ASB
2.19_204.0657m/z	2-{[(3,5-dimethoxyphenyl)(hydroxy)methylidene]amino}acetic acid	C11H13NO5	42.9	20.3	0.65	204.07	1	2.19	0.14	0.012	0.098	-1.04			x		14	Cystitis	ASB
6.62_225.1002n	(2S)-2-amino-3-(4-hydroxy-3-methoxyphenyl)-2-methylpropanoic acid	C11H15NO4	49.6	52.1	0.56	208.10	1	6.62	0.26	0.003	0.054	1.06			x		1	ASB	Cystitis
1.19_256.1485m/z	JWH030 30262	C20H21NO	37.4	0	0.06	256.15	1	1.19	0.08	0.000	0.002	-1.34			x		3	Cystitis	ASB

1.55_90.0551m/z	L-ALANINE-41	C3H7NO2	37.2	0	0.70	90.06	1	1.55	0.35	0.003	0.049	-1.06			x		25	Cystitis	ASB
0.90_211.1418m/z	7,8-diaminononanoic acid	C9H20N2O2	39.1	0	0.74	211.14	1	0.90	0.04	0.000	0.001	1.69			x		5	ASB	Cystitis
8.35_302.1962m/z	3-hydroxy-cis-5-octenoylcarnitine	C15H27NO5	45.3	30.1	0.03	302.20	1	8.35	0.43	0.000	0.007	-1.06			x		6	Cystitis	ASB
12.44_274.2012m/z	Heptanoylcarnitine	C14H27NO4	39	0.0291	-0.25	274.20	1	12.44	0.09	0.001	0.035	1.14			x		1	ASB	Cystitis
12.33_402.2851m/z	O-(13-carboxytridecanoyl)carnitine	C21H39NO6	50.5	57.3	0.17	402.29	1	12.33	0.29	0.009	0.085	1.05			x		8	ASB	Cystitis
10.04_522.2337m/z	DMG-MINO	C27H35N5O8	36.8	0	-1.73	522.23	1	10.04	0.09	0.001	0.020	1.11			x		1	ASB	Cystitis
13.42_372.2745m/z	Sphingofungin B	C20H39NO6	44.4	28.9	0.02	372.27	1	13.42	0.10	0.003	0.049	1.31			x		1	ASB	Cystitis
5.46_344.2278m/z	Lys-Ser-Lys	C15H31N5O5	44.5	32.9	-3.97	344.23	1	5.46	0.27	0.009	0.087	1.03			x		4	ASB	Cystitis
1.00_265.1116m/z	THIAMINE-100	C12H17N4OS	38.7	0	-0.59	265.11	1	1.00	0.05	0.000	0.016	-1.21			x		2	Cystitis	ASB
5.87_420.2229m/z	Trp Ser Lys 11020	C20H29N5O5	37.8	0.929	-3.04	420.22	1	5.87	0.10	0.008	0.081	1.08			x		9	ASB	Cystitis
5.89_418.2072m/z	Trp Val Asn 1792	C20H27N5O5	37.8	0.674	-3.07	418.21	1	5.89	0.10	0.004	0.054	1.14			x		9	ASB	Cystitis
7.91_468.2442m/z	Val-Arg-Arg	C17H35N9O4	38.9	0	-0.32	468.24	1	7.91	0.15	0.009	0.086	-1.05				x	6	Cystitis	ASB
4.36_117.0699m/z	2-Phenylpropionaldehyde	C9H10O	56	85.1	0.40	117.07	1	4.36	0.24	0.002	0.041	-1.03				x	35	Cystitis	ASB
6.51_250.1108m/z	Ametryn	C9H17N5S	37.2	0	4.80	250.11	1	6.51	0.10	0.004	0.058	1.06				x	1	ASB	Cystitis
5.98_250.1108m/z	Ametryn	C9H17N5S	37.2	0	4.85	250.11	1	5.98	0.29	0.011	0.096	1.03				x	1	ASB	Cystitis
0.90_202.9973m/z	2,4-Dihydroxypteridine :: Pteridines :: Polar Metabolites :: 1H-pteridine-2,4-dione	C6H4N4O2	38.8	0	4.29	203.00	1	0.90	0.06	0.000	0.000	-4.37				x	5	Cystitis	ASB
1.40_267.1186m/z	L-(-)-Arabitol, permethyl-	C10H22O5	37.9	0	3.42	267.12	1	1.40	0.12	0.004	0.054	1.55				x	3	ASB	Cystitis
9.75_143.1068m/z	2-Propyl-2-pentenoic acid	C8H14O2	45.1	29.2	1.01	143.11	1	9.75	0.20	0.002	0.044	-1.08				x	127	Cystitis	ASB
5.56_354.1547m/z	L-Arginine-7-amido-4-methylcoumarin	C16H21N5O3	37.9	0	3.08	354.15	1	5.56	0.09	0.000	0.011	-1.09				x	39	Cystitis	ASB
2.07_279.1551m/z	Tri(propylene glycol) propyl ether	C12H26O4	38.4	0	3.40	279.16	1	2.07	0.12	0.006	0.073	1.06				x	1	ASB	Cystitis
4.06_279.1551m/z	Tri(propylene glycol) propyl ether	C12H26O4	37.8	0	3.47	279.16	1	4.06	0.13	0.002	0.041	1.08				x	1	ASB	Cystitis
11.97_242.1387m/z	N-(3-Oxooctanoyl)-L-homoserine lactone	C12H19NO4	39.7	0.695	0.07	242.14	1	11.97	0.14	0.011	0.092	1.09				x	3	ASB	Cystitis
15.64_304.2998m/z	N-[(1R)-2-Hydroxy-1-methylethyl-9Z-octadecenamide	C21H41NO2	39.1	0	-0.08	304.30	1	15.64	0.13	0.010	0.088	1.11				x	4	ASB	Cystitis
10.82_252.1231m/z	Acetyl Tyrosine Ethyl Ester 17404	C13H17NO4	39.2	0	0.24	252.12	1	10.82	0.18	0.001	0.027	1.06				x	7	ASB	Cystitis
2.18_396.1502m/z	Ala Tyr Val 25311	C17H25N3O5	38.3	0	-1.20	396.15	1	2.18	0.20	0.001	0.031	-1.07				x	69	Cystitis	ASB
5.66_454.2007m/z	Arg Glu Gln 13213	C16H29N7O7	38.6	0	-3.24	454.20	1	5.66	0.09	0.001	0.031	-1.19				x	11	Cystitis	ASB
6.75_406.2072m/z	Asn Lys Tyr 3435	C19H29N5O6	37.9	0	-2.97	406.21	1	6.75	0.08	0.008	0.084	1.11				x	17	ASB	Cystitis
6.92_380.1816m/z	Asp Val Phe 9677	C18H25N3O6	56.9	90.2	0.05	380.18	1	6.92	0.12	0.006	0.072	-1.05				x	40	Cystitis	ASB
15.04_432.2382m/z	Met(O)-Lys-Arg	C17H35N7O5S	37.8	0	-1.26	432.24	1	15.04	0.18	0.012	0.098	1.14				x	4	ASB	Cystitis

1.92_269.0590m/z	Ergothioneine 20679	C9H16N3O2S	38.2	0.0282	-2.02	269.06	1	1.92	0.11	0.004	0.056	-1.05				x	7	Cystitis	ASB
8.32_462.2335m/z	Glu-Trp-Lys	C22H31N5O6	44.7	35.2	-2.62	462.23	1	8.32	0.22	0.006	0.073	-1.09				x	3	Cystitis	ASB
10.38_597.3560m/z	GPA(20:5/9:0)	C32H53O8P	35.1	0	1.50	597.36	1	10.38	0.11	0.002	0.039	1.15				x	6	ASB	Cystitis
7.38_516.2711m/z	GPEtn(14:1/4:0)	C23H44NO8P	36.3	0	2.86	516.27	1	7.38	0.09	0.000	0.006	1.12				x	23	ASB	Cystitis
7.60_406.1641m/z	His Met His 1385	C17H25N7O4S	37.5	0	-3.55	406.16	1	7.60	0.28	0.004	0.060	1.03				x	20	ASB	Cystitis
7.92_396.1612m/z	His Pro Val 7439	C16H25N5O4	38.9	0	-1.84	396.16	1	7.92	0.22	0.002	0.043	1.05				x	12	ASB	Cystitis
2.04_206.1025m/z	Tetrahydrobiopterin	C9H15N5O3	45.8	40.7	-4.89	206.10	1	2.04	0.14	0.005	0.062	1.06				x	10	ASB	Cystitis
3.46_162.1125m/z	L-Carnitine	C7H15NO3	39.6	2.05	0.44	162.11	1	3.46	0.11	0.005	0.065	1.16				x	6	ASB	Cystitis
1.34_137.0598m/z	Phenylacetic acid	C8H8O2	38.2	0	0.76	137.06	1	1.34	0.07	0.000	0.003	-1.32				x	63	Cystitis	ASB
1.82_177.1023m/z	Serotonin	C10H12N2O	38.7	0	0.60	177.10	1	1.82	0.16	0.008	0.082	-1.06				x	18	Cystitis	ASB
2.04_171.0652m/z	3,4-Dihydroxyphenylglycol	C8H10O4	38.8	0	0.12	171.07	1	2.04	0.14	0.008	0.083	1.05				x	19	ASB	Cystitis
5.94_155.0703m/z	2-Octenedioic acid	C8H12O4	47.1	40.6	0.43	155.07	1	5.94	0.18	0.011	0.092	1.04				x	36	ASB	Cystitis
11.41_246.1701m/z	2-Methylbutyroylcarnitine	C12H23NO4	39	0	0.27	246.17	1	11.41	0.13	0.007	0.074	1.15				x	8	ASB	Cystitis
9.50_183.1017m/z	2-Hydroxydecanedioic acid	C10H18O5	49.6	52.7	0.72	183.10	1	9.50	0.14	0.002	0.041	1.06				x	38	ASB	Cystitis
6.44_221.0921m/z	5-Hydroxy-L-tryptophan	C11H12N2O3	28	0	0.35	221.09	1	6.44	0.14	0.001	0.030	1.39				x	38	ASB	Cystitis
12.47_257.2263m/z	5a-Androstane-3b,17b-diol	C19H32O2	52	63.9	-0.17	257.23	1	12.47	0.08	0.004	0.055	1.08				x	37	ASB	Cystitis
4.68_361.1129m/z	3-Methoxy-4-hydroxyphenylglycol glucuronide	C15H20O10	38.8	0	-0.13	361.11	1	4.68	0.18	0.010	0.091	-1.14				x	18	Cystitis	ASB
8.45_272.1493m/z	3-Methylglutarylcarnitine	C13H23NO6	39.3	0	0.05	272.15	1	8.45	0.22	0.008	0.081	1.09				x	3	ASB	Cystitis
3.81_159.0653m/z	Succinylacetone	C7H10O4	38.8	0	0.73	159.07	1	3.81	0.17	0.011	0.095	1.06				x	36	ASB	Cystitis
10.56_246.1701m/z	Isovalerylcarnitine	C12H23NO4	39.4	7.24	0.29	246.17	1	10.56	0.15	0.003	0.049	1.15				x	8	ASB	Cystitis
7.13_223.0845n	N-Acetyl-L-tyrosine	C11H13NO4	49.1	49.2	0.37	224.09	1	7.13	0.24	0.007	0.080	1.04				x	15	ASB	Cystitis
2.13_85.0649m/z	Valeric acid	C5H10O2	41.4	10.3	0.85	85.06	1	2.13	0.25	0.012	0.098	-1.07				x	45	Cystitis	ASB
10.56_211.1330m/z	Traumatic acid	C12H20O4	51.5	61.8	0.40	211.13	1	10.56	0.26	0.007	0.074	1.09				x	35	ASB	Cystitis
5.05_208.0605m/z	4-(2-Aminophenyl)-2,4-dioxobutanoic acid	C10H9NO4	53.3	78.4	0.41	208.06	1	5.05	0.16	0.010	0.090	-1.03				x	8	Cystitis	ASB
2.04_295.0327m/z	gamma-Glutamylcysteine	C8H14N2O5S	38.6	0	-3.21	295.03	1	2.04	0.16	0.009	0.086	1.06				x	12	ASB	Cystitis
1.35_237.0870m/z	N'-Formylkynurenine	C11H12N2O4	38.3	0	0.23	237.09	1	1.35	0.06	0.008	0.081	-1.16				x	37	Cystitis	ASB
6.77_196.0606m/z	Dopaquinone	C9H9NO4	50.5	64.1	0.88	196.06	1	6.77	0.24	0.003	0.049	1.05				x	26	ASB	Cystitis
6.33_219.1129m/z	N-Acetylserotonin	C12H14N2O2	38.8	0	0.51	219.11	1	6.33	0.14	0.009	0.088	-1.07				x	56	Cystitis	ASB
6.30_350.0870m/z	1,7-Dimethylguanosine	C12H17N5O5	38.7	0	2.82	350.09	1	6.30	0.12	0.000	0.003	-1.29				x	7	Cystitis	ASB

9.15_232.1544m/z	Butyrylcarnitine	C11H21NO4	41.3	17.1	0.42	232.15	1	9.15	0.19	0.013	0.099	1.05				x	6	ASB	Cystitis
12.17_190.0863m/z	Indole-3-propionic acid	C11H11NO2	54	72.6	0.47	190.09	1	12.17	0.17	0.000	0.004	1.79				x	34	ASB	Cystitis
7.78_244.1544m/z	Tiglylcarnitine	C12H21NO4	38.9	0	0.44	244.15	1	7.78	0.11	0.012	0.098	1.07				x	8	ASB	Cystitis
1.75_181.0608m/z	Nicotinuric acid	C8H8N2O3	38.3	0	0.43	181.06	1	1.75	0.22	0.002	0.043	-1.08				x	13	Cystitis	ASB
13.72_140.0683m/z	5-Aminopentanoic acid	C5H11NO2	39	0	0.75	140.07	1	13.72	0.59	0.001	0.016	-1.08				x	30	Cystitis	ASB
0.93_124.0871m/z	L-Histidinol	C6H11N3O	38.2	0	1.02	124.09	1	0.93	0.04	0.000	0.003	-1.20				x	8	Cystitis	ASB
1.83_161.0922m/z	D-Alanyl-D-alanine	C6H12N2O3	38.4	0	0.58	161.09	1	1.83	0.12	0.008	0.081	1.10				x	12	ASB	Cystitis
1.08_171.0280m/z	Homocitric acid	C7H10O7	37.3	0	-4.09	171.03	1	1.08	0.11	0.011	0.092	1.53				x	23	ASB	Cystitis
9.26_151.1119m/z	Perillyl aldehyde	C10H14O	39.2	0	0.85	151.11	1	9.26	0.19	0.010	0.090	1.06				x	182	ASB	Cystitis
2.63_111.0554m/z	Imidazole-4-acetaldehyde	C5H6N2O	38.9	0	0.72	111.06	1	2.63	0.15	0.009	0.086	-1.15				x	32	Cystitis	ASB
1.64_217.1295m/z	N-a-Acetyl-L-arginine	C8H16N4O3	38.2	0	0.12	217.13	1	1.64	0.05	0.000	0.006	-1.89				x	2	Cystitis	ASB
6.08_350.0869m/z	N2,N2-Dimethylguanosine	C12H17N5O5	38.8	0	2.50	350.09	1	6.08	0.09	0.000	0.000	-1.46				x	7	Cystitis	ASB
1.34_154.0863m/z	p-Octopamine	C8H11NO2	38.7	0	0.37	154.09	1	1.34	0.07	0.000	0.007	-1.14				x	37	Cystitis	ASB
3.76_302.1598m/z	Kyotorphin	C15H23N5O4	38.2	3.67	-4.13	302.16	1	3.76	0.20	0.001	0.023	1.07				x	18	ASB	Cystitis
6.29_332.1339m/z	2-Acetamido-2-deoxy-6-O-a-L-fucopyranosyl-D-glucose	C14H25NO10	40.7	7.64	-0.21	332.13	1	6.29	0.21	0.013	0.101	1.04				x	30	ASB	Cystitis
1.08_203.0318m/z	2-Hydroxy-3-(4-hydroxyphenyl)propenoic acid	C9H8O4	37.8	0	1.98	203.03	1	1.08	0.09	0.006	0.071	-1.21				x	68	Cystitis	ASB
10.71_464.2412n	Dehydroisoandrosterone 3-glucuronide	C25H36O8	52.5	68.3	0.30	429.23	1	10.71	0.14	0.003	0.050	1.09				x	20	ASB	Cystitis
11.18_463.2327m/z	11-Oxo-androsterone glucuronide	C25H36O9	46.9	40	0.13	463.23	1	11.18	0.13	0.000	0.008	1.07				x	38	ASB	Cystitis
12.66_433.2585m/z	3-alpha-Androstanediol glucuronide	C25H40O8	49.4	53.4	0.10	433.26	1	12.66	0.12	0.005	0.062	1.06				x	12	ASB	Cystitis
11.63_465.2485m/z	11-beta-Hydroxyandrosterone-3-glucuronide	C25H38O9	56	86	0.43	465.25	1	11.63	0.15	0.012	0.099	1.04				x	26	ASB	Cystitis
8.98_500.2789m/z	LysoPE(0:0/20:5(5Z,8Z,11Z,14Z,17Z))	C25H42NO7P	40.1	8.74	3.50	500.28	1	8.98	0.11	0.008	0.083	-1.12				x	6	Cystitis	ASB
12.14_572.2705m/z	LysoPE(0:0/22:5(7Z,10Z,13Z,16Z,19Z))	C27H46NO7P	38.1	0.619	-3.45	572.27	1	12.14	0.11	0.002	0.038	1.04				x	9	ASB	Cystitis
1.36_123.0441m/z	4-Hydroxybenzaldehyde	C7H6O2	38.4	0	0.35	123.04	1	1.36	0.10	0.002	0.042	-1.12				x	46	Cystitis	ASB
24.72_180.9899m/z	Dihydroxyacetone Phosphate Acyl Ester	C4H7O7P	38.6	0	1.17	180.99	1	24.72	1.16	0.008	0.082	-1.03				x	23	Cystitis	ASB
1.32_200.1394m/z	Gamma-glutamyl-L-putrescine	C9H19N3O3	38	0	0.32	200.14	1	1.32	0.05	0.009	0.088	-1.16				x	13	Cystitis	ASB
2.33_194.1177m/z	(-)-Salsoline	C11H15NO2	38.8	0	0.88	194.12	1	2.33	0.38	0.001	0.029	-1.05				x	37	Cystitis	ASB
2.28_84.0809m/z	5-Aminopentanal	C5H11NO	38.6	0	0.97	84.08	1	2.28	0.30	0.011	0.094	1.21				x	8	ASB	Cystitis
12.56_357.2787m/z	6,9,12,15,18,21-Tetracosahexaenoic acid	C24H36O2	56.6	87.9	-0.28	357.28	1	12.56	0.14	0.005	0.064	1.06				x	150	ASB	Cystitis
6.70_238.1075m/z	Salsoline-1-carboxylate	C12H15NO4	49.1	49.1	0.28	238.11	1	6.70	0.44	0.006	0.067	1.03				x	5	ASB	Cystitis

8.81_199.0966m/z	Propionylcholine	C8H18NO2+	39.2	0	-1.93	199.10	1	8.81	0.11	0.003	0.052	1.06				x	19	ASB	Cystitis
0.87_167.0129m/z	Bergaptol	C11H6O4	38.2	0	0.72	167.01	1	0.87	0.92	0.000	0.002	1.92				x	3	ASB	Cystitis
3.66_250.0380m/z	Milrinone	C12H9N3O	38.6	2.42	1.43	250.04	1	3.66	0.15	0.001	0.027	1.16				x	3	ASB	Cystitis
1.20_141.0790n	Ethosuximide	C7H11NO2	38.6	0	0.30	164.07	1	1.20	0.12	0.000	0.000	-1.35				x	7	Cystitis	ASB
10.14_212.1282m/z	Orciprenaline	C11H17NO3	47.8	42.9	0.50	212.13	1	10.14	0.16	0.010	0.088	1.03				x	14	ASB	Cystitis
7.32_205.0861m/z	Edrophonium	C10H16NO+	38.9	0	-1.59	205.09	1	7.32	0.15	0.003	0.048	-1.06				x	56	Cystitis	ASB
12.66_301.2525m/z	Allylestrenol	C21H32O	56.1	84.4	-0.15	301.25	1	12.66	0.10	0.006	0.069	1.06				x	50	ASB	Cystitis
10.14_286.1649m/z	Arginyl-Phenylalanine	C15H23N5O3	45.8	39.5	-4.10	286.16	1	10.14	0.19	0.000	0.006	1.25				x	8	ASB	Cystitis
11.31_286.1649m/z	Arginyl-Phenylalanine	C15H23N5O3	43.7	28.5	-4.28	286.16	1	11.31	0.18	0.006	0.068	1.08				x	8	ASB	Cystitis
4.02_325.1757m/z	Arginyl-Tryptophan	C17H24N6O3	41.3	16.8	-3.92	325.18	1	4.02	0.21	0.001	0.024	-1.15				x	18	Cystitis	ASB
3.70_225.1346m/z	Asparaginyl-Lysine	C10H20N4O4	45	29.9	0.06	225.13	1	3.70	0.13	0.009	0.086	-1.04				x	5	Cystitis	ASB
6.58_225.1234m/z	Glutamylleucine	C11H20N2O5	43.5	22.2	0.18	225.12	1	6.58	0.15	0.001	0.022	1.04				x	41	ASB	Cystitis
1.32_227.1754m/z	Isoleucyl-Isoleucine	C12H24N2O3	43.5	21.1	-0.04	227.18	1	1.32	0.09	0.000	0.005	-1.24				x	26	Cystitis	ASB
5.86_185.1286m/z	Leucyl-Alanine	C9H18N2O3	44.3	26	0.75	185.13	1	5.86	0.17	0.004	0.056	-1.09				x	26	Cystitis	ASB
2.35_243.1340m/z	Leucyl-Glutamate	C11H20N2O5	38.9	0	0.37	243.13	1	2.35	0.18	0.003	0.050	-1.05				x	97	Cystitis	ASB
6.58_244.1423n	Leucyl-Hydroxyproline	C11H20N2O4	47.5	50	0.13	245.15	1	6.58	0.34	0.002	0.036	1.03				x	4	ASB	Cystitis
1.97_251.1503m/z	Leucyl-Histidine	C12H20N4O3	46.3	36.7	0.07	251.15	1	1.97	0.15	0.001	0.028	-1.11				x	21	Cystitis	ASB
4.22_227.1754m/z	Leucyl-Leucine	C12H24N2O3	39.1	0	0.10	227.18	1	4.22	0.09	0.000	0.000	3.76				x	29	ASB	Cystitis
9.04_286.1649m/z	Phenylalanyl-Arginine	C15H23N5O3	46.6	44.2	-4.16	286.16	1	9.04	0.16	0.009	0.087	1.13				x	8	ASB	Cystitis
4.81_167.0816m/z	Serylproline	C8H14N2O4	49.2	56.4	0.59	167.08	1	4.81	0.15	0.003	0.051	1.04				x	18	ASB	Cystitis
6.59_251.1027m/z	Seryltyrosine	C12H16N2O5	46.5	36.6	0.08	251.10	1	6.59	0.14	0.000	0.000	1.32				x	37	ASB	Cystitis
7.18_301.1158m/z	Tyrosyl-Proline	C14H18N2O4	38.6	7.24	-0.10	301.12	1	7.18	0.10	0.005	0.066	1.48				x	31	ASB	Cystitis
7.75_233.0922m/z	Tyrosyl-Serine	C12H16N2O5	48.5	47	0.41	233.09	1	7.75	0.28	0.009	0.085	1.02				x	26	ASB	Cystitis
1.36_215.1391m/z	Valyl-Proline	C10H18N2O3	39.2	0	0.53	215.14	1	1.36	0.56	0.011	0.093	-1.03				x	36	Cystitis	ASB
1.34_245.1132m/z	(2S,4S)-Pinnatanine	C10H16N2O5	38.3	0	0.04	245.11	1	1.34	0.16	0.000	0.015	-1.12				x	30	Cystitis	ASB
0.90_163.0189m/z	Tricetin	C15H10O7	37.5	0	-4.73	163.02	2	0.90	0.05	0.000	0.010	-37.38				x	52	Cystitis	ASB
24.75_154.9903m/z	2-Vinylthiophene	C6H6S	37.9	0	0.84	154.99	1	24.75	2.51	0.011	0.096	-1.07				x	3	Cystitis	ASB
10.61_285.1808m/z	9-Pentadecenoic acid	C15H28O2	40.6	11.2	3.12	285.18	1	10.61	0.14	0.000	0.002	1.07				x	49	ASB	Cystitis
10.40_274.1437m/z	(E,E)-Piperlonguminine	C16H19NO3	45.5	31	-0.30	274.14	1	10.40	0.16	0.000	0.000	-1.33				x	4	Cystitis	ASB

10.99_274.1436m/z	(E,E)-Piperlonguminine	C16H19NO3	43.2	20.8	-0.47	274.14	1	10.99	0.12	0.000	0.002	1.51				x	4	ASB	Cystitis
11.43_328.1907m/z	(+)-O-Methylarmepavine	C20H25NO3	39.3	0	-0.16	328.19	1	11.43	0.14	0.008	0.084	1.07				x	7	ASB	Cystitis
6.64_235.0966m/z	(S)-2,3-Dihydro-6-hydroxy-5-(hydroxyacetyl)-2-isopropenylbenzofuran	C13H14O4	38.4	0	0.51	235.10	1	6.64	0.13	0.002	0.035	1.11				x	13	ASB	Cystitis
5.74_459.1293m/z	6''-O-Acetyldaidzin	C23H22O10	48.9	54.7	1.67	459.13	1	5.74	0.11	0.001	0.024	-1.04				x	58	Cystitis	ASB
8.33_411.1551m/z	Isomammein	C22H28O5	38.8	5.98	-4.54	411.16	1	8.33	0.09	0.010	0.089	1.07				x	23	ASB	Cystitis
9.19_215.1279m/z	5-Hexyltetrahydro-2-oxo-3-furancarboxylic acid	C11H18O4	39	0	0.75	215.13	1	9.19	0.13	0.001	0.021	1.09				x	10	ASB	Cystitis
1.54_73.0649m/z	2-Ethoxyethanol	C4H10O2	34.4	0	1.10	73.06	1	1.54	0.15	0.004	0.054	-1.16				x	21	Cystitis	ASB
1.08_175.0036m/z	Fluorocitric acid	C6H7FO7	38.3	0	-0.62	175.00	1	1.08	0.18	0.005	0.065	-1.11				x	2	Cystitis	ASB
9.75_289.1645m/z	1-(beta-D-Glucopyranosyloxy)-3-octanone	C14H26O7	39	0	-0.22	289.16	1	9.75	0.08	0.002	0.043	1.07				x	4	ASB	Cystitis
8.67_289.1645m/z	1-(beta-D-Glucopyranosyloxy)-3-octanone	C14H26O7	38.9	0	-0.07	289.16	1	8.67	0.10	0.012	0.098	1.07				x	4	ASB	Cystitis
5.19_167.1261m/z	Homoagmatine	C6H16N4	38	0	-4.12	167.13	1	5.19	0.19	0.004	0.059	-1.05				x	6	Cystitis	ASB
4.22_113.0841n	1-Piperidinecarboxaldehyde	C6H11NO	38.5	0	0.68	114.09	1	4.22	0.27	0.000	0.000	1.79				x	4	ASB	Cystitis
8.48_250.1206n	Helinorbisabone	C14H18O4	50.8	59.4	0.52	251.13	1	8.48	0.23	0.012	0.098	1.06				x	17	ASB	Cystitis
8.72_181.1224m/z	2-Phenylpropionaldehyde dimethyl acetal	C11H16O2	39.3	0	0.42	181.12	1	8.72	0.10	0.008	0.084	1.08				x	24	ASB	Cystitis
0.90_154.0136m/z	Maclurin	C13H10O6	38.6	0	3.83	154.01	2	0.90	0.04	0.000	0.000	-136.94				x	21	Cystitis	ASB
10.99_354.1005m/z	4-Hydroxybenzyl isothiocyanate 4''-acetylrhamnoside	C16H19NO6S	38.9	0.0827	-0.35	354.10	1	10.99	0.18	0.000	0.000	1.53				x	5	ASB	Cystitis
10.41_354.1005m/z	4-Hydroxybenzyl isothiocyanate 4''-acetylrhamnoside	C16H19NO6S	39.2	1.9	-0.26	354.10	1	10.41	0.28	0.000	0.008	-1.21				x	5	Cystitis	ASB
6.17_236.1030m/z	N-Acetyl-2,6-diethylaniline	C12H17NO	37.6	0	4.34	236.10	1	6.17	0.13	0.002	0.041	1.08				x	22	ASB	Cystitis
3.76_391.1135m/z	Lepidine F	C20H18N4O2	43.7	26.7	-1.85	391.11	1	3.76	0.15	0.010	0.090	1.08				x	96	ASB	Cystitis
8.57_379.2115m/z	(4R,5S,7R,11S)-11,12-Dihydroxy-1(10)-spirovetiven-2-one 11-glucoside	C21H34O8	47.8	46	0.00	379.21	1	8.57	0.12	0.003	0.049	1.07				x	34	ASB	Cystitis
3.84_295.1652m/z	Sinapoylputrescine	C15H22N2O4	38.4	0	0.02	295.17	1	3.84	0.12	0.010	0.091	-1.12				x	44	Cystitis	ASB
1.33_241.1910m/z	Cyclotetradecane	C14H28	38.3	0	3.73	241.19	1	1.33	0.07	0.003	0.049	-1.33				x	8	Cystitis	ASB
0.87_83.0387m/z	(E)-1,11-Tridecadiene-3,5,7,9-tetrayne	C13H8	39.1	0	1.82	83.04	2	0.87	0.16	0.000	0.000	-3.01				x	2	Cystitis	ASB
7.39_222.1126m/z	Hydrocotarnine	C12H15NO3	38.8	0	0.48	222.11	1	7.39	0.22	0.003	0.051	1.03				x	20	ASB	Cystitis
12.17_130.0652m/z	Quinoline	C9H7N	47.3	39.6	0.89	130.07	1	12.17	0.18	0.000	0.004	1.78				x	39	ASB	Cystitis
1.22_108.0808m/z	3,4-Dihydro-5-propanoyl-2H-pyrrole	C7H11NO	49.5	50	0.42	108.08	1	1.22	0.52	0.008	0.081	-1.05				x	33	Cystitis	ASB
10.37_407.2541m/z	Persicaxanthin	C25H36O3	49.6	59.3	-4.14	407.25	1	10.37	0.14	0.010	0.091	1.06				x	8	ASB	Cystitis
1.34_194.1177m/z	2-Methylpropyl 2-aminobenzoate	C11H15NO2	37.7	0	0.73	194.12	1	1.34	0.16	0.000	0.002	-1.21				x	37	Cystitis	ASB
3.71_152.1202n	(1R,4R)-p-Mentha-2,8-dien-1-ol	C10H16O	42.6	16	0.30	153.13	1	3.71	0.13	0.002	0.044	1.05				x	121	ASB	Cystitis

2.04_213.0789m/z	3-(Dimethylaminomethyl)indole	C11H14N2	41	16.8	0.16	213.08	1	2.04	0.18	0.007	0.080	-1.08				x	5	Cystitis	ASB
12.13_265.1435m/z	(10R,11R)-Pterosin L	C15H20O4	51.4	62.9	0.19	265.14	1	12.13	0.11	0.007	0.074	1.16				x	66	ASB	Cystitis
5.61_229.1799m/z	11-Hydroxy-9-tridecenoic acid	C13H24O3	38.9	0	0.37	229.18	1	5.61	0.07	0.004	0.058	1.05				x	14	ASB	Cystitis
8.98_253.1436m/z	3alpha-Hydroxyoreadone	C14H20O4	51.9	64.3	0.55	253.14	1	8.98	0.22	0.008	0.081	1.10				x	3	ASB	Cystitis
5.17_152.1202n	Dihydrocarvone	C10H16O	46.8	35.9	0.48	153.13	1	5.17	0.14	0.001	0.034	1.03				x	123	ASB	Cystitis
9.67_273.1808m/z	Hexyl octanoate	C14H28O2	40.1	8.56	3.15	273.18	1	9.67	0.14	0.008	0.082	1.05				x	51	ASB	Cystitis
9.49_200.1050n	Matsutakic acid A	C10H16O4	45.4	31.7	0.70	201.11	1	9.49	0.13	0.010	0.088	1.07				x	14	ASB	Cystitis
10.64_255.1420m/z	4-[(2-Methyl-3-furanyl)thio]-5-nonanone	C14H22O2S	36.1	0	2.69	255.14	1	10.64	0.21	0.009	0.085	1.05				x	4	ASB	Cystitis
8.75_177.0741m/z	S-2,5-Dimethyl-3-furanyl 3-methylbutanethioate	C11H16O2S	36.3	0	3.86	177.07	1	8.75	0.20	0.008	0.081	1.06				x	3	ASB	Cystitis
9.68_320.1987n	Oryzalide B	C19H28O4	49.2	50	-0.04	303.20	1	9.68	0.16	0.000	0.015	1.05				x	12	ASB	Cystitis
5.10_335.1964m/z	4-Methylphenyl dodecanoate	C19H30O2	38.9	1.76	2.33	335.20	1	5.10	0.18	0.010	0.090	-1.05				x	58	Cystitis	ASB
10.11_219.1381m/z	2-(3-Hydroxy-4-methylphenyl)-5-methyl-4-hexen-3-one	C14H18O2	39.1	0	0.52	219.14	1	10.11	0.14	0.003	0.048	1.10				x	26	ASB	Cystitis
8.43_258.1337m/z	N-(1-Deoxy-1-fructosyl)leucine	C12H23NO7	40.4	5.76	0.30	258.13	1	8.43	0.28	0.004	0.056	1.08				x	4	ASB	Cystitis
1.35_161.1115m/z	Lactarofulvene	C15H16	36.9	0	0.59	161.11	1	1.35	0.12	0.003	0.051	1.10				x	3	ASB	Cystitis
5.40_171.1016m/z	cis-3-Hexenyl pyruvate	C9H14O3	39	0	0.23	171.10	1	5.40	0.12	0.006	0.067	-1.06				x	29	Cystitis	ASB
3.09_218.1024m/z	1-Isothiocyanato-8-(methylthio)octane	C10H19NS2	36.2	0	-3.50	218.10	1	3.09	0.13	0.004	0.054	1.12				x	2	ASB	Cystitis
10.14_251.1280m/z	Kamahine C	C14H20O5	52.4	66.4	0.88	251.13	1	10.14	0.18	0.000	0.016	1.16				x	19	ASB	Cystitis
9.51_169.1224m/z	(1beta,2beta,5beta)-p-Menth-3-ene-1,2,5-triol	C10H18O3	51.8	62.1	0.55	169.12	1	9.51	0.13	0.004	0.056	1.08				x	133	ASB	Cystitis
11.60_204.0657m/z	Methyl 5-hydroxyoxindole-3-acetate	C11H11NO4	52.3	65.7	0.76	204.07	1	11.60	0.11	0.003	0.049	1.57				x	13	ASB	Cystitis
3.58_341.0802m/z	Naphthoherniarin	C22H16O6	38.5	7.31	-1.78	341.08	1	3.58	0.18	0.004	0.056	1.09				x	14	ASB	Cystitis
9.82_234.0762m/z	N-Carboxyacetyl-D-phenylalanine	C12H13NO5	48.1	44.2	0.35	234.08	1	9.82	0.14	0.009	0.086	1.04				x	5	ASB	Cystitis
1.34_222.0874m/z	Pyro-L-glutaminyl-L-glutamine	C10H15N3O5	38.1	0	0.29	222.09	1	1.34	0.08	0.000	0.009	-2.34				x	47	Cystitis	ASB
1.20_150.0915m/z	2,3,6,7-Tetrahydrocyclopent[b]azepin-8(1H)-one	C9H11NO	38.3	0	0.82	150.09	1	1.20	0.17	0.000	0.000	-2.35				x	53	Cystitis	ASB
1.42_437.1631m/z	alpha-L-Rhamnopyranosyl-(1->3)-alpha-D-galactopyranosyl-(1->3)-L-fucose	C18H32O14	36.3	0	-4.79	437.16	1	1.42	0.06	0.013	0.100	1.55				x	5	ASB	Cystitis
6.72_212.1476m/z	2-Heptyl-4,5-dimethylthiazole	C12H21NS	37.4	0	3.80	212.15	1	6.72	0.18	0.002	0.039	1.03				x	2	ASB	Cystitis
3.41_127.1118m/z	(3E,5Z)-3,5-Octadien-1-ol	C8H14O	41.2	9.9	0.67	127.11	1	3.41	0.14	0.011	0.092	1.06				x	125	ASB	Cystitis
8.79_197.0810m/z	4-Hydroxy-6-methyl-3-(1-oxobutyl)-2H-pyran-2-one	C10H12O4	51.6	63	0.63	197.08	1	8.79	0.12	0.009	0.086	1.05				x	47	ASB	Cystitis
12.47_237.1486m/z	Eremopetasidione	C14H20O3	49.3	51	0.19	237.15	1	12.47	0.07	0.001	0.030	1.10				x	15	ASB	Cystitis
11.20_237.1486m/z	Eremopetasidione	C14H20O3	47.1	39.8	0.28	237.15	1	11.20	0.31	0.002	0.046	1.05				x	15	ASB	Cystitis

7.27_301.1758m/z	Ipomeatetrahydrofuran	C15H28O3	39.5	5.59	2.98	301.18	1	7.27	0.31	0.011	0.092	1.03				x	7	ASB	Cystitis
17.41_352.1312n	Artonin U	C21H20O5	37.9	1.11	0.47	353.14	1	17.41	1.11	0.011	0.092	-1.09				x	35	Cystitis	ASB
0.88_314.1040m/z	(+)-Lyoniresinol 9-glucoside	C28H38O13	35.8	0	-2.97	314.10	2	0.88	0.07	0.000	0.002	1.68				x	2	ASB	Cystitis
3.72_326.1445m/z	2-O-alpha-D-Galactopyranosyl-1-deoxynojirimycin	C12H23NO9	42.5	16.7	-0.30	326.14	1	3.72	0.16	0.003	0.052	1.06				x	37	ASB	Cystitis
10.54_189.0740m/z	1-Deoxy-D-glucitol	C6H14O5	37.7	0	4.23	189.07	1	10.54	0.19	0.002	0.038	1.52				x	4	ASB	Cystitis
1.10_201.1599m/z	Hexamethylene bisacetamide	C10H20N2O2	38.3	0	0.53	201.16	1	1.10	0.12	0.008	0.082	-1.07				x	3	Cystitis	ASB
2.40_195.0766m/z	Pyridylacetylglycine	C9H10N2O3	38.7	0	0.86	195.08	1	2.40	0.14	0.011	0.092	-1.31				x	26	Cystitis	ASB
9.94_234.0762m/z	4-Hydroxy-3-methoxy-cinnamoylglycine	C12H13NO5	47.1	39.4	0.36	234.08	1	9.94	0.12	0.001	0.027	1.06				x	5	ASB	Cystitis
5.42_252.0866m/z	4-Hydroxy-3-methoxy-cinnamoylglycine	C12H13NO5	47.5	41.6	-0.13	252.09	1	5.42	0.10	0.002	0.046	1.86				x	5	ASB	Cystitis
7.14_272.1128m/z	1,N2-propanodeoxyguanosine	C13H17N5O4	37.8	0	-4.41	272.11	1	7.14	0.09	0.007	0.076	1.07				x	2	ASB	Cystitis
6.63_153.0911m/z	3,5-Dimethoxytoluene	C9H12O2	38.8	0	0.66	153.09	1	6.63	0.27	0.009	0.084	1.04				x	45	ASB	Cystitis
7.52_397.1109m/z	5-(3',4',5'-trihydroxyphenyl)-gamma-valerolactone-O-methyl-4'-O-glucuronide	C18H22O11	45.7	41.3	-4.79	397.11	1	7.52	0.12	0.012	0.099	-1.05				x	40	Cystitis	ASB
8.26_213.1599m/z	1,4'-Bipiperidine-1'-carboxylic acid	C11H20N2O2	39.1	0	0.53	213.16	1	8.26	0.09	0.009	0.085	1.07				x	21	ASB	Cystitis
3.29_210.0762m/z	3-Carbamoyl-2-phenylpropionic acid	C10H11NO4	37.8	0	0.60	210.08	1	3.29	0.26	0.001	0.021	1.06				x	5	ASB	Cystitis
3.71_368.1452m/z	4-(Methylnitrosamino)-1-(3-pyridyl)-1-butanol glucuronide	C16H23N3O8	31.8	0	0.02	368.15	1	3.71	0.17	0.009	0.086	-1.10				x	52	Cystitis	ASB
4.00_352.1238m/z	N-acetyl-O-acetylneuraminate	C13H21NO10	39.2	0	-0.20	352.12	1	4.00	0.09	0.011	0.095	1.07				x	17	ASB	Cystitis
1.59_182.1177m/z	3-O-Methyl-a-methyldopamine	C10H15NO2	38	0	0.94	182.12	1	1.59	0.14	0.007	0.077	-1.07				x	35	Cystitis	ASB
1.33_208.0969m/z	2-Acetamido-4-methylphenyl acetate	C11H13NO3	37.5	0	0.39	208.10	1	1.33	0.11	0.004	0.058	-1.11				x	27	Cystitis	ASB
10.55_256.1675n	(6R,8Z)-6-Hydroxy-3-oxotetradecenoic acid	C14H24O4	43.7	22.5	0.12	239.16	1	10.55	0.52	0.011	0.095	1.04				x	4	ASB	Cystitis
9.21_262.1649m/z	hydroxyisovaleroyl carnitine	C12H23NO5	39.5	0	0.12	262.16	1	9.21	0.25	0.002	0.040	1.07				x	5	ASB	Cystitis
9.54_262.1649m/z	hydroxyisovaleroyl carnitine	C12H23NO5	38.1	0.0654	0.12	262.16	1	9.54	0.16	0.009	0.088	1.09				x	5	ASB	Cystitis
2.51_248.1129m/z	O-malonyl-L-carnitine	C10H17NO6	38.7	0	0.29	248.11	1	2.51	0.21	0.002	0.039	1.08				x	24	ASB	Cystitis
4.75_230.1024m/z	O-malonyl-L-carnitine	C10H17NO6	39.2	0	0.50	230.10	1	4.75	0.16	0.007	0.074	1.08				x	7	ASB	Cystitis
2.32_279.0976m/z	1-iodo-2-methylundecane	C12H25I	39.1	0	2.55	279.10	1	2.32	0.16	0.000	0.000	1.32				x	42	ASB	Cystitis
2.58_279.0976m/z	1-iodo-2-methylundecane	C12H25I	38.9	0	2.55	279.10	1	2.58	0.32	0.000	0.001	1.16				x	42	ASB	Cystitis
3.15_229.1184m/z	Pyroglutamylvaline	C10H16N2O4	38.9	0	0.49	229.12	1	3.15	0.11	0.008	0.081	1.10				x	117	ASB	Cystitis
11.72_214.1438m/z	8-nonenoylglycine	C11H19NO3	44.9	28.5	0.36	214.14	1	11.72	0.13	0.001	0.025	1.54				x	17	ASB	Cystitis
2.41_229.0708m/z	2-(2,3,5-trihydroxy-4-methoxyphenyl)propanoic acid	C10H12O6	38.6	0	0.64	229.07	1	2.41	0.11	0.001	0.027	-1.11				x	14	Cystitis	ASB
6.56_165.0548m/z	3-(3-hydroxyphenyl)prop-2-enoic acid	C9H8O3	39.1	0	0.93	165.05	1	6.56	0.15	0.003	0.050	1.05				x	100	ASB	Cystitis

4.60_195.0653m/z	3-(3,4-dihydroxy-5-methoxyphenyl)propanoic acid	C10H12O5	54.4	74.4	0.75	195.07	1	4.60	0.18	0.006	0.073	1.06				x	79	ASB	Cystitis
7.11_207.1017m/z	7-methoxy-2,2-dimethyl-3,4-dihydro-2H-1-benzopyran-4,5-diol	C12H16O4	47.2	40.9	0.64	207.10	1	7.11	0.12	0.008	0.082	1.08				x	31	ASB	Cystitis
12.95_379.1751m/z	3,4,5-trihydroxy-6-{[(2Z)-6-hydroxy-2-(phenylmethylidene)heptyl]oxy}oxane-2-carboxylic acid	C20H28O8	50.9	60.5	0.02	379.18	1	12.95	0.12	0.005	0.061	-1.15				x	36	Cystitis	ASB
14.44_297.0760m/z	3,5,7-trihydroxy-2-(4-hydroxy-3,5-dimethoxyphenyl)-5H-chromen-5-yl	C17H16O7	38.1	2.11	0.65	297.08	1	14.44	0.54	0.012	0.098	-1.07				x	143	Cystitis	ASB
5.42_177.0547m/z	3-(4-methoxyphenyl)oxirane-2-carboxylic acid	C10H10O4	53.6	73.1	0.59	177.05	1	5.42	0.11	0.001	0.024	1.40				x	108	ASB	Cystitis
6.70_177.0548m/z	3-(4-methoxyphenyl)oxirane-2-carboxylic acid	C10H10O4	54.5	76	0.67	177.05	1	6.70	0.42	0.007	0.078	1.04				x	108	ASB	Cystitis
3.19_222.0760m/z	2-{[(3,5-dimethoxyphenyl)(hydroxy)methylidene]amino}acetic acid	C11H13NO5	51.6	62.7	-0.38	222.08	1	3.19	0.18	0.010	0.090	1.03				x	4	ASB	Cystitis
5.07_207.0653m/z	6-(hydroxymethyl)-7-methoxy-2H-chromen-2-one	C11H10O4	49.3	53.8	0.35	207.07	1	5.07	0.11	0.005	0.065	-1.09				x	56	Cystitis	ASB
1.33_251.1391m/z	(2E)-N-(3-aminopropyl)-3-(4-hydroxy-3-methoxyphenyl)prop-2-enimidic acid	C13H18N2O3	37.5	0	0.21	251.14	1	1.33	0.06	0.008	0.081	-1.23				x	26	Cystitis	ASB
3.99_241.1183m/z	(2S)-2-hydrazinyl-3-(4-hydroxy-3-methoxyphenyl)-2-methylpropanoic acid	C11H16N2O4	39.1	0	0.00	241.12	1	3.99	0.22	0.012	0.098	1.03				x	84	ASB	Cystitis
5.74_372.0926m/z	Salicyluric beta-D-glucuronide	C15H17NO10	38.7	0	0.26	372.09	1	5.74	0.09	0.005	0.060	-1.06				x	4	Cystitis	ASB
13.84_484.2907m/z	Leukotriene D4-d5 29467	C25H35D5N2O6S	37	0	3.85	484.29	1	13.84	0.10	0.008	0.084	1.07				x	3	ASB	Cystitis
10.41_502.3013m/z	Leukotriene D4-d5 29467	C25H35D5N2O6S	36.9	0	3.80	502.30	1	10.41	0.20	0.007	0.078	1.09				x	3	ASB	Cystitis
1.21_287.1965m/z	LMFA01020162	C15H30O2	36.9	0	2.98	287.20	1	1.21	0.07	0.012	0.097	-1.35				x	44	Cystitis	ASB
4.38_269.1496m/z	LMFA01030594	C14H24O2	46.6	39.5	3.44	269.15	1	4.38	0.22	0.013	0.100	1.05				x	63	ASB	Cystitis
24.75_312.9429m/z	3,3-Dibromo-2-n-hexylacrylic acid	C9H14Br2O2	23.8	0	-1.27	312.94	1	24.75	1.11	0.009	0.088	1.06				x	2	ASB	Cystitis
23.77_140.0683m/z	LMFA01100023	C5H11NO2	38.8	0	0.66	140.07	1	23.77	0.48	0.005	0.060	-1.06				x	31	Cystitis	ASB
5.55_285.1809m/z	5,6-methylenetetradecanoic acid	C15H28O2	39.1	6.71	3.18	285.18	1	5.55	0.09	0.003	0.052	-1.07				x	49	Cystitis	ASB
9.68_257.1900m/z	LMFA02000191	C18H28O3	52.6	66.9	-0.13	257.19	1	9.68	0.12	0.005	0.062	1.05				x	51	ASB	Cystitis
13.40_239.1642m/z	(9R,13R)-1a,1b-dihomo-jasmonic acid	C14H22O3	47.5	40.2	0.13	239.16	1	13.40	0.09	0.008	0.083	1.06				x	13	ASB	Cystitis
9.42_239.1642m/z	(9R,13R)-1a,1b-dihomo-jasmonic acid	C14H22O3	47.3	41.4	0.09	239.16	1	9.42	0.25	0.001	0.021	1.06				x	13	ASB	Cystitis
9.21_191.1068m/z	Tuberonic acid	C12H18O4	52.2	65.4	0.42	191.11	1	9.21	0.18	0.010	0.088	1.05				x	50	ASB	Cystitis
10.64_191.1067m/z	Tuberonic acid	C12H18O4	54.6	76.1	0.30	191.11	1	10.64	0.18	0.002	0.039	1.08				x	50	ASB	Cystitis
6.61_227.1278m/z	Tuberonic acid	C12H18O4	39.2	0	0.22	227.13	1	6.61	0.29	0.010	0.090	1.06				x	9	ASB	Cystitis
7.77_226.1206n	Tuberonic acid	C12H18O4	49.2	50.7	0.58	227.13	1	7.77	0.46	0.004	0.058	1.03				x	6	ASB	Cystitis
11.22_209.1173m/z	Tuberonic acid	C12H18O4	52.3	65.7	0.50	209.12	1	11.22	0.17	0.003	0.052	1.06				x	33	ASB	Cystitis
9.79_191.1067m/z	Tuberonic acid	C12H18O4	53.8	72.6	0.41	191.11	1	9.79	0.14	0.012	0.097	1.05				x	50	ASB	Cystitis
8.45_228.1363n	(-)-12-hydroxy-9,10-dihydrojasmonic acid	C12H20O4	50.5	56.7	0.49	211.13	1	8.45	0.54	0.008	0.081	1.05				x	15	ASB	Cystitis

9.93_228.1363n	(-)-12-hydroxy-9,10-dihydrojasmonic acid	C12H20O4	49.9	52.7	0.51	229.14	1	9.93	0.15	0.006	0.073	1.05				x	14	ASB	Cystitis
8.51_193.1225m/z	(-)-12-hydroxy-9,10-dihydrojasmonic acid	C12H20O4	49.2	51.5	0.91	193.12	1	8.51	0.28	0.012	0.098	1.05				x	63	ASB	Cystitis
10.37_348.2300n	11-deoxy-11-methylene-15-keto-PGD2	C21H32O4	55.1	80.9	-0.31	349.24	1	10.37	0.16	0.000	0.013	1.08				x	21	ASB	Cystitis
9.31_348.2299n	11-deoxy-11-methylene-15-keto-PGD2	C21H32O4	53.6	72.9	-0.37	331.23	1	9.31	0.11	0.004	0.054	1.06				x	21	ASB	Cystitis
9.48_348.2299n	11-deoxy-11-methylene-15-keto-PGD2	C21H32O4	51.8	63.5	-0.33	349.24	1	9.48	0.12	0.006	0.067	1.05				x	19	ASB	Cystitis
13.41_318.2195n	(+/-)-15-HEPE	C20H30O3	54.7	77.1	-0.09	319.23	1	13.41	0.28	0.011	0.094	1.07				x	154	ASB	Cystitis
13.77_302.1962m/z	3-hydroxy-cis-5-octenoylcarnitine	C15H27NO5	41.9	13.3	-0.11	302.20	1	13.77	0.09	0.006	0.071	1.04				x	6	ASB	Cystitis
8.25_330.2275m/z	6-Keto-decanoylcarnitine	C17H31NO5	40.3	6.42	-0.08	330.23	1	8.25	0.09	0.006	0.067	1.05				x	1	ASB	Cystitis
9.74_330.2274m/z	6-Keto-decanoylcarnitine	C17H31NO5	41.3	10.4	-0.23	330.23	1	9.74	0.21	0.000	0.009	-1.03				x	1	Cystitis	ASB
6.02_276.1442m/z	O-glutarylcarnitine	C12H21NO6	38.9	0	0.16	276.14	1	6.02	0.10	0.012	0.098	1.05				x	16	ASB	Cystitis
10.53_560.2973m/z	PS(19:1(9Z)/0:0)	C25H48NO9P	35.8	0	2.56	560.30	1	10.53	0.09	0.010	0.088	1.08				x	5	ASB	Cystitis
1.16_335.0683m/z	LMPK12110173	C18H16O4	36.1	0	1.01	335.07	1	1.16	0.09	0.000	0.000	-6.41				x	23	Cystitis	ASB
9.31_271.2056m/z	1,17-dihydroxy-androstan-3-one	C19H30O3	47.9	44	-0.22	271.21	1	9.31	0.09	0.000	0.001	1.07				x	42	ASB	Cystitis
7.37_302.1882n	3,17-dihydroxy-9,10-seco-androsta-1,3,5(10)-triene-9-one	C19H26O3	53.5	71.1	-0.05	285.18	1	7.37	0.15	0.002	0.038	1.07				x	49	ASB	Cystitis
9.92_345.2061m/z	1alpha,17alpha,21-trihydroxy-20-oxo-22,23,24,25,26,27-hexanorvitamin D3	C21H30O5	48.8	49.3	0.09	345.21	1	9.92	0.10	0.009	0.086	1.09				x	49	ASB	Cystitis
8.06_462.2335m/z	Lys Glu Trp 13042	C22H31N5O6	37.9	0	-2.62	462.23	1	8.06	0.16	0.003	0.049	-1.12				x	11	Cystitis	ASB
7.63_366.1329m/z	Met Ser Glu 5705	C13H23N3O7S	38.5	0	-0.21	366.13	1	7.63	0.11	0.001	0.029	1.08				x	19	ASB	Cystitis
12.91_757.4889m/z	MGDG(11:0/22:5)	C42H70O10	37.2	0	3.84	757.49	1	12.91	0.07	0.009	0.088	1.10				x	9	ASB	Cystitis
9.22_422.2021m/z	Phe Ile Val 9115	C20H31N3O4	38	0	-1.33	422.20	1	9.22	0.14	0.005	0.064	1.04				x	31	ASB	Cystitis
3.75_314.1597m/z	Pro Pro His 1620	C16H23N5O4	37	0	-4.13	314.16	1	3.75	0.21	0.000	0.011	-1.09				x	4	Cystitis	ASB
3.55_282.1447m/z	Pro Pro Ser 20340	C13H21N3O5	38.9	0	-0.31	282.14	1	3.55	0.15	0.012	0.098	-1.05				x	84	Cystitis	ASB
9.95_430.2437m/z	Trp-Pro-Lys	C22H31N5O4	38.7	2.94	-2.76	430.24	1	9.95	0.14	0.007	0.077	1.07				x	2	ASB	Cystitis
8.06_209.0809m/z	Sinapyl aldehyde 24972	C11H12O4	38.9	0	0.55	209.08	1	8.06	0.26	0.005	0.060	1.05				x	61	ASB	Cystitis
0.06_98.5121m/z	thio-m-Toluthioamide 29871	C8H9NS	38	0	1.43	98.51	2	0.06	0.92	0.011	0.092	1.10				x	16	ASB	Cystitis
6.57_489.2921m/z	Trp Lys Arg 3767	C23H36N8O4	37.8	0	-2.22	489.29	1	6.57	0.08	0.002	0.044	1.13				x	7	ASB	Cystitis
8.02_420.2229m/z	Trp Ser Lys 11019	C20H29N5O5	37.7	0	-3.07	420.22	1	8.02	0.10	0.005	0.065	1.07				x	13	ASB	Cystitis
4.90_367.2222n	Val His Leu 7161	C17H29N5O4	57.3	96.3	0.77	368.23	1	4.90	0.13	0.010	0.091	-1.05				x	18	Cystitis	ASB
3.21_334.1860m/z	Val Pro His 10192	C16H25N5O4	37.8	0	-4.00	334.19	1	3.21	0.19	0.002	0.039	1.07				x	36	ASB	Cystitis
4.78_347.1925m/z	Val Thr Gln 12365	C14H26N4O6	38.8	0	-0.06	347.19	1	4.78	0.09	0.001	0.021	1.06				x	108	ASB	Cystitis

PERMISSIONS

Licenses and Copyright

The following policy applies to all PLOS journals, unless otherwise noted.

What Can Others Do with My Original Article Content?

PLOS applies the Creative Commons Attribution (CC BY) license to articles and other works we publish. If you submit your paper for publication by PLOS, you agree to have the CC BY license applied to your work. Under this Open Access license, you as the author agree that anyone can reuse your article in whole or part for any purpose, for free, even for commercial purposes. Anyone may copy, distribute, or reuse the content as long as the author and original source are properly cited. This facilitates freedom in re-use and also ensures that PLOS content can be mined without barriers for the needs of research.

May I Use Content Owned by Someone Else in My Article?

If you have written permission to do so, yes. If your manuscript contains content such as photos, images, figures, tables, audio files, videos, etc., that you or your co-authors do not own, we will require you to provide us with proof that the owner of that content (a) has given you written permission to use it, and (b) has approved of the CC BY license being applied to their content. We provide a form you can use to ask for and obtain permission from the owner. Download the form (PDF).

If you do not have owner permission, we will ask you to remove that content and/or replace it with other content that you own or have such permission to use.

Don't assume that you can use any content you find on the Internet, or that the content is fair game just because it isn't clear who the owner is or what license applies. It's up to you to ascertain what rights you have—if any—to use that content.

May I Use Article Content I Previously Published in Another Journal?

Many authors assume that if they previously published a paper through another publisher, they own the rights to that content and they can freely use that content in their PLOS paper, but that's not necessarily the case – it depends on the license that covers the other paper. Some publishers allow free and unrestricted re-use of article content they own, such as under the CC BY license. Other publishers use licenses that allow re-use only if the same license is applied by the person or publisher re-using the content.

If the paper was published under a CC BY license or another license that allows free and unrestricted use, you may use the content in your PLOS paper provided that you give proper attribution, as explained above.

If the content was published under a more restrictive license, you must ascertain what rights you have under that license. At a minimum, review the license to make sure you can use the content. Contact that publisher if you have any questions about the license terms – PLOS staff cannot give you legal advice about your rights to use third-party content. If the license does not permit you to use the content in a paper that will be covered by an unrestricted license, you must obtain written permission from the publisher to use the content in your PLOS paper. Please do not include any content in your PLOS paper which you do not have rights to use, and always give proper attribution.

What Are Acceptable Licenses for Data Repositories?

If any relevant accompanying data is submitted to repositories with stated licensing policies, the policies should not be more restrictive than CC BY.

Removal of Content Used Without Clear Rights

PLOS reserves the right to remove any photos, captures, images, figures, tables, illustrations, audio and video files, and the like, from any paper, whether before or after publication, if we have reason to believe that the content was included in your paper without permission from the owner of the content.

Statement of Author Rights

ASM Author Center / Preparing Your Manuscript

Authors may post their articles to their institutional repositories

ASM grants authors the right to post their accepted manuscripts in publicly accessible electronic repositories maintained by funding agencies, as well as appropriate institutional or subject-based open repositories established by a government or non-commercial entity.

In preparation for the REF 2021, ASM would like to remind Authors that the current author fee structure, along with the policy outlined above, allows authors to comply with the HEFCE deposition requirements. If authors have paid a fee to make their article "gold" open access then there is no need to worry about these deposition requirements (See section 38 of the "Policy for open access in Research Excellence Framework 2021" document).

Please note that ASM makes the final, typeset articles from its primary-research journals available free of charge on the ASM Journals and PMC websites 6 months after final publication.

Authors may post their articles in full on personal or employer websites

ASM grants the author the right to post his/her article (after publication by ASM) on the author's personal or university-hosted website, but not on any corporate, government, or similar website, without ASM's prior permission, provided that proper credit is given to the original ASM publication.

Once ASM grants permission to the author, ASM requests that the posting release date for the content be no earlier than 6 months after the final publication of the typeset article by ASM.

Authors may make copies of their articles in full

Corresponding authors are entitled to 10 free downloads of their papers. Additionally, all authors may make up to 99 copies of his/her own work for personal or professional use (including teaching packs that are distributed free of charge within your own institution). For orders of 100 or more copies, you should seek ASM's permission or purchase access through Highwire's Pay-Per-View option, available on the ASM online journal sites.

Authors may republish/adapt portions of their articles

ASM also grants the author the right to republish discrete portions of his/her article in any other publication (including print, CD-ROM, and other electronic formats) of which he or she is author or editor, provided that proper credit is given to the original ASM publication. An ASM author also retains the right to reuse the full article in his/her dissertation or thesis. "Proper credit" means either the copyright lines shown on the top of the first page of the PDF version, or "Copyright © American Society for Microbiology, [insert journal name, volume number, year, page numbers and DOI]" of the HTML version. For technical questions about using Rightslink, please contact Customer Support via phone at (877) 622-5543 (toll free) or (978) 777-9929, or e-mail Rightslink customer care at customercare@copyright.com.

Please note that the ASM is in full compliance with NIH Policy.

Keywords: APEC, ExPEC, MAEC/NMEC, UPEC, two-component systems, signal transduction, virulence factors

Citation: Breland EJ, Eberly AR and Hadjifrangiskou M (2017) An Overview of Two-Component Signal Transduction Systems Implicated in Extra-Intestinal Pathogenic *E. coli* Infections. *Front. Cell. Infect. Microbiol.* 7:162. doi: 10.3389/fcimb.2017.00162

Received: 01 March 2017; **Accepted:** 18 April 2017;
Published: 09 May 2017.

Edited by:
Alfredo G. Torres, University of Texas Medical Branch, USA

Reviewed by:
Chitrita Debroy, Pennsylvania State University, USA
Catherine M. Logue, Iowa State University, USA
Sheryl S. Justice, Ohio State University at Columbus, USA

***Correspondence:** Maria Hadjifrangiskou, maria.hadjifrangiskou@vanderbilt.edu

Chapter: 3 Adhesion of bacteria to surfaces and biofilm formation on medical devices
Book: Biofilms and Implantable Medical Devices
Author: K.A. Floyd,A.R. Eberly,M. Hadjifrangiskou
Publisher: Elsevier
Date: 2017

Order Completed

Thank you for your order.

This Agreement between Allison Eberly ("You") and Elsevier ("Elsevier") consists of your license details and the terms and conditions provided by Elsevier and Copyright Clearance Center.

Your confirmation email will contain your order number for future reference.

printable details

License Number	4477730877644
License date	Nov 28, 2018
Licensed Content Publisher	Elsevier
Licensed Content Publication	Elsevier Books
Licensed Content Title	Biofilms and Implantable Medical Devices
Licensed Content Author	K.A. Floyd,A.R. Eberly,M. Hadjifrangiskou
Licensed Content Date	Jan 1, 2017
Licensed Content Pages	49
Type of Use	reuse in a thesis/dissertation
Portion	figures/tables/illustrations
Number of figures/tables/illustrations	1
Format	both print and electronic
Are you the author of this Elsevier chapter?	Yes
Will you be translating?	No
Original figure numbers	Figure 4.2
Title of your thesis/dissertation	Delineating the role of oxygen in biofilm formation in Escherichia coli urinary tract isolates
Expected completion date	Jan 2019
Estimated size (number of pages)	150
Requestor Location	Allison Eberly 3512 Richland Ave #B NASHVILLE, TN 37205 United States Attn: Allison Eberly
Publisher Tax ID	98-0397604
Total	0.00 USD

ORDER MORE | CLOSE WINDOW

Re: Reprint of Manuscript from IJMS for Thesis

Publisher MDPI [publisher@mdpi.com]
Sent: Monday, September 10, 2018 5:13 AM
To: Eberly, Allison R

Dear Allison Eberly,

Thank you very much for your interest in said material.

All MDPI journals are Open Access and subject to the Creative Commons Attribution License (CC BY). The CC BY permits unrestricted use, distribution, and reproduction of the material in any medium, even commercially, ***provided the original work is properly cited***. You do not have to pay anything for permission.

For more information on the CC BY License, please see here:
https://creativecommons.org/licenses/by/4.0/legalcode

Best regards,
Tim Gasser

Am 06/09/2018 um 22:48 schrieb Eberly, Allison R:

> To whom it may concern:
>
> I am writing my dissertation and would like to use portions of manuscript in my doctoral thesis. The article is published in IJMS and titled "Biofilm Formation by Uropathogenic *Escherichia coli* Is Favored under Oxygen Conditions That Mimic the Bladder Environment" from the Special Issue Molecular Research on Urology, IJSM 18012077.
>
> I am emailing to ask permission to use the published material.
>
> Thank you,
>
> Allison Eberly
> PhD Candidate
> Hadjifrangiskou Lab
> Department of Pathology, Microbiology and Immunology

--
Tim Gasser
Communications & Marketing Assistant, MDPI
St. Alban-Anlage 66, 4052 Basel, Switzerland
www.mdpi.com

Tel. +41 61 683 77 34; Fax +41 61 302 89 18
E-mail Accounting: billing@mdpi.com
E-mail: gasser@mdpi.com

MDPI Contact

MDPI
St. Alban-Anlage 66,
4052 Basel, Switzerland
Support contact
Tel. +41 61 683 77 34
Fax: +41 61 302 89 18

For more contact information, see here.

Terms of Use

§ 1 These Terms of Use govern the use of the MDPI websites or any other MDPI online services you access. This includes any updates or releases thereof. By using our online services, you are legally bound by and hereby consent to our Terms of Use and Privacy Policy. These Terms of Use form a contract between MDPI AG, registered at St. Alban-Anlage 66, 4052 Basel, Switzerland ("MDPI") and you as the user ("User"). These Terms of Use shall be governed by and construed in accordance with Swiss law, applicable at the place of jurisdiction of MDPI in Basel, Switzerland.

§ 2 Unless otherwise stated, the website and affiliated online services are the property of MDPI and the copyright of the website belongs to MDPI or its licensors. You may not copy, hack or modify the website or online services, or falsely claim that some other site is associated with MDPI. MDPI is a registered brand protected by the Swiss Federal Institute of Intellectual Property.

§ 3 Unless otherwise stated, articles published on the MDPI websites are labeled as "Open Access" and licensed by the respective authors in accordance with the Creative Commons Attribution (CC-BY) license. Within the limitations mentioned in §4 of these Terms of Use, the "Open Access" license allows for unlimited distribution and reuse as long as appropriate credit is given to the original source and any changes made compared to the original are indicated.

§ 4 Some articles published on this website (especially articles labeled as "Review" or similar) may make use of copyrighted material for which the author(s) have obtained a reprint permission from the copyright holder. Usually such reprint permissions do not allow author(s) and/or MDPI to further license the copyrighted material. The licensing described in §3 of these terms and conditions are therefore not applicable to such kind of material enclosed within articles. It is the user's responsibility to identify reusability of material provided on this website, for which he may take direct contact with the authors of the article.

§ 5 You may register or otherwise create a user account, user name or password (your "Registration") that allows you to access or receive certain content and/or to participate or utilize certain features of our online service, including features in which you interact with us or other users. You represent and warrant that the information provided in your registration is accurate to the best of your knowledge. You are responsible for the use of any password you create as part of your registration and for maintaining its confidentiality, and you agree that MDPI may use this password to identify you. We reserve the right to deny, terminate or restrict your access to any content or feature reached via such registration process for any reason, at our sole discretion. MDPI reserves the right to block or to terminate the user's access to the website at any time and without prior notice.

§ 6 The MDPI website and online services may provide links to other websites or external resources. As part of these Terms of Use, you acknowledge that MDPI is in not responsible for the availability of such external sites or resources, and that MDPI is not liable for any content, services, advertising, or

materials available from such external sites or resources.

§ 7 The website may contain advertising. MDPI does not endorse any responsibility of any kind for the content of the advertisement or sponsorship or the advertised product or service, which is the responsibility of the advertiser or sponsor, unless the advertised product or service is offered by MDPI.

§ 8 There is no warranty for the website and its content, to the extent permitted by applicable law. MDPI, the copyright holders and/or other parties provide the website and its content “as is” without representations or warranties of any kind, either expressed or implied, including, but not limited to, the implied warranties of merchantability, satisfactory quality and fitness for a particular purpose relating to this website, its content or any to which it is linked. No representations or warranties are given as to the accuracy or completeness of the information provided on this website, or any website to which it is linked.

§ 9 In no event, unless required by applicable law shall MDPI, its employees, agents, suppliers, contractors or any other party, be liable to the user for any damages of any nature, including any general, special, incidental or consequential damages, loss, cost, claim or any expense of any kind arising out of the use, inability to access, or in connection with the use of the website, its content and information, even if the user has been advised of the possibility of such damages.

§ 10 MDPI reserves the right to change these Terms of Use at any time by posting changes to this page of the website without prior notice. Please check these Terms of Use periodically for any modifications. Your continued use of any Service following the posting of any changes will mean that you have accepted and agreed to the changes.

§ 11 Basel, Switzerland shall be the place of jurisdiction for all legal disputes arising of these Terms of Use, even if the Customer has her/his domicile outside of Switzerland.

§ 12 Swiss law applicable at the place of jurisdiction of MDPI shall apply exclusively.

§ 13 If any provisions of the Terms of Use should be found invalid, this shall not affect the validity of the remaining provisions. In any such case, the contracting parties shall negotiate on the invalid clause to substitute by a valid arrangement as close as possible to the original provision

Terms of Use MDPI AG

Terms of Use of MDPI (pdf)

These Terms of Use were last updated on 1 March 2017

REFERENCES

1. Foxman B (2010) The epidemiology of urinary tract infection. *Nat Rev Urol* 7(12):653-660.
2. Foxman B (2014) Urinary tract infection syndromes: occurrence, recurrence, bacteriology, risk factors, and disease burden. *Infect Dis Clin North Am* 28(1):1-13.
3. Kennedy EH, Greene MT, & Saint S (2013) Estimating hospital costs of catheter-associated urinary tract infection. *J Hosp Med* 8(9):519-522.
4. Schappert SM & Rechtsteiner EA (2011) Ambulatory medical care utilization estimates for 2007. *Vital Health Stat 13* (169):1-38.
5. Cai T*, et al.* (2012) The role of asymptomatic bacteriuria in young women with recurrent urinary tract infections: to treat or not to treat? *Clin Infect Dis* 55(6):771-777.
6. Evans DA*, et al.* (1978) Bacteriuria in a population-based cohort of women. *J Infect Dis* 138(6):768-773.
7. Bahagon Y, Raveh D, Schlesinger Y, Rudensky B, & Yinnon AM (2007) Prevalence and predictive features of bacteremic urinary tract infection in emergency department patients. *Eur J Clin Microbiol Infect Dis* 26(5):349-352.
8. Al-Hasan MN, Eckel-Passow JE, & Baddour LM (2010) Bacteremia complicating gram-negative urinary tract infections: a population-based study. *J Infect* 60(4):278-285.
9. Ramakrishnan K & Scheid DC (2005) Diagnosis and management of acute pyelonephritis in adults. *Am Fam Physician* 71(5):933-942.
10. Piccoli GB*, et al.* (2011) The clinical and imaging presentation of acute "non complicated" pyelonephritis: a new profile for an ancient disease. *BMC Nephrol* 12:68.
11. Scotland KB & Lange D (2018) Prevention and management of urosepsis triggered by ureteroscopy. *Res Rep Urol* 10:43-49.
12. Dreger NM, Degener S, Ahmad-Nejad P, Wöbker G, & Roth S (2015) Urosepsis--Etiology, Diagnosis, and Treatment. *Dtsch Arztebl Int* 112(49):837-847; quiz 848.
13. Gynecologists ACoOa (2008) ACOG Practice Bulletin No. 91: Treatment of urinary tract infections in nonpregnant women. *Obstet Gynecol* 111(3):785-794.
14. Al-Badr A & Al-Shaikh G (2013) Recurrent Urinary Tract Infections Management in Women: A review. *Sultan Qaboos Univ Med J* 13(3):359-367.
15. McLellan LK & Hunstad DA (2016) Urinary Tract Infection: Pathogenesis and Outlook. *Trends Mol Med* 22(11):946-957.
16. Foxman B, Klemstine KL, & Brown PD (2003) Acute pyelonephritis in US hospitals in 1997: hospitalization and in-hospital mortality. *Ann Epidemiol* 13(2):144-150.
17. Rowe TA & Juthani-Mehta M (2013) Urinary tract infection in older adults. *Aging health* 9(5).

18. Finnell SM, Carroll AE, Downs SM, & Infection SoUT (2011) Technical report—Diagnosis and management of an initial UTI in febrile infants and young children. *Pediatrics* 128(3):e749-770.
19. Nicolle LE (2014) Catheter associated urinary tract infections. *Antimicrob Resist Infect Control* 3:23.
20. Whiteside SA, Razvi H, Dave S, Reid G, & Burton JP (2015) The microbiome of the urinary tract--a role beyond infection. *Nat Rev Urol* 12(2):81-90.
21. Warren JW (2001) Catheter-associated urinary tract infections. *Int J Antimicrob Agents* 17(4):299-303.
22. Czaja CA*, et al.* (2009) Prospective cohort study of microbial and inflammatory events immediately preceding *Escherichia coli* recurrent urinary tract infection in women. *J Infect Dis* 200(4):528-536.
23. Schreiber HL*, et al.* (2017) Bacterial virulence phenotypes of *Escherichia coli* and host susceptibility determine risk for urinary tract infections. *Sci Transl Med* 9(382).
24. Chen SL*, et al.* (2013) Genomic diversity and fitness of *E. coli* strains recovered from the intestinal and urinary tracts of women with recurrent urinary tract infection. *Sci Transl Med* 5(184):184ra160.
25. Amundsen SK, Wang CC, Schwan WR, Duncan JL, & Schaeffer AJ (1988) Role of *Escherichia coli* adhesins in urethral colonization of catheterized patients. *J Urol* 140(3):651-655.
26. Rosen DA, Hooton TM, Stamm WE, Humphrey PA, & Hultgren SJ (2007) Detection of intracellular bacterial communities in human urinary tract infection. *PLoS Med* 4(12):e329.
27. Song J & Abraham SN (2008) Innate and adaptive immune responses in the urinary tract. *Eur J Clin Invest* 38 Suppl 2:21-28.
28. Stamm WE*, et al.* (1982) Diagnosis of coliform infection in acutely dysuric women. *N Engl J Med* 307(8):463-468.
29. Price TK*, et al.* (2016) The Clinical Urine Culture: Enhanced Techniques Improve Detection of Clinically Relevant Microorganisms. *J Clin Microbiol* 54(5):1216-1222.
30. Mediavilla JR*, et al.* (2016) Colistin- and Carbapenem-Resistant *Escherichia coli* Harboring mcr-1 and blaNDM-5, Causing a Complicated Urinary Tract Infection in a Patient from the United States. *MBio* 7(4).
31. Zowawi HM*, et al.* (2015) The emerging threat of multidrug-resistant Gram-negative bacteria in urology. *Nat Rev Urol* 12(10):570-584.
32. Jancel T & Dudas V (2002) Management of uncomplicated urinary tract infections. *West J Med* 176(1):51-55.
33. Gupta K*, et al.* (2011) International clinical practice guidelines for the treatment of acute uncomplicated cystitis and pyelonephritis in women: A 2010 update by the Infectious Diseases Society of America and the European Society for Microbiology and Infectious Diseases. *Clin Infect Dis* 52(5):e103-120.
34. Miller JM*, et al.* (2018) A Guide to Utilization of the Microbiology Laboratory for Diagnosis of Infectious Diseases: 2018 Update by the Infectious Diseases Society of America and the American Society for Microbiology. *Clin Infect Dis* 67(6):813-816.

35. von Wintersdorff CJ*, et al.* (2016) Dissemination of Antimicrobial Resistance in Microbial Ecosystems through Horizontal Gene Transfer. *Front Microbiol* 7:173.
36. Knothe H, Shah P, Krcmery V, Antal M, & Mitsuhashi S (1983) Transferable resistance to cefotaxime, cefoxitin, cefamandole and cefuroxime in clinical isolates of *Klebsiella pneumoniae* and *Serratia marcescens*. *Infection* 11(6):315-317.
37. Rawat D & Nair D (2010) Extended-spectrum β-lactamases in Gram Negative Bacteria. *J Glob Infect Dis* 2(3):263-274.
38. Paterson DL (2000) Recommendation for treatment of severe infections caused by Enterobacteriaceae producing extended-spectrum beta-lactamases (ESBLs). *Clinical microbiology and infection : the official publication of the European Society of Clinical Microbiology and Infectious Diseases* 6(9):460-463.
39. Organization WH (2017) WHO publishes list of bacteria for which new antibiotics are urgently needed. (Online).
40. Lopez D, Vlamakis H, & Kolter R (2010) Biofilms. *Cold Spring Harb Perspect Biol* 2(7):a000398.
41. Flemming H-C*, et al.* (2016) Biofilms: an emergent form of bacterial life. *Nature Reviews Microbiology* 14(9):563-575.
42. Flemming HC & Wingender J (2010) The biofilm matrix. *Nat Rev Microbiol* 8(9):623-633.
43. Kostakioti M, Hadjifrangiskou M, & Hultgren SJ (2013) Bacterial biofilms: development, dispersal, and therapeutic strategies in the dawn of the postantibiotic era. *Cold Spring Harb Perspect Med* 3(4):a010306.
44. Hagan EC, Lloyd AL, Rasko DA, Faerber GJ, & Mobley HL (2010) *Escherichia coli* global gene expression in urine from women with urinary tract infection. *PLoS Pathog* 6(11):e1001187.
45. Lewis K (2005) Persister cells and the riddle of biofilm survival. *Biochemistry (Mosc)* 70(2):267-274.
46. Mitchell JG & Kogure K (2006) Bacterial motility: links to the environment and a driving force for microbial physics. *FEMS Microbiol Ecol* 55(1):3-16.
47. Berg HC & Anderson RA (1973) Bacteria swim by rotating their flagellar filaments. *Nature* 245(5425):380-382.
48. Berg HC (2003) The rotary motor of bacterial flagella. *Annu Rev Biochem* 72:19-54.
49. Atsumi T, McCarter L, & Imae Y (1992) Polar and lateral flagellar motors of marine Vibrio are driven by different ion-motive forces. *Nature* 355(6356):182-184.
50. Kojima S, Yamamoto K, Kawagishi I, & Homma M (1999) The polar flagellar motor of *Vibrio cholerae* is driven by an Na+ motive force. *J Bacteriol* 181(6):1927-1930.
51. McCarter LL (2004) Dual flagellar systems enable motility under different circumstances. *J Mol Microbiol Biotechnol* 7(1-2):18-29.
52. Hranitzky KW, Mulholland A, Larson AD, Eubanks ER, & Hart LT (1980) Characterization of a flagellar sheath protein of *Vibrio cholerae*. *Infect Immun* 27(2):597-603.

53. Macnab RM (1977) Bacterial flagella rotating in bundles: a study in helical geometry. *Proc Natl Acad Sci U S A* 74(1):221-225.
54. Merz AJ, So M, & Sheetz MP (2000) Pilus retraction powers bacterial twitching motility. *Nature* 407(6800):98-102.
55. Skerker JM & Berg HC (2001) Direct observation of extension and retraction of type IV pili. *Proc Natl Acad Sci U S A* 98(12):6901-6904.
56. Mattick JS (2002) Type IV pili and twitching motility. *Annu Rev Microbiol* 56:289-314.
57. Harshey RM (2003) Bacterial motility on a surface: many ways to a common goal. *Annu Rev Microbiol* 57:249-273.
58. Henrichsen J (1972) Bacterial surface translocation: a survey and a classification. *Bacteriol Rev* 36(4):478-503.
59. Zusman DR, Scott AE, Yang Z, & Kirby JR (2007) Chemosensory pathways, motility and development in *Myxococcus xanthus*. *Nat Rev Microbiol* 5(11):862-872.
60. Wolgemuth C, Hoiczyk E, Kaiser D, & Oster G (2002) How *myxobacteria* glide. *Curr Biol* 12(5):369-377.
61. Li Y*, et al.* (2003) Extracellular polysaccharides mediate pilus retraction during social motility of *Myxococcus xanthus*. *Proc Natl Acad Sci U S A* 100(9):5443-5448.
62. Gopalaswamy R, Narayanan S, Jacobs WR, & Av-Gay Y (2008) *Mycobacterium smegmatis* biofilm formation and sliding motility are affected by the serine/threonine protein kinase PknF. *FEMS Microbiol Lett* 278(1):121-127.
63. Briegel A*, et al.* (2009) Universal architecture of bacterial chemoreceptor arrays. *Proc Natl Acad Sci U S A* 106(40):17181-17186.
64. Porter SL, Wadhams GH, & Armitage JP (2011) Signal processing in complex chemotaxis pathways. *Nat Rev Microbiol* 9(3):153-165.
65. Wadhams GH & Armitage JP (2004) Making sense of it all: bacterial chemotaxis. *Nat Rev Mol Cell Biol* 5(12):1024-1037.
66. Brown MT, Delalez NJ, & Armitage JP (2011) Protein dynamics and mechanisms controlling the rotational behaviour of the bacterial flagellar motor. *Curr Opin Microbiol* 14(6):734-740.
67. Miller MB & Bassler BL (2001) Quorum sensing in bacteria. *Annu Rev Microbiol* 55:165-199.
68. Henke JM & Bassler BL (2004) Bacterial social engagements. *Trends Cell Biol* 14(11):648-656.
69. Waters CM & Bassler BL (2005) Quorum sensing: cell-to-cell communication in bacteria. *Annu Rev Cell Dev Biol* 21:319-346.
70. Karatan E & Watnick P (2009) Signals, regulatory networks, and materials that build and break bacterial biofilms. *Microbiol Mol Biol Rev* 73(2):310-347.
71. Engebrecht J, Nealson K, & Silverman M (1983) Bacterial bioluminescence: isolation and genetic analysis of functions from *Vibrio fischeri*. *Cell* 32(3):773-781.
72. Engebrecht J & Silverman M (1984) Identification of genes and gene products necessary for bacterial bioluminescence. *Proc Natl Acad Sci U S A* 81(13):4154-4158.

73. Kleerebezem M, Quadri LE, Kuipers OP, & de Vos WM (1997) Quorum sensing by peptide pheromones and two-component signal-transduction systems in Gram-positive bacteria. *Mol Microbiol* 24(5):895-904.
74. Povolotsky TL & Hengge R (2015) Genome-based comparison of c-di-GMP signaling in pathogenic and commensal *Escherichia coli* strains. *J Bacteriol*.
75. Pesavento C*, et al.* (2008) Inverse regulatory coordination of motility and curli-mediated adhesion in *Escherichia coli*. *Genes Dev* 22(17):2434-2446.
76. Fang X & Gomelsky M (2010) A post-translational, c-di-GMP-dependent mechanism regulating flagellar motility. *Mol Microbiol* 76(5):1295-1305.
77. Tischler AD & Camilli A (2004) Cyclic diguanylate (c-di-GMP) regulates *Vibrio cholerae* biofilm formation. *Mol Microbiol* 53(3):857-869.
78. Tischler AD & Camilli A (2005) Cyclic diguanylate regulates *Vibrio cholerae* virulence gene expression. *Infect Immun* 73(9):5873-5882.
79. Weber H, Pesavento C, Possling A, Tischendorf G, & Hengge R (2006) Cyclic-di-GMP-mediated signalling within the sigma network of *Escherichia coli*. *Mol Microbiol* 62(4):1014-1034.
80. Spurbeck RR, Tarrien RJ, & Mobley HL (2012) Enzymatically active and inactive phosphodiesterases and diguanylate cyclases are involved in regulation of Motility or sessility in *Escherichia coli* CFT073. *MBio* 3(5).
81. Patti JM, Allen BL, McGavin MJ, & Höök M (1994) MSCRAMM-mediated adherence of microorganisms to host tissues. *Annu Rev Microbiol* 48:585-617.
82. Vengadesan K & Narayana SV (2011) Structural biology of Gram-positive bacterial adhesins. *Protein Sci* 20(5):759-772.
83. Foster TJ & Höök M (1998) Surface protein adhesins of *Staphylococcus aureus. Trends Microbiol* 6(12):484-488.
84. Clarke SR & Foster SJ (2006) Surface adhesins of *Staphylococcus aureus*. *Adv Microb Physiol* 51:187-224.
85. Patti JM*, et al.* (1994) The *Staphylococcus aureus* collagen adhesin is a virulence determinant in experimental septic arthritis. *Infect Immun* 62(1):152-161.
86. Soto GE & Hultgren SJ (1999) Bacterial adhesins: common themes and variations in architecture and assembly. *J Bacteriol* 181(4):1059-1071.
87. Koebnik R, Locher KP, & Van Gelder P (2000) Structure and function of bacterial outer membrane proteins: barrels in a nutshell. *Mol Microbiol* 37(2):239-253.
88. Orme R, Douglas CW, Rimmer S, & Webb M (2006) Proteomic analysis of *Escherichia coli* biofilms reveals the overexpression of the outer membrane protein OmpA. *Proteomics* 6(15):4269-4277.
89. Fong JN & Yildiz FH (2015) Biofilm Matrix Proteins. *Microbiol Spectr* 3(2).
90. Toyofuku M, Roschitzki B, Riedel K, & Eberl L (2012) Identification of proteins associated with the *Pseudomonas aeruginosa* biofilm extracellular matrix. *J Proteome Res* 11(10):4906-4915.
91. Kostakioti M & Stathopoulos C (2006) Role of the α-Helical Linker of the C-Terminal Translocator in the Biogenesis of the Serine Protease Subfamily of Autotransporters. *Infection and Immunity* 74(9):4961-4969.

92. Chagnot C, Zorgani MA, Astruc T, & Desvaux M (2013) Proteinaceous determinants of surface colonization in bacteria: bacterial adhesion and biofilm formation from a protein secretion perspective. *Front Microbiol* 4:303.
93. Arenas J*, et al.* (2015) The meningococcal autotransporter AutA is implicated in autoaggregation and biofilm formation. *Environ Microbiol* 17(4):1321-1337.
94. Ulett GC*, et al.* (2007) Functional analysis of antigen 43 in uropathogenic *Escherichia coli* reveals a role in long-term persistence in the urinary tract. *Infect Immun* 75(7):3233-3244.
95. Lauer P*, et al.* (2005) Genome analysis reveals pili in Group B *Streptococcus*. *Science* 309(5731):105.
96. Fronzes R, Remaut H, & Waksman G (2008) Architectures and biogenesis of non-flagellar protein appendages in Gram-negative bacteria. *EMBO J* 27(17):2271-2280.
97. Busch A & Waksman G (2012) Chaperone-usher pathways: diversity and pilus assembly mechanism. *Philos Trans R Soc Lond B Biol Sci* 367(1592):1112-1122.
98. Chen SL*, et al.* (2009) Positive selection identifies an in vivo role for FimH during urinary tract infection in addition to mannose binding. *Proc Natl Acad Sci U S A* 106(52):22439-22444.
99. Dodson KW*, et al.* (2001) Structural basis of the interaction of the pyelonephritic *E. coli* adhesin to its human kidney receptor. *Cell* 105(6):733-743.
100. Waksman G & Hultgren SJ (2009) Structural biology of the chaperone-usher pathway of pilus biogenesis. *Nat Rev Microbiol* 7(11):765-774.
101. Geibel S & Waksman G (2014) The molecular dissection of the chaperone-usher pathway. *Biochim Biophys Acta* 1843(8):1559-1567.
102. Martinez JJ, Mulvey MA, Schilling JD, Pinkner JS, & Hultgren SJ (2000) Type 1 pilus-mediated bacterial invasion of bladder epithelial cells. *Embo J* 19(12):2803-2812.
103. Eto DS, Jones TA, Sundsbak JL, & Mulvey MA (2007) Integrin-mediated host cell invasion by type 1-piliated uropathogenic *Escherichia coli*. *PLoS Pathog* 3(7):e100.
104. Thankavel K*, et al.* (1997) Localization of a domain in the FimH adhesin of *Escherichia coli* type 1 fimbriae capable of receptor recognition and use of a domain-specific antibody to confer protection against experimental urinary tract infection. *J Clin Invest* 100(5):1123-1136.
105. Zhou G*, et al.* (2001) Uroplakin Ia is the urothelial receptor for uropathogenic *Escherichia coli*: evidence from in vitro FimH binding. *J Cell Sci* 114(Pt 22):4095-4103.
106. Thumbikat P*, et al.* (2009) Bacteria-induced uroplakin signaling mediates bladder response to infection. *PLoS Pathog* 5(5):e1000415.
107. Bouckaert J*, et al.* (2005) Receptor binding studies disclose a novel class of high-affinity inhibitors of the *Escherichia coli* FimH adhesin. *Mol Microbiol* 55(2):441-455.
108. Hung CS*, et al.* (2002) Structural basis of tropism of *Escherichia coli* to the bladder during urinary tract infection. *Mol Microbiol* 44(4):903-915.

109. Kuehn MJ, Heuser J, Normark S, & Hultgren SJ (1992) P pili in uropathogenic *E. coli* are composite fibres with distinct fibrillar adhesive tips. *Nature* 356(6366):252-255.
110. Hultgren SJ*, et al.* (1989) The PapG adhesin of uropathogenic *Escherichia coli* contains separate regions for receptor binding and for the incorporation into the pilus. *Proc Natl Acad Sci U S A* 86(12):4357-4361.
111. Chen SL*, et al.* (2006) Identification of genes subject to positive selection in uropathogenic strains of *Escherichia coli*: a comparative genomics approach. *Proc Natl Acad Sci U S A* 103(15):5977-5982.
112. Welch RA*, et al.* (2002) Extensive mosaic structure revealed by the complete genome sequence of uropathogenic *Escherichia coli. Proc Natl Acad Sci U S A* 99(26):17020-17024.
113. Struve C, Bojer M, & Krogfelt KA (2008) Characterization of *Klebsiella pneumoniae* type 1 fimbriae by detection of phase variation during colonization and infection and impact on virulence. *Infect Immun* 76(9):4055-4065.
114. Di Martino P, Cafferini N, Joly B, & Darfeuille-Michaud A (2003) *Klebsiella pneumoniae* type 3 pili facilitate adherence and biofilm formation on abiotic surfaces. *Res Microbiol* 154(1):9-16.
115. Murphy CN, Mortensen MS, Krogfelt KA, & Clegg S (2013) Role of *Klebsiella pneumoniae* type 1 and type 3 fimbriae in colonizing silicone tubes implanted into the bladders of mice as a model of catheter-associated urinary tract infections. *Infect Immun* 81(8):3009-3017.
116. Ayers M, Howell PL, & Burrows LL (2010) Architecture of the type II secretion and type IV pilus machineries. *Future Microbiol* 5(8):1203-1218.
117. Burrows LL (2005) Weapons of mass retraction. *Mol Microbiol* 57(4):878-888.
118. Craig L*, et al.* (2003) Type IV pilin structure and assembly: X-ray and EM analyses of *Vibrio cholerae* toxin-coregulated pilus and *Pseudomonas aeruginosa* PAK pilin. *Mol Cell* 11(5):1139-1150.
119. Cleary J*, et al.* (2004) Enteropathogenic *Escherichia coli* (EPEC) adhesion to intestinal epithelial cells: role of bundle-forming pili (BFP), EspA filaments and intimin. *Microbiology* 150(Pt 3):527-538.
120. Varga JJ*, et al.* (2006) Type IV pili-dependent gliding motility in the Gram-positive pathogen *Clostridium perfringens* and other *Clostridia*. *Mol Microbiol* 62(3):680-694.
121. Ramsugit S & Pillay M (2015) Pili of *Mycobacterium tuberculosis*: current knowledge and future prospects. *Arch Microbiol* 197(6):737-744.
122. Cohen FE & Kelly JW (2003) Therapeutic approaches to protein-misfolding diseases. *Nature* 426(6968):905-909.
123. Collinson SK*, et al.* (1993) Thin, aggregative fimbriae mediate binding of *Salmonella enteritidis* to fibronectin. *J Bacteriol* 175(1):12-18.
124. Nielsen HV*, et al.* (2013) Pilin and sortase residues critical for endocarditis- and biofilm-associated pilus biogenesis in *Enterococcus faecalis*. *J Bacteriol* 195(19):4484-4495.
125. Frans I*, et al.* (2013) Does virulence assessment of *Vibrio anguillarum* using sea bass (*Dicentrarchus labrax*) larvae correspond with genotypic and phenotypic characterization? *PLoS One* 8(8):e70477.

126. Craig L & Li J (2008) Type IV pili: paradoxes in form and function. *Curr Opin Struct Biol* 18(2):267-277.
127. Giltner CL, Nguyen Y, & Burrows LL (2012) Type IV pilin proteins: versatile molecular modules. *Microbiol Mol Biol Rev* 76(4):740-772.
128. Barnhart MM & Chapman MR (2006) Curli biogenesis and function. *Annu Rev Microbiol* 60:131-147.
129. Jordal PB*, et al.* (2009) Widespread abundance of functional bacterial amyloid in mycolata and other gram-positive bacteria. *Appl Environ Microbiol* 75(12):4101-4110.
130. Bian Z & Normark S (1997) Nucleator function of CsgB for the assembly of adhesive surface organelles in *Escherichia coli*. *EMBO J* 16(19):5827-5836.
131. Nenninger AA, Robinson LS, & Hultgren SJ (2009) Localized and efficient curli nucleation requires the chaperone-like amyloid assembly protein CsgF. *Proc Natl Acad Sci U S A* 106(3):900-905.
132. Evans ML & Chapman MR (2014) Curli biogenesis: order out of disorder. *Biochim Biophys Acta* 1843(8):1551-1558.
133. Kikuchi T, Mizunoe Y, Takade A, Naito S, & Yoshida S (2005) Curli fibers are required for development of biofilm architecture in *Escherichia coli* K-12 and enhance bacterial adherence to human uroepithelial cells. *Microbiol Immunol* 49(9):875-884.
134. Evans ML*, et al.* (2015) The bacterial curli system possesses a potent and selective inhibitor of amyloid formation. *Mol Cell* 57(3):445-455.
135. Gallo PM*, et al.* (2015) Amyloid-DNA Composites of Bacterial Biofilms Stimulate Autoimmunity. *Immunity* 42(6):1171-1184.
136. Oppong GO*, et al.* (2015) Biofilm-associated bacterial amyloids dampen inflammation in the gut: oral treatment with curli fibres reduces the severity of hapten-induced colitis in mice. *NPJ Biofilms Microbiomes* 1.
137. Rapsinski GJ*, et al.* (2015) Toll-like receptor 2 and NLRP3 cooperate to recognize a functional bacterial amyloid, curli. *Infect Immun* 83(2):693-701.
138. Oppong GO*, et al.* (2013) Epithelial cells augment barrier function via activation of the Toll-like receptor 2/phosphatidylinositol 3-kinase pathway upon recognition of *Salmonella enterica* serovar Typhimurium curli fibrils in the gut. *Infect Immun* 81(2):478-486.
139. Rapsinski GJ, Newman TN, Oppong GO, van Putten JP, & Tükel Ç (2013) CD14 protein acts as an adaptor molecule for the immune recognition of *Salmonella* curli fibers. *J Biol Chem* 288(20):14178-14188.
140. Nishimori JH*, et al.* (2012) Microbial amyloids induce interleukin 17A (IL-17A) and IL-22 responses via Toll-like receptor 2 activation in the intestinal mucosa. *Infect Immun* 80(12):4398-4408.
141. Tükel C*, et al.* (2010) Toll-like receptors 1 and 2 cooperatively mediate immune responses to curli, a common amyloid from enterobacterial biofilms. *Cell Microbiol* 12(10):1495-1505.
142. Tükel C*, et al.* (2009) Responses to amyloids of microbial and host origin are mediated through toll-like receptor 2. *Cell Host Microbe* 6(1):45-53.
143. Kasper DL (1986) Bacterial capsule--old dogmas and new tricks. *J Infect Dis* 153(3):407-415.

144. Meynell GG & Meynell E (1966) The biosynthesis of poly d-glutamic acid, the capsular material of *Bacillus anthracis*. *J Gen Microbiol* 43(1):119-138.
145. Green BD, Battisti L, Koehler TM, Thorne CB, & Ivins BE (1985) Demonstration of a capsule plasmid in *Bacillus anthracis*. *Infection and Immunity* 49(2):291-297.
146. Schrager HM, Albertí S, Cywes C, Dougherty GJ, & Wessels MR (1998) Hyaluronic acid capsule modulates M protein-mediated adherence and acts as a ligand for attachment of group A *Streptococcus* to CD44 on human keratinocytes. *J Clin Invest* 101(8):1708-1716.
147. Huebner J & Goldmann DA (1999) Coagulase-negative *staphylococci*: role as pathogens. *Annu Rev Med* 50:223-236.
148. Okshevsky M & Meyer RL (2015) The role of extracellular DNA in the establishment, maintenance and perpetuation of bacterial biofilms. *Crit Rev Microbiol* 41(3):341-352.
149. Das T, Sharma PK, Krom BP, van der Mei HC, & Busscher HJ (2011) Role of eDNA on the adhesion forces between *Streptococcus mutans* and substratum surfaces: influence of ionic strength and substratum hydrophobicity. *Langmuir* 27(16):10113-10118.
150. Lappann M*, et al.* (2010) A dual role of extracellular DNA during biofilm formation of *Neisseria meningitidis*. *Mol Microbiol* 75(6):1355-1371.
151. Whitchurch CB, Tolker-Nielsen T, Ragas PC, & Mattick JS (2002) Extracellular DNA required for bacterial biofilm formation. *Science* 295(5559):1487.
152. Absolom DR*, et al.* (1983) Surface thermodynamics of bacterial adhesion. *Applied and Environmental Microbiology* 46(1):90-97.
153. Dickson JS & Koohmaraie M (1989) Cell surface charge characteristics and their relationship to bacterial attachment to meat surfaces. *Applied and Environmental Microbiology* 55(4):832-836.
154. van Loosdrecht MC, Lyklema J, Norde W, Schraa G, & Zehnder AJ (1987) Electrophoretic mobility and hydrophobicity as a measured to predict the initial steps of bacterial adhesion. *Applied and Environmental Microbiology* 53(8):1898-1901.
155. Arnold JW & Bailey GW (2000) Surface finishes on stainless steel reduce bacterial attachment and early biofilm formation: scanning electron and atomic force microscopy study. *Poult Sci* 79(12):1839-1845.
156. Wright KJ, Seed PC, & Hultgren SJ (2007) Development of intracellular bacterial communities of uropathogenic *Escherichia coli* depends on type 1 pili. *Cell Microbiol* 9(9):2230-2241.
157. Mulvey MA*, et al.* (1998) Induction and evasion of host defenses by type 1-piliated uropathogenic *Escherichia coli*. *Science* 282(5393):1494-1497.
158. Hultgren SJ, Schwan WR, Schaeffer AJ, & Duncan JL (1986) Regulation of production of type 1 pili among urinary tract isolates of *Escherichia coli. Infection and Immunity* 54(3):613-620.
159. Schilling JD, Mulvey MA, & Hultgren SJ (2001) Structure and function of *Escherichia coli* type 1 pili: new insight into the pathogenesis of urinary tract infections. *J Infect Dis* 183 Suppl 1:S36-40.

160. Kostakioti M*, et al.* (2012) Distinguishing the contribution of type 1 pili from that of other QseB-misregulated factors when QseC is absent during urinary tract infection. *Infect Immun* 80(8):2826-2834.
161. Lane MC & Mobley HL (2007) Role of P-fimbrial-mediated adherence in pyelonephritis and persistence of uropathogenic *Escherichia coli* (UPEC) in the mammalian kidney. *Kidney Int* 72(1):19-25.
162. Belas R (2014) Biofilms, flagella, and mechanosensing of surfaces by bacteria. *Trends Microbiol* 22(9):517-527.
163. Ellison C & Brun YV (2015) Mechanosensing: a regulation sensation. *Curr Biol* 25(3):R113-115.
164. Ma L, Jackson KD, Landry RM, Parsek MR, & Wozniak DJ (2006) Analysis of *Pseudomonas aeruginosa* conditional psl variants reveals roles for the psl polysaccharide in adhesion and maintaining biofilm structure postattachment. *J Bacteriol* 188(23):8213-8221.
165. Irie Y*, et al.* (2012) Self-produced exopolysaccharide is a signal that stimulates biofilm formation in *Pseudomonas aeruginosa. Proc Natl Acad Sci U S A* 109(50):20632-20636.
166. Zhao K*, et al.* (2013) Psl trails guide exploration and microcolony formation in *Pseudomonas aeruginosa* biofilms. *Nature* 497(7449):388-391.
167. Valentini M & Filloux A (2016) Biofilms and Cyclic di-GMP (c-di-GMP) Signaling: Lessons from *Pseudomonas aeruginosa* and Other Bacteria. *Journal of Biological Chemistry* 291(24):12547-12555.
168. Sutherland IW (2001) The biofilm matrix--an immobilized but dynamic microbial environment. *Trends Microbiol* 9(5):222-227.
169. Branda SS, Vik S, Friedman L, & Kolter R (2005) Biofilms: the matrix revisited. *Trends Microbiol* 13(1):20-26.
170. Izano EA, Amarante MA, Kher WB, & Kaplan JB (2008) Differential roles of poly-N-acetylglucosamine surface polysaccharide and extracellular DNA in *Staphylococcus aureus* and *Staphylococcus epidermidis* biofilms. *Appl Environ Microbiol* 74(2):470-476.
171. Vilain S, Pretorius JM, Theron J, & Brozel VS (2009) DNA as an adhesin: *Bacillus cereus* requires extracellular DNA to form biofilms. *Appl Environ Microbiol* 75(9):2861-2868.
172. Tetz GV, Artemenko NK, & Tetz VV (2009) Effect of DNase and antibiotics on biofilm characteristics. *Antimicrob Agents Chemother* 53(3):1204-1209.
173. Koo H, Xiao J, Klein MI, & Jeon JG (2010) Exopolysaccharides produced by *Streptococcus mutans* glucosyltransferases modulate the establishment of microcolonies within multispecies biofilms. *J Bacteriol* 192(12):3024-3032.
174. Bokranz W, Wang X, Tschape H, & Romling U (2005) Expression of cellulose and curli fimbriae by *Escherichia coli* isolated from the gastrointestinal tract. *J Med Microbiol* 54(Pt 12):1171-1182.
175. Thomas VC*, et al.* (2009) A fratricidal mechanism is responsible for eDNA release and contributes to biofilm development of *Enterococcus faecalis*. *Mol Microbiol* 72(4):1022-1036.
176. Friedman L & Kolter R (2004) Genes involved in matrix formation in *Pseudomonas aeruginosa* PA14 biofilms. *Mol Microbiol* 51(3):675-690.

177. Steinberg N & Kolodkin-Gal I (2015) The Matrix Reloaded: How Sensing the Extracellular Matrix Synchronizes Bacterial Communities. *Journal of Bacteriology* 197(13):2092-2103.
178. Zogaj X, Nimtz M, Rohde M, Bokranz W, & Romling U (2001) The multicellular morphotypes of *Salmonella typhimurium* and *Escherichia coli* produce cellulose as the second component of the extracellular matrix. *Mol Microbiol* 39(6):1452-1463.
179. Hung C*, et al.* (2013) Escherichia coli biofilms have an organized and complex extracellular matrix structure. *MBio* 4(5):e00645-00613.
180. McCrate OA, Zhou X, Reichhardt C, & Cegelski L (2013) Sum of the parts: composition and architecture of the bacterial extracellular matrix. *J Mol Biol* 425(22):4286-4294.
181. Rowe MC, Withers HL, & Swift S (2010) Uropathogenic *Escherichia coli* forms biofilm aggregates under iron restriction that disperse upon the supply of iron. *FEMS Microbiol Lett* 307(1):102-109.
182. Chapman MR*, et al.* (2002) Role of *Escherichia coli* curli operons in directing amyloid fiber formation. *Science* 295(5556):851-855.
183. DePas WH*, et al.* (2013) Iron induces bimodal population development by *Escherichia coli*. *Proc Natl Acad Sci U S A* 110(7):2629-2634.
184. Hollenbeck EC*, et al.* (2018) Phosphoethanolamine cellulose enhances curli-mediated adhesion of uropathogenic *Escherichia coli* to bladder epithelial cells. *Proceedings of the National Academy of Sciences* 115(40):10106-10111.
185. Thongsomboon W*, et al.* (2018) Phosphoethanolamine cellulose: A naturally produced chemically modified cellulose. *Science* 359(6373):334-338.
186. Parsek MR & Greenberg EP (2005) Sociomicrobiology: the connections between quorum sensing and biofilms. *Trends Microbiol* 13(1):27-33.
187. O'Toole GA & Kolter R (1998) Initiation of biofilm formation in *Pseudomonas fluorescens* WCS365 proceeds via multiple, convergent signalling pathways: a genetic analysis. *Mol Microbiol* 28(3):449-461.
188. Hannan TJ*, et al.* (2012) Host-pathogen checkpoints and population bottlenecks in persistent and intracellular uropathogenic *Escherichia coli* bladder infection. *FEMS Microbiol Rev* 36(3):616-648.
189. Justice SS*, et al.* (2004) Differentiation and developmental pathways of uropathogenic *Escherichia coli* in urinary tract pathogenesis. *Proc Natl Acad Sci U S A* 101(5):1333-1338.
190. Lewis K (2007) Persister cells, dormancy and infectious disease. *Nat Rev Microbiol* 5(1):48-56.
191. Allesen-Holm M*, et al.* (2006) A characterization of DNA release in *Pseudomonas aeruginosa* cultures and biofilms. *Mol Microbiol* 59(4):1114-1128.
192. Harmsen M, Yang L, Pamp SJ, & Tolker-Nielsen T (2010) An update on *Pseudomonas aeruginosa* biofilm formation, tolerance, and dispersal. *FEMS Immunol Med Microbiol* 59(3):253-268.
193. Dragoš A*, et al.* (2018) Collapse of genetic division of labour and evolution of autonomy in pellicle biofilms. *Nat Microbiol* 3(12):1451-1460.

194. Ramritu P*, et al.* (2008) A systematic review comparing the relative effectiveness of antimicrobial-coated catheters in intensive care units. *American journal of infection control* 36(2):104-117.
195. Ha US & Cho YH (2006) Catheter-associated urinary tract infections: new aspects of novel urinary catheters. *Int J Antimicrob Agents* 28(6):485-490.
196. Zhu Z, Wang Z, Li S, & Yuan X (2019) Antimicrobial strategies for urinary catheters. *J Biomed Mater Res A* 107(2):445-467.
197. Roy R, Tiwari M, Donelli G, & Tiwari V (2017) Strategies for combating bacterial biofilms: A focus on anti-biofilm agents and their mechanisms of action. *Virulence*:00-00.
198. Franklin MJ, Chang C, Akiyama T, & Bothner B (2015) New Technologies for Studying Biofilms. *Microbiol Spectr* 3(4).
199. Lane MC, Alteri CJ, Smith SN, & Mobley HL (2007) Expression of flagella is coincident with uropathogenic *Escherichia coli* ascension to the upper urinary tract. *Proc Natl Acad Sci U S A* 104(42):16669-16674.
200. Wright KJ, Seed PC, & Hultgren SJ (2005) Uropathogenic *Escherichia coli* flagella aid in efficient urinary tract colonization. *Infect Immun* 73(11):7657-7668.
201. Hultgren SJ, Schwan WR, Schaeffer AJ, & Duncan JL (1986) Regulation of production of type 1 pili among urinary tract isolates of *Escherichia coli. Infect Immun* 54(3):613-620.
202. Bishop BL*, et al.* (2007) Cyclic AMP-regulated exocytosis of *Escherichia coli* from infected bladder epithelial cells. *Nat Med* 13(5):625-630.
203. Song J*, et al.* (2009) TLR4-mediated expulsion of bacteria from infected bladder epithelial cells. *Proc Natl Acad Sci U S A* 106(35):14966-14971.
204. Abraham SN & Miao Y (2015) The nature of immune responses to urinary tract infections. *Nat Rev Immunol* 15(10):655-663.
205. Wu J, Miao Y, & Abraham SN (2017) The multiple antibacterial activities of the bladder epithelium. 5:35-35.
206. Lewis AJ, Richards AC, & Mulvey MA (2016) Invasion of Host Cells and Tissues by Uropathogenic Bacteria. *Microbiol Spectr* 4(6).
207. Hannan TJ, Mysorekar IU, Hung CS, Isaacson-Schmid ML, & Hultgren SJ (2010) Early severe inflammatory responses to uropathogenic *E. coli* predispose to chronic and recurrent urinary tract infection. *PLoS Pathog* 6(8):e1001042.
208. Mysorekar IU & Hultgren SJ (2006) Mechanisms of uropathogenic *Escherichia coli* persistence and eradication from the urinary tract. *Proc Natl Acad Sci U S A* 103(38):14170-14175.
209. Floyd KA*, et al.* (2016) The UbiI (VisC) Aerobic Ubiquinone Synthase Is Required for Expression of Type 1 Pili, Biofilm Formation, and Pathogenesis in Uropathogenic *Escherichia coli*. *J Bacteriol* 198(19):2662-2672.
210. Hadjifrangiskou M*, et al.* (2011) A central metabolic circuit controlled by QseC in pathogenic *Escherichia coli*. *Mol Microbiol* 80(6):1516-1529.
211. Alteri CJ, Smith SN, & Mobley HL (2009) Fitness of *Escherichia coli* during urinary tract infection requires gluconeogenesis and the TCA cycle. *PLoS Pathog* 5(5):e1000448.
212. Hadjifrangiskou M*, et al.* (2012) Transposon mutagenesis identifies uropathogenic *Escherichia coli* biofilm factors. *J Bacteriol* 194(22):6195-6205.

213. Floyd KA*, et al.* (2015) Adhesive fiber stratification in uropathogenic *Escherichia coli* biofilms unveils oxygen-mediated control of type 1 pili. *PLoS Pathog* 11(3):e1004697.
214. Tran QH & Unden G (1998) Changes in the proton potential and the cellular energetics of *Escherichia coli* during growth by aerobic and anaerobic respiration or by fermentation. *Eur J Biochem* 251(1-2):538-543.
215. Unden G & Bongaerts J (1997) Alternative respiratory pathways of *Escherichia coli:* energetics and transcriptional regulation in response to electron acceptors. *Biochim Biophys Acta* 1320(3):217-234.
216. Unden G & Dünnwald P (2008) The Aerobic and Anaerobic Respiratory Chain of *Escherichia coli* and *Salmonella enterica*: Enzymes and Energetics. *EcoSal Plus* 3(1).
217. He G*, et al.* (1999) Noninvasive measurement of anatomic structure and intraluminal oxygenation in the gastrointestinal tract of living mice with spatial and spectral EPR imaging. *Proc Natl Acad Sci U S A* 96(8):4586-4591.
218. Wang ZJ*, et al.* (2008) Urinary oxygen tension measurement in humans using magnetic resonance imaging. *Acad Radiol* 15(11):1467-1473.
219. LEVY MN (1960) Effect of variations of blood flow on renal oxygen extraction. *Am J Physiol* 199:13-18.
220. Mulvey MA, Schilling JD, & Hultgren SJ (2001) Establishment of a persistent *Escherichia coli* reservoir during the acute phase of a bladder infection. *Infect Immun* 69(7):4572-4579.
221. Hung C*, et al.* (2013) *Escherichia coli* Biofilms Have an Organized and Complex Extracellular Matrix Structure. *MBio* 4(5).
222. Cegelski L*, et al.* (2009) Small-molecule inhibitors target *Escherichia coli* amyloid biogenesis and biofilm formation. *Nat Chem Biol* 5(12):913-919.
223. Reichhardt C*, et al.* (2016) Influence of the amyloid dye Congo red on curli, cellulose, and the extracellular matrix in *E. coli* during growth and matrix purification. *Anal Bioanal Chem*.
224. Pinkner JS*, et al.* (2006) Rationally designed small compounds inhibit pilus biogenesis in uropathogenic bacteria. *Proc Natl Acad Sci U S A* 103(47):17897-17902.
225. Velasquez MT, Ramezani A, Manal A, & Raj DS (2016) Trimethylamine N-Oxide: The Good, the Bad and the Unknown. *Toxins (Basel)* 8(11).
226. Morcos E & Wiklund NP (2001) Nitrite and nitrate measurement in human urine by capillary electrophoresis. *Electrophoresis* 22(13):2763-2768.
227. Ghoniem GM, McBride D, Sood OP, & Lewis V (1993) Clinical experience with multiagent intravesical therapy in interstitial cystitis patients unresponsive to single-agent therapy. *World J Urol* 11(3):178-182.
228. Vij M, Srikrishna S, & Cardozo L (2012) Interstitial cystitis: diagnosis and management. *Eur J Obstet Gynecol Reprod Biol* 161(1):1-7.
229. Breland EJ, Eberly AR, & Hadjifrangiskou M (2017) An Overview of Two-Component Signal Transduction Systems Implicated in Extra-Intestinal Pathogenic *E. coli* Infections. *Front Cell Infect Microbiol* 7:162.

230. Greene SE, Hibbing ME, Janetka J, Chen SL, & Hultgren SJ (2015) Human Urine Decreases Function and Expression of Type 1 Pili in Uropathogenic *Escherichia coli. MBio* 6(4):e00820.
231. Greene SE*, et al.* (2014) Pilicide ec240 disrupts virulence circuits in uropathogenic *Escherichia coli*. *MBio* 5(6):e02038.
232. Eberly AR*, et al.* (2017) Biofilm Formation by Uropathogenic *Escherichia coli* Is Favored under Oxygen Conditions That Mimic the Bladder Environment. *Int J Mol Sci* 18(10).
233. Puustinen A, Finel M, Haltia T, Gennis RB, & Wikström M (1991) Properties of the two terminal oxidases of *Escherichia coli*. *Biochemistry* 30(16):3936-3942.
234. Calhoun MW, Oden KL, Gennis RB, de Mattos MJ, & Neijssel OM (1993) Energetic efficiency of *Escherichia coli*: effects of mutations in components of the aerobic respiratory chain. *J Bacteriol* 175(10):3020-3025.
235. Murphy KC & Campellone KG (2003) Lambda Red-mediated recombinogenic engineering of enterohemorrhagic and enteropathogenic *E. coli*. *BMC Mol Biol* 4:11.
236. Shaffer CL*, et al.* (2017) Purine Biosynthesis Metabolically Constrains Intracellular Survival of Uropathogenic *Escherichia coli. Infect Immun* 85(1).
237. O'Toole GA*, et al.* (1999) Genetic approaches to study of biofilms. *Methods Enzymol* 310:91-109.
238. Heydorn A*, et al.* (2000) Quantification of biofilm structures by the novel computer program COMSTAT. *Microbiology* 146 (Pt 10):2395-2407.
239. Vorregaard M (2008) Comstat2 - a modern 3D image analysis environment for biofilms, in Informatics and Mathematical Modelling. (Technical University of Denmark: Kongens Lyngby, Denmark).
240. Anonymous (Comstat2.
241. Hung CS, Dodson KW, & Hultgren SJ (2009) A murine model of urinary tract infection. *Nat Protoc* 4(8):1230-1243.
242. Hobley L*, et al.* (2013) BslA is a self-assembling bacterial hydrophobin that coats the Bacillus subtilis biofilm. *Proc Natl Acad Sci U S A* 110(33):13600-13605.
243. Shepherd M*, et al.* (2016) The cytochrome bd-I respiratory oxidase augments survival of multidrug-resistant *Escherichia coli* during infection. *Sci Rep* 6:35285.
244. Hartland EL & Leong JM (2013) Enteropathogenic and enterohemorrhagic E. coli: ecology, pathogenesis, and evolution. *Frontiers in Cellular and Infection Microbiology* 3.
245. Kehl SC (2002) Role of the Laboratory in the Diagnosis of Enterohemorrhagic *Escherichia coli* Infections. 40(8):2711-2715.
246. Russo TA & Johnson JR (2000) Proposal for a new inclusive designation for extraintestinal pathogenic isolates of *Escherichia coli*: ExPEC. *J Infect Dis* 181(5):1753-1754.
247. Subashchandrabose S & Mobley HL (2015) Virulence and Fitness Determinants of Uropathogenic *Escherichia coli. Microbiol Spectr* 3(4).
248. Garcia EC, Brumbaugh AR, & Mobley HLT (2011) Redundancy and Specificity of *Escherichia coli* Iron Acquisition Systems during Urinary Tract Infection. 79(3):1225-1235.

249. Yep A, McQuade T, Kirchhoff P, Larsen M, & Mobley HL (2014) Inhibitors of TonB function identified by a high-throughput screen for inhibitors of iron acquisition in uropathogenic *Escherichia coli* CFT073. *MBio* 5(2):e01089-01013.
250. Knöbl T*, et al.* (2001) Virulence properties of *Escherichia coli* isolated from ostriches with respiratory disease. *Vet Microbiol* 83(1):71-80.
251. Johnson TJ, Siek KE, Johnson SJ, & Nolan LK (2006) DNA sequence of a ColV plasmid and prevalence of selected plasmid-encoded virulence genes among avian *Escherichia coli* strains. *J Bacteriol* 188(2):745-758.
252. Lloyd AL, Rasko DA, & Mobley HL (2007) Defining genomic islands and uropathogen-specific genes in uropathogenic *Escherichia coli. J Bacteriol* 189(9):3532-3546.
253. Wiles TJ, Kulesus RR, & Mulvey MA (2008) Origins and virulence mechanisms of uropathogenic *Escherichia coli. Exp Mol Pathol* 85(1):11-19.
254. Zhu B & Wu X (2008) Identification of outer membrane protein ompR from rickettsia-like organism and induction of immune response in Crassostrea ariakensis. *Mol Immunol* 45(11):3198-3204.
255. Zhu Ge X*, et al.* (2014) Comparative genomic analysis shows that avian pathogenic *Escherichia coli* isolate IMT5155 (O2:K1:H5; ST complex 95, ST140) shares close relationship with ST95 APEC O1:K1 and human ExPEC O18:K1 strains. *PLoS One* 9(11):e112048.
256. Nazemi A, Mirinargasi M, Merikhi N, & Sharifi SH (2011) Distribution of Pathogenic Genes aatA, aap, aggR, among Uropathogenic *Escherichia coli* (UPEC) and Their Linkage with StbA Gene. *Indian J Microbiol* 51(3):355-358.
257. Spurbeck RR*, et al.* (2011) Fimbrial profiles predict virulence of uropathogenic *Escherichia coli* strains: contribution of ygi and yad fimbriae. *Infect Immun* 79(12):4753-4763.
258. Logue CM*, et al.* (2012) Genotypic and phenotypic traits that distinguish neonatal meningitis-associated *Escherichia coli* from fecal *E. coli* isolates of healthy human hosts. *Appl Environ Microbiol* 78(16):5824-5830.
259. Huja S*, et al.* (2015) Genomic avenue to avian colisepticemia. *MBio* 6(1).
260. Wang S*, et al.* (2015) IbeR facilitates stress-resistance, invasion and pathogenicity of avian pathogenic *Escherichia coli*. *PLoS One* 10(3):e0119698.
261. Wijetunge DS*, et al.* (2015) Characterizing the pathotype of neonatal meningitis causing Escherichia coli (NMEC). *BMC Microbiol* 15(1):211.
262. Wurpel DJ, Beatson SA, Totsika M, Petty NK, & Schembri MA (2013) Chaperone-usher fimbriae of *Escherichia coli. PLoS One* 8(1):e52835.
263. Mellata M (2013) Human and avian extraintestinal pathogenic *Escherichia coli*: infections, zoonotic risks, and antibiotic resistance trends. *Foodborne Pathog Dis* 10(11):916-932.
264. Kaper JB (2005) Pathogenic *Escherichia coli*. *Int J Med Microbiol* 295(6-7):355-356.
265. Antao EM*, et al.* (2009) Signature-tagged mutagenesis in a chicken infection model leads to the identification of a novel avian pathogenic *Escherichia coli* fimbrial adhesin. *PLoS One* 4(11):e7796.

266. Schrimpe-Rutledge AC, Codreanu SG, Sherrod SD, & McLean JA (2016) Untargeted Metabolomics Strategies-Challenges and Emerging Directions. *J Am Soc Mass Spectrom* 27(12):1897-1905.
267. Dobrindt U, Wullt B, & Svanborg C (2016) Asymtomatic Bacteriuria as a Model to Study the Coevolution of Hosts and Bacteria. *Pathogens* 5(1).
268. Wullt B & Svanborg C (2016) Deliberate Establishment of Asymptomatic Bacteriuria-A Novel Strategy to Prevent Recurrent UTI. *Pathogens* 5(3).
269. Hancock V, Ferrieres L, & Klemm P (2007) Biofilm formation by asymptomatic and virulent urinary tract infectious *Escherichia coli* strains. *FEMS Microbiol Lett* 267(1):30-37.
270. Connell I*, et al.* (1996) Type 1 fimbrial expression enhances *Escherichia coli* virulence for the urinary tract. *Proc Natl Acad Sci U S A* 93(18):9827-9832.
271. Bahrani-Mougeot FK*, et al.* (2002) Type 1 fimbriae and extracellular polysaccharides are preeminent uropathogenic *Escherichia coli* virulence determinants in the murine urinary tract. *Mol Microbiol* 45(4):1079-1093.
272. Weiner J*, et al.* (2012) Biomarkers of Inflammation, Immunosuppression and Stress with Active Disease Are Revealed by Metabolomic Profiling of Tuberculosis Patients. 7(7):e40221.
273. Lewis GD*, et al.* (2008) Metabolite profiling of blood from individuals undergoing planned myocardial infarction reveals early markers of myocardial injury. 118(10):3503-3512.
274. Kostakioti M, Hadjifrangiskou M, Pinkner JS, & Hultgren SJ (2009) QseC-mediated dephosphorylation of QseB is required for expression of genes associated with virulence in uropathogenic *Escherichia coli*. *Mol Microbiol* 73(6):1020-1031.
275. Khetrapal V, Mehershahi K, Chen S, & Chen S (2016) Application and Optimization of relE as a Negative Selection Marker for Making Definitive Genetic Constructs in Uropathogenic *Escherichia coli.* 5(1):9.
276. Khetrapal V*, et al.* (2015) A set of powerful negative selection systems for unmodified Enterobacteriaceae. *Nucleic Acids Res* 43(13):e83.
277. Habazettl J, Allan MG, Jenal U, & Grzesiek S (2011) Solution structure of the PilZ domain protein PA4608 complex with cyclic di-GMP identifies charge clustering as molecular readout. *J Biol Chem* 286(16):14304-14314.
278. Guckes KR*, et al.* (2013) Strong cross-system interactions drive the activation of the QseB response regulator in the absence of its cognate sensor. *Proc Natl Acad Sci U S A* 110(41):16592-16597.
279. Pfaffl MW (2001) A new mathematical model for relative quantification in real-time RT-PCR. *Nucleic Acids Res* 29(9):e45.
280. Plate L & Marletta MA (2012) Nitric oxide modulates bacterial biofilm formation through a multicomponent cyclic-di-GMP signaling network. *Mol Cell* 46(4):449-460.
281. Mason MG*, et al.* (2009) Cytochrome bd confers nitric oxide resistance to *Escherichia coli*. *Nat Chem Biol* 5(2):94-96.
282. Barraud N*, et al.* (2009) Nitric oxide signaling in *Pseudomonas aeruginosa* biofilms mediates phosphodiesterase activity, decreased cyclic di-GMP levels, and enhanced dispersal. *J Bacteriol* 191(23):7333-7342.

283. Rybtke MT*, et al.* (2012) Fluorescence-based reporter for gauging cyclic di-GMP levels in *Pseudomonas aeruginosa*. *Appl Environ Microbiol* 78(15):5060-5069.
284. Liu X, Beyhan S, Lim B, Linington RG, & Yildiz FH (2010) Identification and Characterization of a Phosphodiesterase That Inversely Regulates Motility and Biofilm Formation in *Vibrio cholerae*. 192(18):4541-4552.
285. Govantes F, Orjalo AV, & Gunsalus RP (2002) Interplay between three global regulatory proteins mediates oxygen regulation of the *Escherichia coli* cytochrome d oxidase (cydAB) operon. 38(5):1061-1073.
286. Gunsalus RP & Park SJ (1994) Aerobic-anaerobic gene regulation in *Escherichia coli*: control by the ArcAB and Fnr regulons. *Res Microbiol* 145(5-6):437-450.
287. Cotter P (1992) Contribution of the fnr and arcA gene products in coordinate regulation of cytochrome o and d oxidase (cyoABCDE and cydAB) genes in *Escherichia coli.* 91(1):31-36.
288. Mogi T*, et al.* (2009) Antibiotics LL-Z1272 identified as novel inhibitors discriminating bacterial and mitochondrial quinol oxidases. *Biochim Biophys Acta* 1787(2):129-133.
289. Folsom JP, Baker B, & Stewart PS (2011) In vitro efficacy of bismuth thiols against biofilms formed by bacteria isolated from human chronic wounds. *Journal of Applied Microbiology* 111(4):989-996.
290. Wood TK (2009) Insights on *Escherichia coli* biofilm formation and inhibition from whole-transcriptome profiling. 11(1):1-15.
291. Frees D*, et al.* (2004) Clp ATPases are required for stress tolerance, intracellular replication and biofilm formation in *Staphylococcus aureus*. *Mol Microbiol* 54(5):1445-1462.
292. O'Toole GA & Kolter R (1998) Flagellar and twitching motility are necessary for *Pseudomonas aeruginosa* biofilm development. *Mol Microbiol* 30(2):295-304.
293. Ducey T & Dyer D (2002) Rapid identification of EZ:: TN™ transposon insertion sites in the genome of *Neisseria gonorrhoeae*. (EPICENTRE Forum).